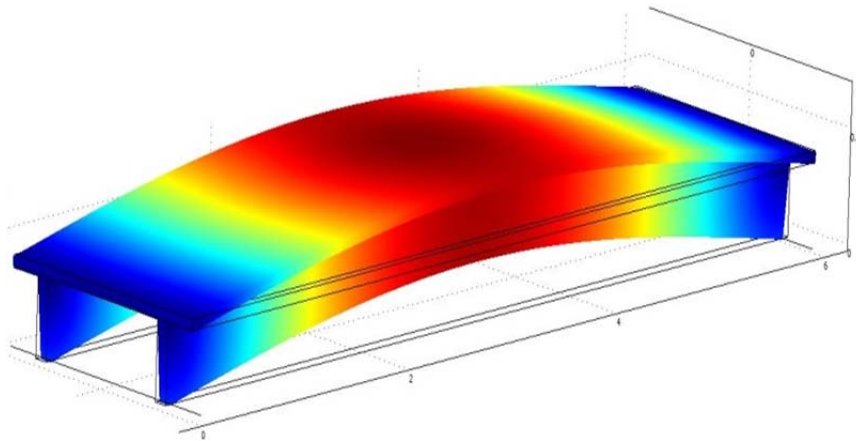


Timber concrete composite floors with prefabricated Fiber Reinforced Concrete



Luca Costa

Avdelningen för Konstruktionsteknik

Lunds Tekniska Högskola

Lunds Universitet, 2011

Avdelningen för Konstruktionsteknik
Lunds Tekniska Högskola

Box 118

221 00 LUND

Department of Structural Engineering
Lund Institute of Technology

Box 118

S-221 00 LUND

Sweden

Timber concrete composite floors with prefabricate Fiber Reinforced Concrete

Luca Costa

2011

Rapport TVBK-5208

ISSN 0349-4969

ISRN: LUTVDG/TVBK-11/5208+189p

Examensarbete

Handledare: Roberto Crocetti

February 2011

1 INTRODUCTION

This chapter presents an introduction to timber-concrete composite systems and their applications, the aims, scope and limitations of the research, and outlines the structure of the thesis.

1.1 Background

Timber-concrete composite structural systems have been investigated for nearly 80 years. Floors of composite timber and concrete have been used successfully in highway bridges, hangar aprons, wharves, piers, buildings and platforms since the early 1940's (Richart and Williams). One of the first projects carried out on timber-concrete composite structures was described by McCullough (1943) who performed experimental tests (known as the *Oregon tests*) on timber-concrete composite beams, prompted by a desire of the Oregon State Highway Department (USA) to develop a cost-effective short-span highway bridge. In many European countries timber-concrete composite constructions are being increasingly used in upgrading and post-strengthening of existing timber floors in residential/office buildings as well as new constructions for buildings and bridges (Ceccotti 1995). In the 1980's and 90's special attention was paid to timber multi-storey buildings and public structures. The most pertinent work was done by Natterer (1996) who proposed a system with vertical nailed planks for floors of new residential and public buildings that was applied in multi-storey buildings. Most research on wood-concrete composite structures has been performed on various types of shear connectors, used together with standard concrete and timber glued laminated beams or wooden decks. However, a few researchers have also explored the possibilities of using different concrete or other wood-based engineering materials.

Most of the research performed to date and currently in progress on wood-concrete composite systems is focused on systems in which "wet" concrete is cast on top of timber beams with mounted shear connector systems (traditional/"wet" timber concrete composite systems). An example of a "wet" timber-concrete composite system with mounted shear connectors is illustrated in next Figure 1.

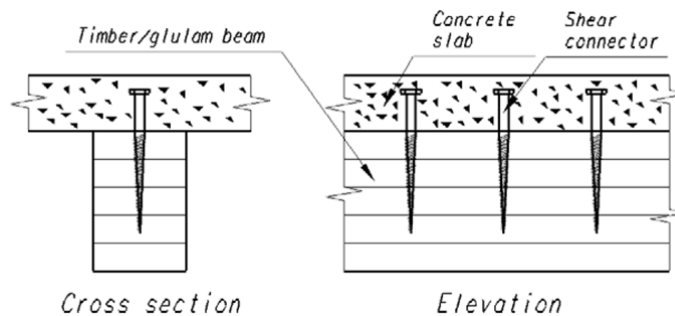


Figure 1: example of "wet" timber-concrete composite system

In timber-concrete composite structure the concrete topping mainly resists compression, while the timber joist resists tension and bending, and the connection system transmits the shear forces between the two components. Advantages over wooden floors include the increased load-carrying capacity, higher stiffness (which leads to reductions in deflections and susceptibility to vibrations), improved acoustic and thermal properties, and higher fire resistance. There are also some advantages relative to normal reinforced concrete floors, notably cracks in the tensile region of reinforced concrete slabs may promote penetration of moisture and corrosion of the steel rebar. Further, the lower part of a concrete slab (40-60% of the depth) is generally ineffective since it is cracked and thus

non-resistant. By replacing that part with a resistant solid wooden deck, the overall depth of the concrete slab can be reduced by about 50% and, thus, the self-weight of the structure can be markedly decreased (Gutkowski 2000). The connection system is a crucial part of any timber-concrete composite structure. It needs to be stiff and strong to maximize the composite action, but its number of components and installation time should be minimal, to make the system cost effective (Deam et al. 2008). Evaluating the connection's stiffness is important because the behavior (static and dynamic) of the composite concrete-wood structure is strongly influenced by the slip between the beam and the slab (Gelfi et al. 2002). Hence, the design of timber-concrete composite structures generally requires consideration of the slip occurring in the joint between the timber and concrete. A method for calculating shear connector loads from mechanically jointed beams or columns is given in Annexes B and C of Eurocode 5 Part 1-1 (EN 1995-1-1:2004), and the design of timber-concrete connections is addressed in Eurocode 5 Part 2 (EN 1995-2:2004). In many cases, however, the load-carrying capacity and slip modulus of the connection have to be determined by empirical tests since Eurocode 5 only provides guidelines to calculate parameters of laterally loaded dowel-type fasteners inserted perpendicular to the shear plane.

However, despite the many advantages of timber-concrete composite structures, the use of wet concrete also has disadvantages, notably:

- the introduction of a "wet" component in the typically "dry" construction processes applied in timber buildings
- the time needed for the concrete to set, which adds to the time required on-site before the next scheduled action can be taken
- low stiffness and high creep while the concrete cures, which is particularly unfavorable for unpropped composite beams, hence propping of beams at midspan is crucial to minimize permanent deflection and enable the development of sufficient initial composite stiffness to sustain the full self-weight of the concrete slab
- the high cost of cast-in-situ concrete slabs, mainly due to the cost of transporting fresh concrete and the use of props, formwork such as planks/particleboard or plywood sheets as composite components, which further increases the self-weight of the structure, and use of separating layer-foil between the concrete and timber to prevent the timber coming into contact with wet concrete

Moreover, excessive shrinkage of concrete causes additional deflection, hence low shrinkage concrete is desirable in timber-concrete composite structures to minimize any permanent deflection.

No previous research has explicitly focused on timber-concrete composite systems in which "dry-dry" shear connectors are embedded in the concrete slabs so the slabs and the timber beams can be connected off-site. Some previous attempts have been made to develop prefabricated composite systems, but in the cited studies wet concrete was still cast on timber beams with inserted shear connectors.

1.2 Aims and scope

The overarching purpose of this research project was to explore the mechanical performance of "dry-dry" shear connectors for mounting in a prefabricated concrete slab in such a way that concrete slab and glulam beams can be connected off-site. Such a prefabricated timber-concrete composite system can significantly reduce all the aforementioned drawbacks of the "wet" systems.

Concrete exhibits creep and drying shrinkage, but by increasing the curing time before the assembly of the prefabricated concrete slab with the glulam beam the long-term deflection can be reduced in comparison to traditional composite floors. Particular focus was placed on thoroughly characterizing the stiffness of the investigated shear connectors, with the target of determining a theoretical formulation for the stiffness of the

connection system. Finally, the influence of various parameters on their long-term (50-years) structural performance was explored,

1.3 Outline of the thesis

This Master Thesis consists of two parts and one Appendix: *Part I* summarizes the research project and contributes additional information about the state of the art. *Part I* also presents background theory related to the analytical and numerical methods applied in studies described in the papers, which present most of the experimental, analytical and numerical results. Furthermore, chapter 4 presents a review of the existing shear connectors used to join across two precast elements as slabs, girders or beams, with some ideas that could be used to provide transversal slab to slab connection. Since *Part I* includes supplementary information, references that were not incorporated in the appended papers are also cited.

Part II contains the detailed description of the innovative systems investigated in this research project, consisting in a fiber reinforced concrete slab lying over glued laminated timber beams, with a theoretical research about the methods to evaluate the stiffness of the shear connectors. Furthermore, there are the results of the experimental tests provided on full-scale specimens. As an introduction of *Part II*, chapter 5 is a brief review concerning the theory of composite elements such as reported on Eurocode.

The *Appendix* presents the evaluation of the stresses and deformations on our system, provided according to the Eurocode 5 theoretical method for composite sections presented on chapter 5. Moreover, we present also an approximate evaluation of the load acting on the transversal slab to slab connection.

2 REFERENCES

This chapter contains all the standards rules and all the paper references used and recalled in the text.

STANDARDS REFERENCE

Analysis, calculations and checks are made on the basis of the requirements provided by the “Norme Tecniche per le Costruzioni” of 14 January 2008, and the relative “Circolare Applicativa” number 617 of February 2, 2009 (respectively Statement [1] and [5] in text).

About some particular checks and issues not covered by that rule, it refers instead to European Standards UNI EN 1992-1-1 (2005): “Design of concrete structures: general rules and rules for buildings” (Statement [2] in text); to European Standards UNI EN 1995-1-1 (2005) and UNI EN 1995-1-1 (2009): “Design of timber structures: general – common rules and rules for buildings” (respectively Statement [3] and [4] in text); to UNI EN 1991-1-4 (2005): “General actions – wind actions” (Statement [6] in text).

About the tests procedure we referred to European Standard EN 26891 (1991): “Timber structures – Joints made with mechanical fasteners – General principles for the determination of strength and deformation characteristic” (Statement [7] in text).

PAPERS REFERENCE

- [I] R. Crocetti, T. Sartori. *Timber-concrete composite structures with prefabricated FRC slab*. WCTE 2010.
- [II] E. Lukaszewska. *Development of prefabricated timber-concrete composite floors*. PhD thesis, Luleå University of Technology 2009.
- [III] M. Piazza, R. Tomasi. *Theoretical and experimental analysis of timber-to-timber joints with inclined screws*. Construction and building materials.
- [IV] M. Ballerini, M. Piazza. *Tecniche di realizzazione di solai composti in legno e calcestruzzo*. CNR 1999.
- [V] H. J. Blass. *Tragfähigkeit von Verbindungen mit selbstbohrenden*. Karlsruher Berichte zum Ingenieurholzbau.
- [VI] M. Ballerini, R. Crocetti, M. Piazza. *An experimental investigation on notched connection for timber concrete composite structures*. WCTE 2002.
- [VII] E. Lukaszewska, H. Johnsson. *Connections for prefabricated Timber-Concrete composite systems*. WCTE 2006.

3 SHEAR CONNECTORS IN TIMBER-CONCRETE COMPOSITE STRUCTURES

This chapter presents a literature review of existing shear connectors used in timber-concrete composite structures. Various applications of traditional composite systems are also presented.

3.1 "Oregon tests" – the first timber-concrete composite connectors

Some of the first full scale bending tests on composite systems were performed between 1938 and 1942 in the Talbot Laboratory, University of Illinois (USA), on 32 composite beams, primarily to compare various shear connections (Richart and Williams 1943).

The shear connections were (i) triangular steel plates with 40 in. (ca. 101.6 mm) long sides (Fig. 2.1a) (in one case inclined 15° inward, mid-span) (ii) triangular steel plates supplemented with spikes, which acted as ties (Fig. 2.1b), (iii) vertical lag screws or railroad spikes (Fig. 2.1c) (also with 45° inclination), and (iv) sloped notches with or without spikes (Fig. 2.1d).

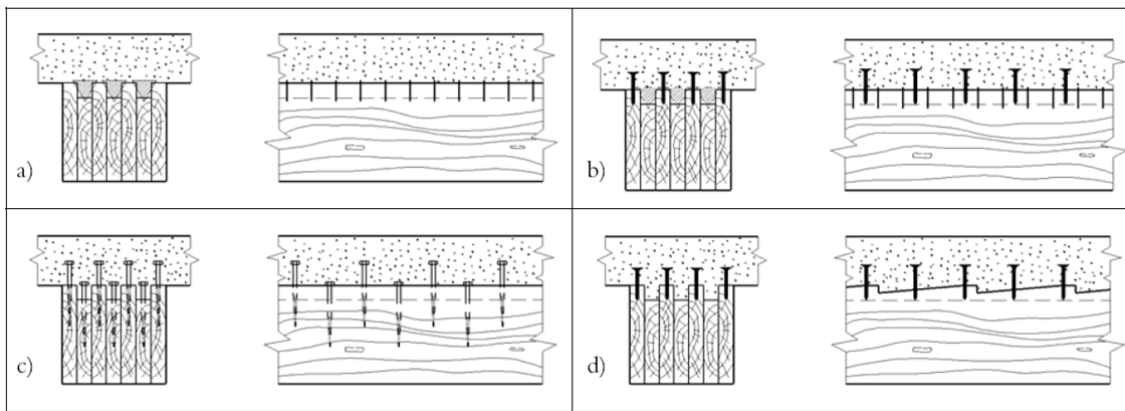


Figure 2: details of composite beams tested by Richart and Williams: (a) triangular plates, vertical, (b) triangular plates and spikes, (c) lag screws or spikes, (d) sloped notched and spikes

The beams with triangular plates units and spikes gave the best results as a group. They had high load carrying capacity, good integral beam action and developed small slip and deflections. Most of the other shear connectors showed fairly satisfactory strength and stiffness (Richart and Williams 1943).

The cited authors were also pioneers in performing long-term tests on timber-concrete composite structures, and their main conclusions were that the differences in volume change (shrinkage or expansion) of the two materials of the composite beam, measured in these tests over a two and a half year period, appeared to have little or no effect upon the strength of the beams, as compared to beams tested 28 days after fabrication. There was no indication of separation of the two elements of the beams and the stiffness and integral action were, if anything, slightly superior for the two and a half years-old beams.

In a study published in the same year 22 full size composite beams were tested to destruction by McCullough (1943). Five types of shear connections were examined, consisting of spikes, daps in the timber, a combination of spikes and daps, pipe dowels and flat steel plates. The main objectives of the tests were: (i) to determine the relative ultimate flexural strength and relative deflection of the composite beams in comparison to plain timber beams of equal

dimensions and under equal load, (ii) to investigate the effect of repeated or alternated loads, (iii) to investigate the effects of thermal changes, (iv) to study the general action of the composite beams under various load increments, the character and extent of shear distortion both elastic and plastic, and (v) to develop a *theory of design* for composite structures.

The following conclusions were drawn from the tests: (i) the ultimate strength of a composite beam is at least twice that of the same elements with no interlayer connection; (ii) the deflection of a composite beam under a given load will be no more than 25% of the corresponding deflection for the same materials, of the same sizes, used independently; (iii) repeated loading did not appear to have any detrimental effect on this type of construction.

The secondary bending resulting from thermal effects does not appear to induce stresses of sufficient magnitude to cause concern; however, the development of tension due to restraint in the lower portions of the concrete slab indicates that adequate longitudinal temperature reinforcement should be provided.

Based upon the results of the Oregon tests a composite design was developed by the Oregon Highway Department and more than 180 bridges, with a total length in excess of 20000 feet (6100 km), have been constructed using it (Baldcock 1941).

3.2 Strengthening of old timber structures and renovation of wooden bridges

In some countries in Europe composite timber-concrete composite structures have become popular for renovation works and strengthening old timber structures (i.e. timber floors in old masonry structures, as shown on next Figure 3 (Ceccotti 1995).

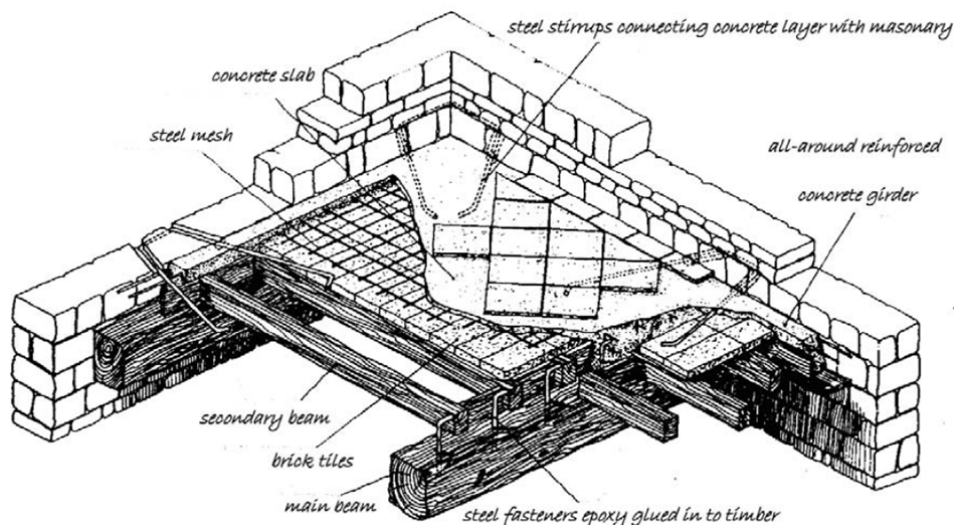


Figure 3: example of seismic strengthening of an existing timber floor in a mid-European masonry building using a timber-concrete composite system (Ceccotti 1995)

One of the first applications in historic buildings was installed in Bratislava, in the former Czechoslovakia, in 1960 and is mentioned by Poštulka (1983). The system, which included use of 6.3 x 180 mm long nails, for strengthening wooden floors led to ca. four-fold increases in load capacity and stiffness, at less than half the costs of building a new floor. In Godycki et al. (1984) the renovation of more than 10000 m² timber floor in Łódź, Poland, is described, using concrete joined with nails. Turrini and Piazza (1983a,b) describe the restoration of historic buildings in Italy using steel dowels glued in timber with a concrete layer poured on the floor.

In other refurbishments of historic buildings in Italy presented by Blasi et al. (1992) corrugated metal sheets were used as lost formwork. In addition, a technique for renovating old timbers by adding a concrete slab and an L-shaped sheet metal nailed plate embedded in the concrete and nailed to wood was proposed by Van der Linden and Blass (1996).

Wooden floors in ancient buildings are not the only structures in need of renovation and strengthening that can be treated in this kind of manner. There are, for instance, many deteriorated short-span wooden bridges to which a concrete layer can be added on top of the old wooden structure, and large numbers of timber-concrete bridges

were built in Australia between the 1950's and 80's with lengths varying between 6 and 37.3 m and in New Zealand in the 70's with spans from 6 m to 24.5 m (Dias 2005, and references therein, including Nolan 2002, and Nauta 1984).

3.3 Timber-concrete connections

Figure 4 summarizes the most commonly used methods of joining concrete to timber, as originally classified by Ceccotti (1995). The shear connectors are grouped, according to their stiffness, in four groups: connectors in group A have the lowest stiffness while connectors in group D are the stiffest (with twice as much bending stiffness as those in group A). With group D type connections it is possible to achieve full composite action between timber and concrete (Ceccotti 2002).

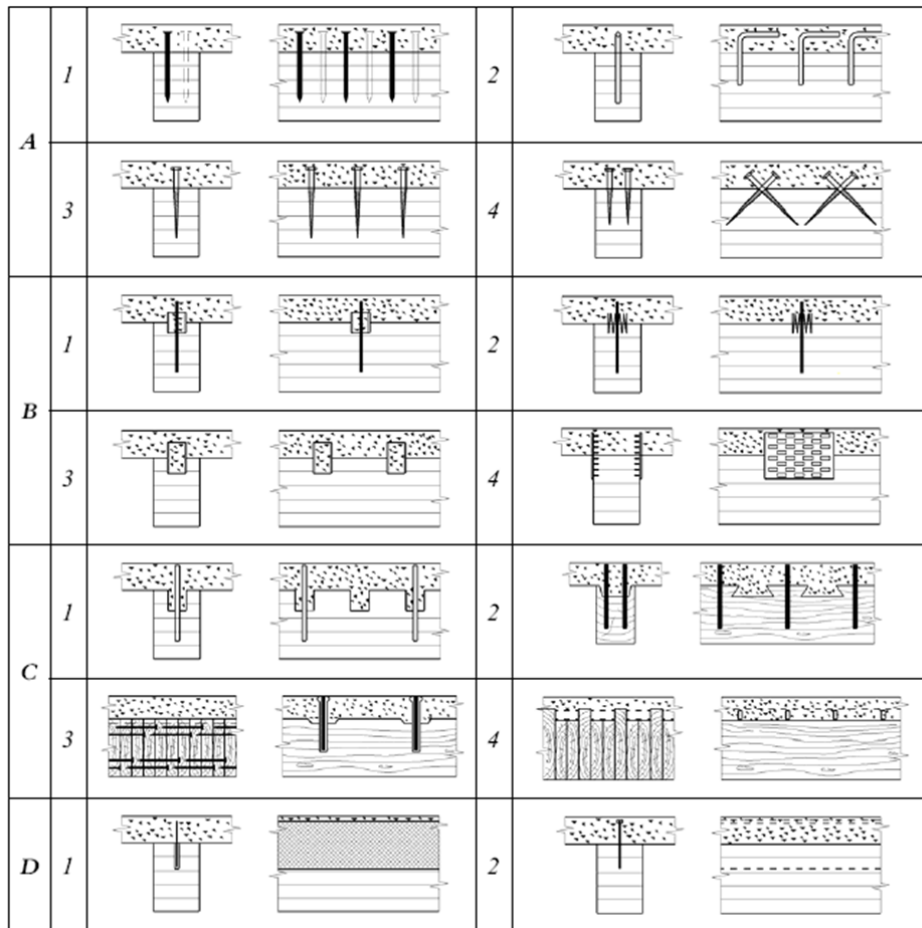


Figure 4: examples of timber-concrete connections with: nails (A1); glued reinforced concrete steel bars (A2); screws (A3); inclined screws (A4); split rings (B1); toothed plates (B2); steel tubes (B3); steel punched metal plates (B4); round indentations in timber, with fasteners preventing uplift (C1); square indentations, ditto (C2); cup indentations and prestressed steel bars (C3); nailed timber planks deck and steel shear plates slotted through the deeper planks (C4); steel lattice glued to timber (D1); and steel plate glued to timber (D2)

Group A connectors have the advantage of being inexpensive and straightforward to install. However, as mentioned above they are generally considered to be the least rigid. Connectors in group B have been shown to have higher rigidity, ductility and ultimate strength than dowel-type connectors (Blass and Schlager 1996, Mungwa et al. 1999). The reason for this is that nails and screws typically cause wood splitting failure, whereas tubular-type connectors (rigid ring connectors, in particular) provide greater rigidity and can cause wood shear plug failure, which generally occurs at higher loads (Clouston et al. 2004). Group C connectors, in which notches

(shear keys) have been cut into the wood and reinforced with anchorage devices such as post-tensioned bolts or lag screws, have been shown to have similar to moderately better strength and slip resistance than group *B* connectors (Blass and Schlager 1996). The horizontal shear forces are transmitted through the shear key with little interlayer slip, while the dowels work in traction to resist the vertical load component. The last (group *D*) connectors are generally considered to have the greatest rigidity, as mentioned above. In this group design calculations for connections can be easily made since there is no slip between the concrete layer and timber member and the concrete section can be “transformed” to an equivalent timber section with the same centre of gravity. In contrast, connections in groups *A-C* are semi-rigid composites, subject to varying levels of slip, which require more complex design procedures (Clouston et al. 2004). Analytical solutions as well as finite element based solutions for partial composite action have been proposed by many researchers.

Existing shear connectors will be discussed further in this chapter in terms of their strength and stiffness as determined in shear tests. The shear connector performance in composite systems will be analyzed in terms of observed efficiency where data are available.

3.3.1 Epoxy glue as a shear connector

Pincus (1969) investigated the use of an epoxy resin compound to bond horizontal concrete flanges to vertical wood beams. Five wood-concrete composite T-beams were tested to destruction. No appreciable slip between the two materials was found prior to the final failure, indicating that the system had true composite action. However, important effects that should be considered in glued wood-concrete beams are (i) environmental conditions before and after bonding, (ii) timber moisture contents and tensile strength variability, (iii) the compatibility with preservative treatments, (iv) effects of repeated and impactive loads, (v) the compatibility of the epoxy and concrete, and (vi) the long-term behavior of the system. These aspects were not considered and therefore remained unknown. Eight composite epoxy bonded wood-concrete T-beams with nails added along the beam to serve as supplementary mechanical shear transfer devices were subsequently tested (Pincus 1970). It was found that applying epoxy glue to vertical boards or wood beams and immediately casting the concrete on the beams is an efficient constructional procedure that results in wood-concrete composite beams. The beams had negligible slip between concrete and timber before final failure. The maximum slip at the end support was 0.305 mm. The small magnitude of the slip is indicative of excellent adhesion compared with the maximum slip of 1.52 mm recorded in the tests performed by Richart and Williams (1943) using mechanical shear connectors. Using nails as additional shear transfer devices increases the horizontal shear capacity at the wood-concrete interface. The nails, which were driven into the wood before application of the epoxy and casting of the concrete, resulted in increases of up to 50% in sliding shear failure load for the specimens tested.

Recently Brunner et al. (2007) proposed a similar approach to the one described by Pincus in 1969: the “wet on wet process”, in which fresh concrete is poured onto epoxy-based adhesive while the adhesive is still wet. This technique provides a rigid connection, but it is a very delicate process, because of the danger of the concrete displacing the adhesive when it is poured.

3.3.2 Epoxy glued-in continuous shear connectors

Piazza and Ballerini (2000) carried out experimental tests on 6 m long full-scale specimens (Fig. 5) with eight different connector types, complemented by push-out tests on single connectors and numerical analyses to verify the influence of the connection systems on the mechanical behavior of the composite beams.

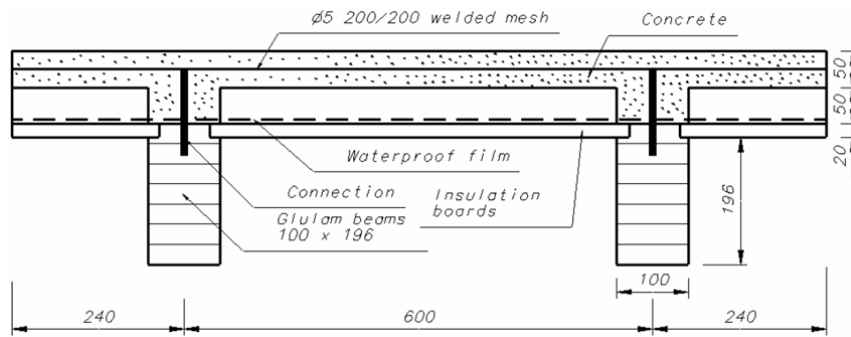


Figure 5: geometry of specimens tested by Piazza and Ballerini (2000) (dimensions in mm)

One of the connection systems was made with 2 mm thick steel sheets epoxy-glued to timber (Fig. 6). The steel sheet connector type showed a linear response nearly right up to failure, followed by a pseudo-plastic branch, due to the progressive failure of the connection (Piazza and Ballerini 2000). The failure occurred due to the shear collapse of the timber nearest the glue surface. Strength at failure was about 30 kN/m^2 , with a corresponding mid-span deflection of about 70 mm. The bending strength of this glued-in system is about 2.5 times higher than that of timber beams. The composite action achieved for this type connector was about 90%.

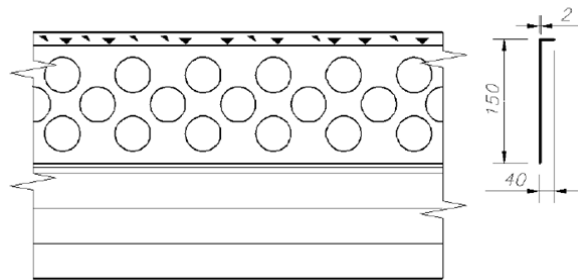


Figure 6: steel sheet (appropriately shaped and drilled) epoxy glued to timber, Piazza and Ballerini 2000 (dimensions in mm)

Bathon and Graf (2000) introduced a continuous wood-concrete composite system in which a steel mesh embedded in a concrete slab is inserted into a continuous slot in the wooden beam and connected by an adhesive, Fig. 7, providing a rigid but ductile connector between the wood and concrete. The ultimate shear failure load was found to be on average ca. 90 kN, with an average displacement of 1.8 mm.

Full-scale specimens (5400 mm long, with 600 mm wide x 70 mm high concrete slabs and wooden beams with cross-section dimensions of 100 mm x 200 mm height) were used in bending tests. The ultimate failure load was on average 70 kN, with an average mid-span deflection of approximately 42 mm (Bathon and Graf 2000).

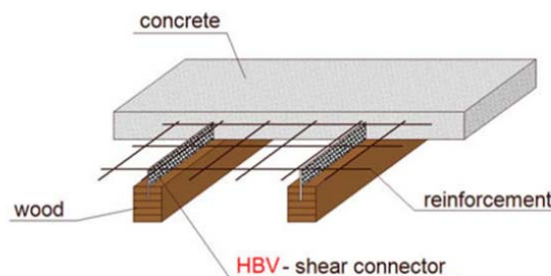


Figure 7: example of prefabricated wood-concrete composite floor panels, Bathon and Graf (2000)

Clouston has investigated the same type of connector for use with U.S. manufactured products (Clouston et al. 2004, Clouston et al. 2005, Clouston and Schreyer 2006) with five different adhesives. The shear connector reached ultimate loads of approximately 52 kN, with a corresponding slip modulus of 22.8 kN/mm. Two bending tests were performed on 4500 mm long specimens with concrete slabs of 76 x 610 mm and Parallel Strand Lumber (PSL) of 89 x 241 mm. The average ultimate capacity was 119 kN, with a corresponding mid-span deflection of about 50 mm. It was found that the wood composite beam behaves as a full composite action system (Clouston et al. 2004). The comprehensive report (Clouston et al. 2005) from tests performed on this continuous steel-mesh connector type showed that the wood concrete composite beam has just 3% lower effective bending stiffness than that of a beam with full composite action.

The continuous steel-mesh solution was approved for the *HBV-Building System*, a prefabricated modular system with wall-, floor-, and roof-elements (Bathon et al. 2006). The prefabricated modular *HBV*-building elements consist of a concrete slab (100 mm thick and 2500 mm wide with varying length) and multiple girders with a cross-section of 76 x 203 mm at 625 mm spacing (Bathon et al. 2006). The long-term performance of the *HBV*-system is described in Bathon et al. (2006). A recommendation from the long-term tests is that in order to compensate for the long-term deflection of the wood-composite system a sufficient negative deflection (cambering of the wooden section) should be included in the design.

3.3.3 Glued-in shear connectors

Floor specimens assembled by means of glued-in steel connectors showed better mechanical responses than those assembled using mechanical connectors. Furthermore, the specimens with glued-in shear connectors are less sensitive to the loading/unloading cycles in terms of residual displacements.

Two glued-in type connectors were tested in the experimental test program presented by Piazza and Ballerini (2000) (Figs. 8 & 9). One connection system was made with $\Phi 16$ mm bent dowels glued to timber (Fig. 8), while the other one included concrete stocky dowels coupled with $\Phi 16$ mm steel ribbed dowels epoxy-glued to timber (Fig. 9).

The behavior of these shear connectors in composite structures was characterized by a quite linear response up to about 50% of the failure load, followed by a post-elastic hardening branch, due mainly to the non linear-behavior of connections. The hardening branch shows a stiffness which ranges between 70% and 85% of composite efficiency for bent dowels and concrete dowels, respectively. Strength at failure was about 25 kN/m², with corresponding mid-span deflection of about 70 mm for bent dowels, while for concrete stocky dowels with steel dowels the strength was about 30 kN/m², with corresponding mid-span deflection of about 50 mm. The bending strength of this glued-in system, with bent and concrete stocky dowels, was about 2.0 and 2.5 times that of timber beams, respectively.

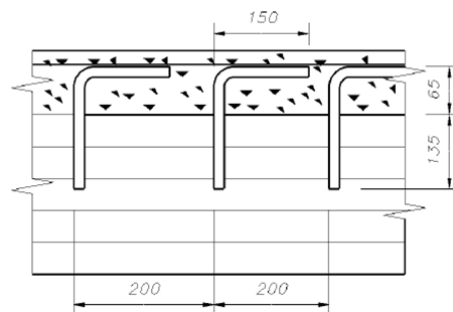


Figure 8: bent dowels epoxy glued into the timber, Piazza and Ballerini 2000 (dimensions in mm)

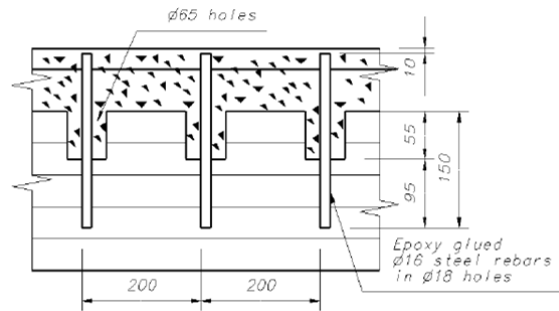


Figure 9: concrete stocky dowel with steel dowels epoxy glued to timber, Piazza and Ballerini 2000 (dimensions in mm)

Ceccotti et al. (2006) reported the outcomes of a comprehensive test performed on a timber-concrete composite system with glued-in connections (Fig. 10), realized using $\Phi 18$ mm corrugated re-bars, which were placed in holes drilled in timber beams and filled with epoxy resin. The spacing of the connectors varied from 150 mm over the supports to 300 and 450 mm in the middle of the span. After a preliminary short-term test, the beam was subjected to sustained load for five years, in outdoor conditions. After the long-term test, the beam was ramp-loaded to failure. The main observation from the test was that the mid-span deflection markedly increased during the first two years of the long-term test, with a final value below the limit adopted by national regulations. The collapse load was 2.44 times the service design load. For the tested beam, the composite efficiency values were 93% and 87% from half the serviceability load and the actual collapse load, respectively, confirming that the connection was very stiff.

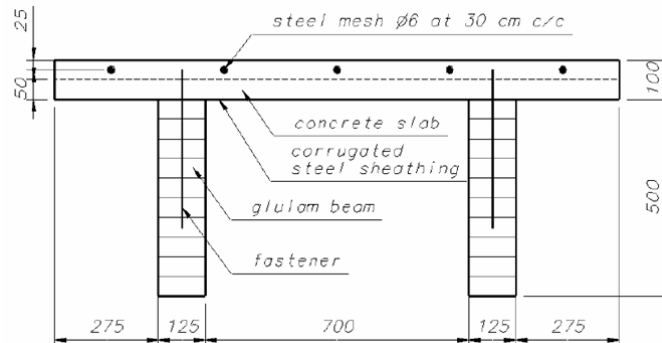


Figure 10: cross-section of the composite beam tested by Ceccotti et al. (2006) (dimensions in mm)

3.3.4 Vertical, inclined nails, screws, bolts and horizontal shear connector types

Unnikrishna (1977) used commercially available 3 mm and 5 mm wire nails as shear connectors in systems subjected to 28 push-out tests. The obtained loads for nails of $\Phi 3$ mm per shear connector were between 2.2 kN for inclined nails (with the head pointing in the opposite direction of the shear) and 4.0 kN for straight nails. For $\Phi 5$ mm nails the loads were between 5.2 kN for inclined nails (with the head pointing in the direction of the shear) and 6.4 kN for straight nails. The corresponding slip was >15 mm. The main conclusions were that the minimum spacing of nails should not be less than 10 times their diameter, the length of embedment of the nail into concrete should be at least 25 mm in the compressive zone and the penetration into the timber beam at least two-thirds of the length of the nail. Placing the nails at an inclination of 45° , with the head pointing in the direction of the shear on the timber surface will result in higher strength and lower slips.

Two different shear connection types, one horizontal and one vertical, were investigated and used in the construction of a composite floor and staircase for an acoustics laboratory (Murthy 1984). In the beams with horizontal shear connectors, timber ribs were slotted over a depth of 37 mm into the concrete topping slab. The shear connectors were made of 13 mm diameter mild steel rods cut from round mild steel reinforcing rods, and

passed horizontally through the holes in the timber rib, ensuring a tight fit by making the holes in the timber of smaller diameter than the rods (Fig. 11a). Two mild steel rods of Φ 6 mm were placed in the longitudinal direction of the beam on either side of the timber rib and held tightly by wires to the shear connectors. The beam with vertical shear connectors did not have timber ribs slotted into the concrete topping slab, but mild steel bolts of Φ 16 mm were used as vertical shear connectors (Fig. 11).

Slip at the interface was high for beams with vertical shear connectors, but for beams with horizontal shear connectors almost full composite action was achieved, particularly for loads below 50% of the ultimate load. Due to considerable slip at the interface of the timber and concrete at ultimate loads the author advised use of a capacity reduction factor of about 0.7 on the ultimate loads calculated assuming full composite action.

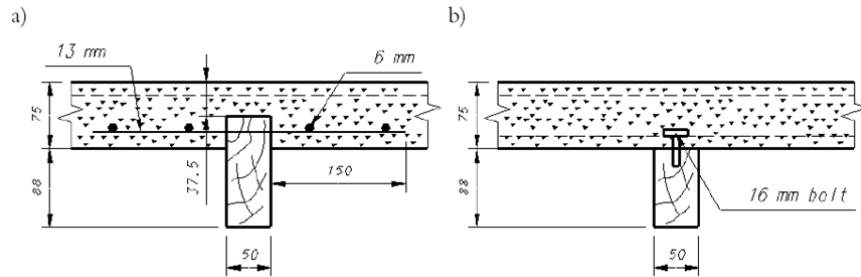


Figure 11: cross-sections of timber-concrete composite beams with horizontal shear connectors (a) and vertical shear connectors (b) (after Murthy 1984) (dimensions in mm)

In the early 1990s the *RF 2000* system was introduced, by Meierhofer (1992), which was one of the first types of steel fasteners produced specifically for timber-concrete composite structures (Figs. 12 & 13). The fastener, which has two heads, allows part of the screw to be fixed in concrete, and the rest in timber. Many researchers have used this type of connector in their studies, including Blass et al. (1995), Van der Linden (1999), Steinberg et al. (2003), Frangi and Fontana (2003), Dias (2005) and Jorge (2005). The system includes a special, high strength *Stadler VB-48-7.5 × 100* steel connector, which is divided into two parts: an upper 50 mm long part with a Φ of 6 mm that acts as an anchor in the concrete and a lower, threaded 100 mm long part with a diameter of 7.5 mm that acts as an anchor in the wood.

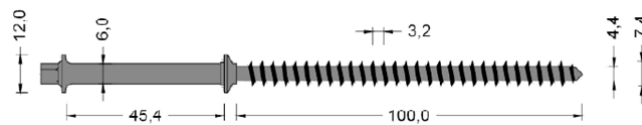


Figure 12: SFS VB screw 48-7.5 x 100 (Jorge 2005) (dimensions in mm)



Figure 13: SFS VB screws in an inclined arrangement in the longitudinal direction (Jorge 2005)

Meierhofer (1992) performed several kinds of tests to evaluate this type of connector's structural performance: short-term pull-out, shear and bending tests and long-term pullout and bending tests of the entire composite

element. Five different arrangements of connectors were tested in configurations with straight or inclined nails at $\pm 45^\circ$ (Fig. 14).

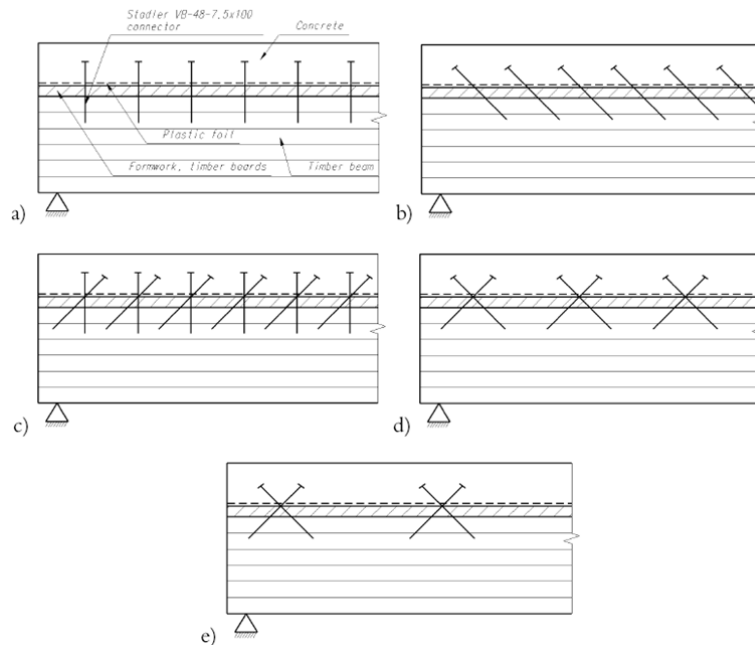


Figure 14: arrangements of the connectors in bending tests described by Meierhofer (1992)

The highest stiffness (of about 60% of composite efficiency) was obtained with the arrangement shown in Fig. 14 d. The maximum load was about 30 kN, with a corresponding mid-span deflection of about 20 mm. The end slip was < 1.5 mm. The lowest stiffness was shown by connectors arranged vertically (Fig. 14 a), for which the maximum load was about 25 kN with corresponding mid-span deflection of 60 mm. The end slip for this arrangement was < 6.5 mm, hence it showed more flexible connection behavior. The long-term test results clearly demonstrated the superiority of the arrangement with the connectors inclined at $\pm 45^\circ$ (Fig. 14 d), for which the mid-span deflection after 250 days was around 7 mm, while for vertically arranged connectors it was around 22 mm. This system has been applied in many projects in Switzerland, in both new structures and for strengthening existing wooden floors (Fig. 15).

In 1992 Delft University and the University of Karlsruhe started a research program focused on the load-carrying capacity of timber-concrete composite beams (Van der Linden 1999, Van der Linden and Blass 1996). The research included shear tests, bending tests, creep tests on composite beams and *Monte Carlo* simulations of floor systems.

Four types of timber-concrete composite beams with different types of connectors were tested.

The concrete slabs and timber beams were connected by means of SFS screws (Fig. 12) installed at $\pm 45^\circ$, with an interlayer of a 28 mm particleboard (Figs. 2.15), nailed plates, bent at an angle of 90° , reinforcement bar with a concrete notch and grooved connections in LVL. The main conclusion was that all connector categories satisfied serviceability and ultimate limit state requirements.

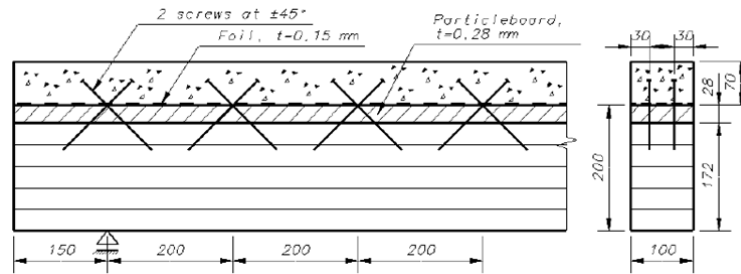


Figure 15: timber-concrete connection with crossed screws (after Van der Linden 1999) (dimensions in mm)

The average strength reached by screws (2 x 2) in the shear tests was around 30 kN, with corresponding slip <1.5 mm. The force decreased with increasing slip once the maximum load had been reached. The strongest composite beams, with the screws arrangement shown in Fig. 15, exhibited almost plastic behavior. The maximum load per jack (in four-point bending tests) was 19 kN, with corresponding mid-span deflection of about 100 mm (Van der Linden 1999).

Ten different kinds of high strength nails employed as shear connectors have been tested under static short-term loading, repeated loading and long-term sustained loading by Ahmadi and Saka (1993). The experimental studies showed that the ultimate load capacity of the proposed composite floor system with two different kinds of nails was twice as high as the non composite system. It was also shown that the deflection of the floor system can be reduced to a fifth of that of the non-composite system. Experimental studies also showed that it is sufficient to drive the nails into the timber joists to a depth of 11 times their diameter. It was concluded that an increase in the stiffness and load-carrying capacity, with at least a 50% saving in the cost of the timber joists compared to non-composite floors, can be achieved by simply providing appropriate shear connectors. The use of two selected nails in composite timber- concrete floors in residential buildings is described by Ahmadi and Saka (1994).

Takac (1996) investigated a full-scale structure (3.2 m span length) with *Bulldog E75M16* type "one-side" dowels (spaced at 200 mm) in a long-term test for 173 days. The timber and concrete was bonded by dowels with wooden bolts, which were sunk 50 mm into the concrete, enabling concrete → bolt → dowel → timber force transfer. The investigations of the rheological behavior indicated that the shift yield is highest during the first seven days after loading.

A flexible tubular connector named *INSA-Hilti* for wood-concrete composite structures was developed by Mungwa (1999). The *INSA-Hilti* connector is essentially a hollow cylinder with varying cross-section and wall thickness. The connector was tested in two static (push-out and composite slab) tests. The connector was classified as a flexible tubular connector with dowel-type behavior, characteristics that were corroborated in push-out tests. The connector showed great ductility, with relative slip observed in the tests of 16 and 22 mm (with maximum corresponding loads per four connectors of 163 and 160 kN), respectively.

Gelfi and Giuriani (1999) performed experimental work with a simple kind of connection, suitable for strengthening, in which stud connectors obtained by simply forcing ordinary smooth steel bars into drilled holes in the wooden beam without resins were used.

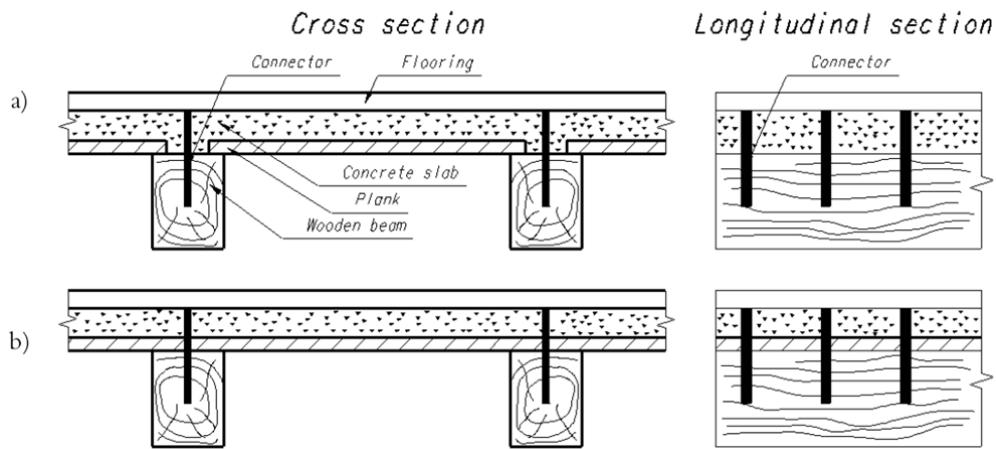


Figure 16: stud shear connectors for stiffening and strengthening wooden floors: direct contact connection (a) and interposed plank connection (b) (after Gelfi and Giuriani 1999)

Two different types of connections were studied: one with the concrete slab in direct contact with the wood beam using Φ 12 mm stud connectors, the other with interposed planks and Φ 16 mm stud connectors (Figs. 16 a & 16 b). The main observation from the study was that wood insertion lengths greater than five times the stud diameter do not considerably improve the connection stiffness and strength. The shear strength for the Φ 12 mm stud ranged from 8.3 to 10.7 kN, with corresponding slip <3.5 mm, and that of the Φ 16 mm stud ranged from 9.9 to 12.7 kN, with corresponding slip between 3 and 3.5 mm.

Benitez (2000) presented three types of shear connectors for potential use in new timber bridges and the rehabilitation of old bridges with timber girders and concrete decks (Fig. 17).

Static and dynamic responses were examined of connectors consisting of: 20 mm plain mild steel dowel inclined at 60° (Fig. 17 a), a circular hollow section (CHS) fitted in a groove of the same diameter in conjunction with $150 \times$ M16 coach screws (Fig. 17 b) and finally a universal column section (UC) fastened to timber using four $75 \times$ M16 coach screws (Fig. 17 c). The average maximum loads (per two connectors) achieved in shear tests were 353 kN, 344 kN and 121 kN for the CHS, UC and steel dowel type connectors, respectively. It was concluded that full composite action can be achieved with universal column sections, which give far better ductility than the CHS with coach screw systems, and the specimens sustained large forces after 100,000 cycles.

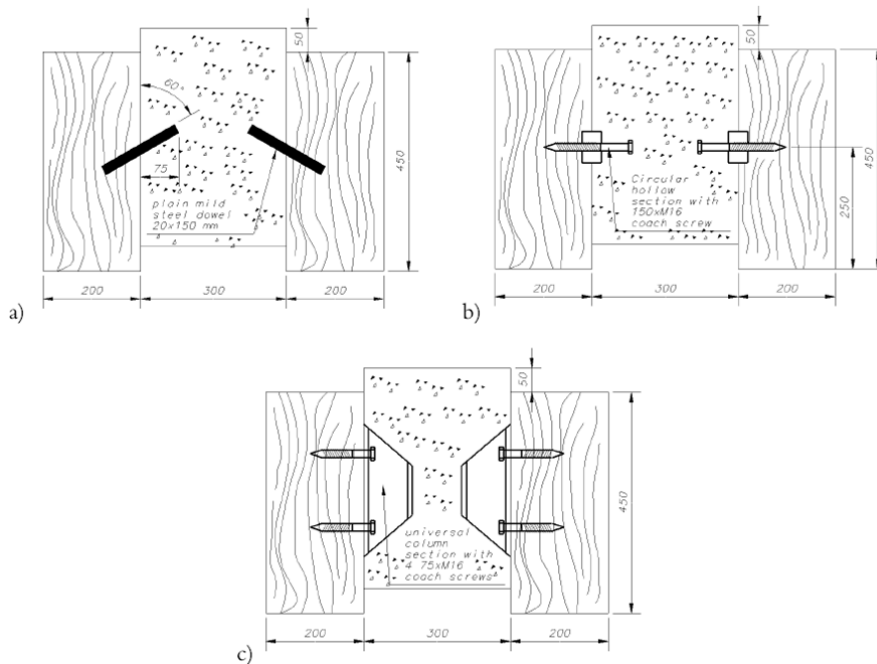


Figure 17: shear connectors for use in composite systems to construct new, or rehabilitate old, timber bridges: (a) 20 mm plain mild steel dowel inclined at 60°; (b) circular hollow section ; (c) universal column section (after Benitez 2000) (dimensions in mm)

Dowel type connectors have also been tested in an experimental test program presented by Piazza and Ballerini (2000) and described in section 3.3.2. One connection system was made with Φ 16 mm screws placed at constant spacing of 200 mm, driven into the timber to about 140 mm (Fig. 18a) while the other consisted of Φ 16 mm ribbed dowels simply placed in Φ 16 mm holes, which were drilled with at $\pm 45^\circ$ inclination (Fig. 18b).

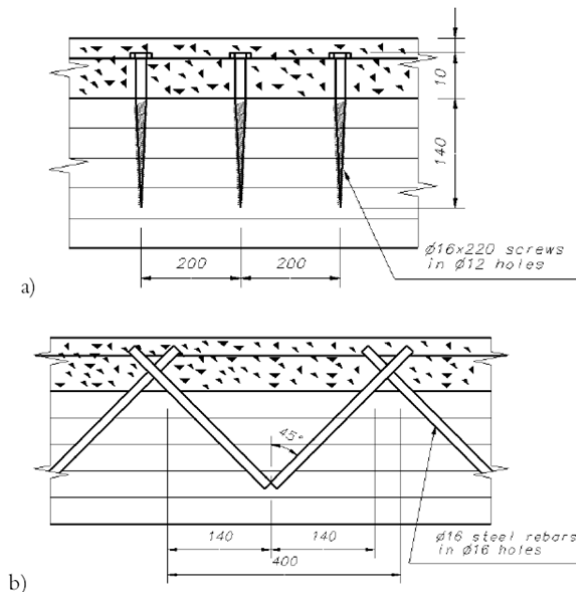


Figure 18: Screws driven into the timber beam (a) and dowels placed into the timber at $\pm 45^\circ$ (b) (after Piazza and Ballerini 2000) (dimensions in mm)

The behavior of screws in composite structures was characterized by a quite linear response up to about 50% of the failure load, followed by a post-elastic hardening branch due mainly to the non-linear behavior of the

connection. The behavior of inclined dowels is non-linear due to the non-elastic responses of unglued dowels (which allow small non-elastic slip).

Strength at failure was about 23 kN/m^2 , with corresponding mid-span deflection of about 55 mm for steel screws, while for inclined steel dowels the strength was about 24 kN/m^2 , with a corresponding mid-span deflection of about 80 mm. The bending strength of this glued-in system was about twice that of the timber beams.

Lehmann et al. (2001) presented a so-called *flat steel lock* connector, which can be utilized to join nail-laminated timber elements with a concrete slab. The steel connector, which has a flat, $5 \times 40 \text{ mm}$ cross-section, is inclined towards shear at an angle of 5° to the vertical (Fig. 19).

Both shear and bending tests were carried out to determine the structural characteristics of the connection. It was found that the shear forces between the timber and concrete can be transferred through the flat-steel lock and the distance between connectors can be kept relatively large in comparison to dowel type connectors. The shear strength achieved in push-out tests was around 100 kN (per two shear connectors), with corresponding slip of about 4 mm.

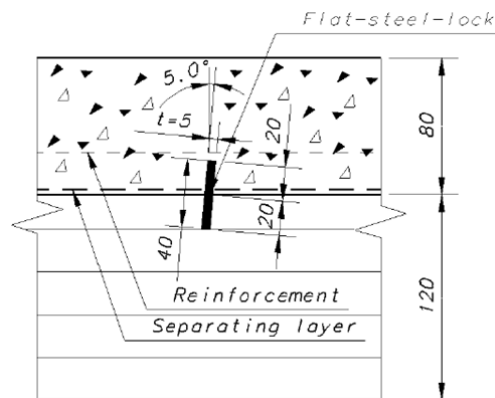


Figure 19: flat steel lock connector (after Lehmann 2001) (dimensions in mm)

Dias performed a large number of experimental shear-tests on dowel type fasteners and notched joints to evaluate their short- and long-term mechanical performance (Dias 2005, Dias et al. 2007). The dowel type fasteners were made of dowel produced from short pieces of steel, smooth or profiled reinforcing bars. Three different types of timber were used (spruce, maritime pine and chestnut), and low strength/lightweight, normal strength and high strength

concrete. The shear test results are presented in Table 1 for all tested dowel type connectors.

Test series	Connector	Timber	Concrete	Strength, F_{max}	Stiffness, K_i
				[kN]	[kN/mm]
8 mm ¹⁾	Ø 8 mm smooth bar	Spruce	MSC*	13.6	13.2
10 mmA ¹⁾	Ø 10 mm smooth bar	Spruce	MSC	22.6	17.2
HSC ¹⁾	Ø 10 mm smooth bar	Spruce	HSC**	23.6	15.7
MP ¹⁾	Ø 10 mm smooth bar	Maritime pine	MSC	25.5	26.4
C ¹⁾	Ø 10 mm smooth bar	Chestnut	MSC	26.2	36.1
LWAC ¹⁾	Ø 10 mm smooth bar	Spruce	LC***	18.5	16.1
10 mmB ²⁾	Ø 10 mm profiled bar	Spruce	MSC	68.8	40.2
INT ²⁾	Ø 10 mm profiled bar	Spruce****	MSC	63.3	26.2

* medium strength concrete, ** high strength concrete, *** lightweight aggregate concrete, **** with additional 20 mm thick interlayer, ¹⁾ two fasteners, ²⁾ four fasteners

Table 1: summary of results for joints with dowel type fasteners (Dias 2005)

The cited author also performed experimental tests (Lopes et al. 2004) on composite beams with nails to evaluate the applicability of the design procedure proposed by Ceccotti (1995). In one series $\Phi 6 \times 100$ mm long nails were used, and in a second series a 20 mm thick intermediate layer of nailed timber boards running perpendicular to the beam direction was used as framework for the concrete cast. In this series $\Phi 6 \times 180$ mm long nails were used. The cited author concluded that the design procedure can be used to predict the deflection of timber-concrete structures, but with errors in the range of 20-30%. Moreover, the experimental deflections of timber-concrete slabs with nails were around twice as large as the expected deflection for full composite action.

3.3.5 Punched metal plate fasteners

The first investigations on punched metal plate fasteners (nail-plates) as timber-concrete connectors were reported by Girhammar (1984), who presented results from 50 push-out tests carried out on nail-plate connectors in order to determine their load-slip and failure characteristics. In all tests, the nail-plates were excessively deformed in shear. The maximum shear strength per nail-plate was about 8 kN, with corresponding slip of 10 mm. This type of connector has been used in timber-concrete wall elements developed in Sweden (Girhammar 1984). Studies on nail-plates were also performed by Van der Linden and Blass (1996), Van der Linden (1999) (Fig. 20) and Jorge (2005) (Fig. 21). The maximum bearing capacity of the nail-plate was reached at a displacement of about 6 mm with corresponding load of 48 kN, whereas failure occurred at about 10 mm slip. The maximum load per jack (in four-point bending tests) was 23 kN with corresponding mid-span deflection of about 80 mm (Van der Linden 1999).

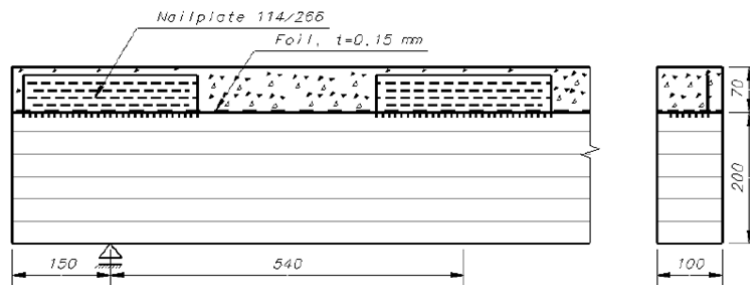


Figure 20: timber-concrete connection with punched metal plate fasteners (after Van der Linden 1999) (dimensions in mm)



Figure 21: nail-plate connector type (Jorge 2005)

Ronca et al. (1991) examined in detail the deformability of composite beams connected with double gang-nails welded together, in terms of both flexibility and slip along the wood-concrete interface, paying particular attention to the system's long-term and cyclic composite performance. The cited authors found that these connectors provided the composite beam with six times greater flexural stiffness than the wooden beam. Moreover, under long-term loading the final deflection was about four times that expected under non-slip theory and about 2.5 times the actual value under short-term load.

Starting in 1997 an investigation was carried out at VTT Building Technology in Finland on wood-concrete composite floors for multi-storey buildings (Toratti and Kevarinmäki 2001, www.sepa.fi). Two kinds of systems with nailplate trusses as shear-connectors were developed, one cast *in situ* (Fig. 22) and one prefabricated with the concrete cast in factory conditions upside-down, without any need for formwork (Fig. 23). Approved by the

Finnish Ministry of the Environment, and designated *SEPA-2000*, both of these wood-concrete composite floor systems are currently produced in Finland.

The maximum allowable span of the floor is determined by its vibration properties. Table 2 summarizes the maximum spans based on the calculations and experiments carried out by Toratti and Kevarinmäki (2001). Using these spans the composite floor structure performs satisfactorily in terms of strength, stiffness, vibrations and point loads. The floor may also be a continuous structure (with three or more supports), in which case the span signifies the largest allowed single span of the floor. However, floors longer than 12 m should be avoided due to handling problems.

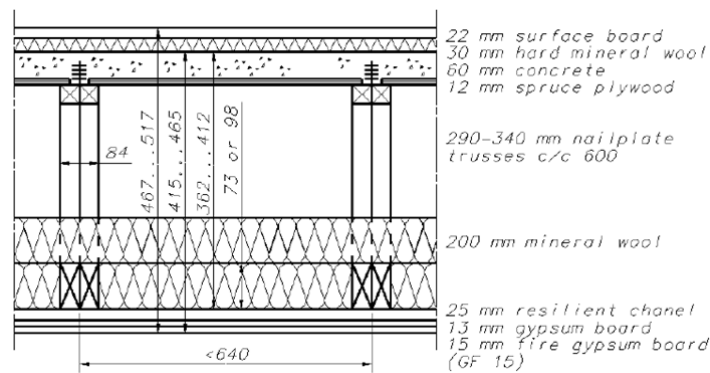


Figure 22: cross-section of the VTT cast-in-situ wood-concrete composite multi-storey house floor system

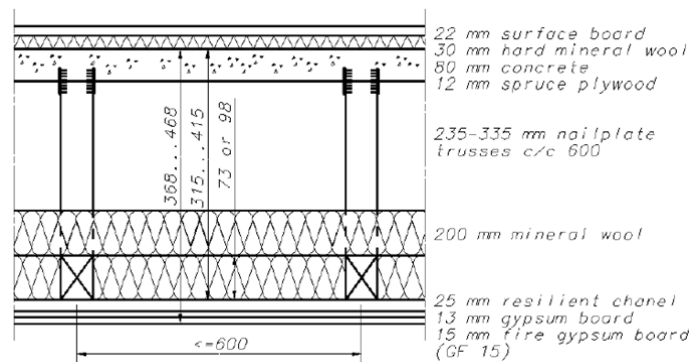


Figure 23: cross-section of the VTT wood-prefabricated concrete composite multi-storey house floor system

Height of truss		Height of composite floor		Full floor height		Max span	
[mm]		[mm]		[mm]		[mm]	
in situ	element	in situ	element	in situ	element	in situ	element
290	235	362	315	415	368	5730	5320
300	250	372	330	425	383	5880	5510
310	265	382	345	435	398	6030	5710
320	280	392	360	445	413	6180	5900
330	295	402	375	455	428	6330	6090
340	310	412	390	465	443	6480	6280
-	320	-	400	-	453	-	6410
-	335	-	415	-	468	-	6600

Table 2: maximum allowable span of the cast-in-situ and prefabricated (element) VTT wood-concrete floor systems, with 600 mm truss spacing (Toratti and Kevarinmäki 2001)

3.3.6 Notch-type connectors with and without dowel

An investigation reported in Yttrup (1996) explores the achievement of composite action by “embedding of the beam prepared with small scale vertical and horizontal dimples into the timber” (Fig. 24). The results suggest that full composite action is achievable without the use of any steel connectors. The small-scale “dimples” used as shear connectors (which are located in the concrete slab) can provide effective shear transfer.

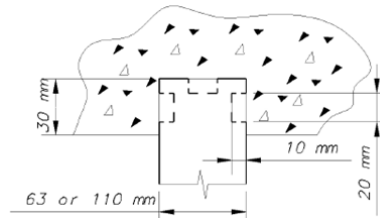


Figure 24: shear key-“dimples” (after Yttrup 1996)

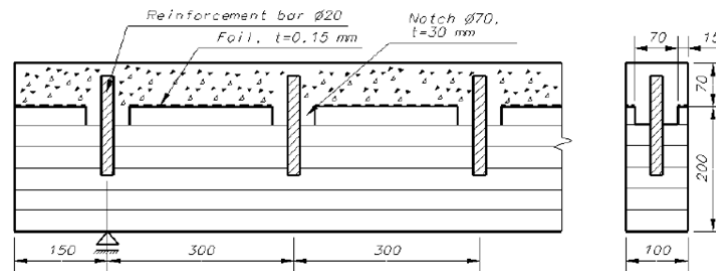


Figure 25: timber-concrete connection with grooved holes and dowels (after Van der Linden 1999) (dimensions in mm)

Grooved connections with dowels were among four different types of shear connectors studied by Van der Linden (1999) and Van der Linden and Blass (1996). In order to manufacture this type of joint, Φ 70 mm grooves were routed 30 mm deep into the timber surface. Within each of these indentations a hole with a diameter of 20 mm was drilled and a steel dowel was driven into the hole (Fig.25).

This type of connector exhibited plastic deformation capability. The maximum shear capacity of the reinforcement bar with concrete notch was reached at a displacement of about 5 mm, with corresponding load of about 52 kN, while failure occurred at about 15 mm slip. The maximum load per jack (in four-point bending tests) was 32 kN, with corresponding mid-span deflection of about 80 mm (Van der Linden 1999).

A similar connection type to that presented by Van der Linden (1999) was studied by Piazza and Ballerini (2000) (Fig. 26). However, the connection contained only concrete stocky dowels (Φ 65 mm x 55 mm high) spaced at 130 mm along the beam length. The stocky concrete dowels showed non-linear responses, probably due to progressive mechanical damage of the “concrete stocky dowels”, through cracking (Piazza and Ballerini 2000). Strength at failure was about 10 kN/m^2 , comparable to the average bending strength of beams (8.5 kN/m^2 , assuming an average bending strength of about 35 MPa) (Piazza and Ballerini 2000).

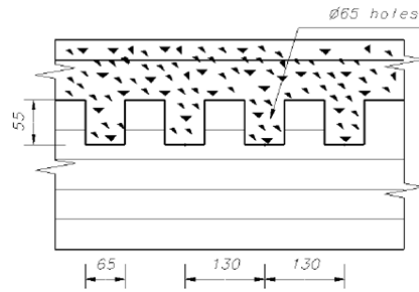


Figure 26: concrete stocky dowels (after Piazza and Ballerini 2000) (dimensions in mm)

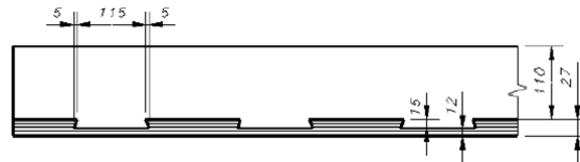


Figure 27: timber (LVL)-concrete connection with grooved indentations in the LVL (after Van der Linden) (dimensions in mm)

Grooved connections (Fig. 27) were also developed for use in composite plate structures in which instead of timber beams laminated veneer lumber (LVL) was used as sheet material in the tensile zone (Van der Linden 1999, Van der Linden and Blass 1996). The maximum shear capacity was reached within a slip of 2 mm and was held or could even increase up to 15 mm, where the test was ended. The average shear load was about 50 kN. The maximum load per jack (in four-point bending tests) was 19 kN, with corresponding mid-span deflection of about 80 mm (Van der Linden 1999).

Interest in wood-concrete composite structures increased in many European countries in the 1980's and 90's, when particular attention was paid to their potential use in multi-storey buildings as well as public structures. The most pertinent work was done by Natterer (1996, 1997), who proposed a floor system for new residential and public buildings, in which the timber component consisted of planks nailed vertically to each other, resulting in a planar surface. The two components are linked by a system of grooves in the wood and dowels that are post-tensioned after the concrete curing period.

The advantage of the post-tensioning is that the gap caused by the concrete's shrinkage is dramatically reduced. It was shown in experimental tests that the connection between the wood and concrete does not depend on the rigidity of the link, but only on the position and the dimensions and spacing of the grooves. The composite efficiency of the connection was found to be 85% to 90 (Natterer 1997).

Capozucca (1998) proposed a development of the system presented by Natterer (1996), but without any indentation in the wood. The redesigned system was based on a connection system involving use of prestressed steel axial connectors that impose a high contact force between the two materials. Using this technique, the initial bonding is increased considerably, without making grooves in the wood, and the connection system may be considered rigid (providing full composite action), thereby eliminating the numerous problems related to the analysis of flexibility of the connector. Use of prestressed axial connectors can increase both the resistance of the structure and its ductility. The maximum bending strength observed was around 120 kN (in four-point bending tests) with corresponding mid-span deflection of about 40 mm for 4000 mm long specimens with 60 x 600 mm concrete slabs and 180 x 250 mm timber beams. It is of fundamental importance to evaluate the stress losses that might occur in this kind of connector due to high humidity levels and/or changes in humidity and temperature. The normal forces applied were equal to 10 kN (specimen 1) and 15 kN (specimen 2) (Capozucca 1998). The loss of

tension after 3 months from the application of preload was about 6% and 10 % of the initial load, for specimens 1 and 2, respectively, with an immediate loss of 2.5%.

Gutkowski (1999) presented a comparable connection system to that developed by Natterer (1996, 1997), with a wooden deck and a concrete slab interconnected by a notched shear key/anchor connection detail (Fig. 28). Sixty slip test specimens were constructed and tested with three different notch configurations (Gutkowski et al. 2004). The highest slip modulus (28.2 kN/mm) was reached by the configuration with notches 152 mm wide and 38 mm deep, with corresponding failure load of 90 kN. The lowest slip modulus (20.3 kN/mm) was obtained for a configuration with notches 102 mm wide and 25 mm deep, with corresponding failure load of 79 kN. The composite efficiencies determined from the measured mid-span deflections of the tested beams were in the range of 57.4-77.0% for 3500 mm spans with four 32 x 128 mm notches. The distance from the edge of the beam to the first notch, and the spacing between notches, was 330 mm. The concrete and wood layer (nailed planks) were 64 mm and 89 mm thick, and 267 and 305 mm wide, respectively.

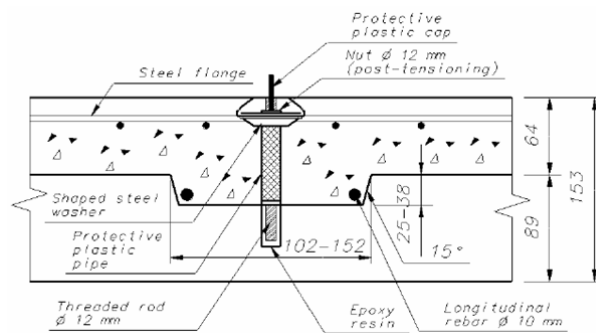


Figure 28: shear key/anchor connection detail (dimensions in mm) (after Gutkowski 1999)

Kuhlmann and co-authors (Kuhlmann and Shänzlin 2001, Kuhlmann and Michelfelder 2006) proposed a timber-concrete connection system consisting of grooves 20 mm deep and 200 mm long in the timber (Fig. 29). They also proposed that screws with a diameter of 12 mm and 250 mm spacing could be installed and tightened after hardening of the concrete, to handle the tensile force in the connection caused by the resulting eccentric bending moment, if necessary.

Several experimental short- and long-term tests, as well as numerical modeling of the system, were performed at the Institute of Structural Design at the University of Stuttgart, Germany, to determine the effects of varying the depth and length of the grooves and numbers of screws.

Interestingly, these tests showed (*inter alia*) that the presence of screws in the grooves had no significant effect on either the load carrying capacity or the stiffness of the connectors, Kuhlmann and Michelfelder (2004).

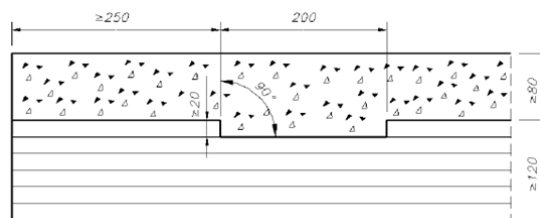


Figure 29: geometry of the grooves studied by Kuhlmann and Michelfelder (2006) (dimensions in mm)

A range of shear connectors, mostly of notch/plug connector types, was proposed and tested in shear-tests by Deam et al. (2008a) and Yeoh et al. (2008) to identify the most efficient and cost-effective shear connectors for an 8 m timber-concrete composite office floor with LVL beams (Figs. 30 & 31). Concrete plugs reinforced with a screw or steel pipe provided the best stiffness, strength and post-peak behavior. For 8 m long spans, 16 reinforced

rectangular concrete plugs, equally spaced along the length of the beam were chosen. Full-scale 6 m long specimens with rectangular notches reinforced with lag screws were subjected to quasi-static and dynamic tests to obtain indications of the structural performance of the LVL-concrete composite systems and their susceptibility to vibration (Deam et al. 2008b). The obtained efficiency for 50 kN load was 93%, and for 150 kN it was 71%, while the failure load was 158 kN (Deam et al. 2008b). The composite system had 295% greater stiffness and 74% greater strength than the bare LVL beam.

Rectangular notches reinforced with lag screw connectors have also been used in a new system for multi-storey pre-stressed timber buildings with timber-concrete composite floors developed in New Zealand (Buchanan 2008). The system, which can be used in multi-storey timber buildings with more than 10 storeys, includes glulam or veneer lumber (LVL) members as part of T-beam floors with concrete topping and post-tensioned connections for ease of building and high-seismic resistance. It consists of 2400 mm wide “M” section panels, built with a single 400 x 63 mm LVL joist on each outer edge and a double LVL joist in the centre (Fig. 32). A plywood interlayer is nailed on top of the LVL joists to provide a permanent formwork for the concrete. A steel mesh is laid above the panels to provide shrinkage control for a 65 mm thick cast-in-situ concrete slab. Notches are cut from the LVL joist before the plywood interlayer is nailed. The span, of between 8 and 10 m, requires six to eight connectors along the length of each joist to provide adequate composite action. The prefabricated 2400 mm panels are placed side by side and connected using either screws or nails, with the concrete slab poured thereafter (Yeoh et al. 2008).





1&2		Type: round plug Plug: \varnothing 48.5 mm, 20 mm depth F_{max} =13.2 kN, $k_{0.4}$ =83.1 kN/mm
3&4		Type: round plug with screw Plug: \varnothing 48.5 mm, 20 mm depth Screw: \varnothing 12 mm, 9 mm predrilled, 150 mm length, 100 mm embedment length F_{max} =31.4 kN, $k_{0.4}$ =105.9 kN/mm
5&6		Type: reinforcement plug Plug: \varnothing 48.5 mm, 20 mm depth Pipe: 40 mm length F_{max} =32.6 kN, $k_{0.4}$ =66.6 kN/mm
7&8		Type: rectangular plug with screw Plug: 50 mm length, 16.5 mm depth Screw: \varnothing 12 mm, 9 mm predrilled, 150 mm length, 103 mm embedment length F_{max} =54.9 kN, $k_{0.4}$ =297.0 kN/mm

Figure 30: characteristics of plug connectors tested by Deam et al. (2008)








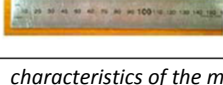
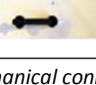
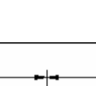
9			Pryda steel brace anchor with rods placed parallel to the beam axis $F_{max}=15.3$ kN, $k_{0.4}=156.9$ kN/mm
10			Pryda steel brace anchor placed parallel to the beam axis $F_{max}=16.6$ kN, $k_{0.4}=170.3$ kN/mm
11			Pryda steel brace anchor placed at a 45° angle to the beam axis $F_{max}=19.3$ kN, $k_{0.4}=77.2$ kN/mm
12	 4 × 65.5 × 45 mm		Pryda steel brace anchor placed perpendicular to the beam axis $F_{max}=16.3$ kN, $k_{0.4}=271.7$ kN/mm
13			Coach screw: Ø 12 mm, 9 mm predrilled, 165 mm length, 115 mm embedment length $F_{max}=21.5$ kN, $k_{0.4}=195.5$ kN/mm
14			Coach screw: Ø 16 mm, 12.5 mm predrilled, 155 mm length, 105 mm embedment length $F_{max}=34.2$ kN, $k_{0.4}=88.3$ kN/mm
15			Pryda framing bracket FB47/76' $F_{max}=16.8$ kN, $k_{0.4}=27.8$ kN/mm
16		 6 × 63 × 40mm	Inverted Pryda framing bracket FB47/76' $F_{max}=15.8$ kN, $k_{0.4}=37.8$ kN/mm
17			Two SFS screws Ø 7.5 × 100 mm inclined at 45° angle $F_{max}=18.5$ kN, $k_{0.4}=14.4$ kN/mm

Figure 31: characteristics of the mechanical connectors tested by Deam et al. (2008)

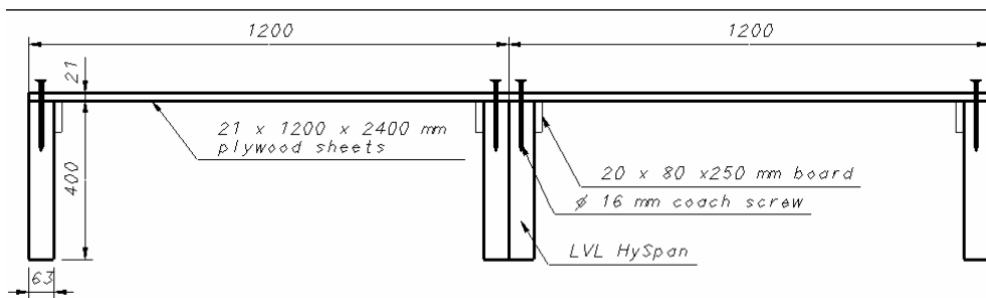


Figure 32 : semi-prefabricated "M" section panel (dimensions in mm) (after Buchanan et al. 2008)

Dias also performed several series of experimental shear-tests on notched joints to evaluate their short- and long-term mechanical performance (Dias 2005, Dias et al. 2007). The notch joints consisted of timber or wood-based timber notches, which were glued to the timber beams (Fig. 33). In the "ON" test series Holm oak notches of 100 x 100 x 15 mm³ were used, in the "dvwN" series densified veneer notches of 100 x 100 x 15 mm³ were used and in the "dvwN1" series densified veneer notches of 100 x 100 x 35 mm³ were used with a 20 mm thick interlayer. Spruce was used for the beams, with normal strength concrete. The maximum shear load and stiffness obtained for all tested notch type connector (with two notches in the connection) in the shear tests are presented in Table 3.

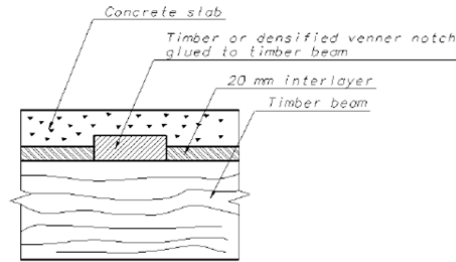


Figure 33: notched joint, Dias (2005)

Test series	Connector	Timber	Concrete	Strength, F_{max} [kN]	Stiffness, K_f [kN/mm]
ON ¹⁾	Oak notch	Spruce	MSC*	59.5	161.2
dvwN ¹⁾	dvw-notch	Spruce	MSC	138.6	317.3
dvwN1 ¹⁾	dvw-notch**	Spruce	MSC	116.2	224.0

*medium strength concrete, **with an additional 20 mm thick interlayer, ¹⁾ two fasteners,

Table 3: summary of results for joints with dowel type fasteners (Dias 2005)

3.3.7 Mechanical continuous shear connectors

A mechanical continuous shear connector – made with a 2 mm thick shaped and drilled steel sheet, fixed to the timber beams with Φ 6 mm screws every 20 mm – has been studied by Piazza and Ballerini (2002) (Fig. 34).

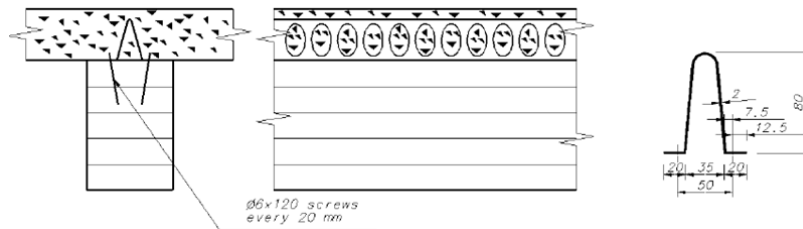


Figure 34: bent and perforated steel sheet fixed to the timber with screws (after Piazza and Ballerini 2000) (dimensions in mm)

The behavior of full-scale specimens is characterized by a quite linear response up to about 50% of the failure load, followed by a post-elastic hardening branch due mainly to the nonlinear-behavior of the connections. The specimens showed strength at failure of about 22 kN/m² with corresponding mid-span deflection of about 72 mm (representing a ca. 200% improvement in strength in comparison to timber beams alone). The composite action displayed by this connector type is in the range of 90% for low load levels (<7 kN/m²) and 30% for failure load (Piazza and Ballerini 2002).

Another system, called slim-floor-profile, Fig. 35, intended for use in tall buildings, has been proposed by Kuhlmann and Schänzlin (2004, 2008).

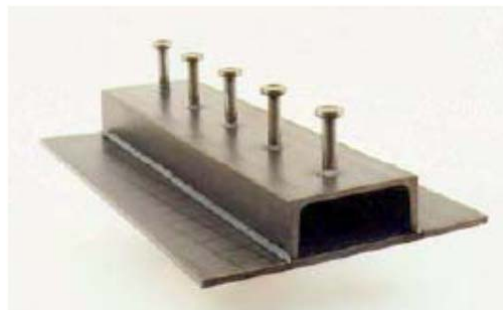


Figure 35: slim-floor-profile (after Kuhlmann and Schänzlin 2008)

An integrated slim-floor profile, designated UPE270, is produced by welding a common U-profile on a flat bar steel and adding headed studs on top of the U-profile to provide the composite action between steel and concrete. Such a system is placed on supports while board stacks are laid on the lower flange of the profile without any secondary support and the concrete is cast over the entire structure. The assembly of this system does not differ from the manufacture of a common concrete slab with prefabricated *Filigree* elements. However, the system has several main advantages that should be mentioned, including reductions of the required number of props (due to the higher bending strength of the board stacks in comparison to prefabricated *Filigree* concrete slabs) and the assembly time (since the amount of cast-in-situ concrete can be reduced by about two thirds due to the greater thickness of the board stacks compared to those of prefabricated *Filigree* slabs).

3.4 Different materials – from lightweight to high performance steel fiber reinforced concrete

Most research on wood-concrete composite structures has been performed on systems consisting of normal concrete and timber/glued laminated beams or wooden decks connected by various types of shear connectors. However, a few researchers have explored the potential utility of other types of concrete or wood-based materials, including the following.

Heiduschke (2003) proposed a composite system in which high performance steel fiber reinforced concrete (HPFRC) and vertically laminated wood were combined to create a composite floor or bridge deck. The composite action of the wood and concrete was facilitated by pouring high shear-strength concrete into 50 or 100 mm circular openings in the wooden deck. The shear strength of the 50 and 100 mm variants, obtained from push-out tests, were around 30 kN and 78 kN, respectively (with corresponding slips of about 1.5 mm in both cases). Preliminary experiments and analyses showed the feasibility of combining vertically laminated wood with HPFRC. However, no significant strength improvement was achieved in comparison to a solid wood section of the same thickness.

Yttrup (1996) used pine LVL beams as an alternative for low cost bridges and floor systems, and an innovative solution for medium- to long-span floors with LVL beams has been recently developed in New Zealand (Figs. 30-32) (Deam 2008). The improved strength, dimensional stability and uniformity that LVL provides in comparison to sawn timber makes it a highly desirable option for floors. However, the improved strength of LVL is not matched by a similar improvement in stiffness, and adding a concrete layer on top of the LVL is expected to be the best method for providing additional stiffness. Regarding the concrete slab reinforcement it is necessary in most cases to restrain shrinkage of the concrete and to ensure that there is sufficient resistance against splitting forces around the shear connectors (Holschemacher et al. 2003). The cited authors mention that in many cases the concrete slab is thicker than necessary to meet the required bearing capacity, and hence the dead load is unnecessarily high.

In some cases steel fiber reinforced concrete (SFRC) has been used in timber-concrete composite systems, initially in the rehabilitation of a timber ceiling in a building in Altengurg/Thuringia (Köhler 2002). Its use followed tests by Holschemacher et al. (2002 & 2003) showing that the normal reinforced concrete usually used in timber-concrete composite systems can generally be replaced by SFRC, and hence the thickness of the concrete slab can be reduced. The experimental program included push-out tests in which Φ 16 x 160 mm long wood screws were tested with a plywood interlayer, in two configurations. In one configuration a hole around the screw was made to create a concrete key while in the other configuration no hole was made in the plywood sheet (Fig. 36).

Based on the push-out tests results the solution with a concrete key was chosen to rehabilitate the timber beam ceiling. The cited authors showed that application of SFRC is more economical than using mesh reinforced concrete and they recommended reducing the concrete slab thickness, depending on the steel fiber geometry, to 35 mm. The ultimate load reached by specimens with SFRC and concrete keys was 19.3 kN (k_s and $k_{0.6}$ stiffness parameters: $K_S = 40.6$ kN/mm and $K_{0.6} = 20.8$ kN/mm). The ultimate load reached by specimens with SFRC lacking concrete keys was 11.0 kN (K_S and $K_{0.6}$ stiffness parameters: 9.1 and 7.6 kN/mm, respectively). Finally, the ultimate

load reached by specimens with plain concrete and concrete keys was 15.2 kN (k_s and $k_{0,6}$ stiffness parameters: 14.6 and 12.5 kN/mm, respectively).

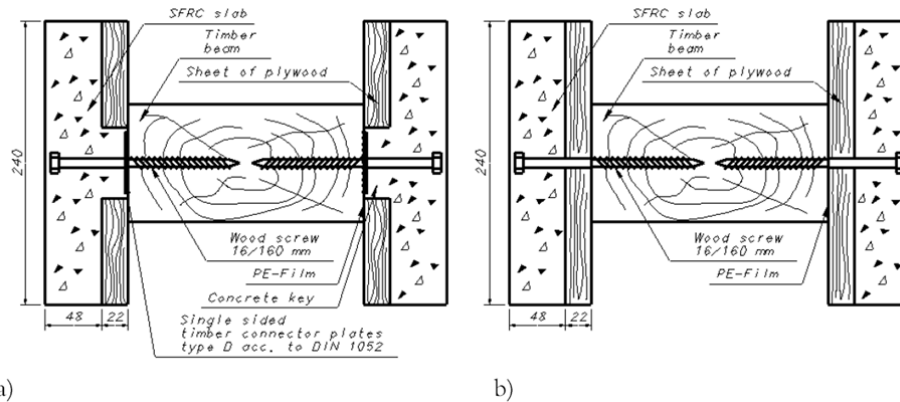


Figure 36: SFRC-timber composite specimen with concrete key (a) and without concrete key (b) (dimensions in mm)

Lightweight concrete (LC) was used in composite floors with five different shear connectors presented by Steinberg (2003). The main observation from the experimental tests was that the dead load of a timber-concrete composite floor can be reduced by 15% by using an LC with a density of 1.6 kN/m^2 instead of a normal weight concrete of 2.3 kN/m^2 . The application of LC provides an attractive alternative in timber-concrete composite structures due to the reduction of the dead load on the timber floors. A lightweight concrete could be a good alternative in renovation situations in which the supporting walls or foundations do not have sufficient strength to support a high extra load (Dias 2005). Fragiaco et al. (2000) also used light-weight concrete while testing *Tecnaria* shear connectors (Fig. 37). The use of lightweight concrete slabs instead of normal weight concrete slabs affected the outcomes of neither collapse push-out tests nor long-term tests (Fragiaco et al. 2006).

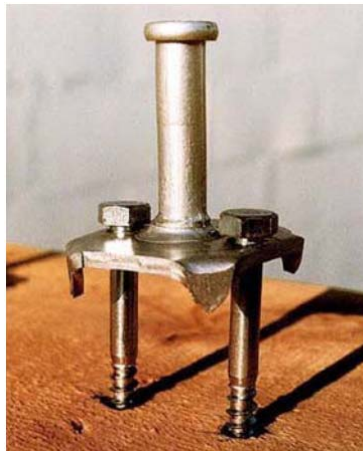


Figure 37: "Tecnaria" connector, Fragiaco et al. (2006)

The use of adhesive in combination with fiber-reinforced ultra-high-performance-concrete (UHPC) was studied by Schäfers (2008). Components of UHPC can be very slim, compared to components of standard concrete, and due to its high surface-tensile-strength gluing is a very efficient way to connect UHPC members with other materials. Cured concrete prisms, 20 mm thick, were cut from a plate and glued on the timber members. This seems to be a very attractive option, but further research is needed, especially regarding the long-term performance of the adhesive joint.

4 SLAB TO SLAB SHEAR CONNECTION

This chapter presents a literature review of existing shear connectors used to connect across two precast elements as slabs, girders or beam. Various applications and examples are also presented. Furthermore, there are some possible ideas interesting for our system's slab to slab transversal connection.

4.1 State of the art

The main purpose of this chapter is to present a general view of the systems used for the lateral connection of two other direction load-bearing systems, such as slabs, girders or beams. Most examples shown come from precast concrete background, so that they could be applicable to our composite structure to join the precast concrete slabs placed side by side, and many following applications originate from prestressed concrete double tee bridges.

4.1.1 Why is cross connection so significant?

The prestressed concrete double tee bridge may be the structure of choice for short- to medium-range spans where speed of construction is a trouble. Primarily used on off-system roads, this mode of construction is receiving more attention because of increasing labor costs associated with the pan form bridge that has been in use for well over 50 years in these circumstances.

An important issue in double tee construction is the type of connection used to join the edges of adjacent tee flanges. When only an asphalt wearing surface is applied to the completed structure, these connections are the only means by which a tee supporting wheel loads is able to share loading with neighboring tees and hence gain the structural efficiency necessary to make this type of construction viable.

4.1.2 Shear connections exploited so far

First application carried (Fig. 38) displays the detail currently used by the Texas Department of Transportation (TxDOT). It is made from a combination of steel plates embedded in the edge of the tee flange during fabrication and a pair of steel angles that are field welded to these embedded plates to complete the connection. The assembly is typically spaced longitudinally at 5-ft (1.50 m) intervals along the length of the structure (usually bridge).

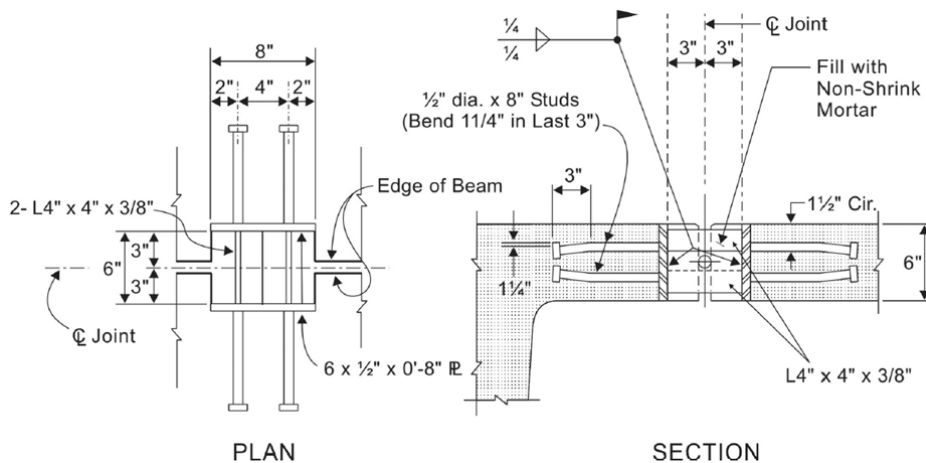


Figure 38: TxDOT lateral connection

A prototype detail, shown in Fig. 39-40, was believed by the same research team to be a less expensive alternative to the current connection because the weld between the steel bar and embedded plates could be accomplished much more easily and consequently more quickly.

The new detail calls for a continuous grout shear key between the adjacent flange edges along the entire length of the bridge. This represents a substantial departure from the current detail that joins the edges only at 5-ft intervals. Although this clearly is an additional expense relative to the current design, the use of a Simple “backer rod” dropped into the crevice created by the (newly designed) sloping flange edges was thought to be a very efficient means for forming the key. The shear key was added primarily to combat deflective longitudinal cracks in the asphalt wearing surface over the area between adjacent tee flanges that had been documented in many of TxDOT’s existing double tee bridges.

The research team developed a series of tests to document the structural performance of the newly proposed connection detail shown in Fig. 39 and 40. Test specimens simulating a 1-ft-wide transverse strip of flange slab and embedded connection were first tested. These tests proved to be enlightening in that in every case the connection failed as a result of inadequate anchorage. Consequently, the 1/2 in. x 8 in. studs that were a carry-over from the old detail in Fig. 39 were replaced with 4 reinforcing bar of sufficient length to fully develop the anchorage. As a final proof-of-concept test, a full-scale section of a bridge was built in TTI’s structural test facility and subjected to a series of simulated wheel loads.

The structure consisted of a pair of 30-ft-long double tees connected laterally at 5-ft intervals with the new welded bar detail and shear key construction. Load cells measured reaction forces, and gages mounted on the shear key measured strains in the bridge.

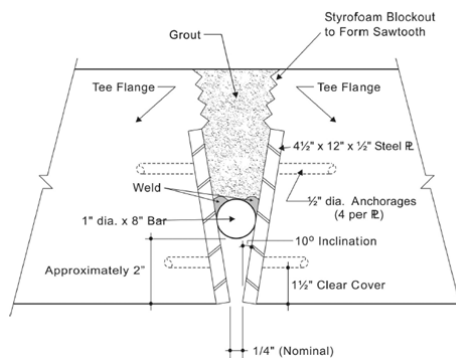


Figure 39: section through bar/plate

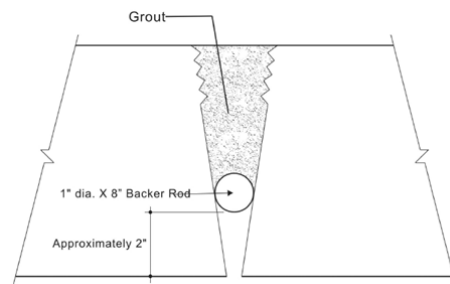


Figure 40: section at other locations

The principal conclusions resulting from this work were that the shear key was indeed a very important component of the connection, and that the welded bar at 5-ft spacing served primarily to keep the flange edges

from separating under load, enabling the shear key to perform most of the lateral load transfer between tees, and the proposed connection in Fig. 39-40 is capable of resisting the largest of those predicted forces.

Fig. 41 shows the details of the double tee to double tee connection developed by Concrete Technology Corporation (“Technical data for detailing double tees”). Each one double tee presents along its edge, at intervals as required by design, an embedded flange, on which is welded a steel lug in order to transfer horizontal forces between the two girders.

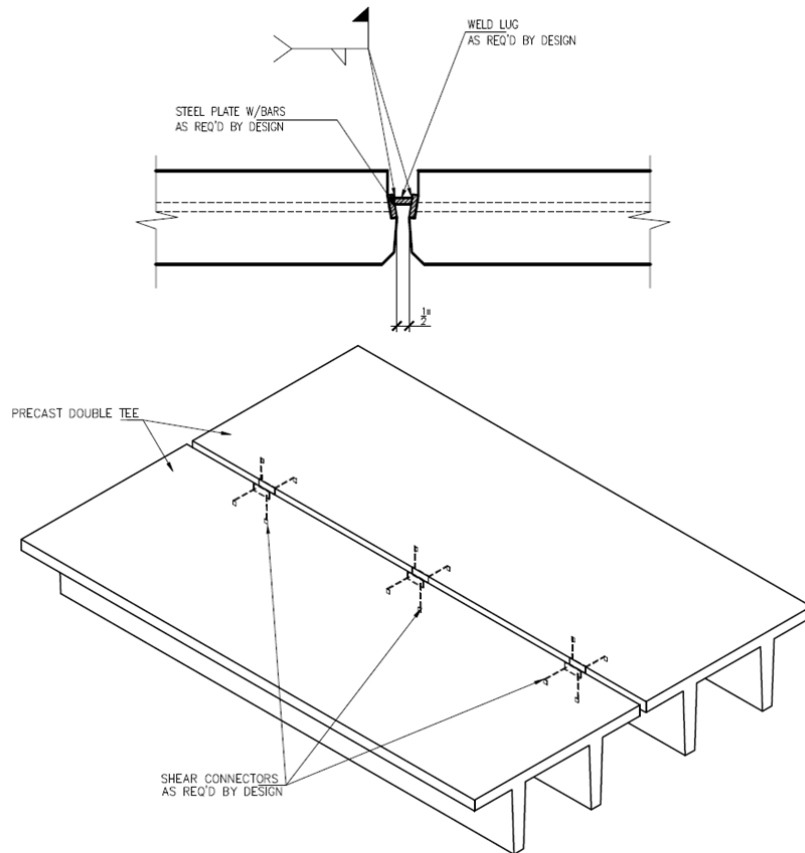


Figure 41: double tee to double tee connection performed by CTC (1980)

The same research group also performed other double tee to double tee connections, as shown in following Fig. 42 and 43. First one connection (Fig. 42) is made with steel T hangers, located at intervals as required by design, allowing simple support between tees. The system needs also a cast-in-place concrete topping to ensure adequate stiffness in plane, in order to transfer seismic and wind load. Furthermore, topping provides to minimize drop between the edge of the tees.

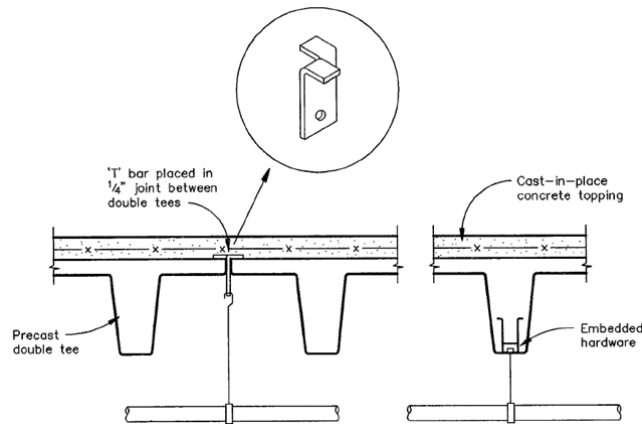


Figure 42: double tee to double tee connection performed by CTC (1980)

According to CTC, hangers can also be installed by field drilling into flange before or after topping is placed, but field drilling into double tee web is not recommended due to the potential damage to prestressing.

Second one (Fig.43 – section A) is realized welding a steel angular profile, at intervals as required by design, to steel plates embedded horizontally in the precast concrete and welded each one to two bars integrated in double tee.

Third one (Fig.43 – section B) is realized welding a steel rod, at intervals as required by design, to steel plates embedded about vertically (with an inclination between 5° and 10°) in the precast concrete and welded each one to two bars integrated in double tee.

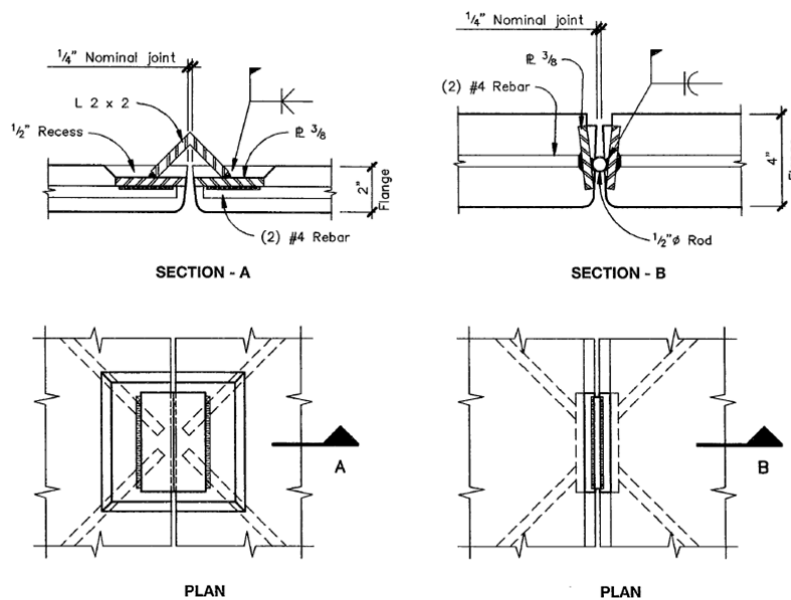


Figure 43: double tee to double tee flange connection performed by CTC (1980)

According to Concrete Technology Corporation these three connection systems provide diaphragm shear transfer. Many researches about the behavior of double tee flange connectors subjected to in-plane loads have been led by Pincheira . His work comprehended experimental investigations in seven mechanical connectors used in 2 and 4 in. (51 and 102 mm) thick double tee flange. The study included five connectors commonly used in practice and two new or modified design. Only most significant connectors tested are described in this section.

Main idea of the author is that, though some existing building model codes require topping slabs to form reliable diaphragm action in high seismic regions, mechanical connectors generally require less labor and are cheaper and

faster to install. Therefore they would be preferable to topping slabs in seismic regions if they could provide similar or better strength and ductility.

The connectors studied by Pincheira are similar to that shown in Fig. 41 and performed by CTC: they consist of two reinforcing bars welded to a steel plate embedded in 2 in. (51 mm) thick flanges. Following advice from a project advisory of Precast Concrete Institute (PCI), four types of flange-to-flange connectors were initially selected for testing as part of a National Science Foundation and PRESSS research program.

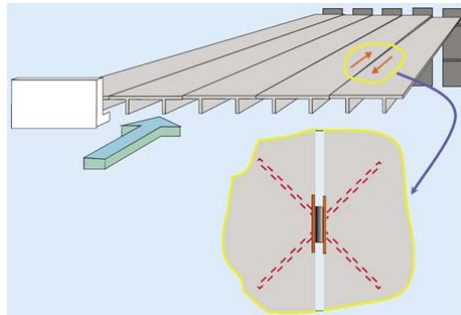


Fig. 44: precast, prestressed double-tee floor system with mechanical connectors

Two of the four types were commonly used in 2 in. (51 mm) double tee flanges: the “hairpin” and the “plate with stud-welded deformed bar anchor” connectors. The third connector type was sometimes used in 4 in. (102 mm) flanges and consisted of a structural tee with two welded reinforcing bars. The fourth connector type consisted of a bent strap of steel (known commercially as Vector) and could be used either in 2 or 4 in. (51 or 102 mm) thick flanges. Three additional connectors were tested in an extension of the initial test program. Two of these connectors, a Vector and a bent plate, were intended for use in 4 in. (102 mm) thick pretopped flanges. The other connectors, an angle attached to the flange mesh reinforcement [mesh and angle (M&A)], had two separate configurations for use in 2 and 4 in. (51 and 102 mm) thick flanges. A more detailed description of the connectors follows.

In each connection, a separate steel bar, or “slug,” is placed between the connectors embedded in the two concrete flanges. The slug is then welded to the connectors for adjoining double tees to complete the connection. One characteristic of all the connectors is important to note. In the experimental tests, one round steel bars were used as the slugs that were dropped between the flange connectors and welded into place to create the connection. In some cases, failures were found to occur in the welds between the round bars and the connector plates. Examination of the welds showed that a consistent thickness groove weld was not being achieved. This was attributed to the difficulty the welders had in accessing the weld location. All of the connectors in the tests described here were intentionally designed to have vertical face plates at the flange edges. Rectangular weld slugs were used to allow fillet welding rather than groove welding. Now we give a brief description of all these kind of connectors.

Two Inch (51 mm) Flange Connectors

Hairpin—Main dimensions and details of this connector are shown in Fig. 45. A 32 in. (813 mm) long ASTM A706 No. 3 reinforcing bar was bent in the form of a “hairpin” with two, 12 in. (305 mm) long legs. The center portion of the bar was then welded to an ASTM A36 steel plate with a 4 in. (102 mm) long, 1/4 in. (6.4 mm) thick flare-bevel weld above and below the bar. The weld was terminated about 1 in. (25.4 mm) from the start of the bar bend, more than the two-bar diameter recommendation to avoid potential crystallization. One connector was fabricated using AISI 304 stainless steel for the plate. All connectors were embedded in the concrete with the intention of having the anchor bar at mid-depth. A minimum cover of 3/4 in. (19 mm) from the top surface of the concrete to the bar was always maintained.

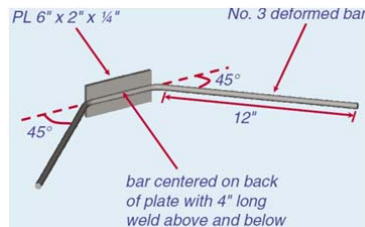


Fig. 45: details and dimensions of the hairpin connector (2 in. flanges)

Stud-Welded DBA—Two, 12 in. (305 mm) long, No. 3 deformed bar anchors (DBA) were stud-welded perpendicular to a plate (see Fig. 46). The DBAs were made of ASTM A496 steel, while the plate was fabricated of ASTM A36 steel. The DBAs were also placed at mid-depth of the flange.

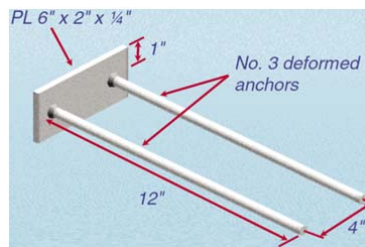


Fig. 46: details and dimensions of the stud-welded anchor and plate connectors (2 in. flanges)

Bent Wing—Main dimensions and details of this connector are shown in Fig. 47. The bent wing connector was designed at the University of Wisconsin and made by cutting and bending a 3/16 in. (4.8 mm) thick steel strap. A 30 in. (762 mm) long, 0.264 in. (6.7 mm) diameter, W5.5 steel wire was fed through a slot (one in each wing) 1 in. (25.4 mm) from the end of the “wings.” This detail was needed to properly anchor the wings and was based on a previous study which showed that the best anchorage could be obtained with a mechanical bar interlock. All connectors were placed in the forms with the top of the face plate at the top of the flange and 3/4 in. (19 mm) cover over the anchor leg.

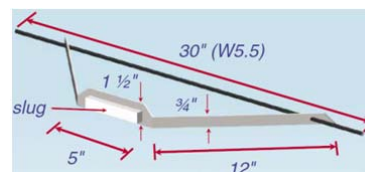


Fig. 47: details and dimensions of the 3/16 in. thick bent wing connector (2 and 4 in. flanges)

M&A—This was an unusual connector in that it did not rely on separate anchor bars to transfer forces into the concrete flanges. The connector was commercially produced as part of the reinforcing mesh normally placed in flanges. It consisted of a steel angle at the flange edge as shown in Fig. 48. The mesh was welded to the bottom of the angle during mesh production. The angle was 3/4 × 3/4 × 1/8 in. thick (19 × 19 × 3 mm) made of ASTM A36 steel and extended the full length of the double tee flange. The joint slug was welded directly to the angle.

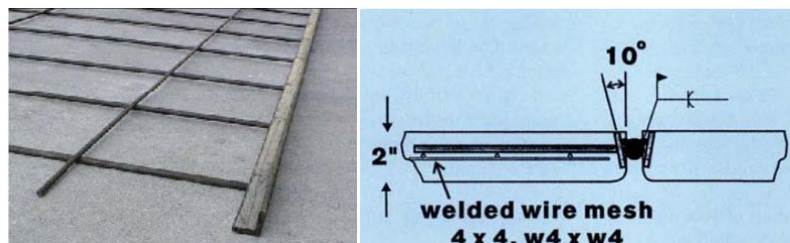


Fig. 48: overall view of mesh and angle (M&A) connector (2 and 4 in. flanges)

Four Inch (102 mm) Flange Connectors

Structural Tee—This connector consisted of two, 16 in. (406 mm) long, No. 4 reinforcing bars welded at a 45° angle to an ASTM A36 structural steel tee section (see Fig. 49). The bars were made of ASTM A706 steel and were welded with 4 in. (102 mm) long, 3/16 in. (4.8 mm) thick, flare-bevel welds on both sides of the bar to the bottom of the stem of the structural tee connector. A 15/8 in. (41 mm) cover was used between the face of the bar and the top concrete surface with the flange of the structural tee connector at the top surface.

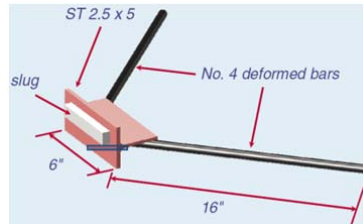


Fig. 49: details and dimensions of the structural tee connector

Bent Wing—The dimensions and details of this connector are similar to those used in the 2 in. (51 mm) flanges described earlier (see Fig. 47). The plate material was also ASTM A36 steel, except that one specimen was made of AISI 304 stainless steel. The concrete cover was 1 in. (25.4 mm) from the top of the concrete surface to the wing anchor bar with the face plate 1/4 in. (6.4 mm) below the flange surface.

Bent Plate—The bent plate was a simple connector fabricated by punching a rectangular hole into and then bending a 1/4 in. (6.4 mm) thick steel plate (see Fig. 50). The hole provided concrete anchorage and the bend left a 5 in. (127 mm) long exposed steel face plate at the edge of the double tee for subsequent welding with a slug. The face plate was set 1/2 in. (12.7 mm) below the flange surface.



Fig. 50: overall view of bent plate connector

Vector—A bent strap, shown in Fig. 50, is a commercially marketed connector referred to as the Vector connector and is similar in concept to the bent wing. While the Vector connector also had a provision for threading a rod through the anchor end, it was tested without the rod present to see if sufficient anchorage existed. Both carbon steel and stainless steel styles of the connector were tested. The face plate of the Vector connectors was set 1/4 in. (6.4 mm) below the flange surface.



Fig. 51: overall view of Vector connector (4 in. flanges)

M&A—A second version of the M&A connector for 4 in. (102 mm) flanges, similar to that used in the 2 in. (51 mm) flange thickness (see Fig. 51), was commercially produced and tested. A larger angle, 11/4 × 11/4 × 1/8 in. thick

(32 × 32 × 3.2 mm), was used in this version and was provided in both plain and galvanized (A36) steel. The mesh was placed at mid-depth of the flange leaving the top of the angle 5/8 in. (15.9 mm) below the flange surface.

The test specimens consisted of a mechanical connector embedded in either a 2 or 4 in. (51 or 102 mm) thick concrete panel, which represented the flange of a double tee girder. The panels were 4 × 4 ft (1.22 × 1.22 m) and were reinforced with 6 × 6 – W2.1 × W2.1 welded wire reinforcement, except for those cast with the M&A connector. The mesh used in the M&A panels was 6 × 12 – W4 × W2.5 in the 2 in. (51 mm) panels, with the W4 wire perpendicular to the flange edge, and 6 × 12 – W6 × W2.5 in the 4 in. (102 mm) panels, with the W6 wire perpendicular to the flange edge. The connectors were subjected to several loading conditions to emulate some of the actions expected in a double-tee floor system. These actions consisted of separate or combined in plane (horizontal) shear and out of plane (vertical) shear. In-plane shear was applied to simulate the forces in the connectors caused by lateral loads (wind or earthquake).

Out-of-plane shear was intended to simulate the forces caused by removal of differential camber in the double tees or by the wheel loads traversing a joint in the floors of parking structures.

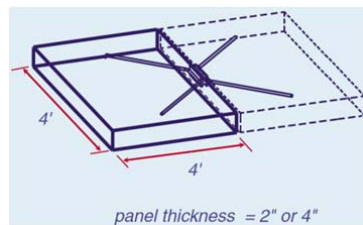


Fig. 52: test specimen dimensions

Based on the results of this investigation, of the connectors tested in 2 in. (51mm) thick flange panels the hairpin had the largest in-plane shear stiffness and strength. This connector displayed also a moderate displacement ductility. The stud-welded DBA connector showed large variability and reached low levels of in-plane shear loads. Its strength depended strongly on the quality of the stud weld between the DBA and the steel plate. This connector had an in-plane shear deformability similar to that of the hairpin but, again, it was strongly dependent on the quality of the weld. The bent wing connector displayed excellent response characteristics under in-plane shear with a strength and stiffness lower than those of the hairpin, but with a larger ductility. Unlike the severe concrete damage observed for the hairpin and the stud-welded DBA connectors, very little concrete cracking or damage was observed for the bent wing connector at ultimate shear load during any of the tests.

Among the connectors tested in 4 in. (102 mm) thick flange panels, the structural tee had both high in-plane shear stiffness and strength. The connector, however, lacked ductility. Damage to the double-tee flange at ultimate in-plane shear load was severe and included large diagonal cracks as well as spalling of the concrete directly above the stem of the structural tee.

The M&A connector had a peak in-plane shear strength and stiffness very close to those of the structural tee. The response of the bent wing connector in a 4 in. (102 mm) thick flange panel was nearly identical to that observed in the 2 in. (51 mm) panels in terms of in-plane shear stiffness and strength, but with even larger displacements due to the ductility. Finally, the Vector connector performed in a manner that was very similar to the bent wing.

In “Guide for concrete floor and slab construction” (ACI Committee 302) it says that to compensate concrete shrinkage post-tensioned slab joints are associated with a jacking gap. The slab edges are strengthened with steel plate embedded in the concrete by metal fasteners (bolt or rod). The filling of jacking gaps should be made with backer rod and elastomeric sealant. Steel plate can be simple (Fig. 52) or performed with an angular profile (Fig. 53).

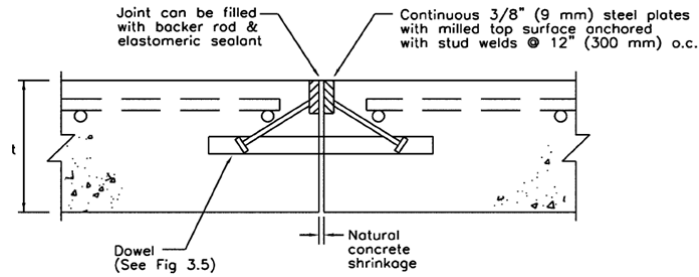


Fig. 52: joint detail according to ACI committee 302 (edge strengthening made by simple steel plate)

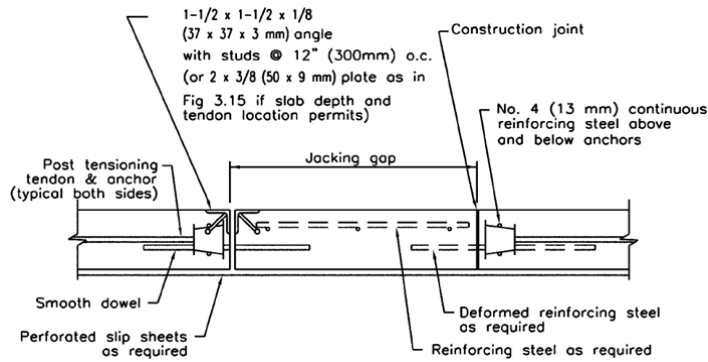


Fig. 53: joint detail according to ACI committee 302 (edge strengthening made by steel angular)

According to Riva (2003), to connect transversally two or more precast units (Fig. 54), we should overlap straight steel bars and integrate with a topping cast-in-situ concrete. This manner guarantees high in plane stiffness and provides diaphragm shear transfer if the thickness of the cast-in-place topping is 40 mm or more (this is also contained at point 7.2.6 of Statement [1]).

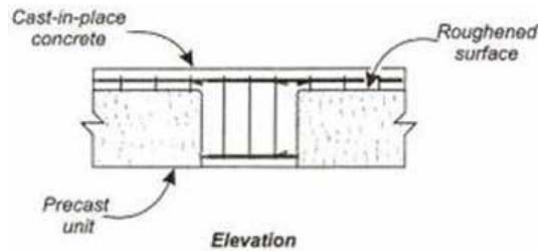


Fig. 54: transversal connection with overlapped bars and cast-in-place concrete topping (Riva)

Mid-Atlantic Precast Association describes two possible types of double tee to double tee connection (Fig. 55 and 56). First one (Fig. 55) is very simple and realized cutting the edge of the girders from bottom to top first vertically (up almost to half height) and then with an angle of 5° - 10° (up to the top), so as it's possible to place some sealant to perform the sideward connection.

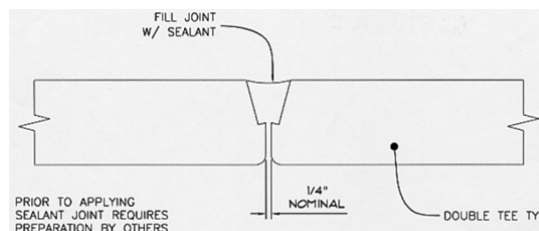


Fig. 55: cut almost vertical (5° - 10°) of the slab edge and filling with sealant

Second one (Fig. 56) is very similar to those realized by Pincheira except for the presence of a sealant cast over the steel bar. It consists of a steel plate embedded almost vertically (inclination of 5° - 10°) in precast concrete along each one slab edge. In each connection, a separate steel bar, or “slug”, is placed between the connectors embedded in the two concrete flange and then welded to the connectors for adjoining the two precast unit to complete the whole system.

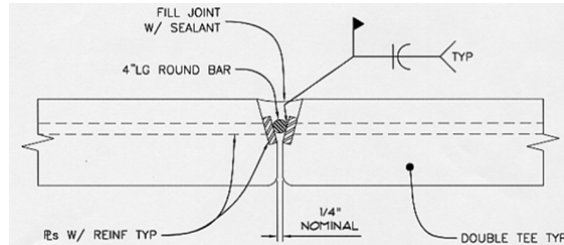


Fig. 56: slug placed between steel plates embedded in the slab edge and final filling with sealant

Over to Issa, a rapid and effective manner to build bridges is achievable by using precast concrete panels, and to provide load transfer between adjacent precast slabs the transverse joint can be grouted using a variety of materials such as grout, epoxy mortar or polymer concrete (Fig. 57). While precast concrete panels perform well under large and highly repetitive loadings, grouted joints behavior can be problematic. Researches lead by the same author (1995) about transverse deck joints evaluated the performance of four different grout materials in precast concrete deck systems: these are Set Grout, Set 45 for normal temperatures, Set 45 for hot weather and polymer concrete.

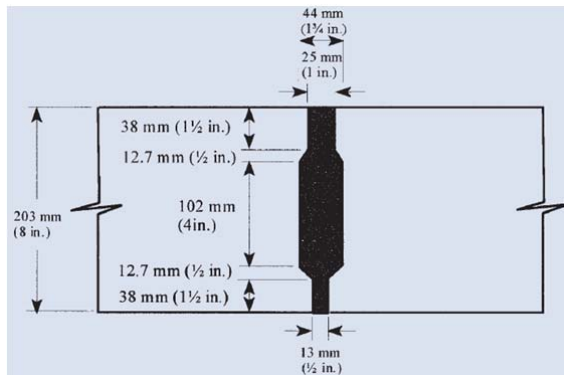


Fig. 57: configuration of panel to panel joint linked with grout

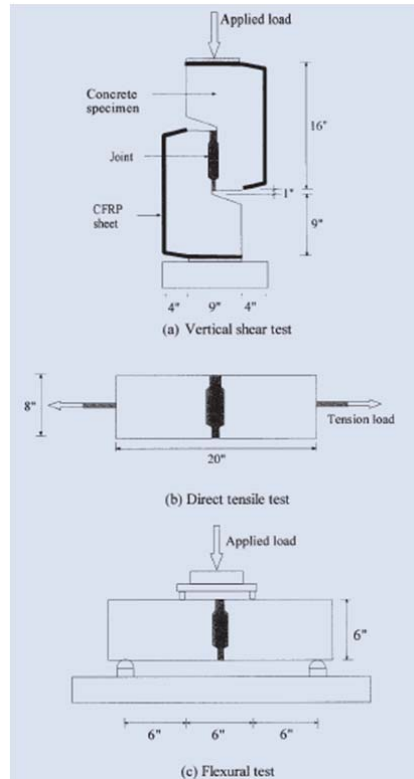


Fig. 58: configuration of the specimen tested (vertical shear, direct tension and flexural test)

A total of 36 full-scale specimen were fabricated and tested for vertical shear, direct tension and flexural capacity (Fig. 58). Polymer concrete was found to be the best material for transverse joint in terms of strength, bond and mode of failure, but it's very expensive and requires careful application, including thorough surface preparation and adequate mixing. However, the use of Set Grout is recommended in transverse deck joints due to its ease of use, fast setting, cheapness and satisfactory performance. In special cases where the joint is subjected to excessive stresses or quick resumption is critical, the proper application of the more expensive polymer is recommended.

In PCI Bridge Manual (Chapter 16) we can read that several panel to panel connection techniques have been developed in response to specific project requirements. Open gaps between panels are sufficiently large to provide for lapped reinforcing bars that project from panel edge. These joints are then filled with cast-in-place concrete. This type of joints diminishes a primary advantage of speed of construction by requiring installation of forms and curing of concrete. In order to avoid these issues, most installation have used keyways that are filled with non-shrink grout or epoxy mortar (Fig. 59).

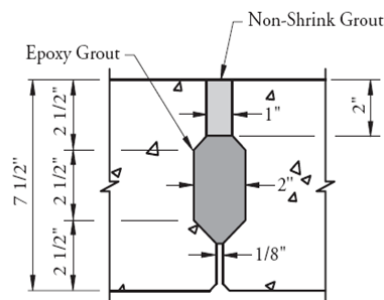


Fig. 59: panel to panel connection performed with grout (PCI Bridge Manual)

Recent analytical studies lead by Naito and Cao and published in PCI journal (spring 2009) have shown that diaphragm joints are subjected to complex shear, tension, and compression deformation demands during an earthquake. To design precast concrete floor diaphragms for seismic demands, methods must be available for estimating the load capacity and deformability of local connections under a combination of in-plane loads. To develop estimates of the strength and deformation capacity of diaphragm connections, a number of experimental studies were conducted. Published research began with hairpin connectors (developed by Pincheira) in 1968 and has continued to recent studies on a variety of mechanical connectors and proprietary connections. Naito and Cao summarized a large portion of these studies and provided a comparison of the responses for connectors examined under both load and deformation demands. Five main type of connectors were examined under in-plane shear and in-plane tension.

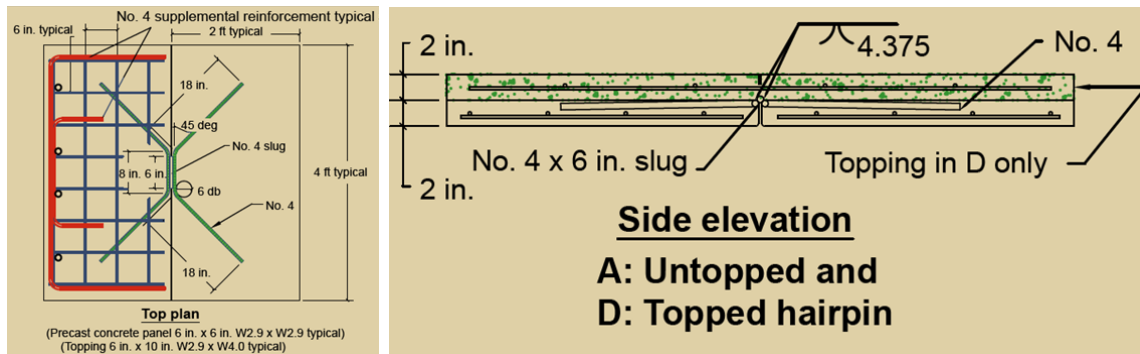


Fig. 60: first type of connection tested by Naito and Cao (hairpin bars, metal slug and concrete topping)

First one analyzed (Fig. 60) was similar to “hairpin” previously reported: it was realized with two reinforcing bar bent in the form of a “hairpin” with two long legs. The center portion of the bar was then welded to a steel plate weld above and below the bar. All connectors were embedded in the concrete with the intention of having the anchor bar at a mid-depth. In each connection, a separate steel bar, or “slug,” is placed between the connectors embedded in the two concrete flanges. The slug is then welded to the connectors for adjoining double tees to complete the connection. To realize diaphragm behavior and complete the system, over the precast slab a concrete 2 in. topping has been cast-in-place.

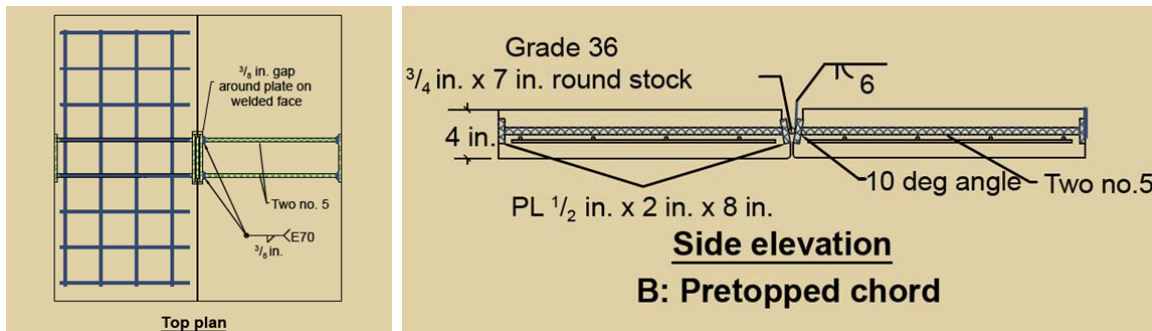


Fig. 61: second type of connection tested by Naito and Cao (steel plate embedded in each slabs and metal slug)

Second one examined (Fig. 61) was made with a 10° inclined with vertical steel plate along the edge of the slab and welded to a pretopped chord embedded in precast concrete. In each connection, a separate steel bar, or “slug,” is placed between the connectors embedded in the two concrete flanges. The slug is then welded to the connectors for adjoining double tees to complete the connection. This type of connection is completely dry and without any cast-in-situ concrete topping.

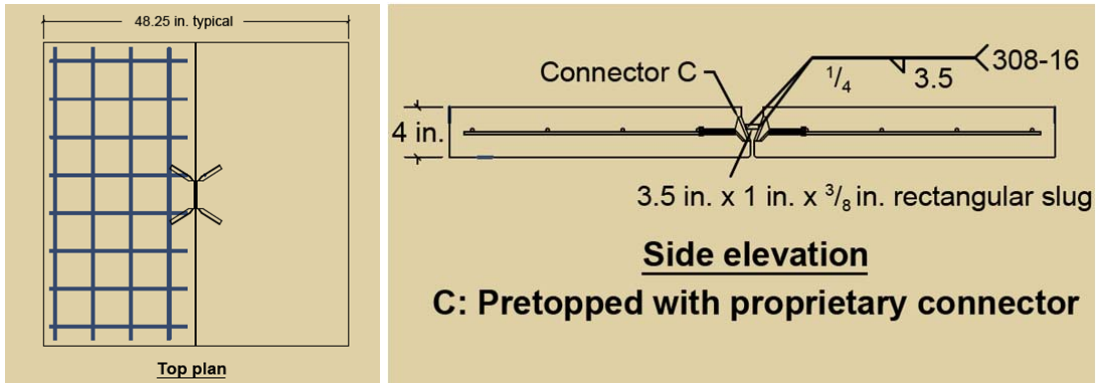


Fig. 62: third type of connection tested by Naito and Cao (steel plate embedded in each slabs and rectangular slug)

Third connection (Fig. 62) was similar to the previous, except for the pretopped chord, replaced here with a steel bent bar with the same shape of the previously described “hairpin”. Inclined steel plates along the edge of each slab are connected by a rectangular slug. As previous, also this system is completely dry and realized without cast-in-place concrete.

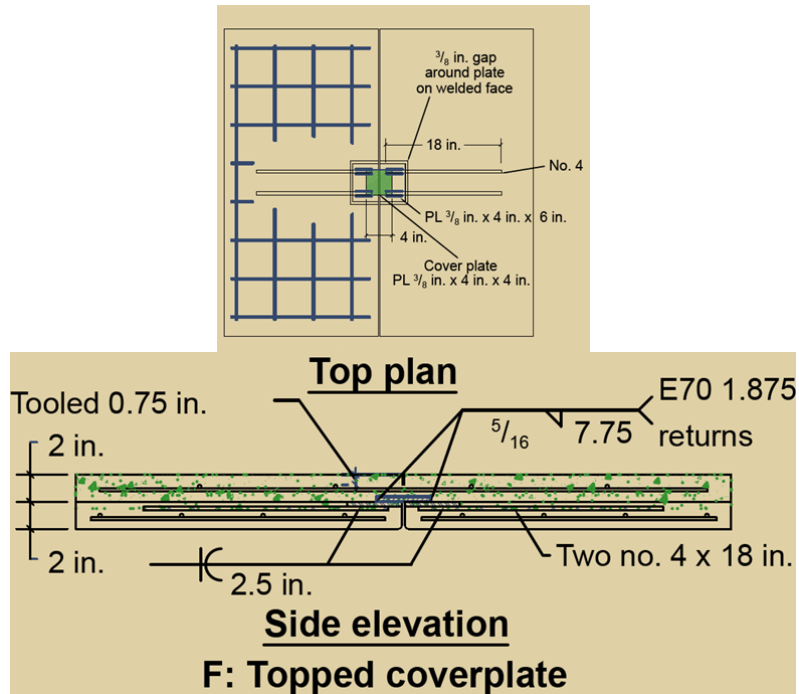


Fig. 63: fourth type of connection tested by Naito and Cao horizontal (steel plate embedded in each slabs and joined with one welded flange and a cast-in-place concrete topping)

Fourth one examined (Fig. 63) was made with a horizontal steel plate over the edge of the slab and welded to straight reinforcing bars embedded in the precast concrete. To join plates of each slabs is then welded one more steel flange, over which is cast a 2 in. topping concrete, in order to obtain diaphragm behavior.

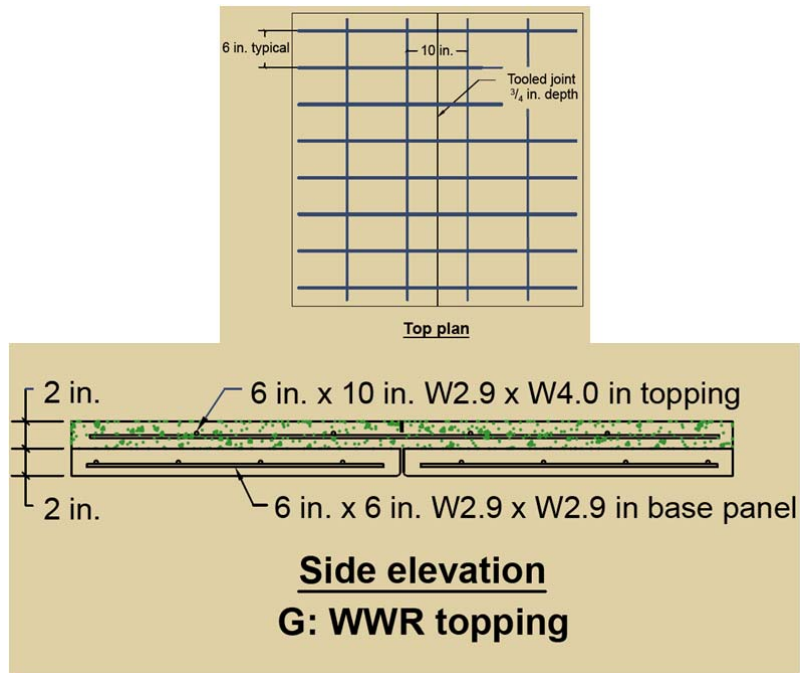


Fig. 64: fifth type of connection tested by Naito and Cao horizontal (slabs placed side by side and joined with a cast-in-situ topping concrete reinforced with a steel mesh)

Fifth connection (Fig. 64) was very simple and realized placing side by side the slabs and casting a 2 in. topping concrete with a steel mesh, or WWR (welded wire reinforcement), in order to obtain diaphragm behavior. According to authors, a ductile option fifth type of connection (but not experimentally tested yet) is shown in Fig. 65, in which we can see that topped connection consists of embedded connectors (steel mesh) and WWR in the topping but only across the joint. In computing the nominal capacity of the topped connectors, the possible assumption we can make is WWR and connector both achieve their yield strengths at the same time and the capacity of WWR is assumed to be additive with that of the underlying connector.

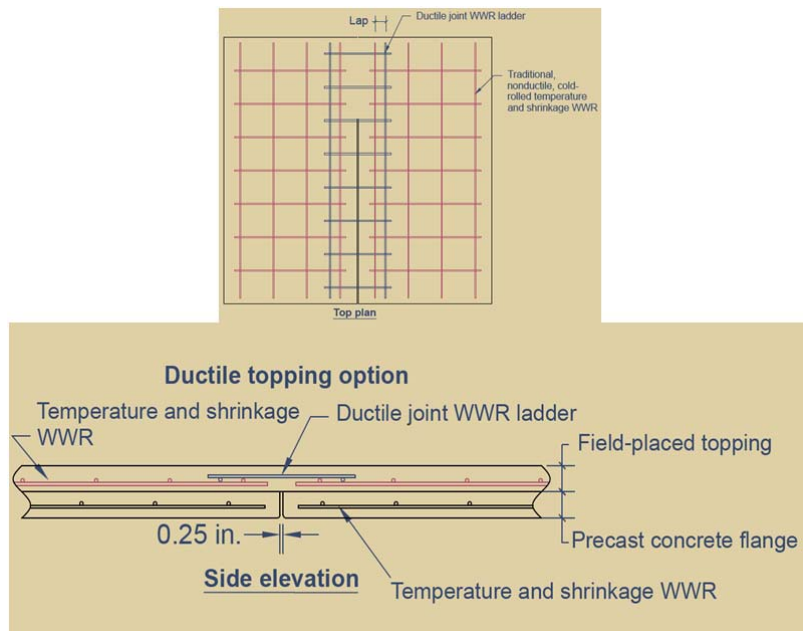


Fig. 65: ductile option to fifth connection: WWR is placed only across the joint

In conclusion, the experimental research program examined the shear performance of seven connections representative of typical pretopped and topped connections commonly used in current U.S. precast concrete construction. From the test observations, the connections exhibited a wide range of shear resistance and deformation capacities. Connections one and three exhibited flexible and ductile shear responses, while connections two, four and five initially exhibited a stiff response with either minimal or no yield plateau. The majority of connections that were examined exhibited brittle concrete crushing and spalling followed by connector fracture. The pretopped chords (second connection), however, did not fracture and was capable of sustaining large deformations.

One more transverse slab to slab connection has been performed by Italian factory Wood Beton. The connection is realized through the casting-in-situ of a 30 cm width topping concrete at the junction between precast panels. In fact panels provide steel bars laterally protruding from slabs that allows the connection between structural elements (Fig. 66 and 67).

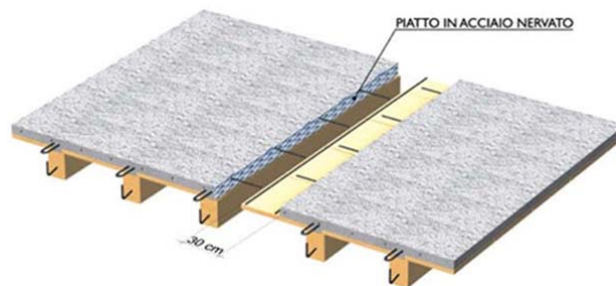


Fig. 66: transversal joint performed by casting of a 30 cm width topping concrete (Wood Beton)

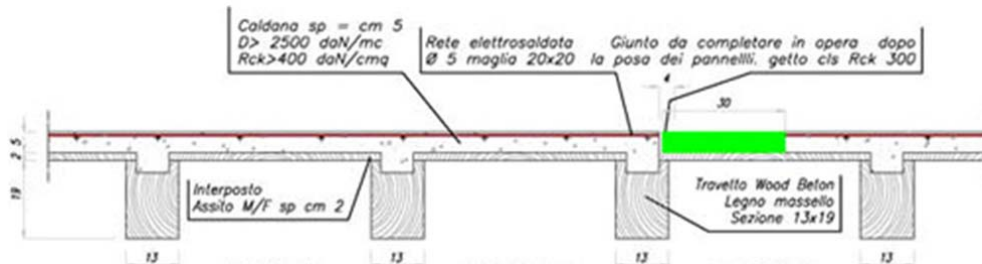


Fig. 67: cross section of transversal joint performed by Wood Beton

Shear connection between precast elements and topping concrete is increased through positioning, during casting phase in establishment, of a vertical ribbed steel plate. The particular conformation of this element allows to increase the contact surface and guarantees a better in-plane loads transmission. This type of joint allows in-plane direct loads transfer, providing also diaphragm shear transfer.

A possible slab to slab connection could be the one shown in Fig. 68. It has been conceived by Mid-Atlantic Precast Association as a wall to wall horizontal joint connection but it could be extended to slabs if the joint doesn't have to transfer vertical shear but only direct tensile and compressive stress. It is realized with an horizontal steel plate over the edge of the slab and welded to straight reinforcing bars embedded in the precast concrete. To join plates of each slabs is then bolted one more steel flange.

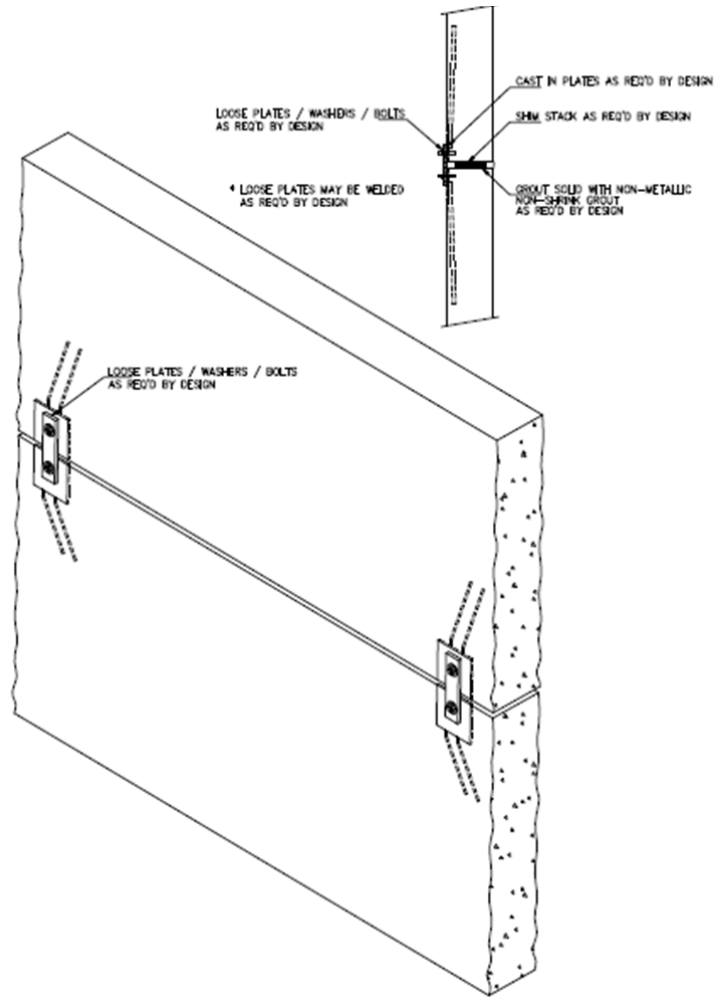


Fig. 68: wall to wall connection performed by MAPA

5 COMPOSITE ACTION OF TIMBER-CONCRETE COMPOSITE SYSTEMS

This chapter presents theoretical models that have been developed for predicting the behavior of composite systems with incomplete composite action between concrete and timber layers. It also presents guidelines for short- and long-term verifications of timber-concrete composite systems according to Eurocode 5. Further, a recently developed approach, which accounts for inelastic strains, for predicting the long-term behavior of timber-concrete composite structures is described. Finally, models for predicting timber-concrete joints' stiffness, strength and overall behavior are presented.

5.1 Background

To manufacture timber-concrete composite systems with high degrees of composite action, the shear between the timber beam and the concrete slab needs to be transferred effectively through the shear connector system. Therefore, the shear connectors are key elements of a composite system, which require particular attention since they determine the system's performance parameters. There are two bounds of composite action:

- a lower bound of fully non-composite action, displayed by timber and concrete layers that are not connected and thus work independently, with no transfer of horizontal force between the two layers via either mechanical bonds or friction (Fig. 69c). The layers have individual neutral axes and there is discontinuous flexural strain at the timber-concrete interface.
- an upper bound of fully composite action, displayed by timber and concrete components that are rigidly connected with no interlayer slip, have cross sections with a single neutral axis and identical flexural strains at the timber-concrete interface (Fig. 38a). Consequently, the transformed section method can be validly applied to analyze stresses in such systems.

The timber and concrete layers are connected by mechanical fasteners in most cases (and/or in a few cases by adhesives). In reality the shear connection system is deformable and most connectors generate at least some horizontal movement ("slip") at the interface. Such behavior is referred to as "partial composite action". The single neutral axis splits and as slip between the layers increases the two neutral axes move farther apart, hence slip between the timber beam and concrete slab reduces the efficiency of the cross section. It is difficult to achieve a rigid connection between timber and concrete, but minor slippage can be advantageous, allowing the redistribution of shear stresses along the shear connectors. Fig. 38b presents strain diagrams for structures with full, partial and no composite action.

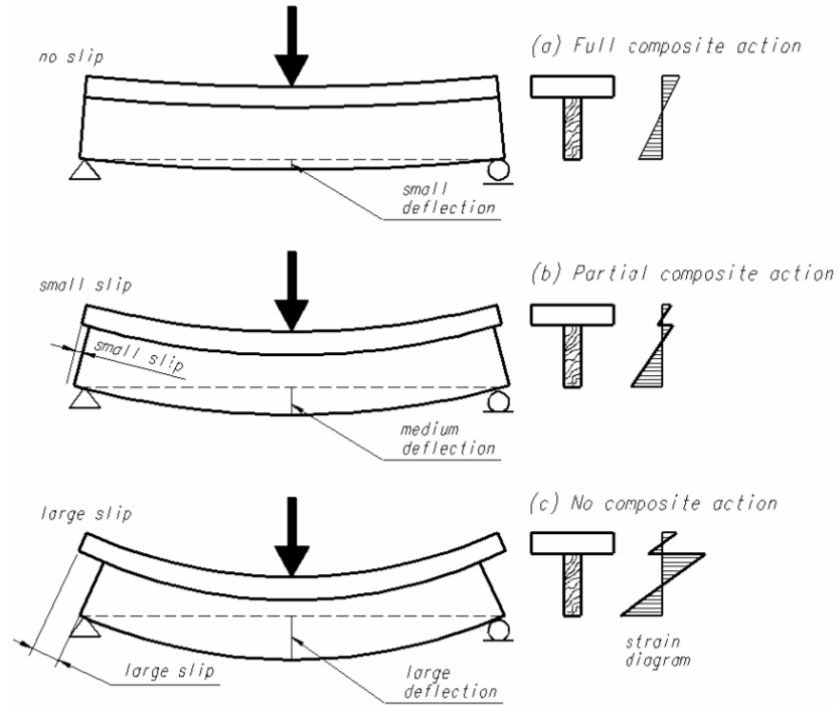


Figure 69: Strain diagrams for composite structures with a rigid connection (a), a deformable connection (b), and no connection between the timber beam and concrete slab (c)

As mentioned above, using an efficient shear connection is the key to achieving strong and stiff composite systems. The efficiency of the shear connection can be measured using the following relationship, suggested by Gutkowski et al. (2008):

$$E = \frac{D_N - D_I}{D_N - D_C}$$

where E is the efficiency of the composite system, D_N is the theoretical fully non-composite deflection (calculated for a layered beam with no interlayer shear transfer), D_C is the theoretical fully composite deflection (calculated by the transformed section method) and D_I the measured deflection of the timber-concrete composite beam. The efficiency can vary between 0% and 100% for ideal cases with no connection and fully rigid connection, respectively. It may also be convenient to define the efficiency of a shear connection for a composite beam, using the following equation, originally proposed by Piazza in 1983 (after Piazza and Ballerini 2000, Ballerini et al. 2002).

$$\eta = \frac{EJ_{real} - EJ_0}{EJ_{\infty} - EJ_0}$$

where: η is the efficiency of the interlayer connection, EJ_{∞} is the bending stiffness of the beam with a theoretical full composite action, EJ_0 is the bending stiffness of the beam with no composite action and EJ_{real} is the actual bending stiffness of the beam. When the shear connection is very stiff EJ_{real} tends to EJ_{∞} and thus $\eta \rightarrow 1$. On the other hand, for a very flexible shear connection EJ_{real} would tend to EJ_0 and thus $\eta \rightarrow 0$.

In order to limit the deflections in composite structures relatively rigid shear connectors should be used. However, rigidity is not the only desirable characteristic of timber-concrete shear connectors. Notably, to prevent undesirable brittle failure in the composite structure, shear connectors should also be sufficiently ductile (Ballerini et al. 2002).

5.2 Theoretical models for incomplete composite action

Generally, analytical models for calculating stresses and deformations in timber-concrete composite structures have been developed for composite structures with semi-rigid connections between two layers (either steel and concrete or wood and wood) and more recently such models have been applied to wood-concrete composite structures. One of the first models was developed in 1943 following small-scale tests carried out on T-beams composed of a concrete slab and a steel I-beam linked together by a shear connector (Newmark 1951). The model is applicable to any types of beams consisting of two interacting layers that satisfy the following assumptions: (i) the shear connection between the upper layer and I-beam can be regarded as continuous along the length of the beam, (ii) the amount of slip permitted per shear connection is directly proportional to the load transmitted, (iii) the distribution of strains throughout the depth of the upper and lower layers is linear, and (iv) both interlayers deflect equal amounts at all points along their length at all times.

A simple linear model that is used widely nowadays and takes into account the slip between two layers of a composite structure is described by many authors, which base their work on Newmark (1951) and Möhler (1956). This linear model found its presence in Eurocode 5 (Statement [3] and [4] in the text) and is based on previously derived differential equations of equilibrium of a composite cross section. The basic assumptions and formulae are described in section 4.3.

Goodman et al. (1968) combined theory with experimental work to develop a procedure for analyzing the nonlinear responses of the connectors used in a 3-layer system made of wood, which can be extended to analyzing systems with more layers. In their procedure, all layers are considered to have the same mechanical properties throughout. Extension of the theory to beams made with layers of varying sizes or properties requires no additional concepts, but the theory has to be modified in order to address time-dependent changes in the behavior of the systems.

Godycki et al. (1984) presented a linear elastic model for calculating properties of timber-concrete composite structures, including the slip of the connectors. The cited authors accounted for time-dependent changes in the behavior of concrete by assuming that its modulus of elasticity declines with time in the model.

Stevanovic (1989 & 1996) proposed an elastic method to calculate forces in composite timber-concrete structures subjected to transverse and axial loading, which takes into account slip between the timber-concrete elements. The developed method, based on an elastic theory, allows deflections and section forces in wood and concrete to be predicted, and the shear force between wood and concrete to be calculated.

In addition, closed form solutions based on Euler-Bernoulli theory for analyzing the behavior of timber-concrete composite beams/columns, with interlayer slip, which include axial load acting together with bending moments and second order ($P-\Delta$) effects have been developed, initially by Girhammar and Gopu (1991). Such solutions are especially applicable when timber-concrete elements are used in wall panels, which are subjected to both axial and transverse loads, hence their design requires the consideration of second order effects. In 1993 the cited authors presented exact first- and second-order functions for composite beam-columns of timber and concrete with partial interaction that are subjected to transverse and axial loading since the procedure they previously presented dealt with only one particular axial loading case.

Girhammar and Pan (2007) subsequently extended and generalized the theories and procedures given by Girhammar and Gopu in 1991. The aim was to derive an exact closed form solution for characteristic equations within the validity domain of Euler-Bernoulli beam theory and the associated buckling length coefficients for partially composite beam-columns. The exact second order analysis, though rigorous, is very elaborate and

extremely cumbersome. Hence, for design applications Girhammar (2008) developed a simplified approach to evaluate the second order effects in composite members with interlayer slip. The approximate procedure allows engineers to analyze and design composite beam-columns with interlayer slip conveniently, but with high accuracy.

Girhammar and Pan (1993) also proposed exact and approximate procedures to analyze composite members with partial interaction that are subjected to general dynamic loading. For both exact and approximate analyses general closed-form solutions for displacement functions and the various internal actions in the composite elements were developed. The theories and procedures published in 1993 have been recently extended and generalized by Girhammar et al. (2009).

A simplified method for analyzing characteristics of composite beams with interlayer slip has also been recently proposed by Girhammar (2009). The principle of the approximate method for partially composite beams is to replace the fully composite bending stiffness (EJ_{sc}) with the partially (effective) composite bending stiffness (EJ_{ef}) in the expressions for deflections, internal actions and stresses in corresponding fully composite beams. The effective bending stiffness reflects the influence of the interlayer slip, and depends on the partial composite action (or shear connector stiffness) parameter (which accounts for the slip modulus, cross-section material, geometry and length of the beam) and relative bending stiffness parameter (the stiffness of the beam, relative to that of a fully composite beam). The major difference between the analytical methods presented by Girhammar (2009) and the one recommended in Eurocode 5 is that the effective beam length equals the buckling length in the corresponding column buckling problem. An approximate method for characterizing mechanically jointed beams given in Eurocode 5, Annex B (further described in section 4.3) was originally developed solely for end-supported conditions. For other boundary conditions Eurocode 5 gives recommendations regarding the “effective” beam length that are generally not as accurate as those provided by the method proposed by Girhammar (2009). However, it should be noted that the recently proposed method by Girhammar gives identical results for composite beams with interlayer slip to those obtained from the approximate method given in Eurocode 5 for simply supported members. For other boundary conditions, the Eurocode 5 procedure may give results with up to 27% errors, depending on the recommended value for the effective beam length.

In 1999 Van der Linden presented a procedure, the so-called *frozen shear force approximation*, to calculate the failure load of a timber-concrete composite beam. The plasticity of the shear connectors is considered by using an elasto-plastic load-slip relationship. The fundamental idea is that the shear forces in all connectors are frozen once the first connector at the support starts to plasticize. The approach discussed by the cited author leads to a lower bound solution, assuming that the concrete and timber still behave in a linear fashion. However, if tests indicate that non-linearities in the behavior of the materials significantly influence the load levels, the derived equations will no longer be valid lower bound solutions, and are likely to overestimate the beam's lower load-bearing capacity (Van der Linden 1999).

Frangi and Fontana (2003) described an elasto-plastic model for predicting the behavior of timber-concrete composite beams with ductile connections. The structural behavior of timber-concrete composite elements is governed by the shear connector type and its performance. If the connection under load remains within the linear elastic range until the timber members fail, linear-elastic behavior of the composite structure may be assumed. However, if the load exceeds the connectors' load carrying capacity, the outermost connectors will deform plastically and the composite structure will begin to behave non-linearly. The elasto-plastic analytical model considers the behavior of the connection by assuming the connectors to be rigid-perfectly plastic in terms of their load-slip relationship. The assumed rigid-perfectly plastic load-slip relationship of the connectors is analogous to

the model assumed in the European Yield Model (Johansen 1949) for designing the load-carrying capacity of dowel-type fastener connections (Frangi and Fontana 2003). In this case the slip modulus of the connectors does not have to be considered, which makes calculations easier and less sensitive to the large coefficient of variation of the slip modulus. For timber, linear elastic behavior is assumed because timber subjected to combined bending and tension exhibits brittle behavior. Linear elastic material behavior is also assumed for concrete because timber members usually fail before the concrete slab plasticizes. The cited authors considered three different cases, which depend on the number of connectors placed in the interlayer:

- (i) in the first case there is no interlayer connection.
- (ii) in the second the interlayer is partially connected, total collapse due to failure of the timber under combined bending and tension takes place once the connectors reach their maximum shear strength. The composite structure in such cases exhibits nonlinear behavior before total collapse occurs.
- (iii) in the last case the interlayer is fully connected and total collapse of the structure is due to failure of the timber before the maximum shear strength of the connectors is exceeded. In this case the composite structure performs linearly before the total collapse occurs.

The fully connected interlayer and the unconnected interlayer represent the upper and lower bounds for the partially connected interlayer. Since the fully connected interlayer and the unconnected interlayer represent the upper and lower bounds for the partially connected interlayer, a simplified linear approximation, which is conservative, may be used to calculate the load-bearing capacity of a partially connected timber-concrete composite beam. The elasto-plastic model gives upper and lower bounds for the load-carrying capacity that are within 5% of those obtained by linear approximation, and the cited authors found it satisfactory for calculating the load-bearing capacity of partially connected composite systems (Fontana and Frangi 2003).

5.3 Design procedure according to Eurocode 5 - “ γ - method”

The design of timber-concrete composite structures must satisfy both ultimate (SLU) and serviceability (SLS) limit states for short- and long-term loads. The ULS is assessed by evaluating the maximum stresses in the component materials (timber, concrete and connection system) using an elastic analysis while the SLS is checked by evaluating the maximum deflection.

Eurocode 5-Part 1-1, Annex B provides a simplified method for calculating these parameters of mechanically jointed beams with flexible elastic connections, under the following assumptions:

- the beam is simply supported with a span l . For continuous beams the expressions may be used with l equal to 0.8 of the relevant span, and twice the cantilever length for cantilevered beams
- the individual parts (of wood, wood-based panels) are either full length or made with glued end joints
- the individual parts are connected to each other by mechanical fasteners with a slip modulus k
- the spacing s between the fasteners is constant or varies uniformly according to the shear force, between s_{min} and s_{max} with $s_{max} \leq 4 s_{min}$
- the load acts in the z-direction giving a moment $M=M(x)$ that varies sinusoidally or parabolically, and a shear force $V=V(x)$.

This method is based on an approximate solution of the differential equation for beams with partial composite action. The simplified design method, the so-called “ γ -method” is closely related to the model initially derived by Möhler (1956) and has proved to provide excellent approximations for composite beams with closely spaced fasteners (Kenel 2000 and Frangi and Fontana 2001). The full derivation of the formulae can be found in Kreuzinger (1995).

According to the γ -method, the effective bending stiffness $(EI)_{eff}$ of a simply supported timber-concrete composite beam is calculated as:

$$EJ_{ef} = \sum_i E_i J_i + \gamma_2 \cdot E_2 \cdot A_2 \cdot a_2^2 + \gamma_1 \cdot E_1 \cdot A_1 \cdot a_1^2$$

with shear γ coefficient and distances a_i given by:

$$\gamma_1 = \left[1 + \pi^2 \cdot E_1 \cdot A_1 \cdot s_{eq} / (K \cdot L^2) \right]^{-1}$$

$$\gamma_2 = 1$$

$$a = h_1/2 + h_2/2 + t$$

$$a_2 = \frac{\gamma_1 \cdot E_1 \cdot A_1 \cdot a}{\gamma_1 \cdot E_1 \cdot A_1 + \gamma_2 \cdot E_2 \cdot A_2}$$

$$a_1 = a - a_2$$

where I_i , A_i and E_i designate the second moment of inertia, area, and modulus of elasticity of the concrete slab ($i=1$) and timber beam ($i=2$), respectively, s is the connector spacing, L is the beam length, k is the slip modulus of the connector, and the other variables are illustrated in Fig. 70 from Eurocode 5. A γ coefficient equal to 0 applies in cases where there is no connection system and the layers act fully independently. A γ coefficient equal to 1 indicates full composite action with no slip at the interface between the timber and concrete.

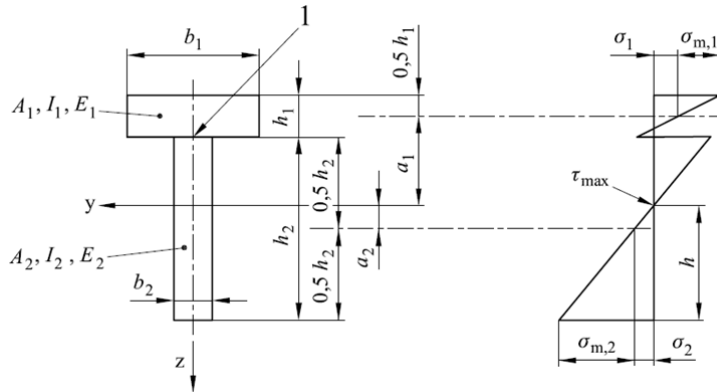


Figure 70: cross-section (left) and stress distribution (right) of a composite beam with partial shear connection (Eurocode 5)

The effective stiffness can be used to calculate the deflection, the stress distribution and the shear load in the fastener, using the following equations:

$$\delta = \frac{5 \cdot q \cdot L^4}{384 \cdot EJ_{ef}}$$

$$\sigma_i = \frac{\gamma_i \cdot E_i \cdot a_i \cdot M}{EJ_{ef}}$$

$$\sigma_{m,i} = \frac{0.5 \cdot E_i \cdot h_i \cdot M}{EJ_{ef}}$$

$$F = \frac{\gamma_1 \cdot E_1 \cdot A_1 \cdot a_1 \cdot s_{eq}}{EJ_{ef}} \cdot V$$

where δ is the mid-span deflection of a simply supported beam, q is the uniformly distributed load, σ_i , $\sigma_{m,i}$ are the stress at the centroid and the flexural component of the stress in the concrete ($i=1$) and timber ($i=2$), F is the shear load in the fastener, M is the bending moment and V is the shear force in the cross-section of interest.

Consequently, the normal stress and bending agents in items 1 and 2, and the maximum shear (that originates where normal tension is equal to zero) are given by the following expressions:

$$N_1 = \frac{\gamma_1 \cdot E_1 \cdot A_1 \cdot a_1}{EJ_{ef}} \cdot M \qquad N_2 = \frac{\gamma_2 \cdot E_2 \cdot A_2 \cdot a_2}{EJ_{ef}} \cdot M$$

$$M_1 = \frac{E_1 \cdot J_1}{EJ_{ef}} \cdot M \qquad M_2 = \frac{E_2 \cdot J_2}{EJ_{ef}} \cdot M$$

$$\tau_{\max} = \frac{0.5 \cdot E_2 \cdot (a_2 + h_2/2)^2}{EJ_{ef}} \cdot V$$

5.4 Short- and long-term verifications

A general effect (such as stress and displacement), caused by the load combination for ultimate (ULS) and serviceability limit (SLS) states, can be calculated using the formulas provided by Eurocode 5. These values depend on the load applied on the beam, and on the Young's and slip moduli of the component materials and can be expressed in the following basic form:

$$E^{SLU} = E^{SLU}(E_{cm}(t_0), E_{0,mean}, k_{ser})$$

$$E^{SLS} = E^{SLS}(E_{cm}(t_0), E_{0,mean}, k_u)$$

where, in general, $k_{ser} \neq k_u$

For the serviceability limit state (SLS) three combinations: (i) characteristic, (ii) frequent and (iii) quasi-permanent are considered, while for the ultimate limit state (SLU) just one design load combination is considered:

$$F_{d,SLE,char} = G_1 + G_2 + P + Q_{K1} + \psi_{02} \cdot Q_{K2} + \psi_{03} \cdot Q_{K3} + \dots$$

$$F_{d,SLE,freq} = G_1 + G_2 + P + \psi_{11} \cdot Q_{K1} + \psi_{22} \cdot Q_{K2} + \psi_{23} \cdot Q_{K3} + \dots$$

$$F_{d,SLE,qp} = G_1 + G_2 + P + \psi_{21} \cdot Q_{K1} + \psi_{22} \cdot Q_{K2} + \psi_{23} \cdot Q_{K3} + \dots$$

$$F_{d,SLU} = \gamma_{G1} \cdot G_1 + \gamma_{G2} \cdot G_2 + \gamma_P \cdot P + \gamma_{Q1} \cdot Q_{K1} + \gamma_{Q2} \cdot \psi_{02} \cdot Q_{K2} + \gamma_{Q3} \cdot \psi_{03} \cdot Q_{K3} + \dots$$

The short-term verifications, at the initial state where loads are applied instantaneously and with no creep effect, can be performed according to the procedure based on the use of Young's moduli for concrete and timber, and the slip modulus of the connection, as described by Ceccotti et al. (2002) and Ceccotti (1995). Since the load-slip relationship of the shear connection is typically non-linear, two different slip moduli are considered for design purposes, as proposed by Ceccotti (1995): k_{ser} for the serviceability limit state (SLS) and k_u for the ultimate limit state (SLU). The slip modulus k_{ser} , which corresponds to the secant value at 40% of the load-carrying capacity of the connection ($k_{0,4}$), is usually evaluated by push-out tests according to EN 26891. For the slip modulus k_u , use of the secant value at 60% ($k_{0,6}$) is recommended; see for example STEP 2 (1995), Fig. 71. However, if experimental data are not available, Eurocode 5-Part 1-1 suggests using the formulae for timber-to-timber connections by multiplying the corresponding values of the slip modulus k_{ser} by 2. The slip modulus k_u may then be taken as 2/3 of k_{ser} (Eurocode 5). Depending on the type of connection involved, this assumption may or may not be adequate. Ceccotti et al. (2007), for example, reported a significant (50%) discrepancy between experimentally and analytically determined properties of connections, and recommended the use of empirically determined values of

connection properties obtained from push-out tests. In Papers I and II the experimental results of shear-tests performed on shear connectors are presented in terms of the slip moduli k_{ser} and k_u , which are further analyzed in the short-term verifications at SLS and SLU.

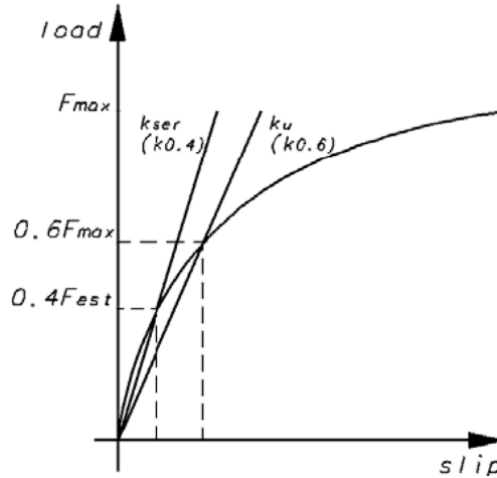


Figure 71: example of load-slip behavior of shear connector and definition of slip moduli: k_{ser} ($k_{0.4}$) at 40% of the estimated load-carrying capacity, k_u ($k_{0.6}$) at 60% of the maximum load-carrying capacity

Thus, the current procedure for short-term solutions for the serviceability and ultimate limit state can be summarized as follows:

1. For the serviceability limit state an elastic solution has been proposed where u_{inst} due to the load characteristic combination is obtained using the elastic moduli:

$$E_c = E_{cm}(t) \quad E_t = E_{0,mean} \quad k = k_{ser}$$

2. For the ultimate limit state an elastic solution has been proposed where stresses due to the load quasi-permanent combination is obtained using the elastic moduli:

$$E_c = E_{cm}(t) \quad E_t = E_{0,mean} \quad k = k_u$$

The verification of a composite beam in the long-term is more problematic, since concrete creep and shrinkage, the creep and mechano-sorption of the timber and connection, and thermal strains of concrete and timber should all be considered. Numerical programs (Fragiacomo and Ceccotti 2006, Schänzlin 2003) and analytical formulas (Fragiacomo 2006, Fragiaco and Ceccotti 2006, Schänzlin and Kuhlmann 2004) have been proposed to provide accurate solutions, but no consensus among researchers has been reached regarding methods to predict the long-term performance of timber-concrete composite structures (after Clouston 2006). Referring to Clouston for steel-concrete construction, the ACI-ASCE Joint Committee recommends using $E_c/2$ as the concrete modulus of elasticity instead of E_c when calculating sustained load creep deflection (after Clouston 2006). The AASHTO Bridge Design Specification, Section 10.38.1.4, suggests using $E_c/3$ (after Clouston 2006). The European Code recommends using creep factors developed from load duration studies to reduce the moduli of the respective materials (Eurocode 5).

The simplified approach suggested by Ceccotti (2002) does not account for shrinkage or thermal strains and is based on the *Effective Modulus Method*, in which the creep and mechano-sorption of the concrete, timber and connection are accounted for by reducing the elastic and slip moduli according to the following expressions:

$$E_{c,fin} = \frac{E_{cm}(t_0)}{1 + \phi(t, t_0)} \quad E_{t,fin} = \frac{E_{0,mean}}{1 + k_{def}} \quad k_{fin} = \frac{k}{1 + k_{def}}$$

For the concrete, Eurocode 2-1-1 provides some guidelines for evaluating the creep coefficient $\phi(t, t_0)$, t and t_0 being the final and loading instants, respectively. Eurocode 5-1-1 provides tables of values of the creep coefficients k_{def} for both timber and the connection. Those moduli are then used in previous equations to solve the beam parameters in long-term loading.

The creep phenomenon has two types of effect on the composite beam: (i) increments with time in strains and displacements and (ii) changes in the distributions with time of stresses and internal forces in the component materials because of the differences in creep properties.

Consequently, creep affects both the ultimate and serviceability limit states, and cannot be neglected in long-term verifications.

The currently proposed procedure (*Effective Modulus Method*) for calculating a long-term solution for the serviceability and ultimate limit states can be summarized as follows:

1. For the serviceability limit state an elastic solution has been proposed where u_{fin} due to the quasi-permanent part of the load combination $F_{d,SLE,qp}$ is obtained using the effective moduli reduced as previously shown to account for shrinkage, creep and mechano-sorption.

The creep effects are due only to the quasi-permanent part of the load $F_{d,SLE,qp}$ considered as acting on the structure for the entire service life. The long-term maximum vertical displacement can be calculated by substituting the long-term displacement due to the quasi-permanent part of the load for the instantaneous displacement due to the difference between the rare and quasi-permanent combinations applied at the end of the service life t :

$$u_{fin} = u_{fin}^{F_{d,SLE,qp}} + u_{inst}^{F_{d,SLE,char} - F_{d,SLE,qp}} = u^{F_{d,SLE,qp}}(E_{c,fin}, E_{t,fin}, k_{ser,fin}) + u^{F_{d,SLE,char} - F_{d,SLE,qp}}(E_{cm}(t), E_{0,mean}, k_{ser})$$

$$F_{d,SLE,char} - F_{d,SLE,qp} = (1 - \psi_{21}) \cdot Q_{K1} + (\psi_{02} - \psi_{22}) \cdot Q_{K2} + (\psi_{03} - \psi_{23}) \cdot Q_{K3} + \dots$$

2. For the ultimate limit state an elastic solution has been proposed where stresses S_{fin} due to the load quasi-permanent combination is obtained using the elastic moduli:

$$E_c = E_{cm}(t) \quad E_t = E_{0,mean} \quad k = k_u$$

In addition, for ultimate limit state verification only the quasi-permanent part of $F_{d,SLE,qp}$ of the combination $F_{d,SLU}$ has to be considered as acting throughout the entire service life. The effects due to the load $F_{d,SLE,qp}$ can be estimated, as mentioned above, using the effective moduli E_{fin} . Moreover, the difference between the ultimate and the quasi-permanent load combination is instead applied instantaneously, therefore for this part of the load the Young's moduli at the instant t have to be used. Consequently, the following formulation can be applied:

$$S_{fin} = S_{fin}^{F_{d,SLE,qp}} + S_{inst}^{F_{d,SLU} - F_{d,SLE,qp}} = S^{F_{d,SLE,qp}}(E_{c,fin}, E_{t,fin}, k_{ser,fin}) + u^{F_{d,SLU} - F_{d,SLE,qp}}(E_{cm}(t), E_{0,mean}, k_u)$$

$$F_{d,SLU} - F_{d,SLE,qp} = \sum_{j \geq 1} (\gamma_{G,j} - 1) \cdot G_{k,j} + (\gamma_{Q,1} - \psi_{21}) \cdot Q_{K1} + \sum_{i > 1} \gamma_{Q,i} \cdot (\psi_{0,i} - \psi_{2,i}) \cdot Q_{K,i}$$

6 STIFFNESS OF THE TIMBER-CONCRETE CONNECTORS

This chapter presents the complete description of both the connection systems between the timber beam and the concrete slab, the T12 and the F45, described and used in experimental tests of reference [1]. Furthermore, there is also a theoretical method to obtain the stiffness of each one of the two considered systems.

6.1 Stiffness of the connection system type T12

The main purpose of this paragraph is to present and analyze one of the two system used in reference [1] to join the glulam beam to the above fiber reinforced concrete slab, or else the T12, of which we report the image below.



Figure 72: beam to slab connection system type T12 used for the researches described in Paper [1]



Figure 73: beam to slab connection system type T12 used for the experimental researches described in this Paper

This kind of connection is made through the insertion in a wood formwork of metal pipes with washer, inclined at 45° and welded to a steel plate. Inside each pipe is then inserted a full-threaded screw of diameter 11 mm, which enters the glulam and joins the slab to the beam. As we can see from following figure 73, the working of the system is like shear-tensile stress.

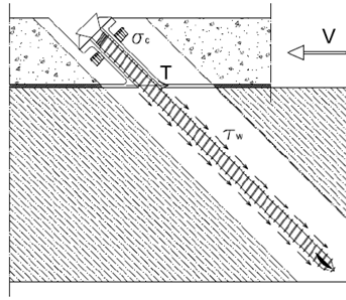


Figure 74: load path of the connection system T12

Shear load V that has to be exchanged between the beam and the slab is divided in two components. First one is transferred directly to the fastener by shear mechanism, and thanks to the high contact stiffness between the screw and the steel pipe. The other component passes from the concrete to the screw's washer as compressive strength σ_c , and is then transferred from screw's head to screw itself throughout the withdrawal capacity of the threaded part of the screw. Furthermore, the vertical component of the screw creates a compression between slab and beam that originates an additional force between the two surfaces due to friction.

From the following image it is possible to see how is made the steel plate, in addition to some geometrical details.

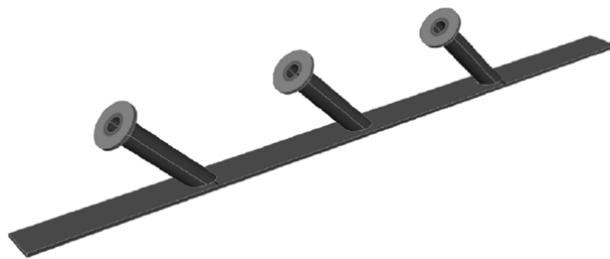


Figure 75: steel plate with welded pipes containing the screws (used in the tests of Paper [1])

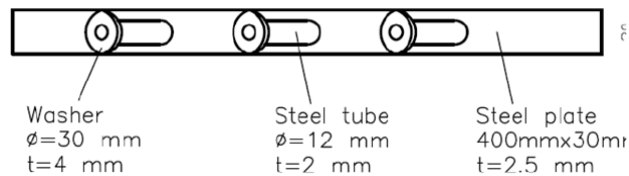


Figure 76: geometrical details of the steel plate



Figure 77: steel plate with welded pipes containing the screws (used in the tests of this Paper)

6.1.1 Stiffness evaluation

The goal that we want now is to obtain and verify a theoretical formulation to describe the mechanical behavior of joint fully assembled through inclined screws in terms of stiffness. In this section we refer to paper [9], containing the theory of Bejtka e Blass regarding the behavior of connecting systems with skewed screws and thus subjected to a shear-tensile stress state.

Since this type of connection is not explicitly provided in Statement [2] the stiffness, or instantaneous slip modulus K_{ser} of joints with inclined screws can be determined with the same formulation related to screws inserted perpendicularly to the shear plane, and thus through the following expression of provided by DIN 1052:2004:

$$K_{ser} = \frac{\rho_k^{1.5} \cdot d}{20}$$

The value of K_{ser} presented in this paragraph is defined by using:

- a value of ρ_k determined experimentally through the laboratory tests performed and described in Paper [1]
- an effective diameter $d_{ef} = 1.1 \times d_{nucleo}$, where d_{nucleo} is the diameter of the non-threaded part of the screw

The previous formulation is valid only for timber to timber joints, while instead for timber to concrete joints, to determine K_{ser} we shall use the same density for the wood element but the obtained values have to be doubled (Piazza).

Following figures show the displacement and stress components in the shear plane, according to the inclination angle α that the screws form with the grain direction.

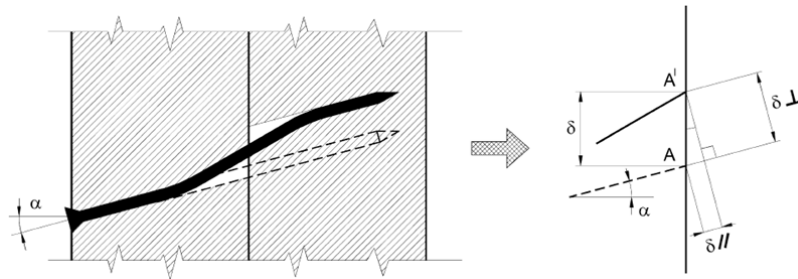


Figure 78: displacement components in the shear plane

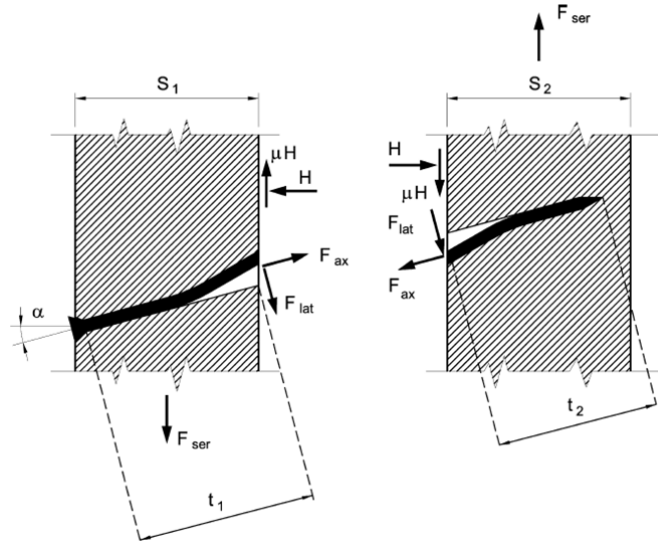


Figure 79: stresses acting in the shear plane

The displacement components δ , with respect to the undeformed configuration of the screw, are:

$$\delta_{||} = \delta \cdot \sin \alpha \quad \delta_{\perp} = \delta \cdot \cos \alpha$$

where δ is the displacement parallel to the shear plane.

If we assume an elastic linear behavior of the screw at the Service Limit State, we can write following equations:

$$F_{ax} = K_{ax} \cdot \delta_{||} \quad F_{lat} = K_{lat} \cdot \delta_{\perp}$$

By imposing now the equilibrium we can obtain:

$$F_{ser} = F_{lat} \cdot (\cos \alpha - \mu \cdot \sin \alpha) + F_{ax} \cdot (\sin \alpha + \mu \cdot \cos \alpha)$$

By substituting the previously reported expressions we can obtain:

$$F_{ser} = K_{ax} \cdot \delta \cdot \sin \alpha \cdot (\sin \alpha + \mu \cdot \cos \alpha) + K_{lat} \cdot \delta \cdot \cos \alpha \cdot (\cos \alpha - \mu \cdot \sin \alpha)$$

Since $K_{ser} = F_{ser} / \delta$, the expression for screws that works in a shear-tensile stress state is:

$$K_{ser} = K_{ax} \cdot \sin \alpha \cdot (\sin \alpha + \mu \cdot \cos \alpha) + K_{lat} \cdot \cos \alpha \cdot (\cos \alpha - \mu \cdot \sin \alpha)$$

where:

K_{lat} indicates the screw lateral stiffness

K_{ax} indicates the screws axial stiffness

μ is the friction coefficient between the two elements

6.1.1.1 Evaluation of K_{lat}

As previously said, the value for the stiffness orthogonally to the screw is given by following expression:

$$K_{lat} = 2 \cdot \frac{\rho_k^{1.5} \cdot d_{ef}}{20} = 2 \cdot \frac{\rho_k^{1.5} \cdot 1.1 \cdot d_{nucleo}}{20} = 2 \times \frac{450^{1.5} \times 1.1 \times 6.5}{20} \left[\frac{N}{mm} \right] = 6825 \left[\frac{N}{mm} \right]$$

6.1.1.2 Evaluation of K_{ax}

For the stiffness in direction parallel to the screw reference [9] suggests to considering separately the contributions of the two (wooden) parts through the following expression:

$$K_{ax} = \frac{1 + \mu \cdot \operatorname{tg} \alpha}{1/K_{ser,ax,1} + 1/K_{ser,ax,2}}$$

where:

μ is the friction coefficient between the two (wooden) elements

In our case one of the two contribution is referred to concrete.

In order to determinate the axial stiffness, previous formulations proposed in reference [9] derive from the results of experimental tests conducted on wood specimens joined by a system of screws subjected to a combination of shear and tensile stress. The basis of Blass theory come from elaboration of experimental data obtained by using screws with diameters contained in a range between 5 and 12 mm, and thus also our 11 mm diameter is within the considered interval. The test instrument through which these experiments were performer is shown in next figure 79.

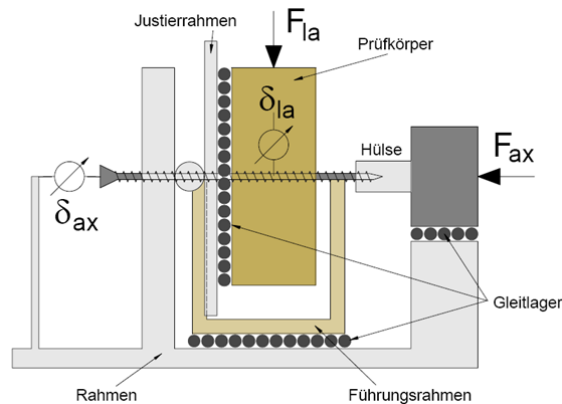


Figure 80: test instrument to determine both shear and withdrawal strength

In accordance with a regression multiple analysis performed over the results of tests carried out on a total of more than 400 specimens, the expression obtained for the axial stiffness of the authors (Blass e Bejtka) is as follows:

$$K_{ax} = 234 \cdot (\rho \cdot d)^{0.2} \cdot l_s^{0.4}$$

where:

d is the screw diameter [mm]

ρ is the timber density [kg/m³]

l_s is the embedment length of the threaded part of the screw in the timber element [mm]

According to the authors, the above expression, obtained on specimens in which the screw was inserted orthogonally to the grain direction, can be extended to cases in which the screw, subjected to shear and tensile stress yet, forms an inclination angle with the grain lower than 90°.

To confirm that there are also the experimental results obtained by Kevarinmaki (2002), which despite the high dispersion present a standard deviation very low if compared to the theoretical value calculated with the expression previously shown.

Moreover, the same authors performed tests to demonstrate how the angle between the screw and the grain influences little the withdrawal behavior of the screw itself. Below is an image containing the schematization of one of the three tested specimens, called G2 because there are two screws for each shear plane. The other two specimens contain respectively 6 (G6) and 11 (G11) screws for each shear plane.

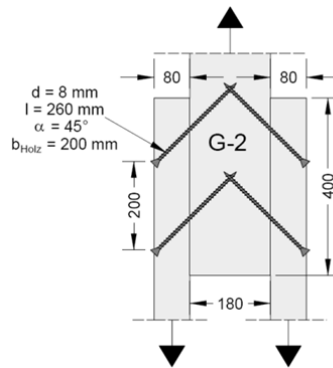


Figure 81: scheme of the tests performed by Blass and Bejtka

The stiffness of system of this type can be determined by the expression (32) of paper [9], below reported:

$$K_{ax} = \frac{1 + \mu \cdot \operatorname{tg} \alpha}{\frac{1}{K_{ax,1}} + \frac{1}{K_{ax,2}}}$$

where:

μ is the friction coefficient

In this case the two elements, joined through the skewed screws, are wood and timber. By assuming an infinite stiffness for the screw when inserted in the concrete element, axial stiffness can be calculated as:

$$K_{ax} = (1 + \mu \cdot \operatorname{tg} \alpha) \cdot K_{ax,1}$$

$K_{ax,1}$ is the axial stiffness of the screw contained in the glulam element

The embedment length l_{ef} of our screw in the glulam element amounts to:

$$l_{ef} = l_{vite} - s_{cls} / \cos \alpha = (250 - 50 / \cos 45^\circ) = 179.3 [\text{mm}]$$

By substituting the values we are able to determine the axial stiffness of the element:

$$K_{ax} = (1 + \mu \cdot \operatorname{tg} \alpha) \cdot K_{ax,1} = \left(1 + 0.4 \times \operatorname{tg} \frac{\pi}{4}\right) \times 10223 = 14312 \left[\frac{N}{\text{mm}}\right]$$

where:

$$K_{ax} = 234 \cdot (\rho \cdot d)^{0.2} \cdot l_s^{0.4} = 234 \times (450 \times 11)^{0.2} \times 179.3^{0.4} = 10223 \left[\frac{N}{\text{mm}}\right]$$

$\mu = 0.4$ is the friction coefficient between timber and concrete according to the German Regulation "Entwurf, Berechnung und Bemessung von Holzbauwerken-Allgemeine Bemessungsregeln für den Hochbau".

In table 4.6 of reference [9] is also shown that this procedure theoretically leads to an underestimation in the evaluation of the stiffness. We don't carry here the above mentioned table to avoid further overloading of the present report, but the ratios between theoretical and experimental stiffness are respectively 66.9% for specimens G2, 65.1% for specimens G6 and 71.4% for specimens G11. This theoretical model leads then to an underestimation of the stiffness value. Therefore, conservatively assuming a value for the underestimation of 70 %, axial stiffness is:

$$K_{ax} = \frac{(1 + \mu \cdot \operatorname{tg} \alpha) \cdot K_{ax,1}}{70\%} = \frac{\left(1 + 0.4 \times \operatorname{tg} \frac{\pi}{4}\right) \times 10223}{0.7} = 20446 \left[\frac{N}{\text{mm}}\right]$$

6.1.1.3 Evaluation of K_{ser}

Once we have obtained both the axial and orthogonal stiffness we are able to estimate the connection stiffness K_{ser} through the previously reported expression.

$$K_{ser} = K_{ax} \cdot \sin \alpha \cdot (\sin \alpha + \mu \cdot \cos \alpha) + K_{lat} \cdot \cos \alpha \cdot (\cos \alpha - \mu \cdot \sin \alpha) = \\ = \left[20446 \times \sin \frac{\pi}{4} \times \left(\sin \frac{\pi}{4} + 0.4 \times \cos \frac{\pi}{4} \right) + 6825 \times \cos \frac{\pi}{4} \times \left(\cos \frac{\pi}{4} - 0.4 \times \sin \frac{\pi}{4} \right) \right] = 16360 \left[\frac{N}{\text{mm}}\right]$$

6.1.1.4 Comparison with the stiffness from reference [1] experimental tests

Let us now compare the just obtained value with those presented in the experimental results reported in Paper [1]. The following image shows the trend of the force-displacement for the first of the two shear tests performed on the same connection type analyzed in this paragraph (T12). These values for the stiffness, evaluated respectively at the SLS (K_{ser}) and at the ULS (K_u) are have been evaluated in agreement with the procedure described in Reference Standard UNI EN 26891 and carried below:

$$K_{ser} = \frac{0.4 \cdot F_{\max}}{\frac{4}{3} \cdot (\nu_{04} - \nu_{01})} = \frac{0.3 \cdot F_{\max}}{(\nu_{04} - \nu_{01})} \qquad K_u = \frac{2}{3} \cdot K_{ser}$$

where:

F_{max} is the maximum load reached during the test

v_{04} is the values of the slip corresponding to 40% of maximum load

v_{01} is the values of the slip corresponding to 10% of maximum load

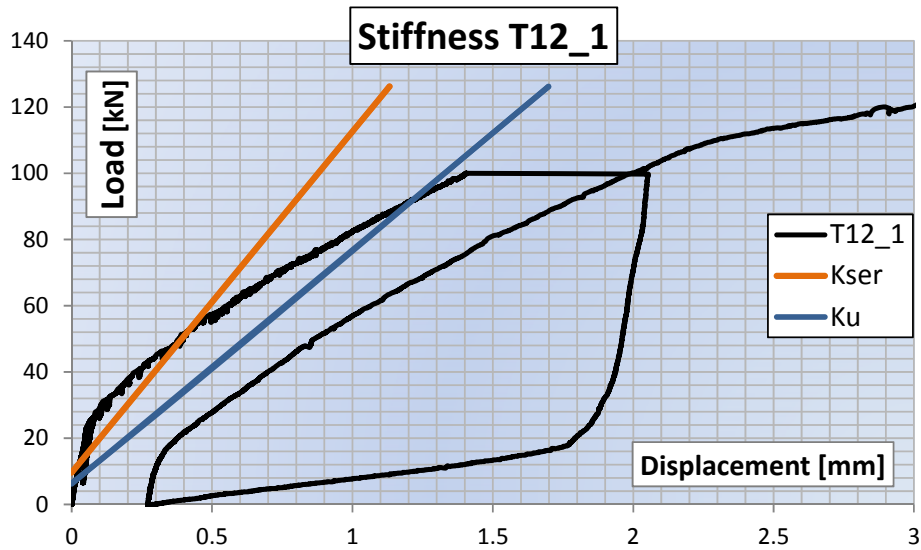


Figure 82: force-displacement graph obtained for the first specimen tested with connection type T12 (reference [1])

By substituting the values obtained for the T12_1 specimen we can get the stiffness:

$$K_{ser, T12_1} = \frac{0.3 \cdot F_{max}}{(v_{04} - v_{01})} = \frac{0.3 \times 126.2}{(0.397 - 0.029)} = 103 \left[\frac{kN}{mm} \right] \quad K_{u, T12_1} = \frac{2}{3} \cdot K_{ser, T12_1} = \frac{2}{3} \times 103 = 69 \left[\frac{kN}{mm} \right]$$

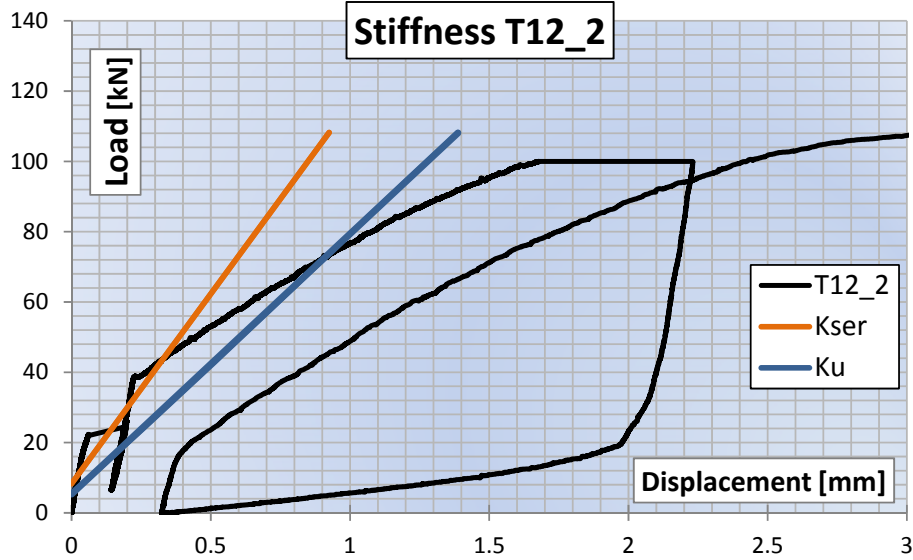


Figure 83: force-displacement graph obtained for the second specimen tested with connection type T12 (reference [1])

By substituting the values obtained for the T12₂ specimen we can get the stiffness:

$$K_{ser,T12_2} = \frac{0.3 \cdot F_{max}}{(v_{04} - v_{01})} = \frac{0.3 \times 108.2}{(0.324 - 0.023)} = 108 \left[\frac{kN}{mm} \right] \quad K_{u,T12_2} = \frac{2}{3} \cdot K_{ser,T12_2} = \frac{2}{3} \times 108 = 72 \left[\frac{kN}{mm} \right]$$

We can now assess the stiffness of the connection system T12, respectively at ULS and at SLS, by calculating an average value:

$$K_{ser,T12} = \frac{(K_{ser,T12_1} + K_{ser,T12_2})}{2} = \frac{(103 + 108)}{2} = 105 \left[\frac{kN}{mm} \right] \quad K_{u,T12} = \frac{2}{3} \cdot K_{ser,T12} = \frac{2}{3} \times 105 = 70 \left[\frac{kN}{mm} \right]$$

Since the connection system T12 is made by three screws, the stiffness of each one is thus:

$$K_{ser,T12,screw} = \frac{K_{ser,T12}}{3} = \frac{105}{3} = 35 \left[\frac{kN}{mm} \right] \quad K_{u,T12,screw} = \frac{2}{3} \cdot K_{ser,T12,screw} = \frac{2}{3} \times 35 = 23 \left[\frac{kN}{mm} \right]$$

Let us now calculate an average value of stiffness, for the connection type T12, through the analysis of the result obtained from paper [1]. We choose to exclude the initial high slope trait (supposedly due to the steel tubes, not considered in the theoretical method).

In order to obtain the stiffness, for both the specimens (T12₁ e T12₂) we can proceed in the following manner:

- we place us in the elastic part and keep two force values F_1 and F_2 so as to exclude the initial high slope branch
- we get the displacement relative to each of the two considered values (d_1 and d_2)
- we obtain the stiffness as the ratio between the load increments and the displacement increments

In order to have more values, we perform the same task with four pairs of values for F_1 and F_2 , both on charge tracks and on re-charge tracks of each one specimen.

First couple of values: $F_1 \approx 60 \text{ KN}$, $F_2 \approx 30 \text{ KN}$

T12_1	F_1 [KN]	F_2 [KN]	d_1 [mm]	d_2 [mm]	K [N/mm]
charge	60.30	29.77	0.569	0.109	66425
re-charge	60.09	30.29	1.067	0.541	56678
T12_2	F_1 [KN]	F_2 [KN]	d_1 [mm]	d_2 [mm]	K [N/mm]
charge	60.28	30.14	0.649	0.204	67879
re-charge	59.91	30.49	1.221	0.621	49101

Whereas the results are referred to the system, consisting of three pipes, the average stiffness for each screw is:

$$K_{ser_60-30} = \frac{1}{3} \cdot \frac{K_{T12_1_carico} + K_{T12_1_ricarico} + K_{T12_2_carico} + K_{T12_2_ricarico}}{4} =$$

$$= \frac{1}{3} \times \frac{66425 + 56678 + 67879 + 49101}{4} \left[\frac{N}{mm} \right] = 20007 \left[\frac{N}{mm} \right]$$

Second couple of values: $F_1 \approx 80 \text{ KN}$, $F_2 \approx 40 \text{ KN}$

T12_1	F_1 [KN]	F_2 [KN]	d_1 [mm]	d_2 [mm]	K [N/mm]
charge	80.02	39.92	0.954	0.224	54999
re-charge	80.23	40.08	1.481	0.699	51384
T12_2	F_1 [KN]	F_2 [KN]	d_1 [mm]	d_2 [mm]	K [N/mm]
charge	79.99	40.01	1.079	0.271	49454
re-charge	80.24	39.09	1.752	0.802	43296

Whereas the results are referred to the system, consisting of three pipes, the average stiffness for each screw is:

$$K_{ser_80-40} = \frac{1}{3} \cdot \frac{K_{T12_1_carico} + K_{T12_1_ricarico} + K_{T12_2_carico} + K_{T12_2_ricarico}}{4} =$$

$$= \frac{1}{3} \times \frac{54999 + 51384 + 49454 + 43296}{4} \left[\frac{N}{mm} \right] = 16594 \left[\frac{N}{mm} \right]$$

Third couple of values: $F_1 \approx 100 \text{ KN}$, $F_2 \approx 50 \text{ KN}$

T12_1	F_1 [KN]	F_2 [KN]	d_1 [mm]	d_2 [mm]	K [N/mm]
charge	99.99	50.05	1.405	0.387	49008
re-charge	100.80	50.01	2.021	0.865	43911
T12_2	F_1 [KN]	F_2 [KN]	d_1 [mm]	d_2 [mm]	K [N/mm]
charge	99.99	50.24	1.679	0.450	40477
re-charge	100.01	50.37	2.426	1.025	35455

Whereas the results are referred to the system, consisting of three pipes, the average stiffness for each screw is:

$$K_{ser_100-50} = \frac{1}{3} \cdot \frac{K_{T12_1_carico} + K_{T12_1_ricarico} + K_{T12_2_carico} + K_{T12_2_ricarico}}{4} =$$

$$= \frac{1}{3} \times \frac{49008 + 43911 + 40477 + 35455}{4} \left[\frac{N}{mm} \right] = 14071 \left[\frac{N}{mm} \right]$$

Fourth couple of values: $F_1 \approx 100 \text{ KN}$, $F_2 \approx 30 \text{ KN}$

T12_1	F_1 [KN]	F_2 [KN]	d_1 [mm]	d_2 [mm]	K [N/mm]
charge	99.99	29.77	1.405	0.109	54174
re-charge	100.80	30.29	2.021	0.541	47632
T12_2	F_1 [KN]	F_2 [KN]	d_1 [mm]	d_2 [mm]	K [N/mm]
charge	99.99	30.14	1.679	0.204	47372
re-charge	100.01	30.49	2.426	0.621	38540

Whereas the results are referred to the system, consisting of three pipes, the average stiffness for each screw is:

$$K_{ser_100-30} = \frac{1}{3} \cdot \frac{K_{T12_1_carico} + K_{T12_1_ricarico} + K_{T12_2_carico} + K_{T12_2_ricarico}}{4} =$$

$$= \frac{1}{3} \times \frac{54174 + 47632 + 47372 + 38540}{4} \left[\frac{N}{mm} \right] = 15643 \left[\frac{N}{mm} \right]$$

6.1.1.5 Stiffness of each screw

We can find the stiffness of each one of the screws of the connection system T12 by averaging the values just obtained. If we substitute these values we have:

$$K_{ser_T12} = \frac{K_{ser_60-30} + K_{ser_80-40} + K_{ser_100-50} + K_{ser_100-30}}{4} =$$

$$= \frac{20007 + 15594 + 14071 + 15643}{4} \left[\frac{N}{mm} \right] = 16329 \left[\frac{N}{mm} \right]$$

This result is in agreement with that obtained using the theoretical method of Blass (and reported at previous paragraph 6.1.1.3 "Evaluation of K_{ser} "), which provided a value for the stiffness of each screw of the connection system type T12 equal to:

$$K_{ser_Blass} = 16360 \left[\frac{N}{mm} \right]$$

6.2 Stiffness of the connection system type F45

The main purpose of this paragraph is to present and analyze the other of the two system used in reference [1] to join the glulam beam to the above fiber reinforced concrete slab, or else the F45, of which we report the image below.

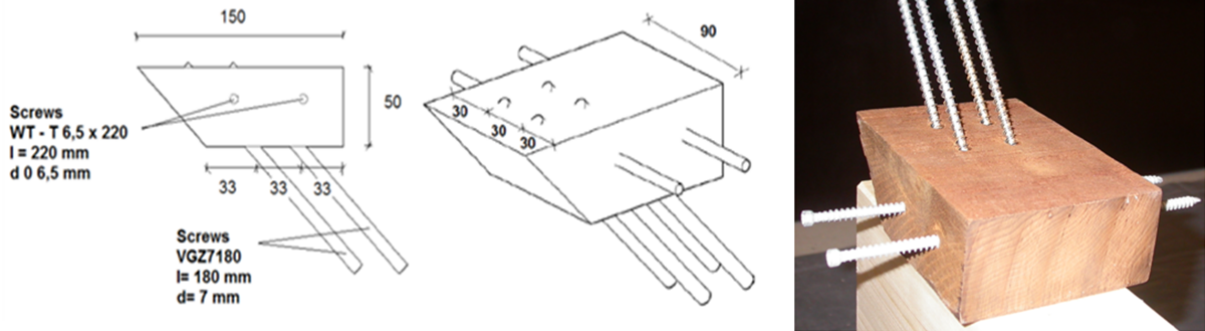


Figure 84: beam to slab connection system type T12

This typology of connection is realized through the use of the furfurylated wood, a kind of material classified as modified wood. This genre of wood is subjected to chemical treatments to improve stability and strength but at the expense of ductility. However, in the end of this process the wood is suitable to be used together with the concrete, and this is due to stability, durability and variation in moisture content consequent the treatment.

The furfurylated wood elements have to be of the same thickness of the concrete slab, and have to be located in formwork before the casting of the concrete in the establishment, as we can see from following figure 83.



Figure 85: furfurylated wood pieces in the formwork (Paper [1])



Figure 86: furfurylated wood pieces in the formwork (tests of this Paper)

Then proceed with the insertion of the screws with an inclination of 45 degrees. Through this procedure is possible to realize a dry system very efficient. The minimum spacing between the screws in the F45 connection of reference [1] (and resulting from Statement [1]) are shown in the table below (Tab. 1 of paper [1]).

Axially loaded screws	
Minimum spacing [mm]	28
Minimum edge distance [mm]	28

The chosen dimensions (indicated in previous figure 82) observe these geometrical disposition. The screws used are VGZ 7x180, with length equal to 180 mm, diameter of the threaded part equal to 7 mm and inner diameter equal to 4.6 mm.

As we can see from following figure 84 the functioning of the system is shear-tensile stress type.

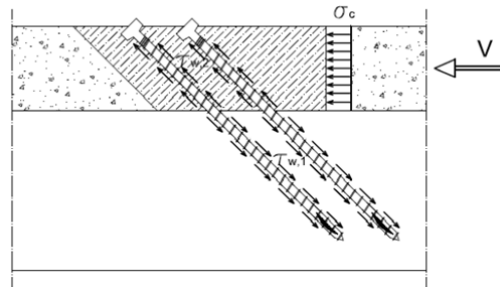


Figure 87: load path of the connection system F45

The shear stress V is passed from concrete slab to furfurylated wood as compressive stress σ_c . This becomes then tangential stress through the four screws, their threaded part and the beam. According to this behavior we can evaluate the stiffness of this type of connection.

One of the main problem in the use of furfurylated wood is its brittle fracture. To avoid it, in each piece are inserted two horizontal screws, useful also in the anchoring of the modified wood element to the concrete slab.

6.2.1 Stiffness evaluation

The goal that we want now is to obtain and verify a theoretical formulation to describe the mechanical behavior of this kind of joint, keeping account both of the modified wood and the inclined screws in terms of stiffness. In this section we refer to paper [9], containing the theories of Bejtka and Blass regarding the behavior of connecting systems with skewed screws and thus subjected to a shear-tensile stress state.

Since this type of connection is not explicitly provided in Statement [2] the stiffness, or instantaneous slip modulus K_{ser} of joints with inclined screws can be determined with the same formulation related to screws inserted perpendicularly to the shear plane, and thus through the following expression of provided by DIN 1052:2004:

$$K_{ser} = \frac{\rho_k^{1.5} \cdot d}{20}$$

- a value of ρ_k determined experimentally through the laboratory tests performed and described in paper [1]

- an effective diameter $d_{ef} = 1.1 \times d_{nucleo}$, where d_{nucleo} is the diameter of the non-threaded part of the screw

The value of K_{ser} presented in this paragraph is defined by using:

- a value of ρ_k that considers the simultaneous presence of two wood wood specimens with different densities, each one in contact with the other. Calling with 1 and 2 respectively the glulam and the modified wood, we assume :

$$\rho_k = \sqrt{\rho_{k,1} \cdot \rho_{k,2}}$$

- an effective diameter $d_{ef} = 1.1 \times d_{nucleo}$, dove d_{nucleo} is the diameter of the non-threaded part of the screw
- counting the presence of four screws in each piece of modified wood (and then multiplying by four the values obtained using the previous formulation)

The previous formulation is valid only for timber to timber joints.

Following figures show the displacement and stress components in the shear plane, according to the inclination angle α that the screws form with the grain direction.

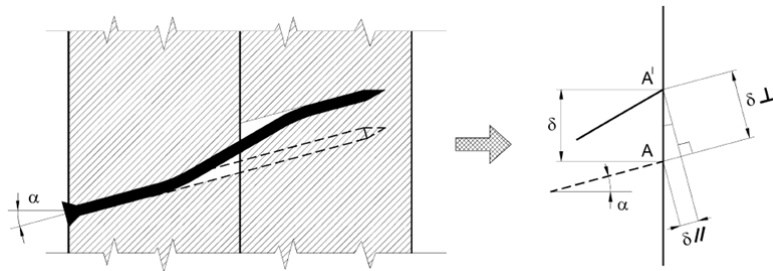


Figure 88: displacement components in the shear plane

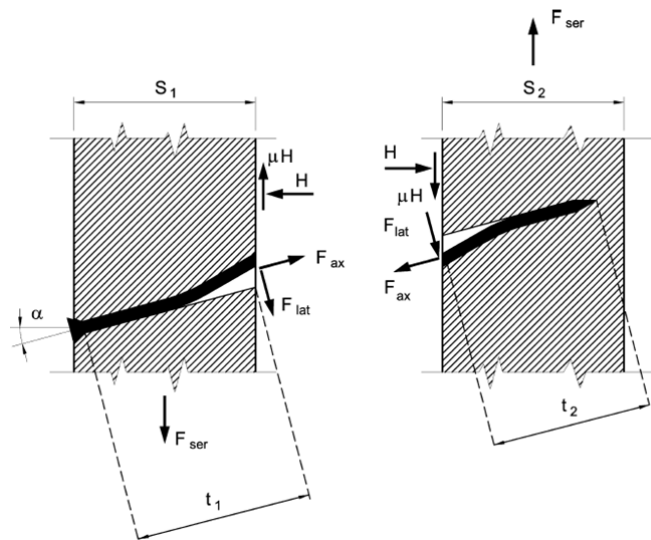


Figure 89: stresses acting in the shear plane

The displacement components δ , with respect to the undeformed configuration of the screw, are:

$$\delta_{\parallel} = \delta \cdot \sin \alpha \quad \delta_{\perp} = \delta \cdot \cos \alpha$$

where δ is the displacement parallel to the shear plane.

If we assume an elastic linear behavior of the screw at the Service Limit State, we can write following equations:

$$F_{ax} = K_{ax} \cdot \delta_{\parallel} \quad F_{lat} = K_{lat} \cdot \delta_{\perp}$$

By imposing now the equilibrium we can obtain:

$$F_{ser} = F_{lat} \cdot (\cos \alpha - \mu \cdot \sin \alpha) + F_{ax} \cdot (\sin \alpha + \mu \cdot \cos \alpha)$$

By substituting the previously reported expressions we can obtain:

$$F_{ser} = K_{ax} \cdot \delta \cdot \sin \alpha \cdot (\sin \alpha + \mu \cdot \cos \alpha) + K_{lat} \cdot \delta \cdot \cos \alpha \cdot (\cos \alpha - \mu \cdot \sin \alpha)$$

Since $K_{ser} = F_{ser} / \delta$, the expression for screws that works in a shear-tensile stress state is:

$$K_{ser} = K_{ax} \cdot \sin \alpha \cdot (\sin \alpha + \mu \cdot \cos \alpha) + K_{lat} \cdot \cos \alpha \cdot (\cos \alpha - \mu \cdot \sin \alpha)$$

where:

K_{lat} indicates the screw lateral stiffness

K_{ax} indicates the screws axial stiffness

μ is the fiction coefficient between the two elements

6.2.1.1 Evaluation of K_{lat}

As previously said, the value for the stiffness orthogonally to the screw is given by following expression:

$$K_{lat} = 4 \cdot \frac{\rho_k^{1.5} \cdot d_{ef}}{20} = 4 \cdot \frac{\rho_k^{1.5} \cdot 1.1 \cdot d_{nucleo}}{20} = 4 \times \frac{636.4^{1.5} \times 1.1 \times 4.6}{20} \left[\frac{N}{mm} \right] = 16247 \left[\frac{N}{mm} \right]$$

where:

$$\rho_k = \sqrt{\rho_{k,1} \cdot \rho_{k,2}} = \sqrt{450 \times 900} \left[\frac{kg}{m^3} \right] = 636.4 \left[\frac{kg}{m^3} \right]$$

6.2.1.2 Evaluation of K_{ax}

For the stiffness in direction parallel to the screw reference [9] suggests to considering separately the contributions of the two (wooden) parts through the following expression:

$$K_{ax} = \frac{1 + \mu \cdot tg \alpha}{1/K_{ser,ax,1} + 1/K_{ser,ax,2}}$$

where:

μ is the fiction coefficient between the two (wooden) elements

In our case one of the two contribution is referred to concrete.

In order to determine the axial stiffness, previous formulations proposed in reference [9] derive from the results of experimental tests conducted on wood specimens joined by a system of screws subjected to a combination of shear and tensile stress. The basis of Blass theory come from elaboration of experimental data obtained by using

screws with diameters contained in a range between 5 and 12 mm, and thus also our 7 mm diameter is within the considered interval. The test instrument through which these experiments were performed is shown in next figure 87.

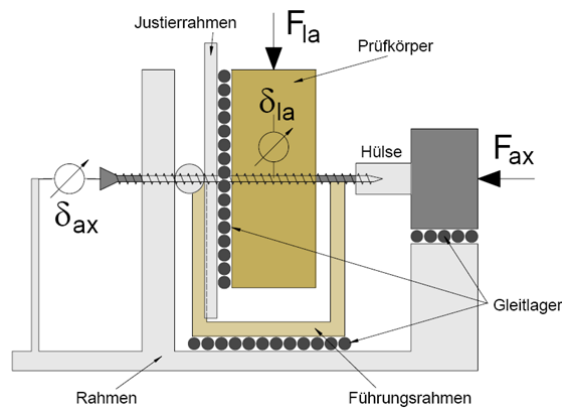


Figure 90: instrument to determine both shear and withdrawal strength

In accordance with a regression multiple analysis performed over the results of tests carried out on a total of more than 400 specimens, the expression obtained for the axial stiffness of the authors (Blass e Bejtka) is as follows:

$$K_{ax} = 234 \cdot (\rho \cdot d)^{0.2} \cdot l_s^{0.4}$$

where:

d is the screw diameter [mm]

ρ is the timber density [kg/m³]

l_s is the embedment length of the threaded part of the screw in the timber element [mm]

According to the authors, the above expression, obtained on specimens in which the screw was inserted orthogonally to the grain direction, can be extended to cases in which the screw, subjected to shear and tensile stress yet, forms an inclination angle with the grain lower than 90°.

To confirm that there are also the experimental results obtained by Kevarinmaki (2002), which despite the high dispersion present a standard deviation very low if compared to the theoretical value calculated with the expression previously shown.

Moreover, the same authors performed tests to demonstrate how the angle between the screw and the grain influences little the withdrawal behavior of the screw itself. Below is an image containing the schematization of one of the three tested specimens, called G2 because there are two screws for each shear plane. The other two specimens contain respectively 6 (G6) and 11 (G11) screws for each shear plane.

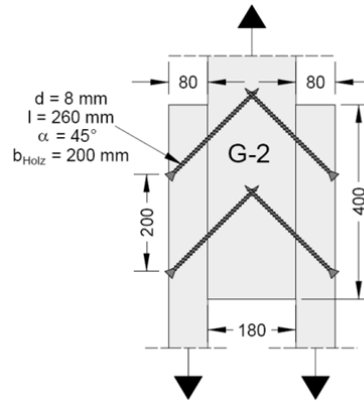


Figure 91: scheme of the tests performed by Blass and Bejtka

The stiffness of system of this type can be determined by the expression (32) of paper [9], below reported:

$$K_{ax} = \frac{1 + \mu \cdot \operatorname{tg} \alpha}{\frac{1}{K_{ax,1}} + \frac{1}{K_{ax,2}}}$$

where:

μ is the friction coefficient

In this case the two elements, joined through the skewed screws, are wood and timber. By assuming an infinite stiffness for the screw when inserted in the concrete element, axial stiffness can be calculated as:

$$K_{ax} = (1 + \mu \cdot \operatorname{tg} \alpha) \cdot K_{ax,1}$$

$K_{ax,1}$ is the axial stiffness of the screw contained in the glulam element

The embedment length l_{ef} of our screw in the glulam element amounts to:

$$l_{ef} = l_{vite} - s_{cls} / \cos \alpha = (180 - 50 / \cos 45^\circ) [mm] = 109.3 [mm]$$

By substituting the values we are able to determine the axial stiffness of the element:

$$K_{ax} = (1 + \mu \cdot \operatorname{tg} \alpha) \cdot K_{ax,1} = \left(1 + 0.4 \times \operatorname{tg} \frac{\pi}{4} \right) \times 30647 \left[\frac{N}{mm} \right] = 42906 \left[\frac{N}{mm} \right]$$

where:

$$K_{ax,1} = 4 \cdot 234 \cdot (\rho \cdot d)^{0.2} \cdot l_s^{0.4} = 4 \times 234 \times (450 \times 7)^{0.2} \times 109.3^{0.4} \left[\frac{N}{mm} \right] = 30647 \left[\frac{N}{mm} \right]$$

$\mu = 0.4$ is the friction coefficient between timber and concrete according to the German Regulation "Entwurf, Berechnung und Bemessung von Holzbauwerken-Allgemeine Bemessungsregeln für den Hochbau".

In table 4.6 of reference [9] is also shown that this procedure theoretically leads to an underestimation in the evaluation of the stiffness. We don't carry here the above mentioned table to avoid further overloading of the

present report, but the ratios between theoretical and experimental stiffness are respectively 66.9% for specimens G2, 65.1% for specimens G6 and 71.4% for specimens G11. This theoretical model leads then to an underestimation of the stiffness value. Therefore, conservatively assuming a value for the underestimation of 70 %, axial stiffness is:

$$K_{ax} = \frac{(1 + \mu \cdot tg \alpha) \cdot K_{ax,1}}{70 \%} = \frac{\left(1 + 0.4 \times tg \frac{\pi}{4}\right) \times 30647}{0.7} \left[\frac{N}{mm} \right] = 61294 \left[\frac{N}{mm} \right]$$

6.2.1.3 Evaluation of K_{ser}

Once we have obtained both the axial and orthogonal stiffness we are able to estimate the connection stiffness K_{ser} through the previously reported expression.

$$K_{ser} = K_{ax} \cdot \sin \alpha \cdot (\sin \alpha + \mu \cdot \cos \alpha) + K_{lat} \cdot \cos \alpha \cdot (\cos \alpha - \mu \cdot \sin \alpha) =$$

$$= \left[61294 \times \sin \frac{\pi}{4} \times \left(\sin \frac{\pi}{4} + 0.4 \times \cos \frac{\pi}{4} \right) + 16247 \times \cos \frac{\pi}{4} \times \left(\cos \frac{\pi}{4} - 0.4 \times \sin \frac{\pi}{4} \right) \right] = 47780 \left[\frac{N}{mm} \right]$$

6.2.1.4 Comparison with the stiffness from reference [1] experimental tests

Let us now compare the just obtained value with those presented in the experimental results reported in Paper [1]. The following image shows the trend of the force-displacement for the first of the two shear tests performed on the same connection type analyzed in this paragraph (F45). These values for the stiffness, evaluated respectively at the SLS (K_{ser}) and at the ULS (K_u) are have been evaluated in agreement with the procedure described in Reference Standard UNI EN 26891 and carried below:

$$K_{ser} = \frac{0.4 \cdot F_{max}}{\frac{4}{3} \cdot (v_{04} - v_{01})} = \frac{0.3 \cdot F_{max}}{(v_{04} - v_{01})} \qquad K_u = \frac{2}{3} \cdot K_{ser}$$

where:

F_{max} is the maximum load reached during the test

v_{04} is the values of the slip corresponding to 40% of maximum load

v_{01} is the values of the slip corresponding to 10% of maximum load

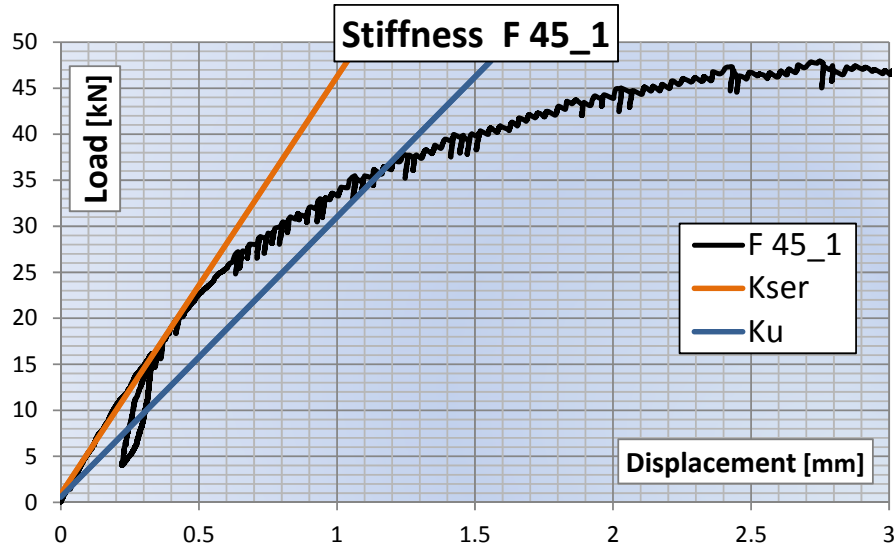


Figure 92: force-displacement graph obtained for the first specimen tested with connection type F45 (reference [1])

By substituting the values obtained for the F45_1 specimen we can get the stiffness:

$$K_{ser, F45_1} = \frac{0.3 \cdot F_{max}}{(\nu_{04} - \nu_{01})} = \frac{0.3 \times 48.0}{(0.403 - 0.086)} = 45 \left[\frac{kN}{mm} \right] \quad K_{u, F45_1} = \frac{2}{3} \cdot K_{ser, F45_1} = \frac{2}{3} \times 45 = 30 \left[\frac{kN}{mm} \right]$$

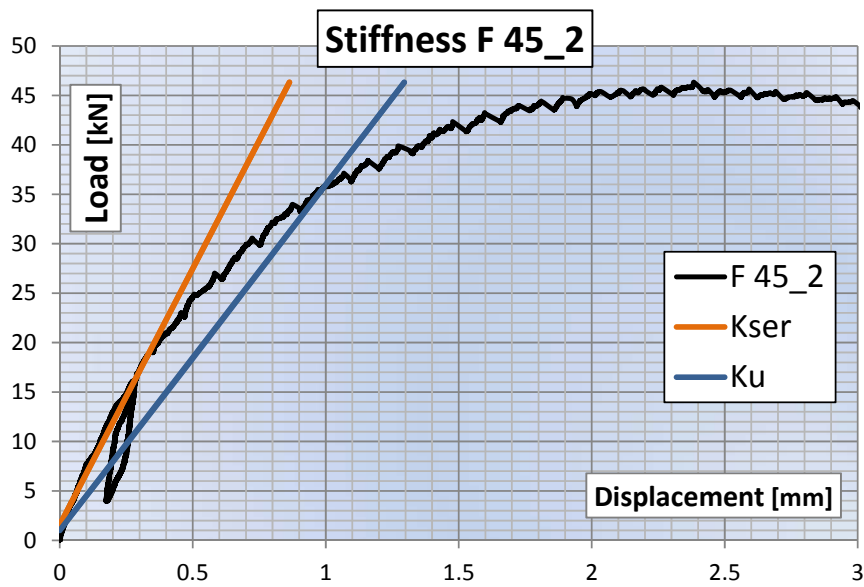


Figure 93: force-displacement graph obtained for the second specimen tested with connection type F45 (reference [1])

By substituting the values obtained for the F45_2 specimen we can get the stiffness:

$$K_{ser, F45_2} = \frac{0.3 \cdot F_{max}}{(\nu_{04} - \nu_{01})} = \frac{0.3 \cdot 46.3}{(0.327 - 0.059)} = 52 \left[\frac{kN}{mm} \right] \quad K_{u, F45_2} = \frac{2}{3} \cdot K_{ser, F45_2} = \frac{2}{3} \cdot 52 = 35 \left[\frac{kN}{mm} \right]$$

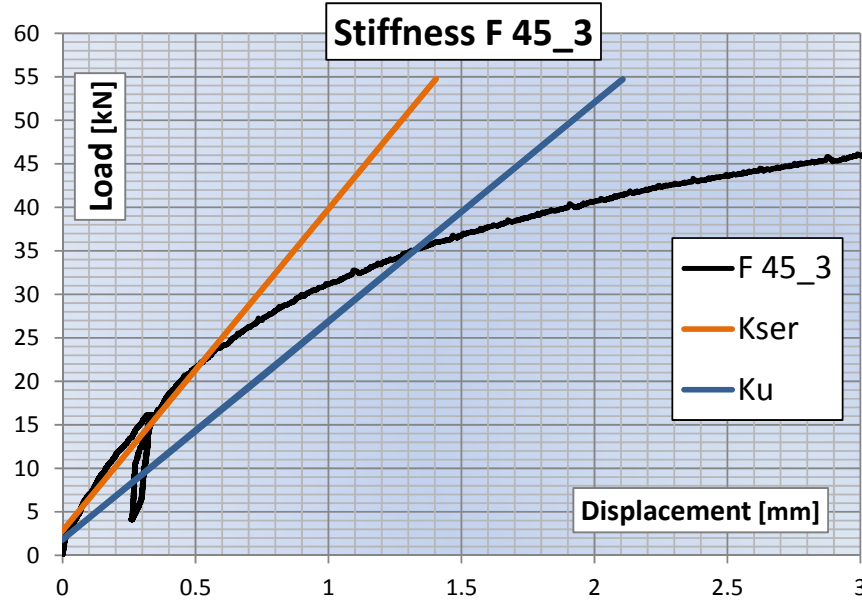


Figure 94: force-displacement graph obtained for the third specimen tested with connection type F45 (reference [1])

By substituting the values obtained for the F45_3 specimen we can get the stiffness:

$$K_{ser, F45_3} = \frac{0.3 \cdot F_{max}}{(\nu_{04} - \nu_{01})} = \frac{0.3 \cdot 54.7}{(0.516 - 0.072)} = 37 \left[\frac{kN}{mm} \right] \quad K_{u, F45_3} = \frac{2}{3} \cdot K_{ser, F45_3} = \frac{2}{3} \cdot 37 = 25 \left[\frac{kN}{mm} \right]$$

We can now assess the stiffness of each piece of modified wood that forms the connection system F45, respectively at ULS and at SLS, by calculating an average value:

$$K_{ser, F45} = \frac{(K_{ser, F45_1} + K_{ser, F45_2} + K_{ser, F45_3})}{3} = \frac{(45 + 52 + 37)}{3} = 45 \left[\frac{kN}{mm} \right]$$

$$K_{u, F45} = \frac{2}{3} \cdot K_{ser, F45} = \frac{2}{3} \cdot 45 = 30 \left[\frac{kN}{mm} \right]$$

6.3 Final values of stiffness

The following summarizing table for both examined connection systems T12 and F45 contains the maximum load reached and the values of the stiffness, obtained by the experimental tests performed and described in reference [1], at the SLS and at the ULS.

<i>Connection system</i>	K_{ser} [kN/mm]	K_u [kN/mm]	F_{max} [kN]
T 12_1	34	23	42
T 12_2	36	24	36
T 12_mean	35	23	39
F 45_1	45	30	48
F 45_2	52	35	46
F 45_3	37	25	55
F 45_mean	45	30	50

7 EXPERIMENTAL TESTS

This chapter presents the experimental shear, bending and dynamic tests program performed on small and full scale specimens.

7.1 Introduction

The experimental tests have been carried out at the laboratory of the Lunds Universitet (Lunds Tekniska Högskola). The experiments included: (i) dynamic tests and (ii) short-time bending tests carried out on two different full-scale specimens. As previously said, since we didn't perform push-out tests, we referred to the results of the experimental research performed and described in Paper [1].

7.2 Shear test program

Shear tests result on which we refer to in this section are described and reported in reference [1].

The aim of the shear test program carried in paper [1] was to investigate the following mechanical parameters of the two type of connection designed for prefabricated timber-concrete composite structures (F45 and T12 previously described): stiffness (slip modulus), shear strength and ductility.

In addition to the investigation of mechanical properties, the feasibility of the proposed prefabrication process was evaluated during the manufacture of the shear test specimens. The connectors used in the tests had mechanical properties ranging from high strength and stiffness with low ductility, to substantially lower strength and stiffness but high ductility. Based on the shear-test results and experience of constructing the specimens two types of shear connectors that appeared to be suitable for the prefabricated timber-concrete composite systems were chosen for further tests.

7.2.1 Test set-up

We are now referring to shear tests performed and described in reference [1], in which direct shear tests were fulfilled on asymmetrical specimens with each of two different connector types F45 and T12, to determine the connectors' load-slip relationships and slip moduli (K_{ser} and K_U), using the experimental set-up illustrated in Fig. 95.

Three specimens were tested with connector type F45 and two specimens were tested with T12. This type of test was chosen because asymmetrical specimens are lighter, cheaper and quicker to construct than symmetric (push-out) specimens, in which the timber beam is connected to two concrete slabs, one on the left- and the other on the right-hand side. A disadvantage of the asymmetrical shear test set-up is that it gives slightly higher estimates of the shear strength and slip modulus than symmetric shear tests (Van der Linden 1999). This is because the overturning moment due to the eccentricity of the axial force results in a compression force at the interface between the concrete and timber, which increases the friction and (thus) improves the apparent mechanical properties of the connection. Calculations based on first principles and the dimensions shown in Fig. 96 indicate that the compression force at the interface between timber and concrete is a sixth of the applied shear force. Hence, assuming a friction coefficient of 0.4 between the timber and concrete, the measured values overestimate true values of strength and slip moduli by ca. 7% (Ceccotti).

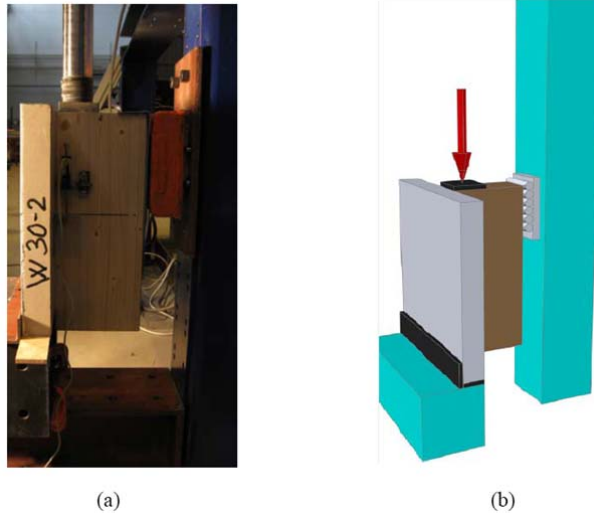


Fig. 95: photo (a) and illustration (b) of test set-up performed in reference [1]

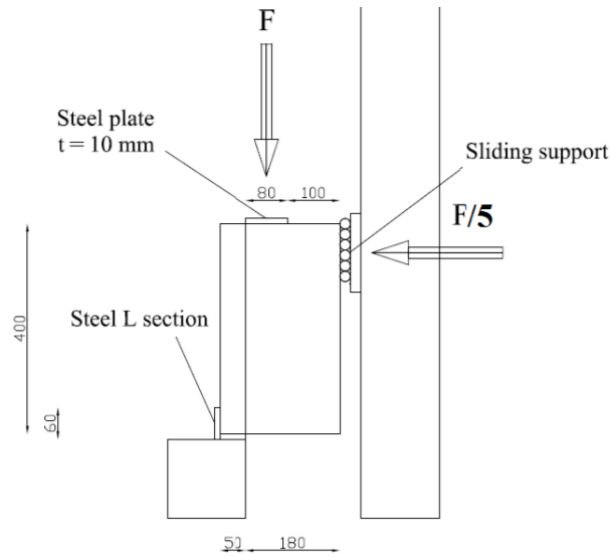


Figure 96: geometry of the test set-up

The load was applied to the wood beam throughout a 10 mm thick steel plate with an area of $80 \times 80 \text{ mm}^2$. The edge of the concrete slab was placed on an L shaped support. A thin strip of fiberboard was placed between the support and the concrete surface in order to distribute the contact stresses evenly. A low friction sliding support was used to minimize the vertical friction force at the upper horizontal support. The relative displacement between the beam and the slab was measured at mid-height of the specimen, at both side of the beam. The load and the displacements were recorded continuously during the test with a frequency of 10 Hz.

The loading procedure was carried out according to EN 26891:1991 [7], see Figure 97. The estimated maximum load, F_{est} , was determined by calculations presented in Appendix 2 of reference [1]. The first load cycle, up to $0.4F_{est}$ and back to $0.1F_{est}$, was carried out in load control and the subsequent loading to failure in displacement control. The load was maintained constant for approximately 30 s between loading and unloading phases.

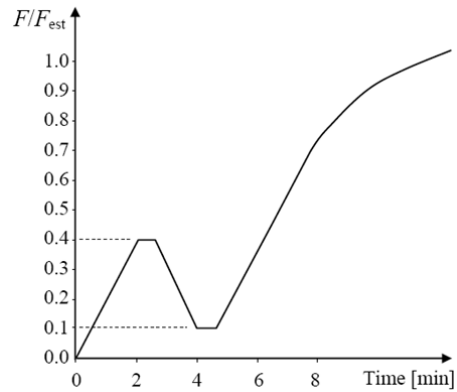


Figure 97: loading procedure

7.2.2 Specimens design and preparation

The specimens were designed based on the findings in the preliminary study presented in Chapter 3 of paper [1]. The geometric properties of the specimens are resumed in Figure 98.

Geometric properties

Slab thickness	5	cm
Slab dimension	40 x 40	cm
Beam height	18	cm
Beam width	9	cm
Beam length	40	cm

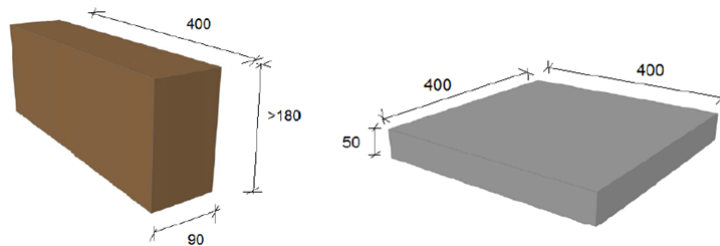


Figure 98: geometry of the specimens

The main processing to obtain the specimens with pieces of wood, F45, are resumed in the next list:

- Cutting pieces of wood with geometry presented in Chapter 6 (“Stiffness of connector system”)
- Pre-drilling pieces where then the screws will be inserted with a drill of 4 mm in diameter
- Inserting transversal screws in the pre-drilled holes (SFS WT-T-6.5 x 190)
- Creating formwork (400 mm x 400 mm x 50 mm)
- Locking pieces of wood in the formwork with provisional screws
- Casting of the concrete
- Cutting of the beam (180 mm x 400 mm x 90 mm)
- Creating the connection by inserting the four screws Rothoblaas VGZ 7 x 180 in the pre-drilled holes
- Painting the specimens of white and applying of black spray to use then ARAMIS system

Instead the main process followed to create the specimens with steel tube connection (T12) are listed below:

- Realization of the steel tubes at the workshop following geometry reported in Chapter 6 (“Stiffness of connector system”)
- Creating formwork (400 mm x 400 mm x 50 mm)
- Locking of the tubes in formwork and insertion of plastic cap to avoid to fill the tubes with the concrete
- Casting of the concrete
- Cutting of the beam (180 mm x 400 mm x 90 mm)
- Creating the connection by inserting the screws Rothoblaas VGS 11 x 250 in the tubes
- Applying a torque moment to the screws equal to 16 KNm
- Painting the specimens of white and applying of black spray to use then ARAMIS system

7.2.3 Optical full-field deformation measurement

Full-field strain measurement was performed on all tested specimens in this study. The commercial non-contact optical deformation measurement system ARAMIS 4M by GOM was used. The system uses a measurement technique based on Digital Image Correlation (DIC) with a stereoscopic camera setup, consisting of two CCD-cameras with 4.0 Mega pixel resolutions (2048 x 2048 pixels). The basic idea behind DIC is to measure the displacement of the specimen under testing by tracking the deformation of a natural occurring, or applied surface speckle pattern in a series of digital images acquired during the loading. This is done by analyzing the displacement of the pattern within discretized pixel subsets or facet elements of the image. In combination with correlation based stereovision technique the measurement of 3D shapes as well as the measurement of 3D displacements fields and surface strain field is possible. The cameras, which are mounted on a rigid bar to avoid relative motion to each other, are placed in front of the specimen at angles and distance that depend on desired measuring volume and the lenses used. In this study the system was calibrated for a measurement volume of approximately 500 x 500 x 500 mm³. In the tests an image pair was captured with a frequency of 1 Hz. In addition, the signals of the load and displacement obtained from the testing machine were recorded also into the ARAMIS system at the same time as each pair of images. The facet size and amount of overlap can be decided by the user on the basis of the spatial resolution and accuracy desired. In this study the facets were 15 x 15 pixels in size and had a two-pixel overlap along the circumference of each facet. This gave a spatial resolution of 13 pixels in the displacement measurement, which for the system set-up employed approximately corresponds to 3.2 mm. The system used in this study is capable of measuring engineering strains from 0.01 up to several 100% with an accuracy of up to 0.01%.

7.2.4 Test results

Push-out tests reported in Paper [1] have been carried out in 2 days. The results in terms of applied force and obtained displacement are shown in the graphs below.

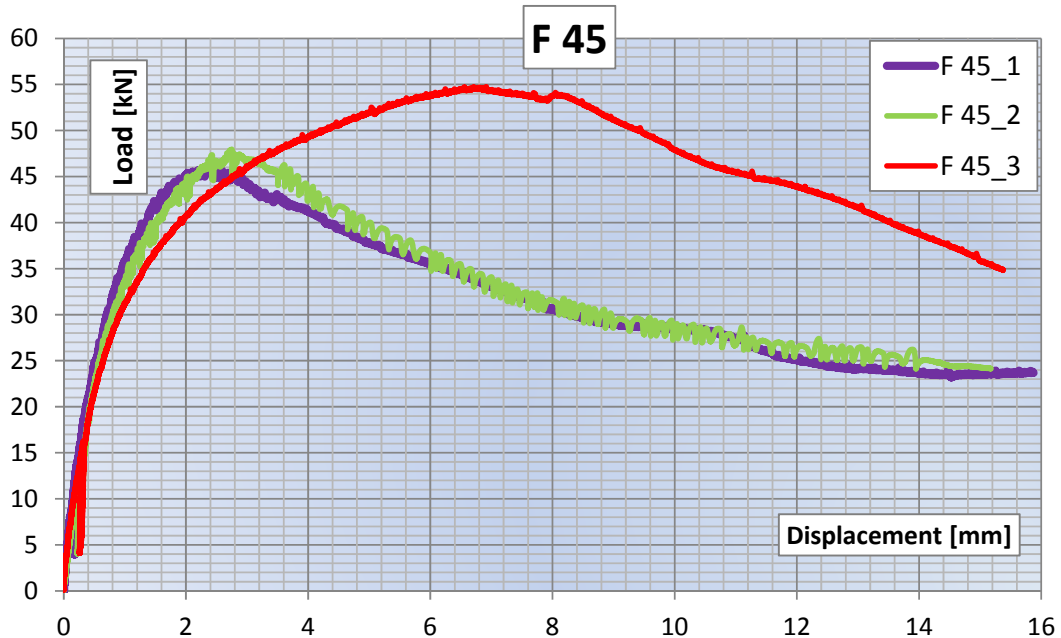


Figure 99: results of the tests on furfurylated wood specimens with (F 45_1, F45_2, F45_3)

The following plots, which represent the results of the tests on the steel tube specimens, should be interpreted taking into account the following aspects. The hydraulic jack used in the tests has a maximum capacity of 120 kN. The load cell used for recording has a capacity of 100 kN. The estimated maximum load was lower than 100 kN but during the tests it was found out that the real ultimate load was greater than this value. During the first load step a value of 120 kN was reached but the recording of the load stopped at 100 kN. After that the specimen was unloaded and led to failure through a hydraulic jack with a greater load capacity. In the plots it can be seen that there is a horizontal plateau at 100 kN due to the reach of the cell load capacity. After this horizontal plateau, the curve continues recovering unloading path of the specimen. Finally, restarting from zero load, the plots follows the path leading to rupture.

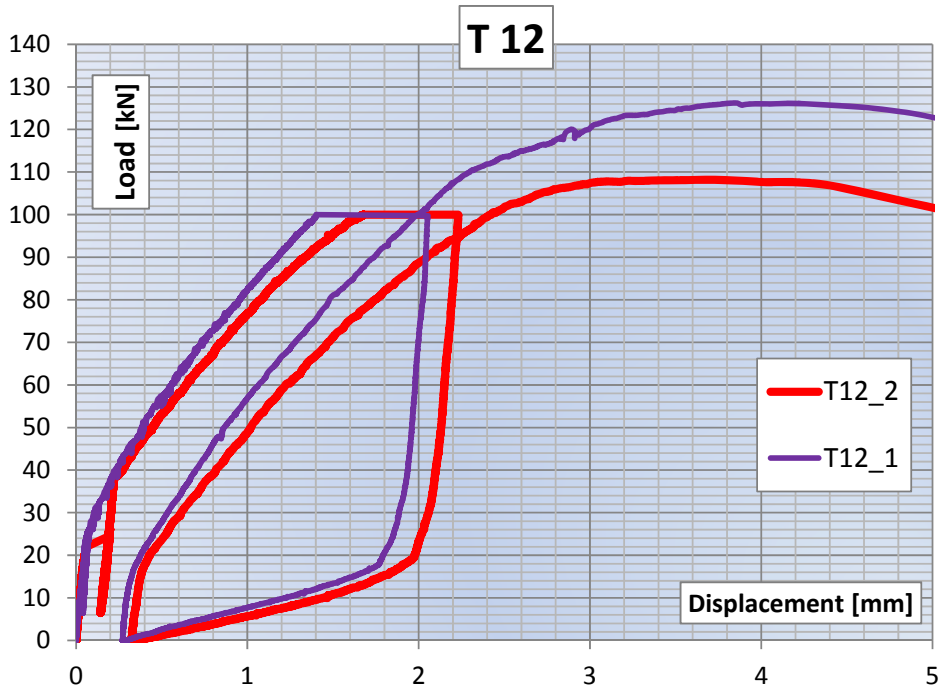


Figure 100: results of the tests of specimens with tubes $d = 12$ mm (T12_1, T12_2)

7.2.5 Results and discussions

In reference [1] were also tested specimens with connector types T14 (steel tubes in which are inserted screws VGS 11 x 250 and filled with mortar) and specimens with normal wood in place of furfurylated wood. The mechanical behavior of the two types of connections that are T12 and T14, are compared in a graph in Reference [1], that we don't show in order to avoid the overloading of this relation. Both of them show similar trends and values of initial stiffness and failure load.

In terms of production of these kind of connections, the tubes of the T14 need also to be filled by mortar during the installation and the mortar must be prepared before. Since both T12 and T14 connections have similar mechanical properties, it seems reasonable to focus on the analysis of type connection T12.

Important indication were achieved with the tests done on the connection made by the piece of furfurylated wood. In the worst conditions, without lateral confinement of the concrete, the furfurylated wood showed no brittle behavior. This leads us to say that this kind of wood, reinforced with transversal screws, is suitable for this type of connection. The use of furfurylated, with respect of normal wood, leads to a better behavior of the connection in term of initial stiffness and maximum achievable load. Due to the higher density of this wood, the failure is moved into the beam below, where the depth of the screw is larger and consequently the maximum load and the stiffness are greater. In conclusion the use of furfurylated wood allows us to get a connection more rigid and more resistant without any brittle behavior.

7.3 Bending tests program

In order to evaluate the mechanical properties and the structural behavior of the composite timber-fiber reinforced concrete system, two bending tests on full scale specimens have been performed. In particular, one experiment has been performed on the model assumed for the office background type while instead the other has been performed on the model related to commercial background type. The specimens tested, representing floor stripes, were constructed and tested to failure.

7.3.1 Specimens design and preparation

The full scale specimens are both made by two glulam GL30 h beams, joined to a fiber reinforced concrete slab with 5 cm thickness, 160 cm depth and length varying according to the floor background type, through the connection systems previously described. The slab is realized by the fiber reinforced concrete described in chapter 1.1 of Appendix 1 ("Fiber reinforced concrete"). Geometrical details are carried below, according to the floor background type.

7.3.2 Bending tests

The bending tests have been performed with the machinery shown on next Figure 101, and in agreement with the scheme reported in Figure 102. The load has been applied on four lines through steel partitioning beams; number and position of these lines have been determined in order to induce in the slab effects (bending moment, maximum shear stress and mid-span deflection) similar to those induced by a uniformly distributed load with same resultant. The force has been applied through an hydraulic jack joined to a reply beam constrained to the laboratory floor, located on axis to the midpoint of the testing beams, and to the partitioning main beam. At the supports and at the load application points have been placed partitioning steel plates 145 mm wide. The supports have been realized through roller, of which one fixed (hinge) and the other allowing longitudinal displacements (roller).

Specimen type	N° specimens	Total length [mm]	Total width [mm]	Connection type	Connection spacing [mm]	Width of the beam [mm]	Depth of the beam [mm]	Beam spacing [mm]
<i>Residential</i>	1	6000	1600	F45	250	90	360	800
<i>Commercial</i>	1	8000	1600	T12	100	90	450	800

Tab. 1: slab samples typologies

In agreement with following Figure 102 the four loads amounting to $P / 4$ (where P is the total load of the composite system, depending on the limit state considered) have to be positioned at a distance (given in function of the slab span L) from one of the two edge of the slab equal to the values carried on following table 2. This values have been determined, as previously said, in order to induce in the slab effects similar to those given by a uniformly distributed load with same resultant.

Values of the load	$P / 4$	$P / 4$	$P / 4$	$P / 4$
Distance from the edge of the slab	$0.125 \cdot L$	$0.375 \cdot L$	$0.625 \cdot L$	$0.875 \cdot L$
Distance from the previous load $P/4$	$0.125 \cdot L$	$0.25 \cdot L$	$0.25 \cdot L$	$0.25 \cdot L$

Tab. 2: positions of the loads



Fig. 101: equipment used to perform the bending tests

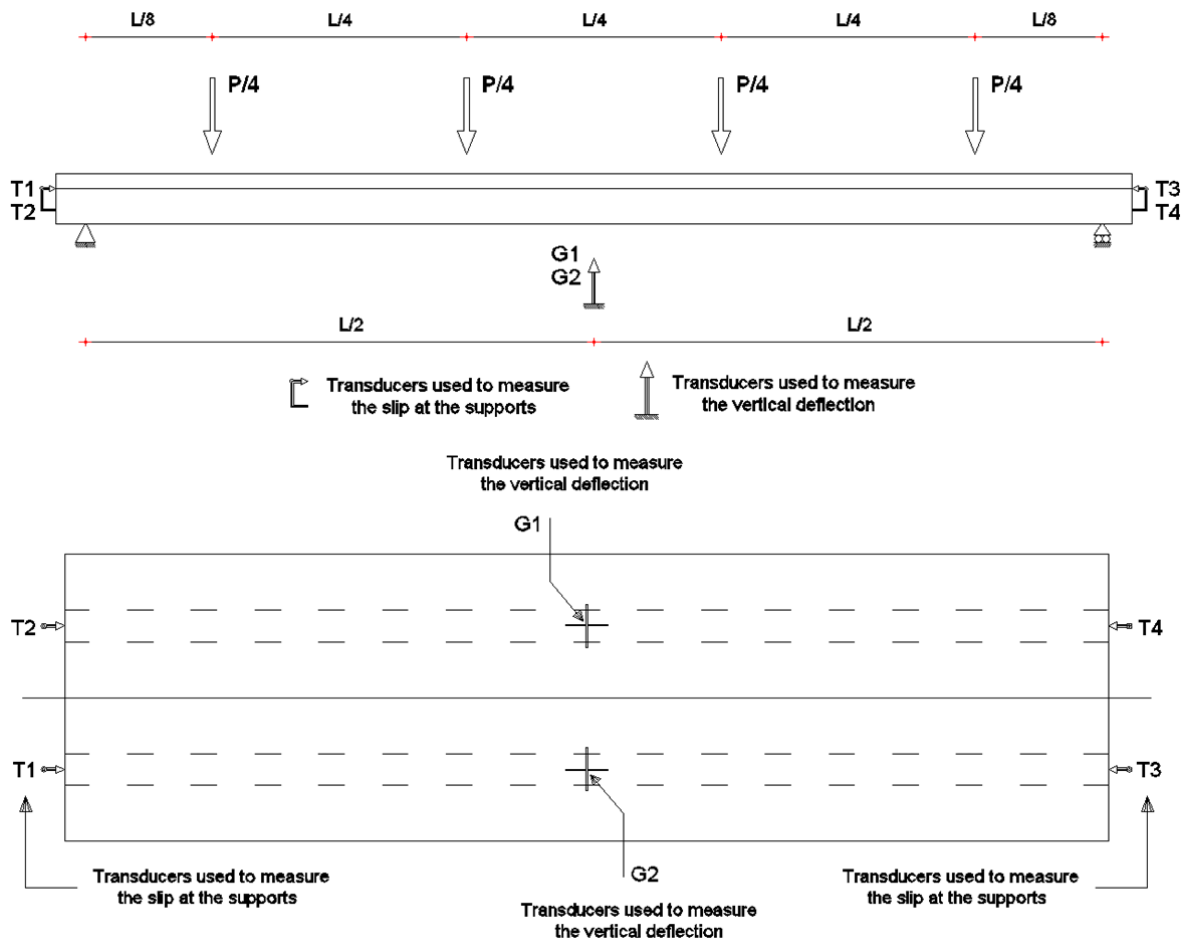


Fig. 102: scheme of the bending test and location of the test instruments

During the experiments have been observed and monitored the total load applied to the specimen, the mid-span deflections (channels G1 and G2) through 2 resistive gauges, and relative slips between slab and beam at the supports (channels T1, T2, T3 e T4) through 4 inductive transducer. The imposed load has been noted through a load cell (with maximum load set in around 500 kN) located between the hydraulic jack and the beam. At the load impressed by the jack must be added the self weight of the partitioning steel beams and joists, equal to the sum of each beam 6.11 kN, corresponding to a uniformly distributed load amounting to 0.48 kN/m² for the commercial background type and to 0.64 kN/m² for the residential background type.

The system of partitioning steel beams is made by one upper HEA 300 with length equal to 5.3 m, two intermediate IPE 160 each one long 2 m and four joists with square section 100 x 100, thickness 5 mm and length equal to 1.6 m. The total self weight of the system is thus:

$$P_{partitioning} = P_{HEA_300} \times 5.3m + 2 \times P_{IPE_160} \times 2m + 4 \times P_{100 \times 100} \times 1.6m =$$

$$= \left(88.3 \frac{kg}{m} \times 5.3m + 2 \times 15.8 \frac{kg}{m} \times 2m + 4 \times 14.4 \frac{kg}{m} \times 1.6m \right) \times g = 6.11 [KN]$$

For each test have been obtained load – slip graphs related to supports and load – deflection, determining also the ultimate load and the slip and deflection values corresponding to fixed load levels.

The maximum load acting on the fastener at the supports have been obtained with the expression $F = V \cdot \gamma_1 \cdot E1 \cdot A1 \cdot a_1 \cdot s_1 / EJ_{ef}$ (for complete discussion go to Chapter 5 “Composite action of timber-concrete composite systems”), determining γ_1 parameter and a_1 e EJ_{ef} values on the basis of stiffness related to Ultimate Limit State, obtained through the experiments described in reference [1].

7.3.2.1 Evaluation of the load P

Experimental tests have been performed according to reference standards UNI EN 26891:1991. For the ULS tests, once we knew the ultimate load of the specimen, P_U (initially estimated on the basis of theoretical evaluations and eventually corrected during the test execution), the following load path has been applied:

- Load increasing until the value $0.4 \cdot P_U$, with an application speed of the load constant and amounting to $0.2 \cdot P_U / min$. Once we arrived at $0.4 \cdot P_U$ the specimen has been kept in this load configuration for 30 s
- Load decreasing until the value $0.1 \cdot P_U$, and maintained constant for 30 s
- Load increasing until the ultimate load or a slip equal to 15 mm; for $P < 0.7 \cdot P_U$ the application speed of the load has been kept constant and amounting to $0.2 \cdot P_U / min$ ($\pm 25\%$), while instead for $P > 0.7 \cdot P_U$ the application speed of the load has been decreased in order to reach the ultimate load, or the 15 mm slip, with an extra-time varying between 3 and 5 minutes ($0.05 \cdot P_U / min$), with the total time for the test amounting to about 10 or 15 minutes.

Anyway, the test has been concluded by reaching the ultimate load and not the slip of 15 mm.

We remember that, in next tables and diagrams, to the load values imposed by the hydraulic jack we must add the self-weight of the partitioning steel beams. In next table 3 we indicate, for each one of the two specimen tested (residential and commercial background type, whose geometric features are reported in previous table 1) the ultimate load P_U estimated. We report two assessment of the ultimate load, depending on the type of failure considered (connection failure or tensile stress in the timber beam).

Specimen type	Total length [mm]	Total width [mm]	Self-weight of the composite system	Self-weight of the partitioning beams	P_U (connection)	P_U (beam)
Residential	6000	1600	12.49 kN	6.11 kN	160	390
Commercial	8000	1600	17.15 kN	6.11 kN	250	460

Tab. 3: ultimate load of the systems

The self-weight of the composite systems are evaluable as:

$$P_{self_weight,RES} = 2 \cdot \left[(g \cdot \rho_{g,k}) \cdot (b_{beam} \cdot h_{beam}) \cdot l + \gamma_{k,FRC} \cdot b_{slab} \cdot h_{slab} \cdot l \right] =$$

$$= 2 \cdot \left[(g \times 390 \times 0.09 \times 0.36 \times 10^{-3} + 22.93 \times 0.80 \times 0.05) \times 6 \right] = 12.49 [KN]$$

$$P_{self_weight,COM} = 2 \cdot \left[(g \cdot \rho_{g,k}) \cdot (b_{beam} \cdot h_{beam}) \cdot l + \gamma_{k,FRC} \cdot b_{slab} \cdot h_{slab} \cdot l \right] =$$

$$= 2 \cdot \left[(g \times 390 \times 0.09 \times 0.45 \times 10^{-3} + 22.93 \times 0.80 \times 0.05) \times 8 \right] = 17.15 [KN]$$

The load due to the self-weight of the partitioning steel beams has been kept into account while performing the experimental tests (the ultimate load obtained by the hydraulic jack was therefore 6.11 KN lower than the real ultimate load of the system).

In the two specimen tested, the ultimate load was due to a first failure of the connection system; after this first failure load one or more restarting of the load have been performed, until the failure of one of the two glulam beams due to bending.

In order to give an evaluation of the ultimate load P_U we operated in the following order:

- we chose a value for the variable uniformly distributed load Q_k in order to reach a value similar to 1 in the strength checking of the connection system (and thus taking account of all the loads, not only permanents)
- we added this value to the load combination at ULS, uniformly distributed per unit area (without considering the weight of the glulam beam)
- we added to the just gotten value the weight of the glulam beam, combined at ULS
- we obtained an esteem for the ultimate load by multiplying this value for the total surface of the slab

For the two specimen tested we proceeded as shown below.

In order to get the ultimate loads on both systems, we used the following mean value for the mechanical properties of the timber GL 30.

$$f_{m,g,m} = 40 [MPa] \quad f_{t,0,g,m} = 35 [MPa] \quad f_{v,g,m} = 4 [MPa]$$

$$E_{0,g,mean} = 12500 [MPa] \quad \rho_{g,m} = 470 [kg/m^3]$$

Residential background type – EC 5 (Statement [3])

Failure of the connection system

By using a value for the variable load amounting to $Q_k = 7.6 \text{ KN/m}^2$ the strength checking (the whole procedure to perform this check is reported on chapter 4.4 of Appendix 1) of the connection system at $t=0$ reaches the following value:

$$\left(\frac{F_{ax,Ed}}{F_{ax,Rd}} \right)^2 + \left(\frac{F_{V,Ed}}{F_{V,Rd}} \right)^2 \approx 1$$

The load combination at ULS, without considering the self-weight of the timber beam (combined at ULS) becomes:

$$P_{slab_RES} = 2 \cdot (\gamma_{G1} \cdot G_1 + \gamma_{G2} \cdot G_2 + \gamma_{Q1} \cdot Q_{K1}) = 2 \cdot (\gamma_{G1} \cdot \gamma_{k,FRC} \cdot h_{slab} + \gamma_{G2} \cdot G_2 + \gamma_{Q1} \cdot Q_{K1}) \cdot l \cdot b =$$

$$= 2 \cdot (1.3 \times 22.93 \times 0.05 + 1.3 \times 2.69 + 1.5 \times 7.6) \times 0.80 \times 6 = 157.32 [KN]$$

The self-weight of the glulam beams combined at ULS is equal to:

$$P_{beam,RES} = 2 \cdot \gamma_{G1} \cdot [(g \cdot \rho_{g,m}) \cdot (b_{beam} \cdot h_{beam}) \cdot l] =$$

$$= 2 \times 1.3 \times [(g \times 470 \times 0.09 \times 0.36 \times 10^{-3}) \times 6] = 2.33 [KN]$$

The estimated ultimate load is therefore:

$$P_{U_RES-EC5} = P_{slab_RES} + P_{beam_RES} = 157.32 + 2.33 \approx 160 [KN]$$

Failure on the wooden beams

By using a value for the variable load amounting to $Q_k = 23.6 \text{ KN/m}^2$ the strength checking (the whole procedure to perform this check is reported on chapter 4.4 of Appendix 1) of the wooden beams at $t=0$ reaches the following value:

$$\frac{\sigma_2}{f_{t,0,d}} + \frac{\sigma_{m2}}{f_{m,d}} \approx 1$$

The load combination at ULS, without considering the self-weight of the timber beam (combined at ULS) becomes:

$$P_{slab_RES} = 2 \cdot (\gamma_{G1} \cdot G_1 + \gamma_{G2} \cdot G_2 + \gamma_{Q1} \cdot Q_{k1}) = 2 \cdot (\gamma_{G1} \cdot \gamma_{k,FRC} \cdot h_{slab} + \gamma_{G2} \cdot G_2 + \gamma_{Q1} \cdot Q_{k1}) \cdot l \cdot b =$$

$$= 2 \times (1.3 \times 22.93 \times 0.05 + 1.3 \times 2.69 + 1.5 \times 23.6) \times 0.80 \times 6 = 387.72 [KN]$$

The self-weight of the glulam beams combined at ULS is equal to:

$$P_{beam,RES} = 2 \cdot \gamma_{G1} \cdot [(g \cdot \rho_{g,m}) \cdot (b_{beam} \cdot h_{beam}) \cdot l] =$$

$$= 2 \times 1.3 \times [(g \times 470 \times 0.09 \times 0.36 \times 10^{-3}) \times 6] = 2.33 [KN]$$

The estimated ultimate load is therefore:

$$P_{U_RES-EC5} = P_{slab_RES} + P_{beam_RES} = 387.72 + 2.33 \approx 390 [KN]$$

Anyway, this value can't be considered real because it doesn't take into account of the fact that the stiffness of the connection system decreases after the failure on the shear connectors.

Commercial background type – EC5 (Statement [3])

By using a value for the variable load amounting to $Q_k = 9.6 \text{ KN/m}^2$ the strength checking (the whole procedure to perform this check is reported on chapter 4.4 of Appendix 1) of the connection system at $t = 0$ reaches the following value:

$$\left(\frac{F_{ax,Ed}}{F_{ax,Rd}} \right)^2 + \left(\frac{F_{V,Ed}}{F_{V,Rd}} \right)^2 \approx 1$$

The load combination at ULS, without considering the self-weight of the timber beam (combined at ULS) becomes:

$$P_{slab_COM} = 2 \cdot (\gamma_{G1} \cdot G_1 + \gamma_{G2} \cdot G_2 + \gamma_{Q1} \cdot Q_{k1}) = 2 \cdot (\gamma_{G1} \cdot \gamma_{k,FRC} \cdot h_{slab} + \gamma_{G2} \cdot G_2 + \gamma_{Q1} \cdot Q_{k1}) \cdot l \cdot b =$$

$$= 2 \times (1.3 \times 22.93 \times 0.05 + 1.3 \times 2.69 + 1.5 \times 9.6) \times 0.80 \times 8 = 248.16 [KN]$$

The self-weight of the glulam beams combined at ULS is equal to:

$$P_{beam,COM} = 2 \cdot \gamma_{G1} \cdot [(g \cdot \rho_{g,m}) \cdot (b_{beam} \cdot h_{beam}) \cdot l] =$$

$$= 2 \times 1.3 \times [(g \times 470 \times 0.09 \times 0.45 \times 10^{-3}) \times 8] = 3.88 [KN]$$

The estimated ultimate load is therefore:

$$P_{U_COM-EC5} = P_{slab_COM} + P_{beam_COM} = 248.16 + 3.88 \approx 252 [KN] \approx 250 [KN]$$

Failure on the wooden beams

By using a value for the variable load amounting to $Q_k = 20.5 \text{ KN/m}^2$ the strength checking (the whole procedure to perform this check is reported on chapter 4.4 of Appendix 1) of the wooden beams at $t=0$ reaches the following value:

$$\frac{\sigma_2}{f_{t,0,d}} + \frac{\sigma_{m2}}{f_{m,d}} \approx 1$$

The load combination at ULS, without considering the self-weight of the timber beam (combined at ULS) becomes:

$$P_{slab_COM} = 2 \cdot (\gamma_{G1} \cdot G_1 + \gamma_{G2} \cdot G_2 + \gamma_{Q1} \cdot Q_{K1}) = 2 \cdot (\gamma_{G1} \cdot \gamma_{k,FRC} \cdot h_{slab} + \gamma_{G2} \cdot G_2 + \gamma_{Q1} \cdot Q_{K1}) \cdot l \cdot b =$$

$$= 2 \times (1.3 \times 22.93 \times 0.05 + 1.3 \times 2.69 + 1.5 \times 20.5) \times 0.80 \times 8 = 457.44 [KN]$$

The self-weight of the glulam beams combined at ULS is equal to:

$$P_{beam,COM} = 2 \cdot \gamma_{G1} \cdot [(g \cdot \rho_{g,m}) \cdot (b_{beam} \cdot h_{beam}) \cdot l] =$$

$$= 2 \times 1.3 \times [(g \times 470 \times 0.09 \times 0.36 \times 10^{-3}) \times 8] = 3.88 [KN]$$

The estimated ultimate load is therefore:

$$P_{U_COM-EC5} = P_{slab_COM} + P_{beam_COM} = 457.44 + 3.88 \approx 461 [KN] \approx 460 [KN]$$

Anyway, this value can't be considered real because it doesn't take into account of the fact that the stiffness of the connection system decreases after the failure on the shear connectors.

7.3.2.2 Other tests performed

In addition to the bending tests until failure, we performed also dynamic tests on both system, with the aim of getting the stiffness of the system and compare it with the one obtained by the push out tests performed and described in Paper [1]. Since there was the possibility, we decided to get the stiffness of both the system not only with the whole connection working, but also with just some screws inserted. With these configurations we also performed a bending test with a reduced load P , equal to a fraction of the ultimate load P_U just evaluated, in order to evaluate the mid-span deflection.

The bending dynamic stiffness, once we knew the eigenfrequency from the accelerogram, could be evaluated by inverting the following relation:

$$f_n = n^2 \cdot \frac{\pi}{2} \cdot \frac{1}{L^2} \cdot \sqrt{\frac{g}{A \cdot \gamma}} \cdot \sqrt{EJ_{dyn}}$$

The accelerometer has been placed in each one of the systems in the middle of the slab, and we excited the system with an hammer in order to induce the vibrations (Fig. 103). With the help of the *FE* software Comsol Multiphysics it has been possible to define which mode of vibration was related with the bending.



Fig. 103: excitation of the system by using an hammer in order to induce vibrations

7.3.2.3 Residential background type

The first test regarded the office background type floor, of which we report the calculation example in Appendix 1. In accordance with following Figure 104 the structure has the following geometrical dimensions.

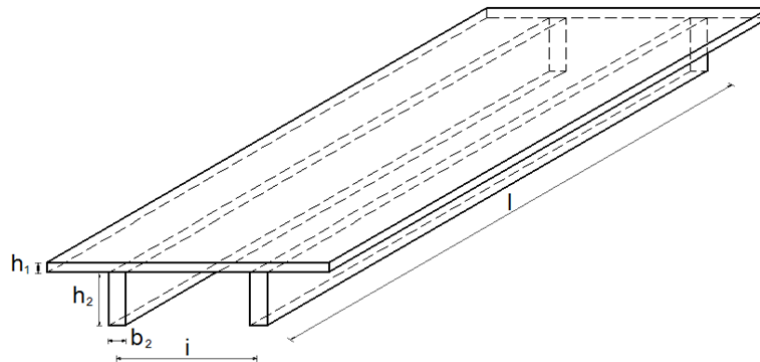


Figure 104: nomenclature indicating some geometrical parameters

l = floor span = length of the concrete slab = length of the glulam beams = 6.00 m

h_1 = thickness of the concrete slab = 50 mm

h_2 = depth of the glulam beams = 360 mm

b_2 = basis of the glulam beams = 90 mm

i = spacing between the glulam beams = 800 mm

The connection typology used for this floor type is the F45 previously described in Chapter 6. The spacing between one furfurylated element and the following amounts to 250 mm, and each modified wood element contains four screws, inclined at 45°. The full description of this system is however presented in Chapter 6 (“Stiffness of the timber-concrete connectors”). In next figure 105 we show the position of the loads and of the transducers used to determine the slip and the deflection, in the full-scale test on the specimen with residential background type.

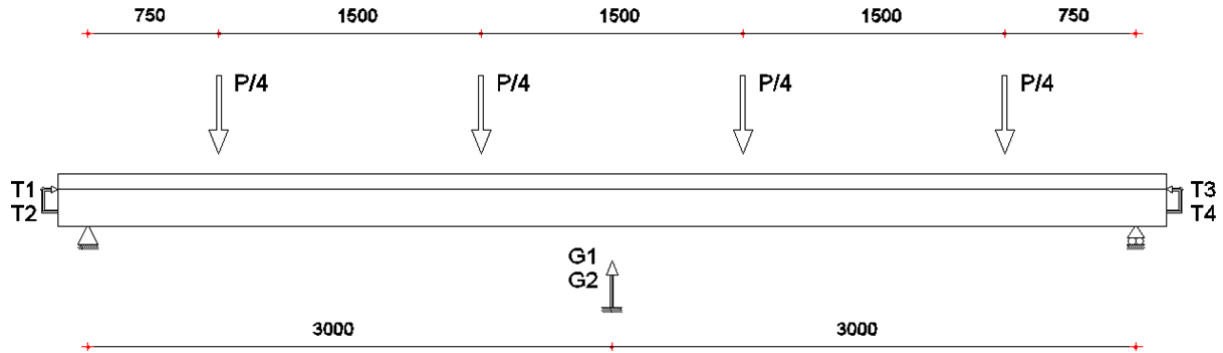


Figure 105: position of the loads and of the transducers on the specimen with residential background type

The load pattern, with referring to the failure of the wooden beam for combined tensile and bending stresses (estimated $P_U \approx 390$ KN), is reported below; to the load applied to the test machine we must take off the self weight of the system and of the partitioning beams (the estimated failure load becomes thus $P_U' = 390 - 6.11 - 12.49 \approx 370$ KN):

- Load increasing until the value $0.4 \cdot P_U = 0.4 \times 370 \approx 150$ KN, with an application speed of the load constant and amounting to $0.2 \cdot P_U/\text{min} = 0.2 \times 370/\text{min} \approx 75$ KN/min. Once we arrived at $0.4 \cdot P_U = 0.4 \times 370 \approx 150$ KN, the specimen has been kept in this load configuration for 30 s
- Load decreasing until the value $0.1 \cdot P_U = 0.1 \times 370 = 35$ KN, and maintained constant for 30 s
- Load increasing until the ultimate load or a slip equal to 15 mm; for $P < 0.7 \cdot P_U = 0.7 \times 370 \approx 260$ KN the application speed of the load has been kept constant and amounting to $0.2 \cdot P_U/\text{min} (\pm 25\%) = 0.2 \times 370/\text{min} (\pm 25\%) \approx 75$ KN/min ($\pm 25\%$), while instead for $P > 0.7 \cdot P_U = 0.7 \times 370 \approx 260$ KN the application speed of the load has been decreased in order to reach the ultimate load, or the 15 mm slip, with an extra-time varying between 3 and 5 minutes ($0.05 \cdot P_U/\text{min} = 0.05 \times 370/\text{min} \approx 18.5$ KN/min), with the total time for the test amounting to about 10 or 15 minutes.

This concrete slab has been cast on December the 17th on the laboratory of the University of Lund (LTH). Before casting the slab we provided the insertion of the connection system F45 on the formwork, as shown in next Figure 106, and the bending test has been performed on February the 14th, exactly 59 days after the casting of the material. The slab has been lifted up in four points, then lowered and made resting on the underlying glulam beams. The lifting check is shown on next Chapter 5 of Appendix 1 (“Lifting check”).

In order to give strength against the self weight during the lifting of the slab, we provided the insertion of some fiber-glass bars along the length of the system (Figure 107). Then the screws already inserted in the furfurylated wooden pieces have been inserted on the glulam beams, until the head of some screws (only the first two wooden pieces in each edge of the timber beams, in order to perform the dynamic tests also in this configuration) was completely inserted on the modified wood elements. In this configuration we provided the transportation of the system under the test machine (Figure 109).



Figure 106: formwork before the casting of the concrete, with the connection system F45

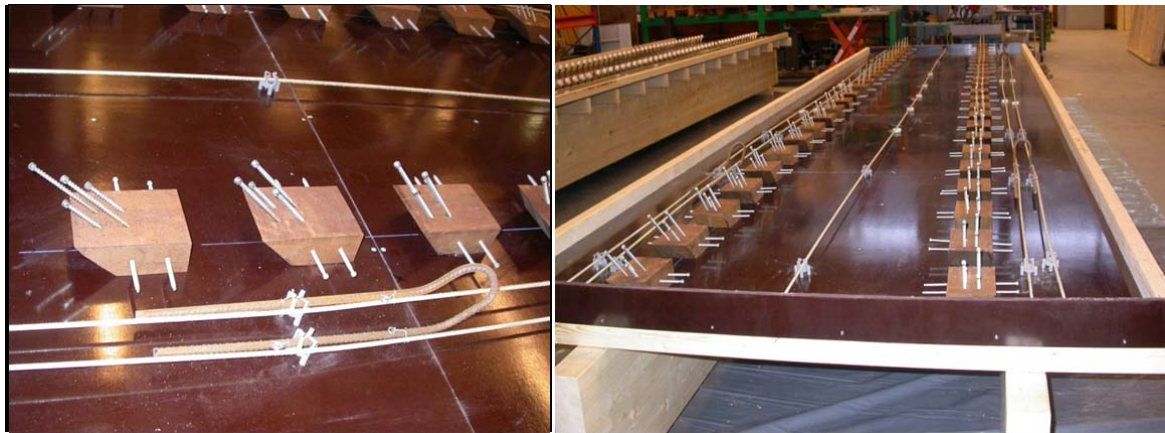


Figure 107: fiber glass bars and hangs to lift-up the slab



Figure 109: lifting-up of the system



Figure 110: residential background type specimen before the bending tests

The ultimate load has been reached by the failure at the bottom of one of the two wooden beams (Figure 113). For a P load, applied by the test machine, amounting to about 300 kN and thus for a q load, uniformly distributed per unit area, equal to about 31 kN/m^2 (the q load is obtained by dividing the P load for the total surface of the slab, $1600 \times 6000 \text{ mm}^2$ – we remember that this has been possible only because we located the partitioning steel beams in the exact positions in order to induce in the system the same results in terms of bending effects of the ones obtained with a uniformly distributed load per unit area with same resultant) both the glulam beams started breaking for compression perpendicular to grain at the fixed supports (Figure 111). This fact is probably due to the indentation consequent to the high pressure and to the fact that the beams couldn't slide and slip but only rotate. Anyway, these breaks did not condition the failure mode of the system (reached for a P load amounting to around 400 kN and a q load of 42 kN/m^2). It's really interesting to notice that, at the failure load, the compressive stress perpendicular to grain, at the supports, was around 7.5 MPa, or else three times the characteristic strength value for a GL 30 (2.5 MPa). The configuration of the cross-section at the supports is shown in following Figure 112.



Figure 111: the timber beams start breaking for compression perpendicular to grain at the fixed support



Figure 112: cross-section of the two timber beams at the fixed supports at the failure load

The failure of the system occurred for a P load, applied by the test machine, equal to 388 kN (or else 405 kN considering the self-weight of the system and of the steel partitioning beams, and thus $q \approx 42 \text{ kN/m}^2$). Suddenly and at the same time two cracks parallel to the grain appeared in one of the two beams (Figure 113). The lower crack was located at the interface between the second and the third lamella (or else to a depth of around 90 mm evaluated from the bottom of the timber beam), while the upper at the end of the pointside penetration length of the screws (or else to a depth of around 110 mm evaluated from the top of the timber beam).

Anyway, even if the failure mode has supposedly been reached for shear, since there is a plateau observable from the load – mid-span deflection trend (that we'll see in next page), we can consider the system as ductile.



Figure 113: one of the timber beams collapsed (failure load)

In next graphs are shown the following curves:

- $q - f$ (load – mid span deflection) in Figure 114
- the real stiffness $EJ_{\text{real}} = 5 \cdot q \cdot L^4 / (f \cdot 384)$ in function of the applied load q in Figure 115, compared with the values of theoretical effective stiffness of the system EJ_{eff} as obtained with the theoretical method for composite sections presented in Annex B of Eurocode 5, infinite stiffness of the connection system (or else system with rigid behavior and full-composite action) EJ_{∞} , and null stiffness of the connection system (or else, stiffness of the system considered without connection, with the slab separated from the underlying timber beam) EJ_0
- the real efficiency of the connection $\eta_{\text{real}} = (EJ_{\text{real}} - EJ_0) / (EJ_{\infty} - EJ_0)$, as proposed by Piazza, in function of the applied load q , compared with the theoretical efficiency $\eta_{\text{eff}} = (EJ_{\text{eff}} - EJ_0) / (EJ_{\infty} - EJ_0)$, Figure 118
- $q - \delta$ (load – slip at the supports) in Figure 119

The parameters needed to define these curves are evaluated in the following lines, with reference to the experimental researches reported in reference [1]. They are assessed with referring to short term conditions ($t = 0$) and to ULS. By assuming the same nomenclature adopted by the Eurocode 5, we have:

$$E_1 \cdot J_1 = E_{cm} \cdot \frac{i \cdot h_1^3}{12} = 36210 \times \frac{800 \times 50^3}{12} = 3.02 \times 10^{11} [Nmm^2]$$

$$E_2 \cdot J_2 = E_{0,mean} \cdot \frac{b_2 \cdot h_2^3}{12} = 12500 \times \frac{90 \times 360^3}{12} = 4.37 \times 10^{12} [Nmm^2]$$

$$E_1 \cdot A_1 = E_{cm} \cdot i \cdot h_1 = 36210 \times 800 \times 50 = 1.45 \times 10^9 [N]$$

$$E_2 \cdot A_2 = E_{0,mean} \cdot b_2 \cdot h_2 = 12500 \times 90 \times 360 = 4.05 \times 10^8 [N]$$

$$(EJ)_0 = E_1 \cdot J_1 + E_2 \cdot J_2 = 3.02 \times 10^{11} + 4.37 \times 10^{12} = 4.68 \times 10^{12} [Nmm^2]$$

$$(EA)_0 = \frac{E_1 \cdot A_1 \cdot E_2 \cdot A_2}{E_1 \cdot A_1 + E_2 \cdot A_2} = \frac{1.45 \times 10^9 \times 4.05 \times 10^8}{1.45 \times 10^9 + 4.05 \times 10^8} = 3.17 \times 10^8 [N]$$

As we saw in previous chapter 6 (“Stiffness of the timber-concrete connectors”), containing the full description of the connection system, we have, for the F45 connection system:

$$K_U = 30000 \text{ N/mm}$$

$$s_{eq} = s = 250 \text{ mm}$$

Thus, by substituting values on the expressions at point B.2 of Eurocode 5, we obtain:

$$\gamma_2 = 1$$

$$\gamma_1 = \left[1 + \pi^2 \cdot E_1 \cdot A_1 \cdot s_{eq} / (K \cdot l^2) \right]^{-1} = \left[1 + \pi^2 \times 1.45 \times 10^9 \times 250 / (30000 \times 6000^2) \right]^{-1} = 0.23$$

$$a = h_1/2 + h_2/2 = (50/2 + 360/2) = 205 \text{ mm}$$

$$a_2 = \frac{\gamma_1 \cdot E_1 \cdot A_1 \cdot a}{\gamma_1 \cdot E_1 \cdot A_1 + \gamma_2 \cdot E_2 \cdot A_2} = \frac{0.23 \times 1.45 \times 10^9}{0.23 \times 1.45 \times 10^9 + 1 \times 4.05 \times 10^8} \times 205 = 93 \text{ mm}$$

$$a_1 = a - a_2 = (205 - 93) = 112 \text{ mm}$$

$$EJ_{ef} = \sum_i E_i J_i + \gamma_2 \cdot E_2 \cdot A_2 \cdot a_2^2 + \gamma_1 \cdot E_1 \cdot A_1 \cdot a_1^2 =$$

$$= (3.02 \times 10^{11} + 4.37 \times 10^{12} + 1 \times 4.05 \times 10^8 \times 93^2 + 0.23 \times 1.45 \times 10^9 \times 112^2) = 1.24 \times 10^{13} [Nmm^2]$$

$$EJ_{\infty} = (EJ)_0 + (EA)_0 \cdot a^2 = (4.68 \times 10^{12} + 3.17 \times 10^8 \times 205^2) = 1.80 \times 10^{13} [Nmm^2]$$

$$\eta = \frac{EJ_{ef} - (EJ)_0}{EJ_{\infty} - (EJ)_0} = \frac{1.24 \times 10^{13} - 4.68 \times 10^{12}}{1.80 \times 10^{13} - 4.68 \times 10^{12}} = 0.58$$

The service loads P_{SER} and $q_{SER} = P_{SER}/A$ amount to:

$$P_{SER} = 2 \cdot (G_1 + G_2 + Q_{K1}) = 2 \cdot [\gamma_{k,FRC} \cdot h_1 \cdot b_1 + (g \cdot \rho_{g,k} \cdot h_2 \cdot b_2) + G_2 \cdot b_1 + Q_{K1} \cdot b_1] \cdot l =$$

$$= 2 \times [22.93 \times 0.05 \times 0.8 + (g \times 390 \times 0.36 \times 0.09 \times 10^{-3}) + 2.69 \times 0.8 + 2.00 \times 0.8] \times 6 = 57.5 [kN]$$

$$q_{SER} = \frac{P_{SER}}{A} = \frac{P_{SER}}{2 \cdot b_1 \cdot l} = \frac{57.5}{2 \times 0.8 \times 6} = 6 \left[\frac{kN}{m^2} \right]$$

With referring to this value of load we can get from the following curve in Figure 115:

$$EJ_{real} = 1.60 \times 10^{13} [Nmm^2]$$

By substituting values we can get the efficiency of the connection, related to the service load:

$$\eta_{real} = \frac{EJ_{real} - (EJ)_0}{EJ_{\infty} - (EJ)_0} = \frac{1.60 \times 10^{13} - 4.68 \times 10^{12}}{1.80 \times 10^{13} - 4.68 \times 10^{12}} = 0.85$$

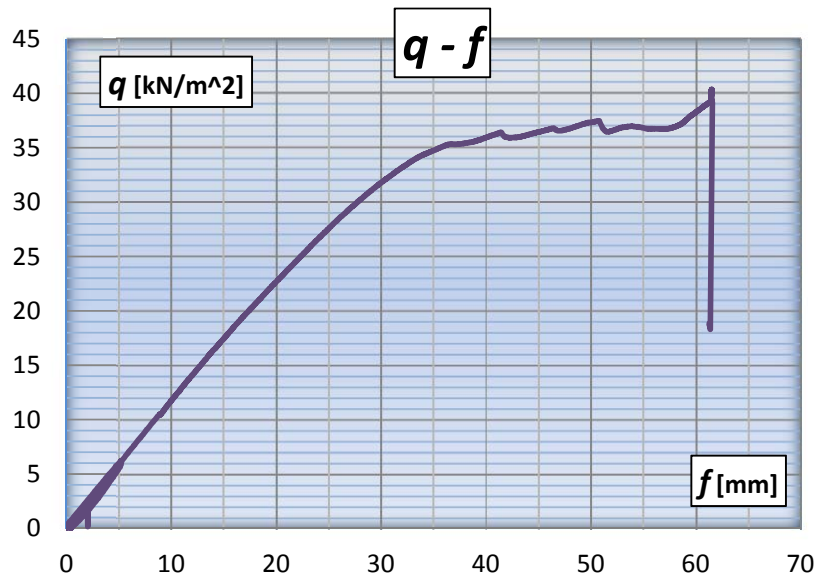


Figure 114: load-mid span deflection curve

The load-carrying capacity of the system is really high (the ultimate load is higher than 40 kN/m² and the service load, usually assessed as 60% of the failure load, is around 24 kN/m², while a normal residential or commercial floor seldom goes over 8-10 kN/m². We remember that to these value of load q we must add the weight of the reply steel beams.

As previously said, even if the failure was supposedly due to shear, since there is a sort of plateau clearly observable from the trend load – mid-span deflection, the behavior of the system can be considered as ductile.

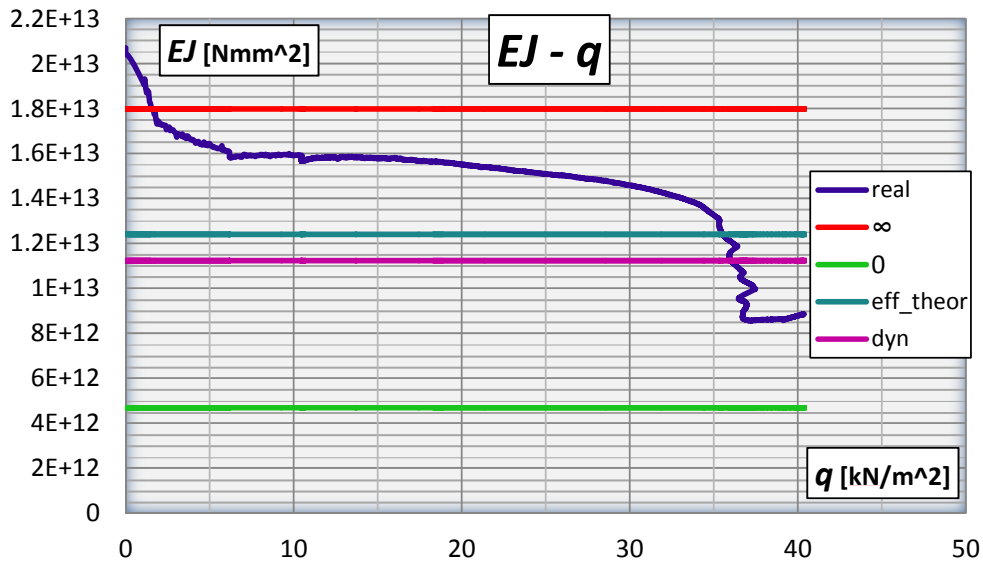


Figure 115: bending stiffness of the system, compared with the theoretical cases of $k=0$ and $k=\infty$, and with both the effective and dynamic stiffness

As we can see, the real stiffness is higher than the effective one. This is supposedly due to the fact that the push-out tests described in Paper [1] have been performed by using for each specimen only one piece of furfurylated wood, and also without the benefit of the surrounding concrete and the transversal screws. In this case, in addition to the transversal screws and the confinement by the concrete, we can think that the effective numbers of connections inserted is higher than the real number, and this is probably due to the high compression applied on the system and thus to the increased friction between the elements (slab and beams).

We can also see that the dynamic stiffness (violet line) is a bit lower than the static one, and this could be due to the fact that the connections don't lead the system to a full-composite action.

The dynamic stiffness has been evaluated by inverting the following expression, referred to the eigenfrequency:

$$f_n = n^2 \cdot \frac{\pi}{2} \cdot \frac{1}{L^2} \cdot \sqrt{\frac{g}{A \cdot \gamma}} \cdot \sqrt{EJ_{dyn}}$$

Once we knew from the *FE* software Comsol Multiphysics that the first vibration mode is the one related to the bending of the system (Figure 117), and the eigenfrequency of the system from the accelerogram, $f_1 \approx 14$ Hz, (Figure 118) we can obtain the dynamic stiffness by inserting $n = 1$ in the previous formulation:

$$EJ_{dyn} = f_n^2 \cdot \left(\frac{2}{\pi}\right)^2 \cdot \frac{L^4}{n^4} \cdot \frac{A \cdot \gamma}{g} =$$

$$= 14^2 \times \left(\frac{2}{\pi}\right)^2 \times \frac{6000^4}{1^4} \times \frac{22.93 \times 50 \times 800 \times 10^{-6} + (390 \times 9.81) \times 90 \times 360 \times 10^{-9}}{9.81} \times 10^{-3} = 1.12 \times 10^{13} [Nmm^2]$$

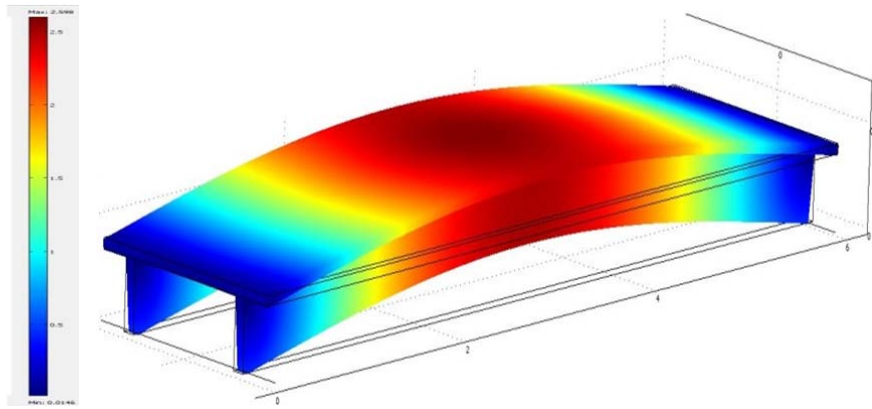


Figure 116: first mode of vibration of the system, related to bending

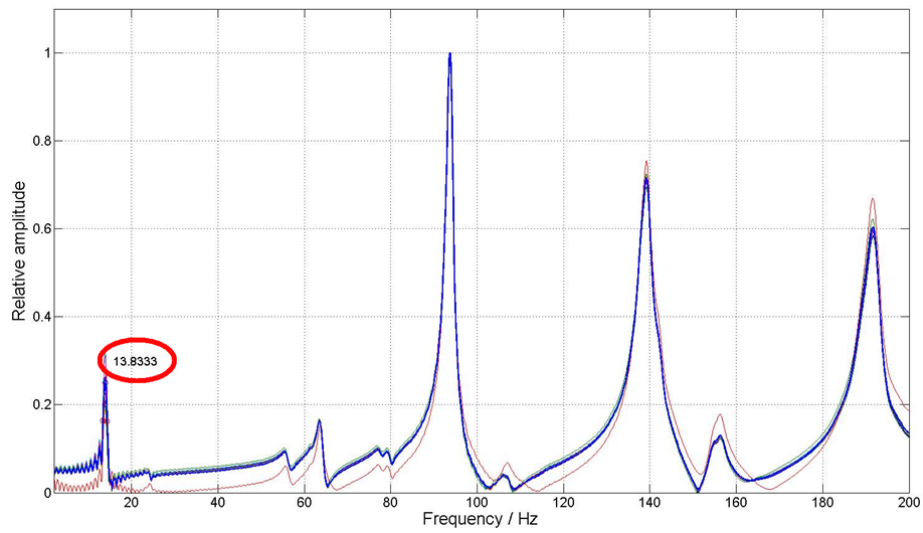


Figure 117: accelerogram of the system, showing the eigenfrequencies related to the relative waving amplitude

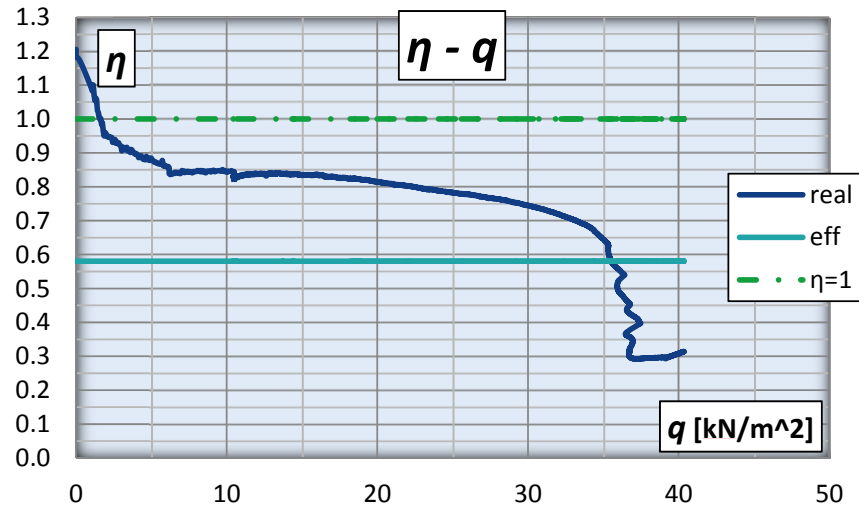


Figure 118: efficiency, real and effective, of the system

The real efficiency of the system, with the same trend of the stiffness, is higher than the effective one and we can see that, for normal service load (always lower than 8-10 kN/m²), we have almost 85% of the full-composite action.

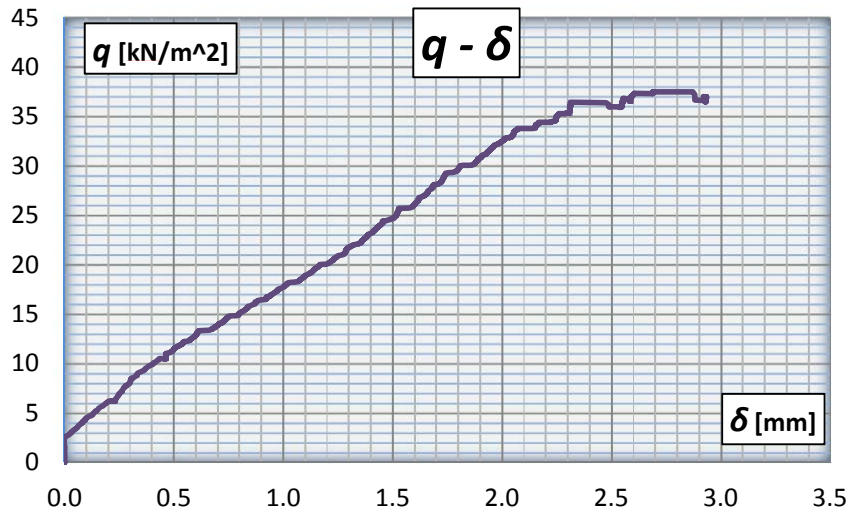


Figure 119: load – slip trend

This graph shows the trend of the relative slip between the concrete slab and the timber beams, in function of the load. We can see that, as direct consequence of the rigidity of the shear connectors, the values of slip are almost null (at the failure load we have around 3 mm while for a normal floor load we have less than 1 mm).

We remember that to these value of load q we must add the self-weight of the system and the weight of the reply steel partitioning beams.

In next table we show the stiffness EJ_{real} and the efficiency of the system, with referring to the service load previously evaluated $q_{SER} = 6 \text{ kN/m}^2$, and compared with the theoretical values obtained by using the experimental researches described in reference [1].

<i>real values</i>		<i>theoretical values</i>	
$EJ_{real} \text{ [Nmm}^2\text{]}$	η_{real}	$EJ_{ef} \text{ [Nmm}^2\text{]}$	η
1.60×10^{12}	0.85	1.24×10^{13}	0.58

Conclusions

This system can be considered highly resistant, by referring to normal floor-loads at SLS, and the best result obtained from this experimental research performer on the slab with the F 45 shear connectors concerns about the huge stiffness of the system, whose efficiency is near to 1 (0,85) and that can be regarded as almost rigid.

7.3.2.4 Commercial background type

Second test regarded the commercial background type floor. In accordance with following Figure 120 the structure has the following geometrical dimensions.

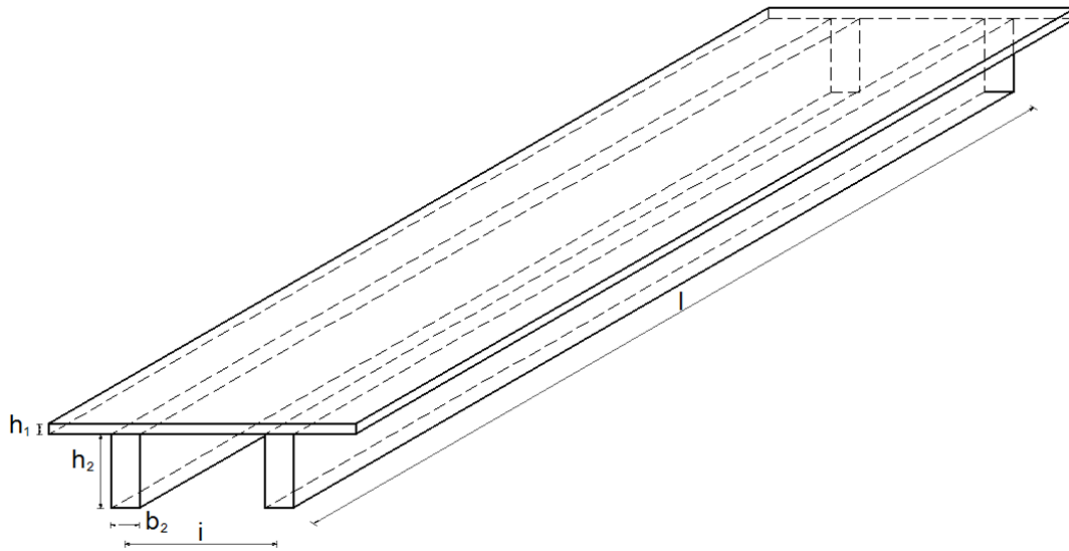


Figure 120: nomenclature indicating some geometrical parameters

l = floor span = length of the concrete slab = length of the glulam beams = 8.00 m

h_1 = thickness of the concrete slab = 50 mm

h_2 = depth of the glulam beams = 450 mm

b_2 = basis of the glulam beams = 90 mm

i = spacing between the glulam beams = 800 mm

The connection typology used for this background type is the T12 previously described in Chapter 5 (“Stiffness of the timber-concrete connectors”). The spacing between the screws, which are VGS 11x250, varies between a minimum value of 8 cm in the tract that extends from supports to a distance of 2.4 m from supports themselves, and a value of 10 cm at the central remaining tract. The full description of this system is however presented in Chapter 6 (“Stiffness of the timber-concrete connectors”). In next figure 121 we show the position of the loads and of the transducers used to determine the slip and the deflection on the specimen with commercial background type.

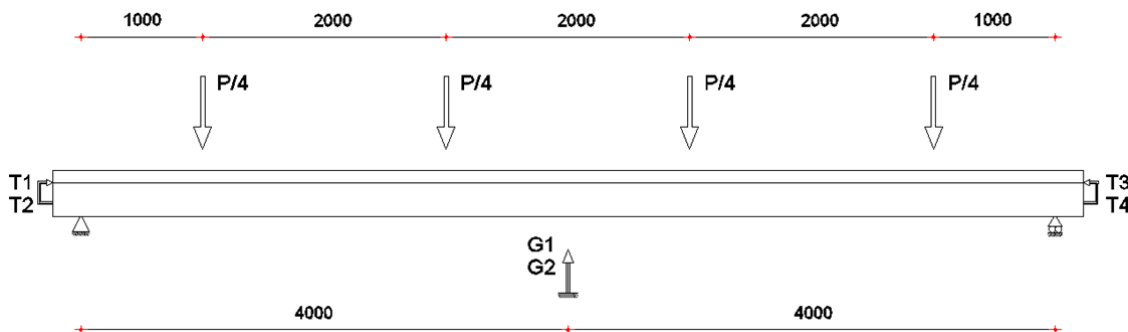


Figure 121: position of the loads and of the transducers on the specimen with commercial background type

The load pattern, with referring to the failure of the wooden beam for combined tensile and bending stresses (estimated $P_U \approx 460$ KN), is reported below; to the load applied to the test machine we must take off the self weight of the system and of the partitioning beams (the estimated failure load becomes thus $P_U' = 460 - 6.11 - 12.49 \approx 440$ KN):

- Load increasing until the value $0.4 \cdot P_U = 0.4 \times 440 \approx 180$ KN, with an application speed of the load constant and amounting to $0.2 \cdot P_U/\text{min} = 0.2 \times 440/\text{min} \approx 90$ KN/min. Once we arrived at $0.4 \cdot P_U = 0.4 \times 440 \approx 180$ KN, the specimen has been kept in this load configuration for 30 s
- Load decreasing until the value $0.1 \cdot P_U = 0.1 \times 440 \approx 45$ KN, and maintained constant for 30 s
- Load increasing until the ultimate load or a slip equal to 15 mm; for $P < 0.7 \cdot P_U = 0.7 \times 440 \approx 310$ KN the application speed of the load has been kept constant and amounting to $0.2 \cdot P_U/\text{min} (\pm 25\%) = 0.2 \times 440/\text{min} (\pm 25\%) \approx 90$ KN/min ($\pm 25\%$), while instead for $P > 0.7 \cdot P_U = 0.7 \times 440 \approx 310$ KN the application speed of the load has been decreased in order to reach the ultimate load, or the 15 mm slip, with an extra-time varying between 3 and 5 minutes ($0.05 \cdot P_U/\text{min} = 0.05 \times 440/\text{min} \approx 20$ KN/min), with the total time for the test amounting to about 10 or 15 minutes.

This concrete slab has been cast on December the 17th on the laboratory of the University of Lund (LTH). Before casting the slab we provided the insertion of the connection system T 12 on the formwork, as shown in next Figure 122, and the bending test has been performed on February the 18th, exactly 63 days after the casting of the material. Like for the system with the F 45 shear connectors, the slab has been lifted up in four points, then lowered and made resting on the underlying glulam beams. The lifting check is shown on next Chapter 5 of Appendix 1 (“Lifting check”).

In order to give strength against the self weight during the lifting of the slab, we provided the insertion of some fiber-glass bars along the length of the system (Figure 123). Then only some screws have been inserted in the pipes and in the underlying glulam beams (only the first five screws in each edge of the timber beams, in order to perform the dynamic tests also in this configuration). In this configuration we provided the transportation of the system under the test machine.



Figure 122: formwork before the casting of the concrete, with the connection system T12



Figure 123: fiber glass bars and hangs to lift-up the slab

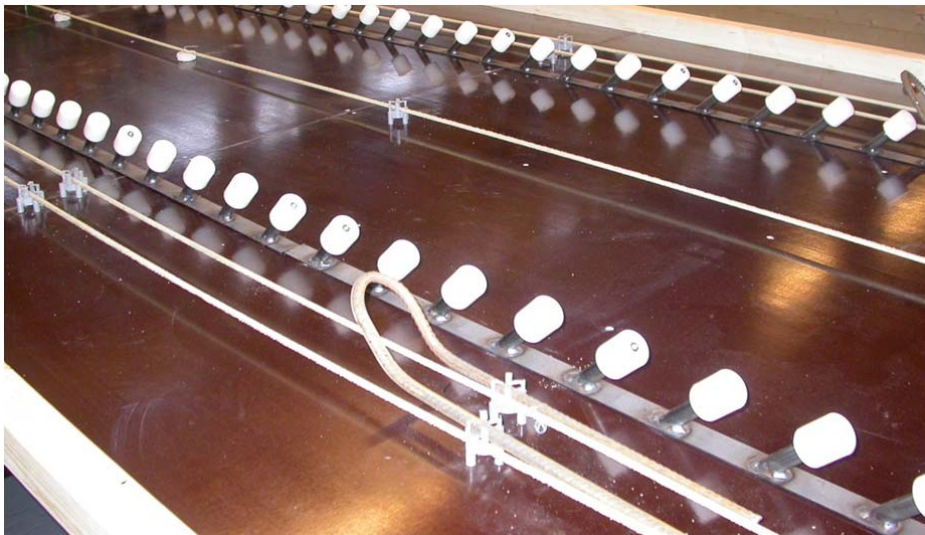


Figure 124: particular of one hang to lift-up the slab



Figure 125: commercial background type specimen before the bending tests

The ultimate load has been reached by the failure at the bottom of both the wooden beams for combined tensile and bending stress. For a P load, applied by the test machine, amounting to about 285 kN and thus for a q load, uniformly distributed per unit area, equal to about 24 kN/m² (the q load is obtained by dividing the sum of the P load applied by the test machine, the self-weight of the system and the self-weight of the steel partitioning beams for the total surface of the slab, 1600x8000 mm² – we remember that this has been possible only because we located the partitioning steel beams in the exact positions in order to induce in the system the same results in terms of bending effects of the ones obtained with a uniformly distributed load per unit area with same resultant) in one of the two beams one finger joint broke, in the lowest lamella (Figure 126).



Figure 126: first failure of the system, due to the breaking of one finger joint in one timber beam

After this first failure, the P load decreased until a value of about 245 kN, and then has been increased again until the collapse of the system: for a P load amounting to about 300 kN, and thus $q \approx 25$ kN/m², in the other beam one knot broke in the lowest lamella (Figure 127).



Figure 127: second and final failure of the system, due to the breaking of one knot in the other timber beam

In next graphs are shown the following curves:

- $q - f$ (load – mid span deflection) in Figure 128
- the real stiffness $EJ_{\text{real}} = 5 \cdot q \cdot L^4 / (f \cdot 384)$ in function of the applied load q in Figure 129, compared with the values of theoretical effective stiffness of the system EJ_{eff} as obtained with the theoretical method for composite sections presented in Annex B of Eurocode 5, infinite stiffness of the connection system (or else system with rigid behavior and full-composite action) EJ_{∞} , and null stiffness of the connection system (or else, stiffness of the system considered without connection, with the slab separated from the underlying timber beam) EJ_0
- the real efficiency of the connection $\eta_{\text{real}} = (EJ_{\text{real}} - EJ_0) / (EJ_{\infty} - EJ_0)$, as proposed by Piazza, in function of the applied load q , compared with the theoretical efficiency $\eta_{\text{eff}} = (EJ_{\text{eff}} - EJ_0) / (EJ_{\infty} - EJ_0)$, Figure 132
- $q - \delta$ (load – slip at the supports) in Figure 133

The parameters needed to define these curves are evaluated in the following lines, with reference to the experimental researches reported in reference [1]. They are assessed with referring to short term conditions ($t = 0$) and to ULS. By assuming the same nomenclature of previous Figure xx (the same adopted by the Eurocode 5), we have:

$$E_1 \cdot J_1 = E_{cm} \cdot \frac{i \cdot h_1^3}{12} = 36210 \times \frac{800 \times 50^3}{12} = 3.02 \times 10^{11} [Nmm^2]$$

$$E_2 \cdot J_2 = E_{0,mean} \cdot \frac{b_2 \cdot h_2^3}{12} = 12500 \times \frac{90 \times 450^3}{12} = 8.54 \times 10^{12} [Nmm^2]$$

$$E_1 \cdot A_1 = E_{cm} \cdot i \cdot h_1 = 36210 \times 800 \times 50 = 1.45 \times 10^9 [N]$$

$$E_2 \cdot A_2 = E_{0,mean} \cdot b_2 \cdot h_2 = 12500 \times 90 \times 450 = 5.06 \times 10^8 [N]$$

$$(EJ)_0 = E_1 \cdot J_1 + E_2 \cdot J_2 = 3.02 \times 10^{11} + 8.54 \times 10^{12} = 8.84 \times 10^{12} [Nmm^2]$$

$$(EA)_0 = \frac{E_1 \cdot A_1 \cdot E_2 \cdot A_2}{E_1 \cdot A_1 + E_2 \cdot A_2} = \frac{1.45 \times 10^9 \times 5.06 \times 10^8}{1.45 \times 10^9 + 5.06 \times 10^8} = 3.75 \times 10^8 [N]$$

As we saw in previous chapter 6 (“Stiffness of the timber-concrete connectors”), containing the full description of the connection system, we have, for the T12 connection system:

$$K_U = 23000 \text{ N/mm}$$

$$s_{eq} = s = 100 \text{ mm}$$

Thus, by substituting values on the expressions at point B.2 of Eurocode 5, we obtain:

$$\gamma_2 = 1$$

$$\gamma_1 = \left[1 + \pi^2 \cdot E_1 \cdot A_1 \cdot s_{eq} / (K \cdot l^2) \right]^{-1} = \left[1 + \pi^2 \times 1.45 \times 10^9 \times 100 / (23000 \times 8000^2) \right]^{-1} = 0.51$$

$$a = h_1/2 + h_2/2 = (50/2 + 450/2) = 250 \text{ mm}$$

$$a_2 = \frac{\gamma_1 \cdot E_1 \cdot A_1 \cdot a}{\gamma_1 \cdot E_1 \cdot A_1 + \gamma_2 \cdot E_2 \cdot A_2} = \frac{0.51 \times 1.45 \times 10^9}{0.51 \times 1.45 \times 10^9 + 1 \times 5.06 \times 10^8} \times 250 = 148 \text{ mm}$$

$$a_1 = a - a_2 = (250 - 148) = 102 \text{ mm}$$

$$EJ_{ef} = \sum_i E_i J_i + \gamma_2 \cdot E_2 \cdot A_2 \cdot a_2^2 + \gamma_1 \cdot E_1 \cdot A_1 \cdot a_1^2 =$$

$$= (3.02 \times 10^{11} + 8.54 \times 10^{12} + 1 \times 5.06 \times 10^8 \times 148^2 + 0.51 \times 1.45 \times 10^9 \times 102^2) = 2.76 \times 10^{13} [Nmm^2]$$

$$EJ_\infty = (EJ)_0 + (EA)_0 \cdot a^2 = (8.84 \times 10^{12} + 3.75 \times 10^8 \times 250^2) = 3.23 \times 10^{13} [Nmm^2]$$

$$\eta = \frac{EJ_{ef} - (EJ)_0}{EJ_\infty - (EJ)_0} = \frac{2.76 \times 10^{13} - 8.84 \times 10^{12}}{3.23 \times 10^{13} - 8.84 \times 10^{12}} = 0.80$$

The service loads P_{SER} and $q_{SER} = P_{SER} / A$ amount to:

$$P_{SER} = 2 \cdot (G_1 + G_2 + Q_{K1}) = 2 \cdot [\gamma_{k,FRC} \cdot h_1 \cdot b_1 + (g \cdot \rho_{g,k} \cdot h_2 \cdot b_2) + G_2 \cdot b_1 + Q_{K1} \cdot b_1] \cdot l =$$

$$= 2 \times [22.93 \times 0.05 \times 0.8 + (g \times 390 \times 0.45 \times 0.09 \times 10^{-3}) + 2.69 \times 0.8 + 4.00 \times 0.8] \times 8 = 103 [kN]$$

$$q_{SER} = \frac{P_{SER}}{A} = \frac{P_{SER}}{2 \cdot b_1 \cdot l} = \frac{103}{2 \times 0.8 \times 8} = 8 \left[\frac{kN}{m^2} \right]$$

With referring to this value of load we can get from the following curve in Figure 129:

$$EJ_{real} = 2.65 \times 10^{13} [Nmm^2]$$

By substituting values we can get the efficiency of the connection, related to the service load:

$$\eta_{real} = \frac{EJ_{real} - (EJ)_0}{EJ_{\infty} - (EJ)_0} = \frac{2.65 \times 10^{13} - 8.84 \times 10^{12}}{3.23 \times 10^{13} - 8.84 \times 10^{12}} = 0.75$$

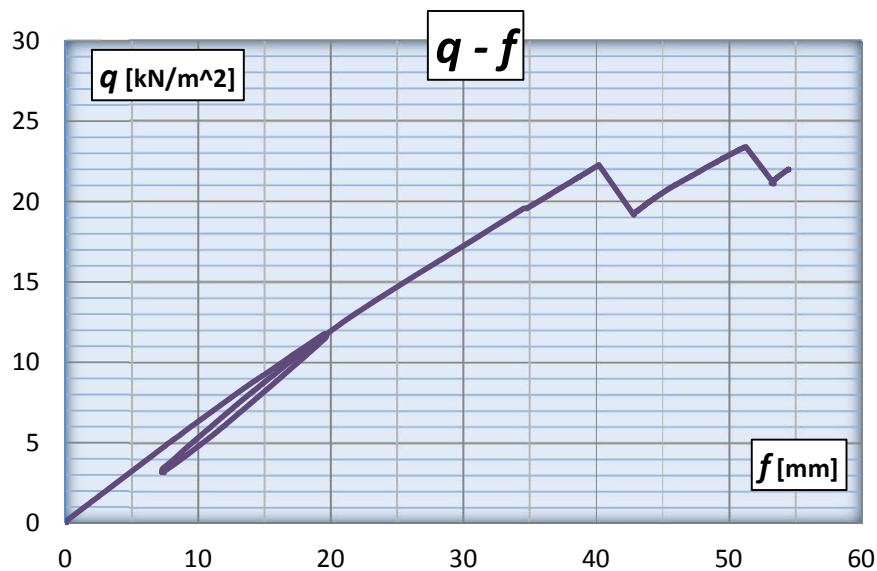


Figure 128: load-mid span deflection curve

Even if it's a bit lower than the previous case with the connection system F 45, also for this system the load-carrying capacity of the is really high (the ultimate load is higher than 25 kN/m² and the service load, usually assessed as 60% of the failure load, is around 15 kN/m², while a normal residential or commercial floor seldom goes over 8-10 kN/m². We remember that to these value of load q shown in the graph we must add the self-weight of slab and timber beams and the weight of the reply steel partitioning beams.

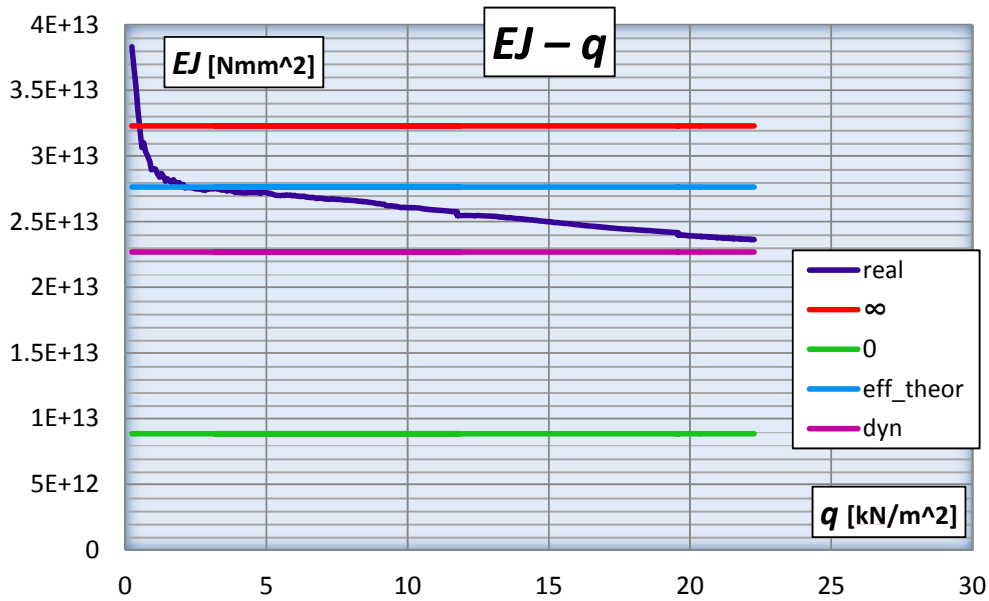


Figure 129: bending stiffness of the system, compared with the theoretical cases of $k=0$ and $k=\infty$, and with both the effective and dynamic stiffness

As we can see, the real stiffness is a bit lower than the effective one, evaluated on the basis of the stiffness of the shear connectors obtained from the results of the push-out tests performed and described in Paper [1] and in agreement with the theoretical method of Eurocode 5 for composite sections. This is supposedly due to the fact that some screws could not be inserted because in some of the steel pipes there was stuck concrete that we have not been able to take out.

We can also see that, like in the previous case, the dynamic stiffness (violet line) is a bit lower than the static one, and this could be due to the fact that the connections don't lead the system to a full-composite action.

The dynamic stiffness has been evaluated by inverting the following expression, referred to the eigenfrequency:

$$f_n = n^2 \cdot \frac{\pi}{2} \cdot \frac{1}{L^2} \cdot \sqrt{\frac{g}{A \cdot \gamma}} \cdot \sqrt{EJ_{dyn}}$$

Once we knew from the FE software Comsol Multiphysics that the first vibration mode is the one related to the bending of the system (Figure 130), and the eigenfrequency of the system from the accelerogram, $f_1 \approx 11$ Hz, (Figure 131) we can obtain the dynamic stiffness by inserting $n = 1$ in the previous formulation:

$$EJ_{dyn} = f_n^2 \cdot \left(\frac{2}{\pi}\right)^2 \cdot \frac{L^4}{n^4} \cdot \frac{A \cdot \gamma}{g} =$$

$$= 11^2 \times \left(\frac{2}{\pi}\right)^2 \times \frac{8000^4}{1^4} \times \frac{22.93 \times 50 \times 800 \times 10^{-6} + (390 \times 9.81) \times 90 \times 450 \times 10^{-9}}{9.81} \times 10^{-3} = 2.2 \times 10^{13} [Nmm^2]$$

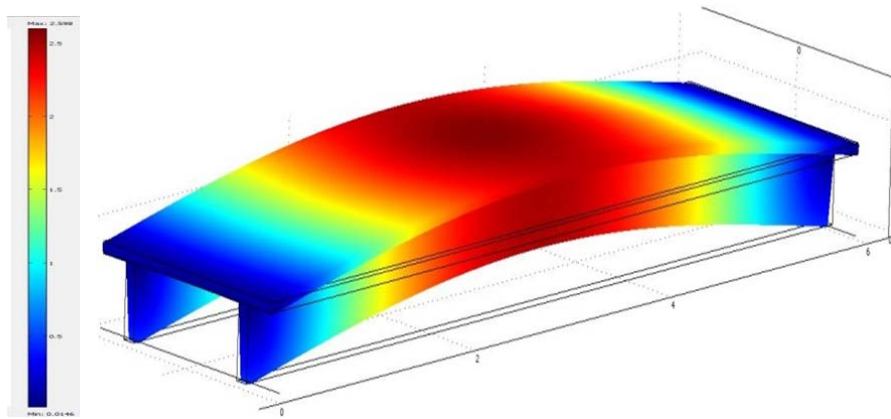


Figure 130: first mode of vibration of the system, related to bending

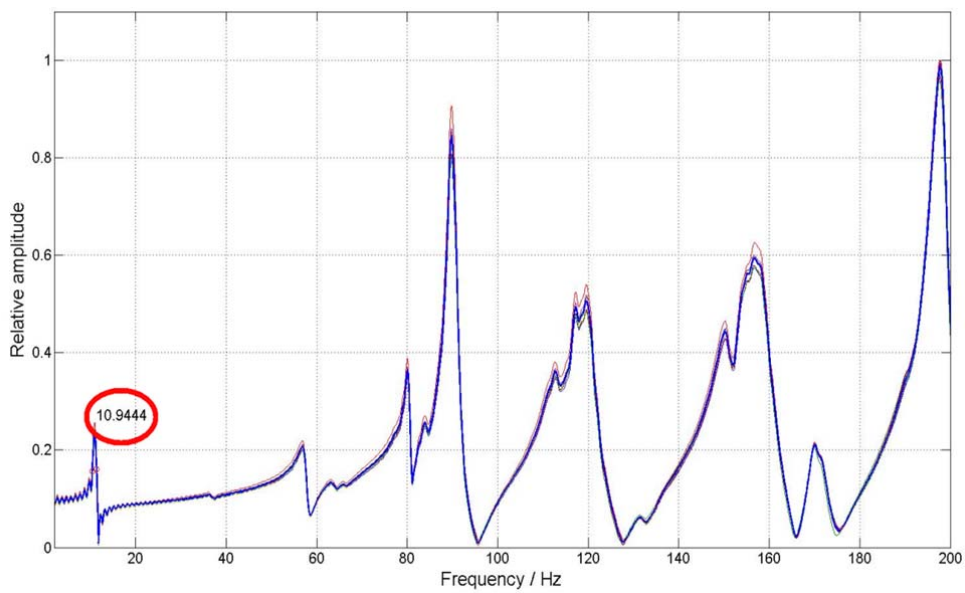


Figure 131: accelerogram of the system, showing the eigenfrequencies related to the relative waving amplitude

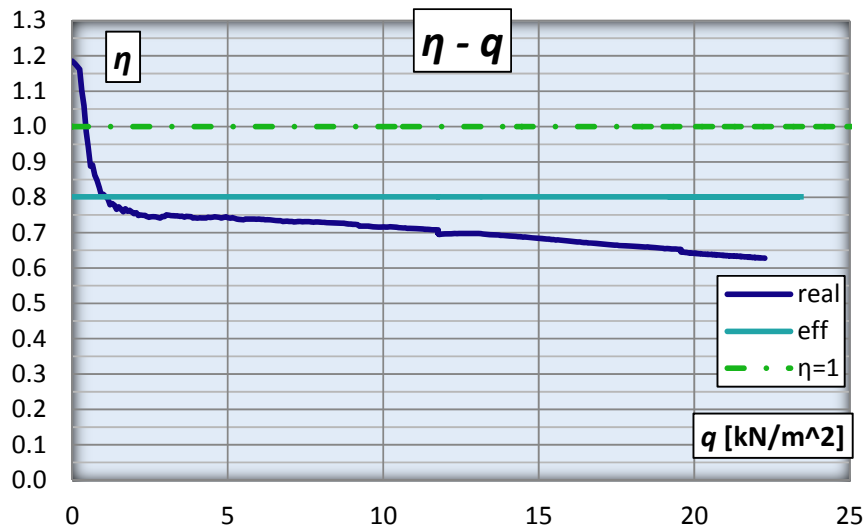


Figure 132: efficiency, real and effective, of the system

Differently from the previous case, the real efficiency for the system with the T 12 connections, with the same trend of the stiffness, is a bit lower than the effective, but it's anyway a high value and we can see that, for normal service floor-loads (always lower than 8-10 kN/m²), we have almost 75% of the full-composite action.

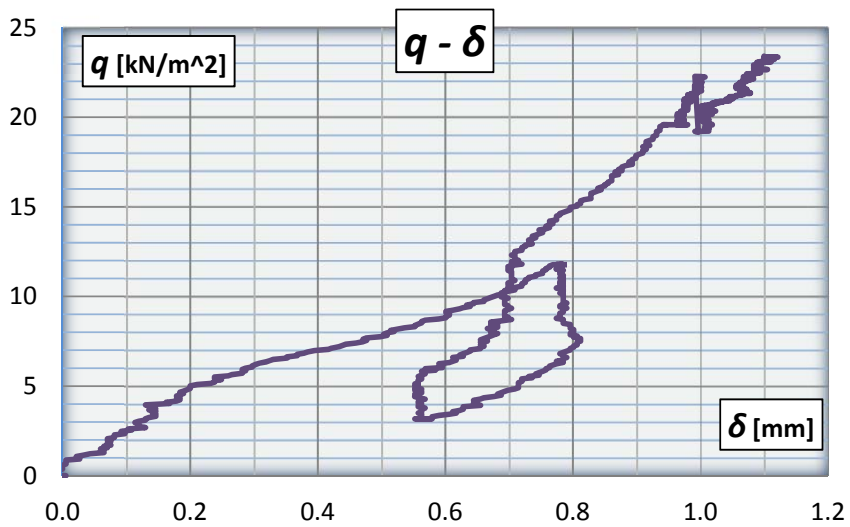


Figure 133: load – slip trend

This graph shows the trend of the relative slip between the concrete slab and the timber beams, in function of the load. We can see that, as direct consequence of the rigidity of the shear connectors, the values of slip are almost null and always lower than 1 mm.

In next table we show the stiffness EJ_{real} and the efficiency of the system, with referring to the service load previously evaluated $q_{SER} = 8 \text{ kN/m}^2$, and compared with the theoretical values obtained by using the experimental researches described in reference [1].

real values		theoretical values	
$EJ_{real} \text{ [Nmm}^2\text{]}$	η_{real}	$EJ_{ef} \text{ [Nmm}^2\text{]}$	η
2.65×10^{12}	0.75	2.76×10^{13}	0.80

Conclusions

Also this system can be considered highly resistant, by referring to normal floor-loads at SLS. The good result obtained from this experimental research performer on the slab with the T 12 shear connectors concerns about the high value of stiffness of the system, whose efficiency leads to 75% of rigid behavior and full-composite action.

7.3.2.5 Comparison between the two systems

Since the geometrical dimensions of the two system tested are different, it doesn't have any sense to compare the loads reached and the stiffness obtained. Though, in next Figure 134 we carry the trend of the efficiency, related to the load q . As conclusion, we remark that both system had shown a resistant and rigid behavior, if related to normal floor-loads evaluated at SLS. The most important result concerns the huge bending stiffness of the system, whose efficiency are near to 1.

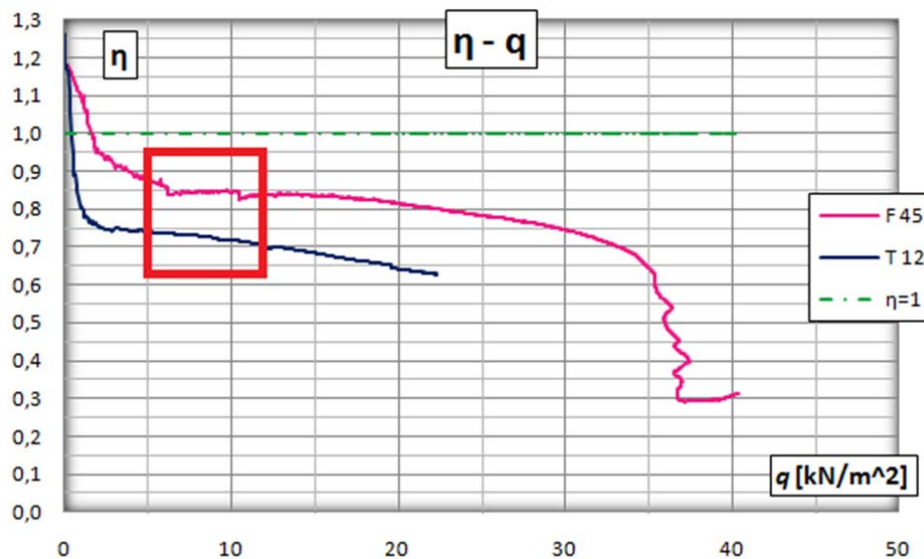


Figure 134: comparison between the efficiencies of the two system

APPENDIX 1

This annex presents a calculation example of a timber concrete composite slab, based on the theoretical method for composite sections suggested in Chapter 5 (“Composite Action of Timber-Concrete composite systems”). The main purpose of this appendix is to obtain maximum dimension of items belonging to a composite slab (thickness of the concrete plate, height of the timber beam and spacing of the connectors), with reference to background destination.

1 MATERIALS

1.1 Fiber reinforced concrete

The fiber reinforced concrete we are referring to is the one used in the experimental tests described in Paper [1]. Thus, mechanical characteristics are obtained from uniaxial compression tests performed and reported in the same paper.

Reason of the use of fiber reinforced concrete

The main issue of a composite system like the one we are analyzing, firstly due to long-term actions, is the shrinkage of both elements, timber and concrete. To face this problem a great alternative is made up by fiber reinforced concrete, in which the reinforce is formed by steel fibers (but in business is possible to find also different types of fibers, natural and artificial), that start working when the first cracking originates in concrete. Furthermore, these fibers contribute improving strength parameters of the material with benefits on the composite system behavior.

Characteristics of fiber reinforced concrete

Fiber reinforced concrete used in the experimental tests carried in reference [1] is made of 375 kg/m³ of cement and 45 kg/m³ of steel fibers type ZP 30/.40 (Dramix).

Characteristic strength R_{ck} is defined according to values obtained by uniaxial compression tests on 150 mm wide cubic specimens, matured 28 days. Characteristic strength f_{ck} is instead defined using cylindrical specimens with 300 mm height and 150 mm diameter. Between the two values there is the following relation:

$$f_{ck} = 0.83 \cdot R_{ck}$$

Concrete strength class is based upon cubic characteristic compression strength (R_{ck}), defined as the value beneath which lies only 5 % of whole samples resistance values (lower fractile at 5 %).

By using normal Gauss distribution (most common statistic distribution), lower fractile at 5 % can be calculated according to the following expression:

$$R_{ck} = R_m - 1.64 \cdot sqm$$

Where:

R_m is the average specimens resistance

sqm is the standard deviation, computable as:

$$sqm = \sqrt{\frac{\sum_{i=1}^{n=3} (R_i - R_m)^2}{n-1}}$$

where:

R_i is the resistance of each specimen

n is the number of specimens tested

In our case the test to determine compression resistance have been provided leading to rupture three cubic specimens. Strengths of each specimen have successively been reported in the following Table 4 (taken from reference [1]).

Nr	ID	a mm	b mm	h mm	A mm ²	Weight kg	ρ g/cm ³	F_m kN	σ_m N/mm ²
1	1	150,8	150,8	149,8	22736,5	8,099	2,38	1314,77	57,83
2	2	150,8	150,8	149,8	22729,3	8,044	2,36	1276,22	56,15
3	3	151,0	151,0	149,8	22787,7	8,028	2,35	1319,39	57,90

Results after 28 days

Table 4: mechanical parameters of the concrete specimen tested

As we can see from Table 4, three specimens have been tested and the values we are interested in are in the last column (compression resistances after 28 days). By substituting values we can get first standard deviation and then compression characteristic resistances:

$$R_m = \sum_{i=1}^{n=3} \frac{R_i}{n} = \frac{57.83 + 56.15 + 57.90}{3} = 57.29 [MPa]$$

$$sqm = \sqrt{\sum_{i=1}^{n=3} \frac{(R_i - R_m)^2}{n-1}} = \sqrt{\frac{(57.83 - 57.29)^2 + (56.15 - 57.29)^2 + (57.90 - 57.29)^2}{2}} = 0.99 [MPa]$$

$$R_{ck} = R_m - 1.64 \cdot sqm = (57.29 - 1.64 \times 0.99) = 55.67 [MPa]$$

The characteristic resistance evaluation is also possible by using the method proposed by reference [1] at 11.2.5, concerning acceptance checks. Acceptation check is passed and concrete accepted if both inequalities in Table 11.2.1 of standard [1] are verified. If the number of specimens tested is three, we have to respect following inequalities:

$$R_1 \geq R_{ck} - 3.5$$

$$R_m \geq R_{ck} + 3.5$$

Where:

R_1 is minimum value of specimen resistance

By substituting all values we obtain:

$$R_{ck} \leq R_m - 3.5 = (57.29 - 3.5) = 53.79 [MPa]$$

$$R_1 = 56.15 [MPa] \geq R_{ck} - 3.5 = (53.79 - 3.5) = 50.29 [MPa]$$

Since the test has been provided on a small number of specimens (equal to three), the approach suggested by standard [1] results more precautionary than the theoretical Gauss method.

Thus, the cubic compression characteristic resistance chosen is:

$$R_{ck} = 53.79[MPa]$$

Mechanical characteristics of concrete can be deducted by formulations indicated at 11.2.10 of Statement [1], successively reported. For matters not covered we can refer to standard [2].

$$f_{ck} = 0.83 \cdot R_{ck} = 0.83 \times 53.79 = 44.65[MPa]$$

$$f_{cm} = f_{ck} + 8 = (44.65 + 8) = 52.65[MPa]$$

$$f_{ctm} = 0.3 \cdot (f_{ck})^{2/3} = 0.3 \times (44.65)^{2/3} = 3.78[MPa]$$

$$f_{ctk,0.05} = 0.7 \cdot f_{ctm} = 0.7 \times 3.78 = 2.64[MPa]$$

$$f_{ctk,0.95} = 1.3 \cdot f_{ctm} = 1.3 \times 3.78 = 4.91[MPa]$$

$$E_{cm} = 22000 \cdot (f_{cm}/10)^{0.3} = 22000 \times (52.65/10)^{0.3} = 36210[MPa]$$

Concrete design compressive strength

The design compressive strength of the fiber reinforced concrete f_{cd} can be obtained by expression (4.1.4) of reference [1]:

$$f_{cd} = \frac{\alpha_{cc} \cdot f_{ck}}{\gamma_c} = \frac{0.85 \times 44.65}{1.5} = 25.30[MPa]$$

Where:

$\alpha_{cc} = 0.85$ is the reductive coefficient for long term strengths

$\gamma_c = 1.5$ is the concrete partial safety factor

Concrete design tensile strength

The design tensile strength of the fiber reinforced concrete f_{ctd} can be obtained by expression (4.1.5) of reference [1]:

$$f_{ctd} = \frac{f_{ctk,0.05}}{\gamma_c} = \frac{2.64}{1.5} = 1.76[MPa]$$

Where:

$\gamma_c = 1.5$ is the concrete partial safety factor

From Table 4 we can also get the fiber reinforced concrete specific weight. In particular we can first calculate the specimens average value and then the characteristic value, still by using a normal Gauss distribution. If we substitute values we can obtain the average value, the standard deviation and finally the characteristic value:

$$\gamma_{m,FRC} = \sum_{i=1}^{n=3} \frac{\gamma_i}{n} = g \times \frac{2.38+2.36+2.35}{3} = g \times 2.36 \left[\frac{g}{cm^3} \right] = 23.17 \left[\frac{KN}{m^3} \right]$$

$$sqm = g \times \sqrt{\sum_{i=1}^{n=3} \frac{(\rho_i - \rho_m)^2}{n-1}} = g \times \sqrt{\frac{(2.38-2.36)^2 + (2.36-2.36)^2 + (2.35-2.36)^2}{2}} =$$

$$= g \times 1.53 \times 10^{-2} \left[\frac{g}{cm^3} \right] = 0.15 \left[\frac{KN}{m^3} \right]$$

$$\gamma_{k,FRC} = \gamma_{m,FRC} - 1.64 \cdot sqm = (23.17 - 1.64 \cdot 0.15) = 22.93 \left[\frac{KN}{m^3} \right]$$

1.2 Glulam

Structural timber used for beam is glued laminated timber GL30 h. Below we carry characteristic strength and elastic moduli significant values, and density, given by prEN 14080:2008.

$$f_{m,g,k} = 30[MPa] \quad f_{t,0,g,k} = 20[MPa] \quad f_{t,90,g,k} = 0.5[MPa]$$

$$f_{c,0,g,k} = 25[MPa] \quad f_{c,90,g,k} = 2.5[MPa] \quad f_{v,g,k} = 3.5[MPa]$$

$$E_{0,g,mean} = 12500[MPa] \quad E_{0,g,0.05} = 10100[MPa] \quad E_{90,g,mean} = 300[MPa] \quad G_{g,mean} = 650[MPa]$$

$$\rho_{g,k} = 390[kg/m^3]$$

The project values of general resistance properties (X_d) and stiffness (K_d) can be obtained from characteristic (X_k) and medium (K_{mean}) values by following relations:

$$X_d = k_{mod} \cdot X_k / \gamma_M \quad K_d = K_{mean} / \gamma_M$$

Where:

γ_M is the partial safety factor for the material properties, such as recommended in Table 2.3 of Statement [3] (reported below).

Table 2.3 – Recommended partial factors γ_M for material properties and resistances

Fundamental combinations:	
Solid timber	1,3
Glued laminated timber	1,25
LVL, plywood, OSB,	1,2
Particleboards	1,3
Fibreboards, hard	1,3
Fibreboards, medium	1,3
Fibreboards, MDF	1,3
Fibreboards, soft	1,3
Connections	1,3
Punched metal plate fasteners	1,25
Accidental combinations	1,0

In our case (Glulam) the partial safety factor is: $\gamma_M = 1.25$.

k_{mod} is the correction factor which considers the effect of, on resistances parameters, both the load duration and the moisture content. Values are presented in following Table 3.1 of Statement [3].

Table 3.1 – Values of k_{mod}

Material	Standard	Service class	Load-duration class				
			Permanent action	Long term action	Medium term action	Short term action	Instantaneous action
Solid timber	EN 14081-1	1	0,60	0,70	0,80	0,90	1,10
		2	0,60	0,70	0,80	0,90	1,10
		3	0,50	0,55	0,65	0,70	0,90
Glued laminated timber	EN 14080	1	0,60	0,70	0,80	0,90	1,10
		2	0,60	0,70	0,80	0,90	1,10
		3	0,50	0,55	0,65	0,70	0,90
LVL	EN 14374, EN 14279	1	0,60	0,70	0,80	0,90	1,10
		2	0,60	0,70	0,80	0,90	1,10
		3	0,50	0,55	0,65	0,70	0,90
Plywood	EN 636 Part 1, Part 2, Part 3 Part 2, Part 3 Part 3	1	0,60	0,70	0,80	0,90	1,10
		2	0,60	0,70	0,80	0,90	1,10
		3	0,50	0,55	0,65	0,70	0,90
OSB	EN 300 OSB/2 OSB/3, OSB/4 OSB/3, OSB/4	1	0,30	0,45	0,65	0,85	1,10
		1	0,40	0,50	0,70	0,90	1,10
		2	0,30	0,40	0,55	0,70	0,90
Particle-board	EN 312 Part 4, Part 5 Part 5 Part 6, Part 7 Part 7	1	0,30	0,45	0,65	0,85	1,10
		2	0,20	0,30	0,45	0,60	0,80
		1	0,40	0,50	0,70	0,90	1,10
		2	0,30	0,40	0,55	0,70	0,90
Fibreboard, hard	EN 622-2 HB.LA, HB.HLA 1 or 2 HB.HLA1 or 2	1	0,30	0,45	0,65	0,85	1,10
		2	0,20	0,30	0,45	0,60	0,80
Fibreboard, medium	EN 622-3 MBH.LA1 or 2 MBH.HLS1 or 2 MBH.HLS1 or 2	1	0,20	0,40	0,60	0,80	1,10
		1	0,20	0,40	0,60	0,80	1,10
		2	–	–	–	0,45	0,80
Fibreboard, MDF	EN 622-5 MDF.LA, MDF.HLS MDF.HLS	1	0,20	0,40	0,60	0,80	1,10
		2	–	–	–	0,45	0,80

Since our elements stay indoors we refer to Service Class 1 (elements protected from weather such as placed inside buildings), according to the point 2.3.1.3 of Statement [3].

Effects must be assigned at one of the load duration categories given in Table 2.1 of Statement [3], indicating a class for each known load duration.

Table 2.1 – Load-duration classes

Load-duration class	Order of accumulated duration of characteristic load
Permanent	more than 10 years
Long-term	6 months – 10 years
Medium-term	1 week – 6 months
Short-term	less than one week
Instantaneous	

In this case we refer to two different load duration categories: permanent, in which there are only the elements self weights, structural and non, and medium duration category, in which in addition to self weights there is also the accidental load. Thus we assume:

$$k_{mod_permanent} = 0.60 \qquad k_{mod_medium-term} = 0.80$$

Regarding service checks (SLS), we must introduce K_{def} factor to estimate viscoelastic deformation, according to the relative service category. k_{def} values are given in following Table 4.4.V of reference [1].

Table 3.2 – Values of k_{def} for timber and wood-based materials

Material	Standard	Service class		
		1	2	3
Solid timber	EN 14081-1	0,60	0,80	2,00
Glued Laminated timber	EN 14080	0,60	0,80	2,00
LVL	EN 14374, EN 14279	0,60	0,80	2,00
Plywood	EN 636			
	Part 1	0,80	–	–
	Part 2	0,80	1,00	–
	Part 3	0,80	1,00	2,50
OSB	EN 300	2,25	–	–
	OSB/2	1,50	2,25	–
	OSB/3, OSB/4			
Particleboard	EN 312			
	Part 4	2,25	–	–
	Part 5	2,25	3,00	–
	Part 6	1,50	–	–
	Part 7	1,50	2,25	–
Fibreboard, hard	EN 622-2			
	HB.LA HB.HLA1, HB.HLA2	2,25 2,25	– 3,00	– –
Fibreboard, medium	EN 622-3			
	MBH.LA1, MBH.LA2	3,00	–	–
	MBH.HLS1, MBH.HLS2	3,00	4,00	–
Fibreboard, MDF	EN 622-5			
	MDF.LA	2,25	–	–
	MDF.HLS	2,25	3,00	–

In this case, as previously said, we refer to Service Class 1 (indoors elements). Thus we can assume:

$$k_{def} = 0.60$$

Before calculating strength parameters project values, with regard to the load duration category, we now estimate the characteristic density value of the material:

$$\gamma_{k,GL} = g \cdot \rho_{g,k} = g \times 390 \left[\text{kg/m}^3 \right] = 3.82 \left[\text{KN/m}^3 \right]$$

Medium duration conditions

Flexural strength

$$f_{m,d} = k_{mod} \cdot f_{m,g,k} / \gamma_M = 0.80 \times 30 / 1.25 = 19.2 \left[\text{MPa} \right]$$

Tensile strength parallel to the grain

$$f_{t,0,d} = k_{mod} \cdot f_{t,0,g,k} / \gamma_M = 0.80 \times 20 / 1.25 = 12.8 \left[\text{MPa} \right]$$

Tensile strength perpendicular to the grain

$$f_{t,90,d} = k_{mod} \cdot f_{t,90,g,k} / \gamma_M = 0.80 \times 0.5 / 1.25 = 0.32 \left[\text{MPa} \right]$$

Compressive strength parallel to the grain

$$f_{c,0,d} = k_{mod} \cdot f_{c,0,g,k} / \gamma_M = 0.80 \times 25 / 1.25 = 16 \left[\text{MPa} \right]$$

Compressive strength perpendicular to the grain

$$f_{c,90,d} = k_{\text{mod}} \cdot f_{c,90,g,k} / \gamma_M = 0.80 \times 2.5 / 1.25 = 1.6 [\text{MPa}]$$

Shear strength

$$f_{v,d} = k_{\text{mod}} \cdot f_{v,g,k} / \gamma_M = 0.80 \times 3.5 / 1.25 = 2.24 [\text{MPa}]$$

Normal modulus of elasticity parallel to the grain

$$E_{0,d} = E_{0,g,\text{mean}} / \gamma_M = 12500 / 1.25 = 10000 [\text{MPa}]$$

Normal modulus of elasticity perpendicular to the grain

$$E_{90,d} = E_{90,g,\text{mean}} / \gamma_M = 300 / 1.25 = 240 [\text{MPa}]$$

Tangential modulus of elasticity

$$G_d = G_{g,\text{mean}} / \gamma_M = 650 / 1.25 [\text{GPa}] = 520 [\text{GPa}]$$

Permanent load duration

Flexural strength

$$f_{m,d} = k_{\text{mod}} \cdot f_{m,g,k} / \gamma_M = 0.60 \times 30 / 1.25 = 14.4 [\text{MPa}]$$

Tensile strength parallel to the grain

$$f_{t,0,d} = k_{\text{mod}} \cdot f_{t,0,g,k} / \gamma_M = 0.60 \times 20 / 1.25 = 9.6 [\text{MPa}]$$

Tensile strength perpendicular to the grain

$$f_{t,90,d} = k_{\text{mod}} \cdot f_{t,90,g,k} / \gamma_M = 0.60 \times 0.5 / 1.25 = 0.24 [\text{MPa}]$$

Compressive strength parallel to the grain

$$f_{c,0,d} = k_{\text{mod}} \cdot f_{c,0,g,k} / \gamma_M = 0.60 \times 25 / 1.25 = 12 [\text{MPa}]$$

Compressive strength perpendicular to the grain

$$f_{c,90,d} = k_{\text{mod}} \cdot f_{c,90,g,k} / \gamma_M = 0.60 \times 2.5 / 1.25 = 1.2 [\text{MPa}]$$

Shear strength

$$f_{v,d} = k_{\text{mod}} \cdot f_{v,g,k} / \gamma_M = 0.60 \times 3.5 / 1.25 = 1.68 [\text{MPa}]$$

Normal modulus of elasticity parallel to the grain

$$E_{0,d} = E_{0,g,mean} / \gamma_M = 12500 / 1.25 = 10000 [MPa]$$

Normal modulus of elasticity perpendicular to the grain

$$E_{90,d} = E_{90,g,mean} / \gamma_M = 300 / 1.25 = 240 [MPa]$$

Tangential modulus of elasticity

$$G_d = G_{g,mean} / \gamma_M = 650 / 1.25 [GPa] = 520 [GPa]$$

2 LOAD COMBINATIONS

For the limit states verifications we refer to the following combination rules, such as reported at 2.5.3 of reference [1].

- Basic combination, used for SLU:

$$\gamma_{G1} \cdot G_1 + \gamma_{G2} \cdot G_2 + \gamma_P \cdot P + \gamma_{Q1} \cdot Q_{K1} + \gamma_{Q2} \cdot \psi_{02} \cdot Q_{K2} + \gamma_{Q3} \cdot \psi_{03} \cdot Q_{K3} + \dots$$

- Characteristic combination, used for irreversible SLS:

$$G_1 + G_2 + P + Q_{K1} + \psi_{02} \cdot Q_{K2} + \psi_{03} \cdot Q_{K3} + \dots$$

- Frequent combination:

$$G_1 + G_2 + P + \psi_{11} \cdot Q_{K1} + \psi_{22} \cdot Q_{K2} + \psi_{23} \cdot Q_{K3} + \dots$$

- Quasi-permanent combination, used for long term effects:

$$G_1 + G_2 + P + \psi_{21} \cdot Q_{K1} + \psi_{22} \cdot Q_{K2} + \psi_{23} \cdot Q_{K3} + \dots$$

In our case we have only G_1 (structural permanent load), G_2 (non structural permanent load) and Q_{K1} (leading variable action).

Partial safety factors γ_{Gi} e γ_{Qj} are presented in following Table 2.6.l of Statement [1]:

		Coefficiente γ_F	EQU	A1 STR	A2 GEO
Carichi permanenti	favorevoli	γ_{G1}	0,9	1,0	1,0
	sfavorevoli		1,1	1,3	1,0
Carichi permanenti non strutturali ⁽¹⁾	favorevoli	γ_{G2}	0,0	0,0	0,0
	sfavorevoli		1,5	1,5	1,3
Carichi variabili	favorevoli	γ_{Qi}	0,0	0,0	0,0
	sfavorevoli		1,5	1,5	1,3

⁽¹⁾Nel caso in cui i carichi permanenti non strutturali (ad es. carichi permanenti portati) siano compiutamente definiti si potranno adottare per essi gli stessi coefficienti validi per le azioni permanenti.

In this case we refer to the structure's strength limit state (STR), by using following values for safety partial factors:

- $\gamma_{G1_favourable} = 1$; $\gamma_{G1_unfavourable} = 1.3$.
- $\gamma_{G2_favourable} = 1$; $\gamma_{G2_unfavourable} = 1.3$.
- $\gamma_{Q,i_favourable} = 0$; $\gamma_{Q,i_unfavourable} = 1.5$.

The partial safety factors related to non structural permanent loads are the same used for structural permanent actions because also these kind of loads are completely defined, as we'll see in the next paragraph 2.2 ("Non structural permanent load").

The combination factors values ψ_{ij} are indicated in next Table 2.5.I of reference [1], according to the following variable action categories:

Categoria/Azione variabile	Ψ_{0j}	Ψ_{1j}	Ψ_{2j}
Categoria A Ambienti ad uso residenziale	0,7	0,5	0,3
Categoria B Uffici	0,7	0,5	0,3
Categoria C Ambienti suscettibili di affollamento	0,7	0,7	0,6
Categoria D Ambienti ad uso commerciale	0,7	0,7	0,6
Categoria E Biblioteche, archivi, magazzini e ambienti ad uso industriale	1,0	0,9	0,8
Categoria F Rimesse e parcheggi (per autoveicoli di peso ≤ 30 kN)	0,7	0,7	0,6
Categoria G Rimesse e parcheggi (per autoveicoli di peso > 30 kN)	0,7	0,5	0,3
Categoria H Coperture	0,0	0,0	0,0
Vento	0,6	0,2	0,0
Neve (a quota ≤ 1000 m s.l.m.)	0,5	0,2	0,0
Neve (a quota > 1000 m s.l.m.)	0,7	0,5	0,2
Variazioni termiche	0,6	0,5	0,0

Below is the procedure for determining respectively of structural permanent load (G_1), non structural permanent load (G_2) and accidental load (Q_1).

2.1 Structural permanent load

Permanent structural load is given by self weight of timber beam and preformed concrete slab above. In accordance with below Figure 135, the procedure for calculating the structural load per unit length and per unit area is:

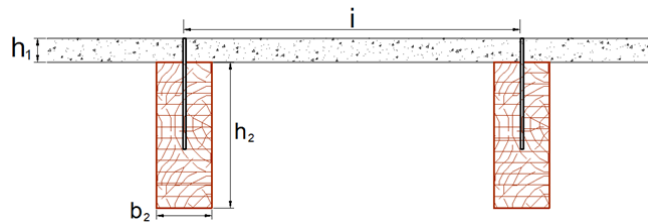


Figure 135: scheme for self-weight calculation

$$g_1 = \gamma_{k,CAP} \cdot h_1 \cdot i + \gamma_{k,GL} \cdot h_2 \cdot b_2$$

$$G_1 = \frac{g_1}{i} = \gamma_{k,FRC} \cdot h_1 + \frac{\gamma_{k,GL} \cdot h_2 \cdot b_2}{i}$$

2.2 Non structural permanent load

In addition to structural permanent load there is also a carried permanent action, due to elements above the concrete plate. We can assume the material layers presented below, each one with his own self load per unit area:

- screed:

$$p_{screed} = 24 \left[\text{KN} / \text{m}^3 \right] \times 0.05 \text{m} = 1.2 \left[\text{KN} / \text{m}^2 \right]$$

- insulation:

$$p_{insulation} = 1 \left[\text{KN} / \text{m}^3 \right] \times 0.05 \text{m} = 0.05 \left[\text{KN} / \text{m}^2 \right]$$

- floor:

$$p_{floor} = 22 \left[\text{KN} / \text{m}^3 \right] \times 0.01 \text{m} = 0.22 \left[\text{KN} / \text{m}^2 \right]$$

We also have to add to these items the weight of internal partitions, briefed to a permanent load per unit area, as suggested by reference [1] al 3.1.3.1.

Internal partitions, not yet present, can be conservatively considered with a 11 cm thickness and thus made up by bricks 8 cm thickness and external plasters 1.5 cm on both sides.

For internal partition we can use bricks which show following characteristics:

- dimensions S x L x H (cm): 8 x 25 x 25
- apparent density: 6 KN/m³

If we consider an height between floors equal to 3 m, the load for unit length of these internal partitions is:

$$p_{partitions} = \{ 16 \left[\text{KN} / \text{m}^3 \right] \times (0.015 \text{m} + 0.015 \text{m}) + 6 \left[\text{KN} / \text{m}^3 \right] \times 0.08 \text{m} \} \times 3 \text{m} = 2.9 \left[\text{KN} / \text{m} \right]$$

The previous value is associated to the following permanent load per unit area, according to reference [1] at point 3.1.3.1:

$$p_{partitions} = 1.2 \left[\text{KN} / \text{m}^2 \right]$$

Non structural permanent load of the slab is given by the sum of all above-mentioned contributions. By substituting all the values we obtain:

$$G_2 = p_{PERMANENT} = p_{screed} + p_{insulation} + p_{floor} + p_{partitions} = 2.69 \left[\text{KN} / \text{m}^2 \right]$$

2.3 Variable load

With the aim of completely determining the loads acting over the slab we choose two background types, according to standard [1]. Each one chosen background has its own variable load value and combination factors that we have to use when we'll do all checks provided by regulations.

Background categories

The two background categories that we'll analyze are:

- residential
- commercial

The variable load associated to each background type can be deducted from next Table 3.1.II (reference [1]):

Tabella 3.1.II – Valori dei carichi d'esercizio per le diverse categorie di edifici

Cat.	Ambienti	q_k [kN/m ²]	Q_k [kN]	H_k [kN/m]
A	Ambienti ad uso residenziale. Sono compresi in questa categoria i locali di abitazione e relativi servizi, gli alberghi. (ad esclusione delle aree suscettibili di affollamento)	2,00	2,00	1,00
B	Uffici. Cat. B1 Uffici non aperti al pubblico Cat. B2 Uffici aperti al pubblico	2,00 3,00	2,00 2,00	1,00 1,00
C	Ambienti suscettibili di affollamento Cat. C1 Ospedali, ristoranti, caffè, banche, scuole Cat. C2 Balconi, ballatoi e scale comuni, sale convegni, cinema, teatri, chiese, tribune con posti fissi Cat. C3 Ambienti privi di ostacoli per il libero movimento delle persone, quali musei, sale per esposizioni, stazioni ferroviarie, sale da ballo, palestre, tribune libere, edifici per eventi pubblici, sale da concerto, palazzetti per lo sport e relative tribune	3,00 4,00 5,00	2,00 4,00 5,00	1,00 2,00 3,00
D	Ambienti ad uso commerciale. Cat. D1 Negozi Cat. D2 Centri commerciali, mercati, grandi magazzini, librerie...	4,00 5,00	4,00 5,00	2,00 2,00
E	Biblioteche, archivi, magazzini e ambienti ad uso industriale. Cat. E1 Biblioteche, archivi, magazzini, depositi, laboratori manifatturieri Cat. E2 Ambienti ad uso industriale, da valutarsi caso per caso	$\geq 6,00$ —	6,00 —	1,00* —
F-G	Rimesse e parcheggi. Cat. F Rimesse e parcheggi per il transito di automezzi di peso a pieno carico fino a 30 kN Cat. G Rimesse e parcheggi per transito di automezzi di peso a pieno carico superiore a 30 kN: da valutarsi caso per caso	2,50 —	2 x 10,00 —	1,00** —
H	Coperture e sottotetti Cat. H1 Coperture e sottotetti accessibili per sola manutenzione Cat. H2 Coperture praticabili Cat. H3 Coperture speciali (impianti, eliporti, altri) da valutarsi caso per caso	0,50 — —	1,20 secondo categoria di appartenenza —	1,00 — —

* non comprende le azioni orizzontali eventualmente esercitate dai materiali immagazzinati
** per i soli parapetti o partizioni nelle zone pedonali. Le azioni sulle barriere esercitate dagli automezzi dovranno essere valutate caso per caso

Thus we have the following loads value:

- residential (Cat. A): $q_k = 2.00 \text{ KN/m}^2$
- commercial (Cat. D1): $q_k = 4.00 \text{ KN/m}^2$

3 DATA

As previously said on introducing chapter, we choose to keep some problem's objects as variable, while instead some other are kept as data, changeless and contained in a definite interval of values, mainly due to constructive requirements.

3.1 Spans

We assume, according to the background type, the following values for maximum spans, indicated with 'l':

- residential (Cat. A): $l = 6 \text{ m}$
- commercial (Cat. D1): $l = 8 \text{ m}$
-

3.2 Width of the glulam beams

The choice of the basis dimension has been taken by considering most common values used to create glulam beam. By indicating with 'b' the width of the glulam beam, we assume $b = 90 \text{ mm}$.

3.3 Spacing between glulam beams

Also this choice has been taken by considering most common values in business. By indicating with 'i' the spacing between the glulam beam, we assume $i = 800 \text{ mm}$.

3.4 Connection system

According to 4.4.9 of standard [1], is possible to make use of special connection systems as well their behavior is clearly defined either theoretically or experimentally. In our case we refer to experimental tests results described in Paper [1]. However, the complete description of the two connection system used is reported on Chapter 6 ("Stiffness of the timber-concrete connectors").

3.5 Check of the connection

According to 8.7.3 of Statement [3], the strength check for connection system made up by screws loaded both axially and laterally provides the satisfying of the following relation (expression (8.28) of standard [3]):

$$\left(\frac{F_{ax,Ed}}{F_{ax,Rd}} \right)^2 + \left(\frac{F_{V,Ed}}{F_{V,Rd}} \right)^2 \leq 1$$

If we call α the angle between the screw axis and the grain, previous expression becomes:

$$\left(\frac{F \cdot \cos \alpha}{F_{ax,Rd}} \right)^2 + \left(\frac{F \cdot \sin \alpha}{F_{V,Rd}} \right)^2 \leq 1$$

where F , fastener load, has to be taken as (as suggested at point B.5 of standard [3]):

$$F = \frac{\gamma_1 \cdot E_1 \cdot A_1 \cdot a_1 \cdot s_{eq}}{EJ_{ef}} \cdot V$$

where:

V is the maximum shear load

The withdrawal strength $F_{ax,k,Rk}$ should be taken by using expression (8.38) of standard reference [4]:

$$F_{ax,k,Rk} = \frac{n_{ef} \cdot f_{ax,k} \cdot d \cdot l_{ef} \cdot k_d}{1.2 \cdot \cos^2 \alpha + \sin^2 \alpha}$$

where:

$$f_{ax,k} = 0.52 \cdot d^{-0.5} \cdot l_{ef}^{-0.1} \cdot \rho_k^{0.8}$$

$$k_d = \min\{d/8; 1\}$$

$$n_{ef} = n^{0.9}$$

d is the diameter of each connector (outer diameter of the threaded part)

n is the number of screws acting together in a connection

The characteristic shear strength of screw laterally loaded can be calculated by using expression (8.10) of standard [3], which also considers the rope effect caused by screws withdrawal strength and evaluable, in absence of experimentation, with the quantity $F_{ax,Rk}/4$ (point 8.2.1 of standard [3]):

$$F_{V,Rk} = \min \left\{ \begin{array}{l} n \cdot f_{h,o,k} \cdot l_{ef} \cdot \phi \\ n \cdot f_{h,o,k} \cdot l_{ef} \cdot \phi \cdot \left[\sqrt{2 + \frac{4 \cdot M_{y,Rk}}{f_{h,o,k} \cdot l_{ef}^2 \cdot \phi}} - 1 \right] + \frac{F_{ax,Rk}}{4} \\ n \cdot 2,3 \cdot \sqrt{M_{y,k} \cdot f_{h,o,k} \cdot \phi} + \frac{F_{ax,Rk}}{4} \end{array} \right\}$$

where:

l_{ef} is the pointside penetration length of the threaded part minus one screw diameter, in mm

$M_{y,Rk}$ is the characteristic value for the yield moment, in Nmm

$f_{h,o,k}$ is the characteristic embedment strength, in Nmm

The connection check imposes to calculate the characteristic embedment strength of the screws (evaluable with expression (8.16) of standard [3]) and the characteristic yield moment (evaluable with expression (8.14) of standard [3]):

$$f_{h,o,k} = 0.082 \cdot (1 - 0.01\phi) \cdot \rho_k$$

$$M_{y,Rk} = 0.3 \cdot f_{u,k} \cdot \phi^{2,6}$$

These relations are valid if the screws has not a threaded part. Otherwise, according to point 8.7.1 of standard [3], the screw load-carrying capacity should be calculated using an effective diameter d_{ef} taken as 1.1 times the thread root diameter.

By passing from characteristic to project value we have to consider also k_{mod} factors (previously described in chapter 1 of this appendix) and material safety factors γ_M . His value can be taken from next Table 4.4.III of standard [1].

Table 2.3 – Recommended partial factors γ_M for material properties and resistances

Fundamental combinations:	
Solid timber	1,3
Glued laminated timber	1,25
LVL, plywood, OSB,	1,2
Particleboards	1,3
Fibreboards, hard	1,3
Fibreboards, medium	1,3
Fibreboards, MDF	1,3
Fibreboards, soft	1,3
Connections	1,3
Punched metal plate fasteners	1,25
Accidental combinations	1,0

In case of connections the partial factor is equal to: $\gamma_M = 1.3$.

4 CALCULATION EXAMPLE

In this section we bring, as an example, the whole calculation and check proceeding for a definite background type and a definite connection system. For the other possible combinations between background type and connection system successively we'll bring only the results of the checks.

We assume a residential background and the F45 connection system, previously described on Chapter 6 “Stiffness of the timber-concrete connectors”.

The data related to residential background, regarding span and variable load, are equal to:

- $l = 6 \text{ m}$
- $Q_k = 2.00 \text{ KN/m}^2$

We assume the following dimensions for the structural part, according to Figure 136 reported below:

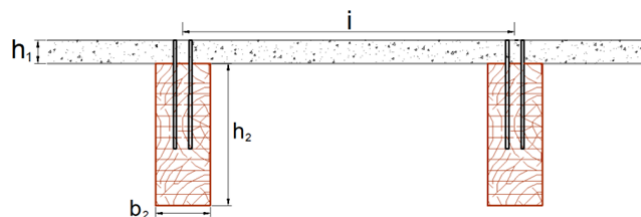


Figure 136: nomenclature and symbols used to define the system

$$i = 800 \text{ mm}$$

$$h_1 = 50 \text{ mm}$$

$$b_2 = 90 \text{ mm}$$

$$h_2 = 360 \text{ mm}$$

With reference to two side-by-side glulam beam spacing we can determinate the loads per unit length acting on each joist, obtained by considering both the glulam beam and a part of the concrete slab with depth equal to spacing between glulam beams.

$$g_1 = \gamma_{k,CAP} \cdot h_1 \cdot i + \gamma_{k,GL} \cdot h_2 \cdot b_2 = 22.93 \times 0.05 \times 0.8 + 3.82 \times 0.36 \times 0.09 = 1.04 \left[\frac{KN}{m} \right]$$

$$g_2 = G_2 \cdot i = 2.69 \times 0.8 = 2.15 \left[\frac{KN}{m} \right]$$

$$q_1 = Q_1 \cdot i = 2.00 \times 0.8 = 1.60 \left[\frac{KN}{m} \right]$$

We can now determinate external action values, with reference to load combinations required for checks.

4.1 Load combinations

Checks, to consider the different load duration categories and the long term behavior, will be done both at early time (implementation of the system) and at infinite time.

In early time SLU checks we consider two different actions combination, one made up by only permanent loads (Combination I) and the other with all loads included variable action (Combination II). Instead, at final time we consider only the second Combination, including all loads. By substituting the values previously obtained we have:

$$q_{SLU,I} = 1.3 \cdot g_1 + 1.3 \cdot g_2 = 1.3 \times (1.04 + 2.15) = 4.15 \left[\frac{KN}{m} \right]$$

$$q_{SLU,II} = 1.3 \cdot g_1 + 1.3 \cdot g_2 + 1.5 \cdot q_1 = (1.3 \times 1.04 + 1.3 \times 2.15 + 1.5 \times 1.60) = 6.55 \left[\frac{KN}{m} \right]$$

The values of actions combined at SLS are equal to:

$$q_{SLE,characteristic} = g_1 + g_2 + q_1 = (1.04 + 2.15 + 1.60) = 4.79 \left[\frac{KN}{m} \right]$$

$$q_{SLE_{-qp}} = g_1 + g_2 + \psi_{21} \cdot q_1 = (1.04 + 2.15 + 0.3 \times 1.60) = 3.67 \left[\frac{KN}{m} \right]$$

4.1.1 External actions

Now we calculate the project value of bending moment at mid-span (M_d) and shear at the end of the beam (T_d), according to the two significant load combinations at SLU.

$$T_{d,I} = \frac{q_{SLU,I} \cdot l}{2} = \frac{4.15 \times 6}{2} = 12.46 [KN]$$

$$M_{d,I} = \frac{q_{SLU,I} \cdot l^2}{8} = \frac{4.15 \times 6^2}{8} = 18.69 [KNm]$$

$$T_{d,II} = \frac{q_{SLU,II} \cdot l}{2} = \frac{6.55 \times 6}{2} = 19.66 [KN]$$

$$M_{d,II} = \frac{q_{SLU,II} \cdot l^2}{8} = \frac{6.55 \times 6^2}{8} = 29.49 [KNm]$$

4.2 Properties of the connection system

As previously said, in this example we use connection system F45. We choose to maintain spacing between two successive connectors constant and equal to 250 mm, thus in 1 meter there are four connectors (we remember that each one connector is formed by one element made up by furfurylated wood in which are inserted four inclined screws VGZ 7 x 180).

Stiffness related to each connection element can be deduced from experimental tests provided in reference [1] and presented in at point 6.2.2 of this paper. In this case we have:

$$K_{ser} = 45000 \text{ N/mm}$$

$$K_u = 30000 \text{ N/mm}$$

With reference to following Figure 137 and to its indicated nomenclature, each screw is embedded in the two different items for a definite length, reported below.

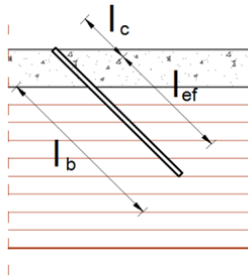


Figure 137: embedment lengths of the screws on each element

$$l_b = 180 \text{ mm (total length of the screw)}$$

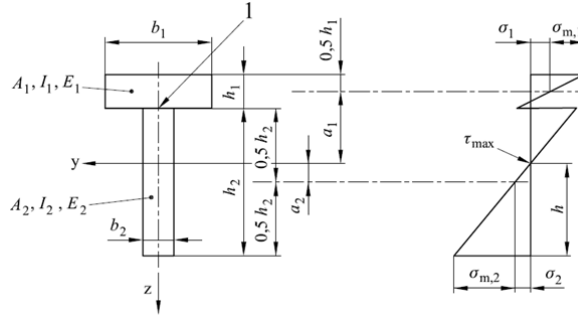
$$l_c = h_1 / \cos 45^\circ = (50 / \cos 45^\circ) \text{ mm} \approx 70 \text{ mm (embedment length of the screw in the furfurylated wood)}$$

$$l_{ef} = l_b - l_c = (180 - 70) \text{ mm} \approx 110 \text{ mm (embedment length of the screw in the glulam beam)}$$

4.3 Stiffness properties of composite system

In this section we'll assess the stiffness values, first relative to single items and then relative to composite system. These values are evaluate both at early time ($t = 0$) and final time ($t = \infty$). The calculation is made by using for the stiffness average values. Now we give an esteem of these properties evaluated at ULS, while instead the properties at SLS will be calculated on following paragraph 4.5 ("Deformation checks").

We refer to symbols adopted on Fig. B.1 of standard [3].



Short term ($t = 0$)

$$E_1 \cdot J_1 = E_{cm} \cdot \frac{i \cdot h_1^3}{12} = 36210 \times \frac{800 \times 50^3}{12} = 3.02 \times 10^{11} [Nmm^2]$$

$$E_2 \cdot J_2 = E_{0,mean} \cdot \frac{b_2 \cdot h_2^3}{12} = 12500 \times \frac{90 \times 360^3}{12} = 4.37 \times 10^{12} [Nmm^2]$$

$$E_1 \cdot A_1 = E_{cm} \cdot i \cdot h_1 = 36210 \times 800 \times 50 mm^2 = 1.45 \times 10^9 [N]$$

$$E_2 \cdot A_2 = E_{0,mean} \cdot b_2 \cdot h_2 = 12500 \times 90 \times 360 = 4.05 \times 10^8 [N]$$

$$(EJ)_0 = E_1 \cdot J_1 + E_2 \cdot J_2 = (3.02 \times 10^{11} + 4.37 \times 10^{12}) = 4.68 \times 10^{12} [Nmm^2]$$

$$(EA)_0 = \frac{E_1 \cdot A_1 \cdot E_2 \cdot A_2}{E_1 \cdot A_1 + E_2 \cdot A_2} = \frac{1.45 \times 10^9 \times 4.05 \times 10^8}{1.45 \times 10^9 + 4.05 \times 10^8} = 3.17 \times 10^8 [N]$$

$$EJ_{ef} = \sum_i E_i J_i + \gamma_2 \cdot E_2 \cdot A_2 \cdot a_2^2 + \gamma_1 \cdot E_1 \cdot A_1 \cdot a_1^2$$

$$EJ_{\infty} = \sum_i (E_i \cdot J_i + E_i \cdot A_i \cdot a_i^2) = (EJ)_0 + (EA)_0 \cdot a^2$$

$$\eta = \frac{EJ_{ef} - (EJ)_0}{EJ_{\infty} - (EJ)_0}$$

Where, according to the point B.2 of reference [4], we have:

$$a = h_1/2 + h_2/2 + t$$

$$a_2 = \frac{\gamma_1 \cdot E_1 \cdot A_1 \cdot a}{\gamma_1 \cdot E_1 \cdot A_1 + \gamma_2 \cdot E_2 \cdot A_2}$$

$$a_1 = a - a_2$$

$$\gamma_2 = 1$$

$$\gamma_1 = \left[1 + \pi^2 \cdot E_1 \cdot A_1 \cdot s_{eq} / (K \cdot l^2) \right]^{-1}$$

η is a dimensionless parameter which quantifies the connection efficiency

As we saw in previous paragraph, containing a brief description of the connection system, we have:

$$K_U = 30000 \text{ N/mm}$$

$$s_{eq} = s = 250 \text{ mm}$$

Thus, by substituting values we obtain:

$$\gamma_2 = 1$$

$$\gamma_1 = \left[1 + \pi^2 \cdot E_1 \cdot A_1 \cdot s_{eq} / (K \cdot I^2) \right]^{-1} = \left[1 + \pi^2 \times 1.45 \times 10^9 \times 250 / (30000 \times 6000^2) \right]^{-1} = 0.23$$

$$a = h_1/2 + h_2/2 = (50/2 + 360/2) = 205 \text{ mm}$$

$$a_2 = \frac{\gamma_1 \cdot E_1 \cdot A_1 \cdot a}{\gamma_1 \cdot E_1 \cdot A_1 + \gamma_2 \cdot E_2 \cdot A_2} = \frac{0.23 \times 1.45 \times 10^9}{0.23 \times 1.45 \times 10^9 + 1 \times 4.05 \times 10^8} \times 205 \text{ mm} = 93 \text{ mm}$$

$$a_1 = a - a_2 = (205 - 93) = 112 \text{ mm}$$

$$\begin{aligned} EJ_{ef} &= \sum_i E_i J_i + \gamma_2 \cdot E_2 \cdot A_2 \cdot a_2^2 + \gamma_1 \cdot E_1 \cdot A_1 \cdot a_1^2 = \\ &= (3.02 \times 10^{11} + 4.37 \times 10^{12} + 1 \times 4.05 \times 10^8 \times 93^2 + 0.23 \times 1.45 \times 10^9 \times 112^2) = 1.24 \times 10^{13} [\text{Nmm}^2] \end{aligned}$$

$$EJ_{\infty} = (EJ)_0 + (EA)_0 \cdot a^2 = (4.68 \times 10^{12} + 3.17 \times 10^8 \times 205^2) = 1.80 \times 10^{13} [\text{Nmm}^2]$$

$$\eta = \frac{EJ_{ef} - (EJ)_0}{EJ_{\infty} - (EJ)_0} = \frac{1.24 \times 10^{13} - 4.68 \times 10^{12}}{1.80 \times 10^{13} - 4.68 \times 10^{12}} = 0.58$$

Long term ($t = \infty$)

With respect to the short term the glulam elastic modulus changes:

$$E_{0,mean,\infty} = \frac{E_{0,mean}}{1 + k_{def}} = \frac{12500}{1 + 0.6} = 7813 [\text{MPa}]$$

$$E_1 \cdot J_1 = E_{cm} \cdot \frac{i \cdot h_1^3}{12} = 36210 \times \frac{800 \times 50^3}{12} = 3.02 \times 10^{11} [\text{Nmm}^2]$$

$$E_2 \cdot J_2 = E_{0,mean,\infty} \cdot \frac{b_2 \cdot h_2^3}{12} = 7813 \times \frac{90 \times 360^3}{12} = 2.73 \times 10^{12} [\text{Nmm}^2]$$

$$E_1 \cdot A_1 = E_{cm} \cdot i \cdot h_1 = 36210 \times 800 \times 50 \text{ mm}^2 = 1.45 \times 10^9 [\text{N}]$$

$$E_2 \cdot A_2 = E_{0,mean,\infty} \cdot b_2 \cdot h_2 = 7813 \times 90 \times 360 = 2.53 \times 10^8 [\text{N}]$$

$$(EJ)_0 = E_1 \cdot J_1 + E_2 \cdot J_2 = (3.02 \times 10^{11} + 2.73 \times 10^{12}) = 3.04 \times 10^{12} [\text{Nmm}^2]$$

$$(EA)_0 = \frac{E_1 \cdot A_1 \cdot E_2 \cdot A_2}{E_1 \cdot A_1 + E_2 \cdot A_2} = \frac{1.45 \times 10^9 \times 2.53 \times 10^8}{1.45 \times 10^9 + 2.53 \times 10^8} = 2.15 \times 10^8 [\text{N}]$$

$$EJ_{ef} = \sum_i E_i J_i + \gamma_2 \cdot E_2 \cdot A_2 \cdot a_2^2 + \gamma_1 \cdot E_1 \cdot A_1 \cdot a_1^2$$

$$EJ_{\infty} = \sum_i (E_i \cdot J_i + E_i \cdot A_i \cdot a_i^2) = (EJ)_0 + (EA)_0 \cdot a^2$$

$$\eta = \frac{EJ_{ef} - (EJ)_0}{EJ_{\infty} - (EJ)_0}$$

Where, according to the point B.2 of reference [4], we have:

$$a = h_1/2 + h_2/2 + t$$

$$a_2 = \frac{\gamma_1 \cdot E_1 \cdot A_1 \cdot a}{\gamma_1 \cdot E_1 \cdot A_1 + \gamma_2 \cdot E_2 \cdot A_2}$$

$$a_1 = a - a_2$$

$$\gamma_2 = 1$$

$$\gamma_1 = \left[1 + \pi^2 \cdot E_1 \cdot A_1 \cdot s_{eq} / (K \cdot l^2)\right]^{-1}$$

η is a dimensionless parameter which quantifies the connection efficiency

As we saw in previous paragraph, containing a brief description of the connection system, we have:

$$K_U = 30000 \text{ N/mm}$$

$$s_{eq} = s = 250 \text{ mm}$$

Furthermore we have:

$$K_{U,\infty} = K_U / (1 + k_{def}) = 30000 / (1 + 0.6) \text{ Nmm} = 18750 \text{ Nmm}$$

$$s_{eq} = s = 250 \text{ mm}$$

Thus, by substituting values we obtain:

$$\gamma_2 = 1$$

$$\gamma_1 = \left[1 + \pi^2 \cdot E_1 \cdot A_1 \cdot s_{eq} / (K \cdot l^2)\right]^{-1} = \left[1 + \pi^2 \times 1.45 \times 10^9 \times 250 / (18750 \times 6000^2)\right]^{-1} = 0.16$$

$$a = h_1/2 + h_2/2 = (50/2 + 360/2) = 205 \text{ mm}$$

$$a_2 = \frac{\gamma_1 \cdot E_1 \cdot A_1 \cdot a}{\gamma_1 \cdot E_1 \cdot A_1 + \gamma_2 \cdot E_2 \cdot A_2} = \frac{0.16 \times 1.45 \times 10^9}{0.16 \times 1.45 \times 10^9 + 1 \times 2.53 \times 10^8} \times 205 = 98 \text{ mm}$$

$$a_1 = a - a_2 = (205 - 98) = 107 \text{ mm}$$

$$EJ_{ef} = \sum_i E_i J_i + \gamma_2 \cdot E_2 \cdot A_2 \cdot a_2^2 + \gamma_1 \cdot E_1 \cdot A_1 \cdot a_1^2 =$$

$$= (3.02 \times 10^{11} + 2.73 \times 10^{12} + 1 \times 2.53 \times 10^8 \times 98^2 + 0.16 \times 1.45 \times 10^9 \times 107^2) = 8.10 \times 10^{12} [\text{Nmm}^2]$$

$$EJ_{\infty} = (EJ)_0 + (EA)_0 \cdot a^2 = (3.04 \times 10^{12} + 2.15 \times 10^8 \times 205^2) = 1.21 \times 10^{12} [\text{Nmm}^2]$$

$$\eta = \frac{EJ_{ef} - (EJ)_0}{EJ_{\infty} - (EJ)_0} = \frac{8.10 \times 10^{12} - 3.04 \times 10^{12}}{1.21 \times 10^{12} - 3.04 \times 10^{12}} = 0.56$$

4.4 Strength verifications

Strength verifications regard the glulam beam, the concrete slab and the connection system, and have to be performed both at short term ($t = 0$) and long term ($t = \infty$), according to the load duration conditions (short term and long term-permanent). In our case we refer to symbols adopted in Figure B.1 of Statement [3], already presented in Chapter 5 (“Composite action of timber-concrete composite systems”). Verifications that must be achieved are indicated below:

- Compressive strength on concrete (at upper side of the concrete plate)
- Tensile strength on concrete (eventual, at lower side of the concrete plate)
- Combined bending and axial tension in glulam (at lower side of the glulam beam)
- Shear strength in glulam
- Combined shear and axial load on the connection system

We carry below the formulations suggested in Appendix B of standard [3] to evaluate the stresses in the elements:

$$\tau_{\max} = \frac{0.5 \cdot E_2 \cdot (a_2 + h_2/2)^2}{EJ_{ef}} \cdot V$$

$$\sigma_i = \frac{\gamma_i \cdot E_i \cdot a_i \cdot M}{EJ_{ef}}$$

$$\sigma_{m,i} = \frac{0.5 \cdot E_i \cdot h_i \cdot M}{EJ_{ef}}$$

4.4.1 Strength verifications at $t = 0$ with only permanent loads

External stresses, previously calculated, are equal to: $T_{d,l} = 12.46 \text{ KN}$; $M_{d,l} = 18.69 \text{ KNm}$.

By substituting these values we can evaluate stresses acting in each element.

$$\sigma_1 = \frac{\gamma_1 \cdot E_1 \cdot a_1}{EJ_{ef}} \cdot M_{d,l} = \frac{0.23 \times 36210 \times 112}{1.24 \times 10^{13}} \times 18.69 \times 10^6 = 1.42 [\text{MPa}]$$

$$\sigma_{m,1} = \frac{0.5 \cdot E_1 \cdot h_1}{EJ_{ef}} \cdot M_{d,l} = \frac{0.5 \times 36210 \times 50}{1.24 \times 10^{13}} \times 18.69 \times 10^6 = 1.37 [\text{MPa}]$$

$$\sigma_2 = \frac{\gamma_2 \cdot E_2 \cdot a_2}{EJ_{ef}} \cdot M_{d,l} = \frac{1 \times 12500 \times 93}{1.24 \times 10^{13}} \times 18.69 \times 10^6 = 1.75 [\text{MPa}]$$

$$\sigma_{m,2} = \frac{0.5 \cdot E_2 \cdot h_2}{EJ_{ef}} \cdot M_{d,l} = \frac{0.5 \times 12500 \times 360}{1.24 \times 10^{13}} \times 18.69 \times 10^6 = 3.39 [\text{MPa}]$$

$$\tau_{\max} = \frac{0.5 \cdot E_2 \cdot (a_2 + h_2/2)^2}{EJ_{ef}} \cdot T_{d,l} = \frac{0.5 \times 12500 \times (93 + 360/2)^2}{1.24 \times 10^{13}} \times 12.46 \times 10^3 = 0.47 [\text{MPa}]$$

Compressive and tensile strength in concrete (both considered positive) are equal to:

$$\sigma_{C1} = \sigma_1 + \sigma_{m,1} = 1.42 + 1.37 = 2.79 [\text{MPa}]$$

$$\sigma_{T1} = \sigma_{m,1} - \sigma_1 = 1.37 - 1.42 = -0.05 [\text{MPa}]$$

The load acting on the fastener is equal to:

$$F = \frac{\gamma_1 \cdot E_1 \cdot A_1 \cdot a_1 \cdot s_{eq}}{EJ_{ef}} \cdot T_{d,l} = \frac{0.23 \times 1.45 \times 10^9 \times 112 \times 250}{1.24 \times 10^{13}} \times 12.46 = 9.47 [\text{KN}]$$

Now we can perform all the checks provided by the statements.

Compressive strength in concrete

$$\frac{\sigma_{C1}}{f_{cd}} = \frac{2.79}{25.30} = 0.11 \leq 1$$

Tensile strength in concrete

$$\frac{\sigma_{T1}}{f_{ctd}} = \frac{-0.05}{1.76} \leq 1$$

Combined bending and axial tension in glulam

$$\frac{\sigma_2}{f_{t,0,d}} + \frac{\sigma_{m2}}{f_{m,d}} = \frac{1.75}{10.10} + \frac{3.39}{15.15} = 0.40 \leq 1$$

where:

$$f_{t,0,d} = k_h \cdot \frac{k_{\text{mod}} \cdot f_{t,0,k}}{\gamma_m} = 1.05 \times \frac{0.6 \times 20}{1.25} = 10.10 [\text{MPa}]$$

$$f_{m,d} = k_h \cdot \frac{k_{\text{mod}} \cdot f_{m,k}}{\gamma_m} = 1.05 \times \frac{0.6 \times 30}{1.25} = 15.15 [\text{MPa}]$$

$$k_h = \min \left\{ \left(\frac{600}{h_2} \right)^{0.1}; 1.1 \right\} = \min \left\{ \left(\frac{600}{360} \right)^{0.1}; 1.1 \right\} = 1.05$$

Shear in glulam

$$\frac{\tau_{\max}}{f_{v,d}} = \frac{0.47}{1.68} = 0.28 \leq 1$$

Combined shear and axial load on connection system

With reference to the point 8.7.2 of Statement [3] (“Axially loaded screws”), to evaluate the withdrawal capacity we can use the following expression:

$$F_{ax,k,Rk} = \frac{n_{ef} \cdot f_{ax,k} \cdot d \cdot l_{ef} \cdot k_d}{1.2 \cdot \cos^2 \alpha + \sin^2 \alpha}$$

where:

$$f_{ax,k} = 0.52 \cdot d^{-0.5} \cdot l_{ef}^{-0.1} \cdot \rho_k^{0.8} = 0.52 \times 7^{-0.5} \times 110^{-0.1} \times 390^{0.8} = 14.53 [MPa]$$

$$k_d = \min\{d/8; 1\} = \min\{7/8; 1\} = 0.88$$

$$n_{ef} = n^{0.9} = 4^{0.9} = 3.48$$

$$F_{ax,k,Rk} = \frac{n_{ef} \cdot f_{ax,k} \cdot d \cdot l_{ef} \cdot k_d}{1.2 \cdot \cos^2 \alpha + \sin^2 \alpha} = \frac{3.48 \times 14.52 \times 7 \times 110 \times 0.88}{1.2 \times \cos^2 45^\circ + \sin^2 45^\circ} \times 10^{-3} = 30.80 [kN]$$

Characteristic strength of both laterally and axially loaded screws can be evaluated by using expression (8.10) of reference [3]:

$$F_{V,Rk} = \min \left\{ \begin{array}{l} n \cdot f_{h,o,k} \cdot l_{ef} \cdot \phi \\ n \cdot f_{h,o,k} \cdot l_{ef} \cdot \phi \cdot \left[\sqrt{2 + \frac{4 \cdot M_{y,Rk}}{f_{h,o,k} \cdot l_{ef}^2 \cdot \phi}} - 1 \right] + \frac{F_{ax,Rk}}{4} \\ n \cdot 2,3 \cdot \sqrt{M_{y,k} \cdot f_{h,o,k} \cdot \phi} + \frac{F_{ax,Rk}}{4} \end{array} \right\}$$

where:

$$\phi = 1.1 \cdot d_{nucleo} = 1.1 \times 4.6 = 5.06 mm$$

$d_{nucleo} = 4.6 mm$ is the inner diameter of the screw

$$f_{h,o,k} = 0.082 \cdot (1 - 0.01\phi) \cdot \rho_k = 0.082 \times (1 - 0.01 \times 5.06) \times 390 = 30.36 [MPa]$$

$$M_{y,Rk} = 0.3 \cdot f_{u,k} \cdot \phi^{2.6} = 0.3 \times 1000 \times 5.06^{2.6} = 20319 [Nmm]$$

$f_{uk} = 1000 N/mm^2$ is the ultimate strength of the connector

If we substitute these values we can obtain:

$$F_{V,Rk} = \min \left\{ \begin{array}{l} n \cdot f_{h,o,k} \cdot l_{ef} \cdot \phi \\ n \cdot f_{h,o,k} \cdot l_{ef} \cdot \phi \cdot \left[\sqrt{2 + \frac{4 \cdot M_{y,Rk}}{f_{h,o,k} \cdot l_{ef}^2 \cdot \phi}} - 1 \right] + \frac{F_{ax,Rk}}{4} \\ n \cdot 2,3 \cdot \sqrt{M_{y,k} \cdot f_{h,o,k} \cdot \phi} + \frac{F_{ax,Rk}}{4} \end{array} \right\}$$

$$= \min \left\{ \begin{array}{l} 4 \times 30.36 \times 110 \times 5.06 \\ 4 \times 30.36 \times 110 \times 5.06 \times \left[\sqrt{2 + \frac{4 \times 20319}{30.36 \times 110^2 \times 5.06}} - 1 \right] + \frac{30800}{4} \\ 4 \times 2.3 \times \sqrt{20319 \times 30.36 \times 5.06} + \frac{30800}{4} \end{array} \right\} = \min \left\{ \begin{array}{l} 67161 \\ 36566 \\ 23956 \end{array} \right\} [N] = 23.96 [KN]$$

We can now get the design strength values and check the connection:

$$F_{ax,Rd} = k_{mod,I} \cdot \frac{F_{ax,k,Rk}}{\gamma_{connection}} = \frac{0.6 \times 30.80}{1.30} = 14.22 [KN]$$

$$F_{V,Rd} = k_{mod,I} \cdot \frac{F_{V,Rk}}{\gamma_{connection}} = \frac{0.6 \times 23.96}{1.30} = 11.06 [KN]$$

$$\left(\frac{F_{ax,Ed}}{F_{ax,Rd}} \right)^2 + \left(\frac{F_{V,Ed}}{F_{V,Rd}} \right)^2 = \left(\frac{F \cdot \cos \alpha}{F_{ax,Rd}} \right)^2 + \left(\frac{F \cdot \sin \alpha}{F_{V,Rd}} \right)^2 = \left(\frac{9.47 \times \cos \alpha}{14.22} \right)^2 + \left(\frac{9.47 \times \sin \alpha}{11.06} \right)^2 = 0.59 \leq 1$$

Stresses in the cross-section

Next graph shows the path of the stress σ on the cross section, at $t = 0$ and with only the permanent loads acting.

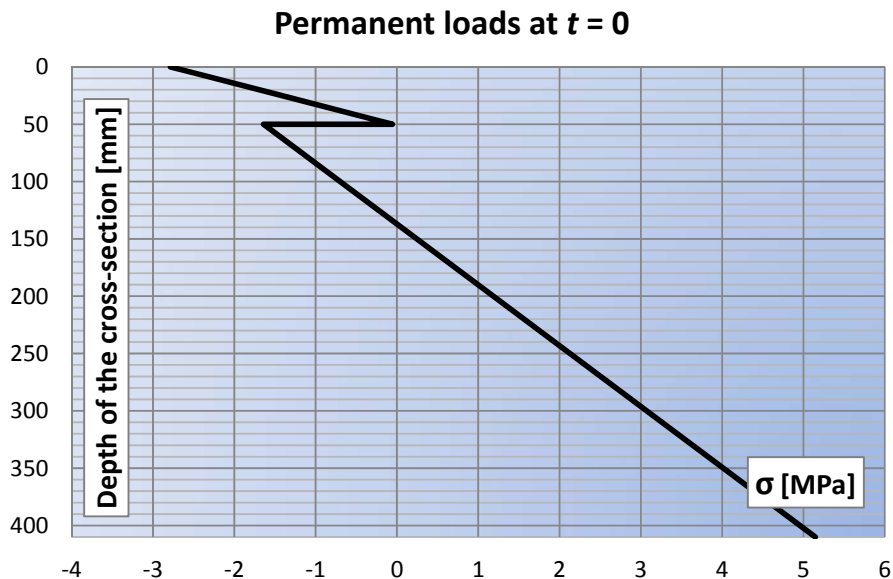


Figure 138: stress path on the cross-section with only the permanent load acting, at $t = 0$

4.4.2 Strength verifications at $t = 0$ with all loads

External stresses, previously calculated, are equal to: $T_{d,II} = 19.66 \text{ KN}$; $M_{d,II} = 29.49 \text{ KNm}$.

By substituting these values we can evaluate stresses acting in each element.

$$\sigma_1 = \frac{\gamma_1 \cdot E_1 \cdot a_1}{EJ_{ef}} \cdot M_{d,II} = \frac{0.23 \times 36210 \times 112}{1.24 \times 10^{13}} \times 29.49 \times 10^6 = 2.24 [\text{MPa}]$$

$$\sigma_{m,1} = \frac{0.5 \cdot E_1 \cdot h_1}{EJ_{ef}} \cdot M_{d,II} = \frac{0.5 \times 36210 \times 50}{1.24 \times 10^{13}} \times 29.49 \times 10^6 = 2.15 [\text{MPa}]$$

$$\sigma_2 = \frac{\gamma_2 \cdot E_2 \cdot a_2}{EJ_{ef}} \cdot M_{d,II} = \frac{1 \times 12500 \times 93}{1.24 \times 10^{13}} \times 29.49 \times 10^6 = 2.77 [\text{MPa}]$$

$$\sigma_{m,2} = \frac{0.5 \cdot E_2 \cdot h_2}{EJ_{ef}} \cdot M_{d,II} = \frac{0.5 \times 12500 \times 360}{1.24 \times 10^{13}} \times 29.49 \times 10^6 = 5.35 [\text{MPa}]$$

$$\tau_{\max} = \frac{0.5 \cdot E_2 \cdot (a_2 + h_2/2)^2}{EJ_{ef}} \cdot T_{d,II} = \frac{0.5 \times 12500 \times (93 + 360/2)^2}{1.24 \times 10^{13}} \times 19.66 \times 10^3 = 0.74 [\text{MPa}]$$

Compressive and tensile strength in concrete (both considered positive) are equal to:

$$\sigma_{C1} = \sigma_1 + \sigma_{m,1} = 2.24 + 2.15 = 4.39 [\text{MPa}]$$

$$\sigma_{T1} = \sigma_{m,1} - \sigma_1 = 2.15 - 2.24 = -0.09 [\text{MPa}]$$

The load acting on the fastener is equal to:

$$F = \frac{\gamma_1 \cdot E_1 \cdot A_1 \cdot a_1 \cdot s_{eq}}{EJ_{ef}} \cdot T_{d,II} = \frac{0.23 \times 1.45 \times 10^9 \times 112 \times 250}{1.24 \times 10^{13}} \times 19.66 = 14.93 [\text{KN}]$$

Now we can perform all the checks provided by the statements.

Compressive strength in concrete

$$\frac{\sigma_{C1}}{f_{cd}} = \frac{4.39}{25.30} = 0.17 \leq 1$$

Tensile strength in concrete

$$\frac{\sigma_{T1}}{f_{ctd}} = \frac{-0.09}{1.76} \leq 1$$

Combined bending and axial tension in glulam

$$\frac{\sigma_2}{f_{t,0,d}} + \frac{\sigma_{m,2}}{f_{m,d}} = \frac{2.77}{13.47} + \frac{5.35}{20.21} = 0.47 \leq 1$$

where:

$$f_{t,0,d} = k_h \cdot \frac{k_{\text{mod}} \cdot f_{t,0,k}}{\gamma_m} = 1.05 \times \frac{0.8 \times 20}{1.25} = 13.47 [\text{MPa}]$$

$$f_{m,d} = k_h \cdot \frac{k_{\text{mod}} \cdot f_{m,k}}{\gamma_m} = 1.05 \times \frac{0.8 \times 30}{1.25} = 20.21 [\text{MPa}]$$

$$k_h = \min \left\{ \left(\frac{600}{h_2} \right)^{0.1}; 1.1 \right\} = \min \left\{ \left(\frac{600}{360} \right)^{0.1}; 1.1 \right\} = 1.05$$

Shear in glulam

$$\frac{\tau_{\text{max}}}{f_{v,d}} = \frac{0.74}{2.24} = 0.33 \leq 1$$

Combined shear and axial load on connection system

With reference to the point 8.7.2 of Statement [3] (“Axially loaded screws”), to evaluate the withdrawal capacity we can use the following expression:

$$F_{ax,k,Rk} = \frac{n_{ef} \cdot f_{ax,k} \cdot d \cdot l_{ef} \cdot k_d}{1.2 \cdot \cos^2 \alpha + \sin^2 \alpha}$$

where:

$$f_{ax,k} = 0.52 \cdot d^{-0.5} \cdot l_{ef}^{-0.1} \cdot \rho_k^{0.8} = 0.52 \times 7^{-0.5} \times 110^{-0.1} \times 390^{0.8} = 14.53 [\text{MPa}]$$

$$k_d = \min\{d/8; 1\} = \min\{7/8; 1\} = 0.88$$

$$n_{ef} = n^{0.9} = 4^{0.9} = 3.48$$

$$F_{ax,k,Rk} = \frac{n_{ef} \cdot f_{ax,k} \cdot d \cdot l_{ef} \cdot k_d}{1.2 \cdot \cos^2 \alpha + \sin^2 \alpha} = \frac{3.48 \times 14.52 \times 7 \times 110 \times 0.88}{1.2 \times \cos^2 45^\circ + \sin^2 45^\circ} \times 10^{-3} = 30.80 [\text{KN}]$$

Characteristic strength of both laterally and axially loaded screws can be evaluate by using expression (8.10) of reference [3]:

$$F_{V,Rk} = \min \left\{ \begin{array}{l} n \cdot f_{h,o,k} \cdot l_{ef} \cdot \phi \\ n \cdot f_{h,o,k} \cdot l_{ef} \cdot \phi \cdot \left[\sqrt{2 + \frac{4 \cdot M_{y,Rk}}{f_{h,o,k} \cdot l_{ef}^2 \cdot \phi}} - 1 \right] + \frac{F_{ax,Rk}}{4} \\ n \cdot 2.3 \cdot \sqrt{M_{y,k} \cdot f_{h,o,k} \cdot \phi} + \frac{F_{ax,Rk}}{4} \end{array} \right\}$$

where:

$$\phi = 1.1 \cdot d_{\text{nucleo}} = 1.1 \times 4.6 = 5.06 \text{ mm}$$

$d_{\text{nucleo}} = 4.6 \text{ mm}$ is the inner diameter of the screw

$$f_{h,0,k} = 0.082 \cdot (1 - 0.01\phi) \cdot \rho_k = 0.082 \times (1 - 0.01 \times 5.06) \times 390 = 30.36 [\text{MPa}]$$

$$M_{y,Rk} = 0.3 \cdot f_{u,k} \cdot \phi^{2.6} = 0.3 \times 1000 \times 5.06^{2.6} = 20319 [\text{Nmm}]$$

$f_{uk} = 1000 \text{ N/mm}^2$ is the ultimate strength of the connector

If we substitute these values we can obtain:

$$F_{V,Rk} = \min \left\{ \begin{array}{l} n \cdot f_{h,o,k} \cdot l_{ef} \cdot \phi \\ n \cdot f_{h,o,k} \cdot l_{ef} \cdot \phi \cdot \left[\sqrt{2 + \frac{4 \cdot M_{y,Rk}}{f_{h,o,k} \cdot l_{ef}^2 \cdot \phi}} - 1 \right] + \frac{F_{ax,Rk}}{4} \\ n \cdot 2.3 \cdot \sqrt{M_{y,k} \cdot f_{h,o,k} \cdot \phi} + \frac{F_{ax,Rk}}{4} \end{array} \right\}$$

$$= \min \left\{ \begin{array}{l} 4 \times 30.36 \times 110 \times 5.06 \\ 4 \times 30.36 \times 110 \times 5.06 \times \left[\sqrt{2 + \frac{4 \times 20319}{30.36 \times 110^2 \times 5.06}} - 1 \right] + \frac{30800}{4} \\ 4 \times 2.3 \times \sqrt{20319 \times 30.36 \times 5.06} + \frac{30800}{4} \end{array} \right\} = \min \left\{ \begin{array}{l} 67161 \\ 36566 \\ 23956 \end{array} \right\} [N] = 23.99 [KN]$$

We can now get the strength project values and check the connection:

$$F_{ax,Rd} = k_{mod,II} \cdot \frac{F_{ax,k,Rk}}{\gamma_{connection}} = \frac{0.8 \times 30.80}{1.30} = 18.96 [KN]$$

$$F_{V,Rd} = k_{mod,II} \cdot \frac{F_{V,Rk}}{\gamma_{connection}} = \frac{0.8 \times 23.96}{1.30} = 14.74 [KN]$$

$$\left(\frac{F_{ax,Ed}}{F_{ax,Rd}} \right)^2 + \left(\frac{F_{V,Ed}}{F_{V,Rd}} \right)^2 = \left(\frac{F \cdot \cos \alpha}{F_{ax,Rd}} \right)^2 + \left(\frac{F \cdot \sin \alpha}{F_{V,Rd}} \right)^2 = \left(\frac{14.93 \times \cos \alpha}{18.96} \right)^2 + \left(\frac{14.93 \times \sin \alpha}{14.74} \right)^2 = 0.82 \leq 1$$

Stresses in the cross-section

In next diagram we can see the path of the stress σ on the cross section of both concrete and glulam, at $t = 0$ and with all loads acting.

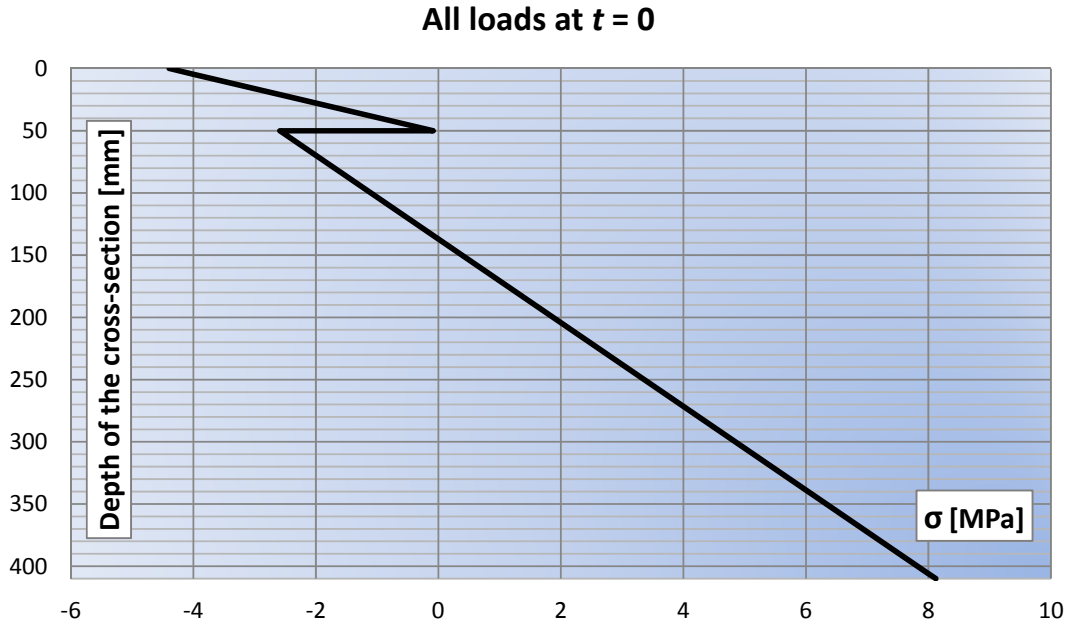


Figure 139: stress path on the cross-section with only the permanent load acting, at $t = 0$

4.4.3 Strength checks at $t = \infty$ with all loads

External stresses, previously calculated, are equal to: $T_{d,II} = 19.66 \text{ KN}$; $M_{d,II} = 29.49 \text{ KNm}$.

By substituting these values we can evaluate stresses acting in each element.

$$\sigma_1 = \frac{\gamma_1 \cdot E_1 \cdot a_1}{EJ_{ef}} \cdot M_{d,II} = \frac{0.16 \times 36210 \times 107}{8.10 \times 10^{12}} \times 29.49 \times 10^6 = 2.25 [\text{MPa}]$$

$$\sigma_{m,1} = \frac{0.5 \cdot E_1 \cdot h_1}{EJ_{ef}} \cdot M_{d,II} = \frac{0.5 \times 36210 \times 50}{8.10 \times 10^{12}} \times 29.49 \times 10^6 = 3.30 [\text{MPa}]$$

$$\sigma_2 = \frac{\gamma_2 \cdot E_2 \cdot a_2}{EJ_{ef}} \cdot M_{d,II} = \frac{1 \times 7813 \times 98}{8.10 \times 10^{12}} \times 29.49 \times 10^6 = 2.78 [\text{MPa}]$$

$$\sigma_{m,2} = \frac{0.5 \cdot E_2 \cdot h_2}{EJ_{ef}} \cdot M_{d,II} = \frac{0.5 \times 7813 \times 360}{8.10 \times 10^{12}} \times 29.49 \times 10^6 = 5.12 [\text{MPa}]$$

$$\tau_{\max} = \frac{0.5 \cdot E_2 \cdot (a_2 + h_2/2)^2}{EJ_{ef}} \cdot T_{d,II} = \frac{0.5 \times 7813 \times (98 + 360/2)^2}{8.10 \times 10^{12}} \times 19.66 \times 10^3 = 0.73 [\text{MPa}]$$

Compressive and tensile strength in concrete (both considered positive) are equal to:

$$\sigma_{C1} = \sigma_1 + \sigma_{m,1} = 2.25 + 3.30 = 5.55[\text{MPa}]$$

$$\sigma_{T1} = \sigma_{m,1} - \sigma_1 = 3.30 - 2.25 = 1.05[\text{MPa}]$$

The load acting on the fastener is equal to:

$$F = \frac{\gamma_1 \cdot E_1 \cdot A_1 \cdot a_1 \cdot s_{eq}}{EJ_{ef}} \cdot T_{d,II} = \frac{0.16 \times 1.45 \times 10^9 \times 107 \times 250}{8.10 \times 10^{12}} \times 19.66 = 14.99[\text{KN}]$$

Now we can perform all the checks provided by the statements.

Compressive strength in concrete

$$\frac{\sigma_{C1}}{f_{cd}} = \frac{5.55}{25.30} = 0.22 \leq 1$$

Tensile strength in concrete

$$\frac{\sigma_{T1}}{f_{ctd}} = \frac{1.05}{1.76} = 0.60 \leq 1$$

Combined bending and axial tension in glulam

$$\frac{\sigma_2}{f_{t,0,d}} + \frac{\sigma_{m2}}{f_{m,d}} = \frac{2.78}{13.47} + \frac{5.12}{20.21} = 0.46 \leq 1$$

where:

$$f_{t,0,d} = k_h \cdot \frac{k_{\text{mod}} \cdot f_{t,0,k}}{\gamma_m} = 1.05 \times \frac{0.8 \times 20}{1.25} = 13.47[\text{MPa}]$$

$$f_{m,d} = k_h \cdot \frac{k_{\text{mod}} \cdot f_{m,k}}{\gamma_m} = 1.05 \times \frac{0.8 \times 30}{1.25} = 20.21[\text{MPa}]$$

$$k_h = \min \left\{ \left(\frac{600}{h_2} \right)^{0.1}; 1.1 \right\} = \min \left\{ \left(\frac{600}{360} \right)^{0.1}; 1.1 \right\} = 1.05$$

Shear in glulam

$$\frac{\tau_{\text{max}}}{f_{v,d}} = \frac{0.73}{2.24} = 0.33 \leq 1$$

Combined shear and axial load on connection system

With reference to the point 8.7.2 of Statement [3] (“Axially loaded screws”), to evaluate the withdrawal capacity we can use the following expression:

$$F_{ax,k,Rk} = \frac{n_{ef} \cdot f_{ax,k} \cdot d \cdot l_{ef} \cdot k_d}{1.2 \cdot \cos^2 \alpha + \sin^2 \alpha}$$

where:

$$f_{ax,k} = 0.52 \cdot d^{-0.5} \cdot l_{ef}^{-0.1} \cdot \rho_k^{0.8} = 0.52 \times 7^{-0.5} \times 110^{-0.1} \times 390^{0.8} = 14.53 [MPa]$$

$$k_d = \min\{d/8; 1\} = \min\{7/8; 1\} = 0.88$$

$$n_{ef} = n^{0.9} = 4^{0.9} = 3.48$$

$$F_{ax,k,Rk} = \frac{n_{ef} \cdot f_{ax,k} \cdot d \cdot l_{ef} \cdot k_d}{1.2 \cdot \cos^2 \alpha + \sin^2 \alpha} = \frac{3.48 \times 14.52 \times 7 \times 110 \times 0.88}{1.2 \times \cos^2 45^\circ + \sin^2 45^\circ} \times 10^{-3} = 30.80 [KN]$$

Characteristic strength of both laterally and axially loaded screws can be evaluate by using expression (8.10) of reference [3]:

$$F_{V,Rk} = \min \left\{ \begin{array}{l} n \cdot f_{h,o,k} \cdot l_{ef} \cdot \phi \\ n \cdot f_{h,o,k} \cdot l_{ef} \cdot \phi \cdot \left[\sqrt{2 + \frac{4 \cdot M_{y,Rk}}{f_{h,o,k} \cdot l_{ef}^2 \cdot \phi}} - 1 \right] + \frac{F_{ax,Rk}}{4} \\ n \cdot 2,3 \cdot \sqrt{M_{y,k} \cdot f_{h,o,k} \cdot \phi} + \frac{F_{ax,Rk}}{4} \end{array} \right\}$$

where:

$$\phi = 1.1 \cdot d_{nucleo} = 1.1 \times 4.6 = 5.06 mm$$

$d_{nucleo} = 4.6 mm$ is the inner diameter of the screw

$$f_{h,o,k} = 0.082 \cdot (1 - 0.01\phi) \cdot \rho_k = 0.082 \times (1 - 0.01 \times 5.06) \times 390 = 30.36 [MPa]$$

$$M_{y,Rk} = 0.3 \cdot f_{u,k} \cdot \phi^{2,6} = 0.3 \times 1000 \times 5.06^{2,6} = 20319 [Nmm]$$

$f_{uk} = 1000 N/mm^2$ is the ultimate strength of the connector

If we substitute these values we can obtain:

$$F_{V,Rk} = \min \left\{ \begin{array}{l} n \cdot f_{h,o,k} \cdot l_{ef} \cdot \phi \\ n \cdot f_{h,o,k} \cdot l_{ef} \cdot \phi \cdot \left[\sqrt{2 + \frac{4 \cdot M_{y,Rk}}{f_{h,o,k} \cdot l_{ef}^2 \cdot \phi}} - 1 \right] + \frac{F_{ax,Rk}}{4} \\ n \cdot 2,3 \cdot \sqrt{M_{y,k} \cdot f_{h,o,k} \cdot \phi} + \frac{F_{ax,Rk}}{4} \end{array} \right\}$$

$$= \min \left\{ \begin{array}{l} 4 \times 30.36 \times 110 \times 5.06 \\ 4 \times 30.36 \times 110 \times 5.06 \times \left[\sqrt{2 + \frac{4 \times 20319}{30.36 \times 110^2 \times 5.06}} - 1 \right] + \frac{30800}{4} \\ 4 \times 2.3 \times \sqrt{20319 \times 30.36 \times 5.06} + \frac{30800}{4} \end{array} \right\} = \min \left\{ \begin{array}{l} 67161 \\ 36566 \\ 23956 \end{array} \right\} [N] = 23.96 [KN]$$

We can now get the strength project values and check the connection:

$$F_{ax,Rd} = k_{mod,II} \cdot \frac{F_{ax,k,Rk}}{\gamma_{connection}} = \frac{0.8 \times 30.80}{1.30} = 18.96 [KN]$$

$$F_{V,Rd} = k_{mod,II} \cdot \frac{F_{V,Rk}}{\gamma_{connection}} = \frac{0.8 \times 23.96}{1.30} = 14.74 [KN]$$

$$\left(\frac{F_{ax,Ed}}{F_{ax,Rd}} \right)^2 + \left(\frac{F_{V,Ed}}{F_{V,Rd}} \right)^2 = \left(\frac{F \cdot \cos \alpha}{F_{ax,Rd}} \right)^2 + \left(\frac{F \cdot \sin \alpha}{F_{V,Rd}} \right)^2 = \left(\frac{14.99 \times \cos \alpha}{18.96} \right)^2 + \left(\frac{14.99 \times \sin \alpha}{14.74} \right)^2 = 0.83 \leq 1$$

Stresses in the cross-section

Next graph shows the path of the stress σ on the cross section, at $t = \infty$ and with all loads acting.

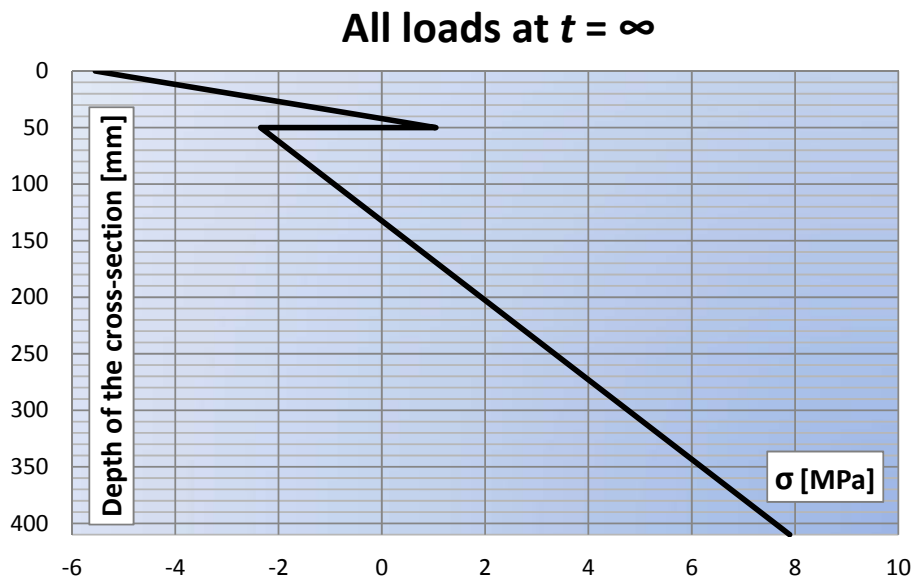


Figure 139: stress path on the cross-section with only the permanent load acting, at $t = 0$

If we compare the three stress paths (only permanent loads at t = 0, all loads at t = 0 and all loads at t = ∞) we obtain the following graph:

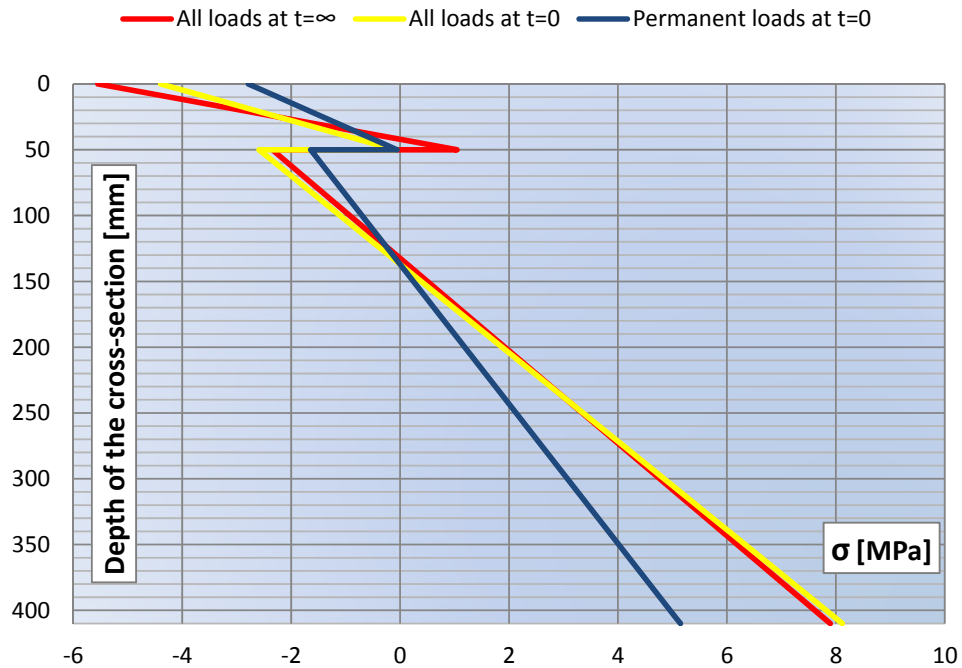


Figure 140: comparison between the three stress paths analyzed

4.5 SLS verifications

SLS verifications provide the direct evaluation of the beam mid-span deflection, and the control of the vibrations. The value of the mid-span deflection has to be compared with appropriate limit values indicated in regulations. According to point 7.2 of standard [3], it is recommended to assume limit values presented in following Table 7.2.

Table 7.2 – Examples of limiting values for deflections of beams

	w_{inst}	$w_{net,fin}$	w_{fin}
Beam on two supports	$l/300$ to $l/500$	$l/250$ to $l/350$	$l/150$ to $l/300$
Cantilevering beams	$l/150$ to $l/250$	$l/125$ to $l/175$	$l/75$ to $l/150$

The net deflection below a straight line between the supports should be calculated by using expression (7.2) of reference [3], below reported:

$$w_{net,fin} = w_{inst} + w_{creep} - w_c = w_{fin} - w_c$$

where:

w_c is the precamber (if applied)

w_{inst} is the instantaneous deflection

w_{creep} is the creep deflection

w_{fin} is the final deflection

$w_{net,fin}$ is the net final deflection

in the deflection checks, the effective stiffness properties of the composite structure have to be calculated according to the stiffness service value $K_{ser} = 45000 \text{ N/mm}$.

Now we calculate stiffness values, first relative to single items and then relative to composite system. These values are evaluate both at early time ($t = 0$) and final time ($t = \infty$). The calculation is made by using for the stiffness average values.

We refer to symbols adopted on Fig. B.1 of standard [3], previously reported.

Short term ($t = 0$)

$$E_1 \cdot J_1 = E_{cm} \cdot \frac{i \cdot h_1^3}{12} = 36210 \times \frac{800 \times 50^3}{12} = 3.02 \times 10^{11} [\text{Nmm}^2]$$

$$E_2 \cdot J_2 = E_{0,mean} \cdot \frac{b_2 \cdot h_2^3}{12} = 12500 \times \frac{90 \times 360^3}{12} = 4.37 \times 10^{12} [\text{Nmm}^2]$$

$$E_1 \cdot A_1 = E_{cm} \cdot i \cdot h_1 = 36210 \times 800 \times 50 = 1.45 \times 10^9 [\text{N}]$$

$$E_2 \cdot A_2 = E_{0,mean} \cdot b_2 \cdot h_2 = 12500 \times 90 \times 360 = 4.05 \times 10^8 [\text{N}]$$

$$(EJ)_0 = E_1 \cdot J_1 + E_2 \cdot J_2 = 3.02 \times 10^{11} + 4.37 \times 10^{12} = 4.68 \times 10^{12} [\text{Nmm}^2]$$

$$(EA)_0 = \frac{E_1 \cdot A_1 \cdot E_2 \cdot A_2}{E_1 \cdot A_1 + E_2 \cdot A_2} = \frac{1.45 \times 10^9 \times 4.05 \times 10^8}{1.45 \times 10^9 + 4.05 \times 10^8} = 3.17 \times 10^8 [\text{N}]$$

$$EJ_{ef} = \sum_i E_i J_i + \gamma_2 \cdot E_2 \cdot A_2 \cdot a_2^2 + \gamma_1 \cdot E_1 \cdot A_1 \cdot a_1^2$$

$$EJ_{\infty} = \sum_i (E_i \cdot J_i + E_i \cdot A_i \cdot a_i^2) = (EJ)_0 + (EA)_0 \cdot a^2$$

Where, according to the point B.2 of reference [4], we have:

$$a = h_1/2 + h_2/2 + t$$

$$a_2 = \frac{\gamma_1 \cdot E_1 \cdot A_1 \cdot a}{\gamma_1 \cdot E_1 \cdot A_1 + \gamma_2 \cdot E_2 \cdot A_2}$$

$$a_1 = a - a_2$$

$$\gamma_2 = 1$$

$$\gamma_1 = \left[1 + \pi^2 \cdot E_1 \cdot A_1 \cdot s_{eq} / (K \cdot l^2)\right]^{-1}$$

As we saw in the previous paragraph, containing a brief description of the connection system, we have:

$$K_{ser} = 45000 \text{ N/mm}$$

$$s_{eq} = s = 250 \text{ mm}$$

Thus, by substituting values we obtain:

$$\gamma_2 = 1$$

$$\gamma_1 = \left[1 + \pi^2 \cdot E_1 \cdot A_1 \cdot s_{eq} / (K \cdot l^2)\right]^{-1} = \left[1 + \pi^2 \times 1.45 \times 10^9 \times 250 / (45000 \times 6000^2)\right]^{-1} = 0.31$$

$$a = h_1/2 + h_2/2 = (50/2 + 360/2) \text{ mm} = 205 \text{ mm}$$

$$a_2 = \frac{\gamma_1 \cdot E_1 \cdot A_1 \cdot a}{\gamma_1 \cdot E_1 \cdot A_1 + \gamma_2 \cdot E_2 \cdot A_2} = \frac{0.31 \times 1.45 \times 10^9}{0.31 \times 1.45 \times 10^9 + 1 \times 4.05 \times 10^8} \times 205 \text{ mm} = 108 \text{ mm}$$

$$a_1 = a - a_2 = 205 - 108 = 97 \text{ mm}$$

$$EJ_{ef,t=0,SLS} = \sum_i E_i J_i + \gamma_2 \cdot E_2 \cdot A_2 \cdot a_2^2 + \gamma_1 \cdot E_1 \cdot A_1 \cdot a_1^2 =$$

$$= 3.02 \times 10^{11} + 4.37 \times 10^{12} + 1 \times 4.05 \times 10^8 \times 108^2 + 0.31 \times 1.45 \times 10^9 \times 97^2 = 1.36 \times 10^{13} [\text{Nmm}^2]$$

$$EJ_{\infty,t=0,SLS} = (EJ)_0 + (EA)_0 \cdot a^2 = 4.68 \times 10^{12} + 3.17 \times 10^8 \times 205^2 = 1.80 \times 10^{13} [\text{Nmm}^2]$$

Long term ($t = \infty$)

With respect to short term the glulam elastic modulus changes:

$$E_{0,mean,\infty,SLS} = \frac{E_{0,mean}}{1 + \psi_{2Q} \cdot k_{def}} = \frac{12500}{1 + 0.3 \times 0.6} = 10593 [\text{MPa}]$$

$$E_1 \cdot J_1 = E_{cm} \cdot \frac{i \cdot h_1^3}{12} = 36210 \times \frac{800 \times 50^3}{12} = 3.02 \times 10^{11} [\text{Nmm}^2]$$

$$E_2 \cdot J_2 = E_{0,mean} \cdot \frac{b_2 \cdot h_2^3}{12} = 10593 \times \frac{90 \times 360^3}{12} = 3.71 \times 10^{12} [\text{Nmm}^2]$$

$$E_1 \cdot A_1 = E_{cm} \cdot i \cdot h_1 = 36210 \times 800 \times 50 = 1.45 \times 10^9 [\text{N}]$$

$$E_2 \cdot A_2 = E_{0,mean} \cdot b_2 \cdot h_2 = 10593 \times 90 \times 360 = 3.43 \times 10^8 [\text{N}]$$

$$(EJ)_0 = E_1 \cdot J_1 + E_2 \cdot J_2 = 3.02 \times 10^{11} + 3.71 \times 10^{12} = 4.01 \times 10^{12} [\text{Nmm}^2]$$

$$(EA)_0 = \frac{E_1 \cdot A_1 \cdot E_2 \cdot A_2}{E_1 \cdot A_1 + E_2 \cdot A_2} = \frac{1.45 \times 10^9 \times 3.43 \times 10^8}{1.45 \times 10^9 + 3.43 \times 10^8} = 2.77 \times 10^8 [\text{N}]$$

$$EJ_{ef} = \sum_i E_i J_i + \gamma_2 \cdot E_2 \cdot A_2 \cdot a_2^2 + \gamma_1 \cdot E_1 \cdot A_1 \cdot a_1^2$$

$$EJ_{\infty} = \sum_i (E_i \cdot J_i + E_i \cdot A_i \cdot a_i^2) = (EJ)_0 + (EA)_0 \cdot a^2$$

Where, according to the point B.2 of reference [4], we have:

$$a = h_1/2 + h_2/2 + t$$

$$a_2 = \frac{\gamma_1 \cdot E_1 \cdot A_1 \cdot a}{\gamma_1 \cdot E_1 \cdot A_1 + \gamma_2 \cdot E_2 \cdot A_2}$$

$$a_1 = a - a_2$$

$$\gamma_2 = 1$$

$$\gamma_1 = \left[1 + \pi^2 \cdot E_1 \cdot A_1 \cdot s_{eq} / (K \cdot l^2)\right]^{-1}$$

η is a dimensionless parameter which quantifies the connection efficiency

Furthermore we have:

$$K_{ser,\infty} = K_{ser} / (1 + \psi_{2Q} k_{def}) = 45000 / (1 + 0.3 \times 0.6) = 38136 \text{ Nmm}$$

$$s_{eq} = s = 250 \text{ mm}$$

Thus, by substituting values we obtain:

$$\gamma_2 = 1$$

$$\gamma_1 = \left[1 + \pi^2 \cdot E_1 \cdot A_1 \cdot s_{eq} / (K \cdot l^2)\right]^{-1} = \left[1 + \pi^2 \times 1.45 \times 10^9 \times 250 / (38136 \times 6000^2)\right]^{-1} = 0.28$$

$$a = h_1/2 + h_2/2 = (50/2 + 360/2) = 205 \text{ mm}$$

$$a_2 = \frac{\gamma_1 \cdot E_1 \cdot A_1 \cdot a}{\gamma_1 \cdot E_1 \cdot A_1 + \gamma_2 \cdot E_2 \cdot A_2} = \frac{0.28 \times 1.45 \times 10^9}{0.28 \times 1.45 \times 10^9 + 1 \times 3.43 \times 10^8} \times 205 = 111 \text{ mm}$$

$$a_1 = a - a_2 = 205 - 111 = 94 \text{ mm}$$

$$EJ_{ef,\infty,SLS} = \sum_i E_i J_i + \gamma_2 \cdot E_2 \cdot A_2 \cdot a_2^2 + \gamma_1 \cdot E_1 \cdot A_1 \cdot a_1^2 =$$

$$= 3.02 \times 10^{11} + 3.71 \times 10^{12} + 1 \times 3.43 \times 10^8 \times 111^2 + 0.28 \times 1.45 \times 10^9 \times 94^2 = 1.18 \times 10^{13} [\text{Nmm}^2]$$

$$EJ_{\infty,t=\infty,SLS} = (EJ)_0 + (EA)_0 \cdot a^2 = 4.01 \times 10^{12} + 2.78 \times 10^8 \times 205^2 = 1.57 \times 10^{12} [\text{Nmm}^2]$$

4.5.1 Mid span deflection check at $t = 0$

The instantaneous deflection is evaluated on the basis of the characteristic SLS action combination. Conservatively we assume a shear deflection equal to about 10% of bending deflection.

$$w_{inst} = 1.1 \cdot \frac{5}{384} \cdot \frac{q_{SLS_characteristic} \cdot l^4}{EJ_{ef,t=0,SLS}} = 1.1 \times \frac{5}{384} \times \frac{4.79 \times 6000^4}{1.36 \times 10^{13}} = 7mm \approx \frac{l}{850}$$

This value is much smaller than the lower limit carried on Table 7.2. In fact we have:

$$w_{inst} = 7mm \approx \frac{l}{850} < w_{inst_LIMIT} = \frac{l}{500} = 12mm$$

4.5.2 Mid span deflection check at $t = \infty$

The net final deflection is evaluated on the basis of the quasi-permanent SLS action combination. Conservatively we assume a shear deflection equal to about 10% of bending deflection.

$$w_{net,fin} = 1.1 \cdot \frac{5}{384} \cdot \frac{q_{SLE-QP} \cdot l^4}{EJ_{ef,t=\infty,SLE}} = 1.1 \times \frac{5}{384} \times \frac{3.67 \times 6000^4}{1.80 \times 10^{13}} = 4mm \approx \frac{l}{1500}$$

This value is much smaller than lower limit carried on Table 7.2. In fact we have:

$$w_{net,fin} = 4mm \approx \frac{l}{1500} < w_{net,fin_LIMIT} = \frac{l}{350} = 17mm$$

4.5.3 Vibrations checks at $t = 0$

In agreement with point 7.3 of Statement [3] we have:

$$f_{lim} = 8 \text{ Hz}$$

$$m = \frac{g_1 + g_2}{i} \cdot \frac{1}{g} = \frac{1.04 + 2.15}{0.8} \cdot \frac{1}{9.81} \times 10^3 = 407 \left[\frac{kg}{m^2} \right]$$

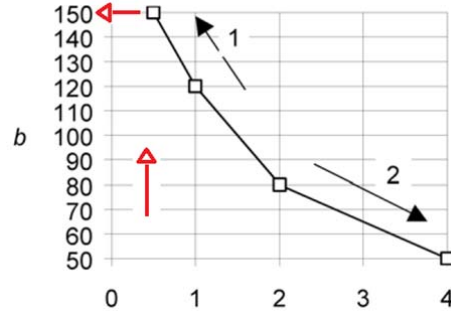
$$(EI)_l = \frac{EJ_{ef,t=0,SLS}}{i} = \frac{1.36 \times 10^{13}}{800} \times 10^{-3} = 1.71 \times 10^7 \left[\frac{Nm^2}{m} \right]$$

$$f_1 = \frac{\pi}{2 \cdot l^2} \cdot \sqrt{\frac{(EI)_l}{m}} = \frac{\pi}{2 \times 6^2} \times \sqrt{\frac{1.71 \times 10^7}{407}} = 9Hz > f_{lim} = 8Hz$$

$$(EI)_b = E_{cm} \cdot \frac{h_1^3}{12} = 36210 \times \frac{50^3}{12} \times 10^{-3} = 3.77 \times 10^5 \frac{Nm^2}{m}$$

$$\frac{w}{F} = \frac{l^3}{48 \cdot EJ_{ef,t=0,SLS}} = \frac{6^3}{48 \times 1.36 \times 10^{13}} \times 10^{12} = 0.3 \frac{mm}{kN}$$

With this value we enter the Figure 7.2 (reported below) at point 7.3.3 of Statement [1] and conservatively we can obtain the limit value $b = 150$.



$$b^{(f_1 \cdot \zeta - 1)} = 150^{(9 \times 0.01 - 1)} = 10^{-2}$$

where the recommended value for the modal damping ratio of a residential floor is: $\zeta = 0.01$

$$\eta_{40} = \left\{ \left[\left(\frac{40}{f_1} \right)^2 - 1 \right] \cdot \left(\frac{i}{l} \right)^4 \cdot \frac{(EI)_l}{(EI)_b} \right\}^{0.25} = \left\{ \left[\left(\frac{40}{9} \right)^2 - 1 \right] \times \left(\frac{0.8}{6} \right)^4 \times \frac{1.71 \times 10^7}{3.77 \times 10^5} \right\}^{0.25} = 0.7$$

$$v = \frac{4 \cdot (0.4 + 0.6 \cdot \eta_{40})}{m \cdot b \cdot l + 200} = \frac{4 \times (0.4 + 0.6 \times 0.7)}{407 \times 0.8 \times 6 + 200} = 1.5 \times 10^{-3}$$

By substituting the values we can see that the system is verified with respect to the vibrations.

$$v = 1.5 \times 10^{-3} < b^{f_1 \cdot \zeta - 1} = 10^{-2} = 10 \times 10^{-3}$$

4.5.4 Vibrations checks at $t = \infty$

In agreement with point 7.3 of Statement [3] we have:

$$f_{lim} = 8 \text{ Hz}$$

$$m = \frac{g_1 + g_2}{i} \cdot \frac{1}{g} = \frac{1.04 + 2.15}{0.8} \cdot \frac{1}{9.81} \times 10^3 = 407 \left[\frac{kg}{m^2} \right]$$

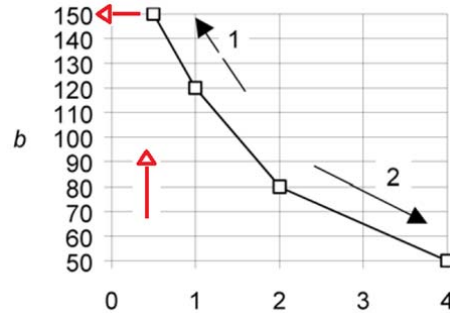
$$(EI)_l = \frac{EJ_{ef,t=\infty,SLS}}{i} = \frac{1.18 \times 10^{13}}{800} \times 10^{-3} = 1.48 \times 10^7 \left[\frac{Nm^2}{m} \right]$$

$$f_1 = \frac{\pi}{2 \cdot l^2} \cdot \sqrt{\frac{(EI)_l}{m}} = \frac{\pi}{2 \times 6^2} \times \sqrt{\frac{1.48 \times 10^7}{407}} = 8.3 \text{ Hz} > f_{lim} = 8 \text{ Hz}$$

$$(EI)_b = E_{cm} \cdot \frac{h_i^3}{12} = 36210 \times \frac{50^3}{12} \times 10^{-3} = 3.77 \times 10^5 \frac{Nm^2}{m}$$

$$\frac{w}{F} = \frac{l^3}{48 \cdot EJ_{ef,t=0,SLS}} = \frac{6^3}{48 \times 1.18 \times 10^{13}} \times 10^{12} = 0.4 \frac{mm}{kN}$$

With this value we enter the Figure 7.2 (reported below) at point 7.3.3 of Statement [1] and conservatively we can obtain the limit value $b = 150$.



$$b^{(f_1 \cdot \zeta^{-1})} = 150^{(9 \times 0.01^{-1})} = 10^{-2}$$

where the recommended value for the modal damping ratio of a residential floor is: $\zeta = 0.01$

$$\eta_{40} = \left\{ \left[\left(\frac{40}{f_1} \right)^2 - 1 \right] \cdot \left(\frac{i}{l} \right)^4 \cdot \frac{(EI)_h}{(EI)_b} \right\}^{0.25} = \left\{ \left[\left(\frac{40}{9} \right)^2 - 1 \right] \times \left(\frac{0.8}{6} \right)^4 \times \frac{1.48 \times 10^7}{3.77 \times 10^5} \right\}^{0.25} = 0.7$$

$$v = \frac{4 \cdot (0.4 + 0.6 \cdot \eta_{40})}{m \cdot b \cdot l + 200} = \frac{4 \times (0.4 + 0.6 \times 0.7)}{407 \times 0.8 \times 6 + 200} = 1.5 \times 10^{-3}$$

By substituting the values we can see that the system is with respect to the vibrations.

$$v = 1.5 \times 10^{-3} < b^{f_1 \cdot \zeta^{-1}} = 10^{-2} = 10 \times 10^{-3}$$

5 LIFTING CHECK

In this section we verify, with a numerical FE software SAP 2000, that the fiber reinforced concrete slab, with its definite dimensions, doesn't break under its own self-weight when carried. The concrete slabs are transported alone and separately from wooden beams.

Since after the elevation of the bigger plate (the one with 8 m of span) a little crack opened at the bottom, close to mid-span, we want to analyze other different manner of lifting, in addition to the real used in this experimental research (already described in Chapter 7 "Test results"). Thus, we analyze the following four manners of transportation, indicated in Figure 141 and described below:

- Upraising the plate at two points, symmetrical to the center, orthogonally to the plane of the slab (first manner)
- Upraising the plate at four points, symmetrical to the center, orthogonally to the plane of the slab (second and real manner used to lift the slab during the tests)
- Upraising the plate at two points, symmetrical to the center, parallel to the plane of the slab (third manner)
- Upraising the plate at three points, symmetrical to the center, orthogonally to the plane of the slab (fourth manner)

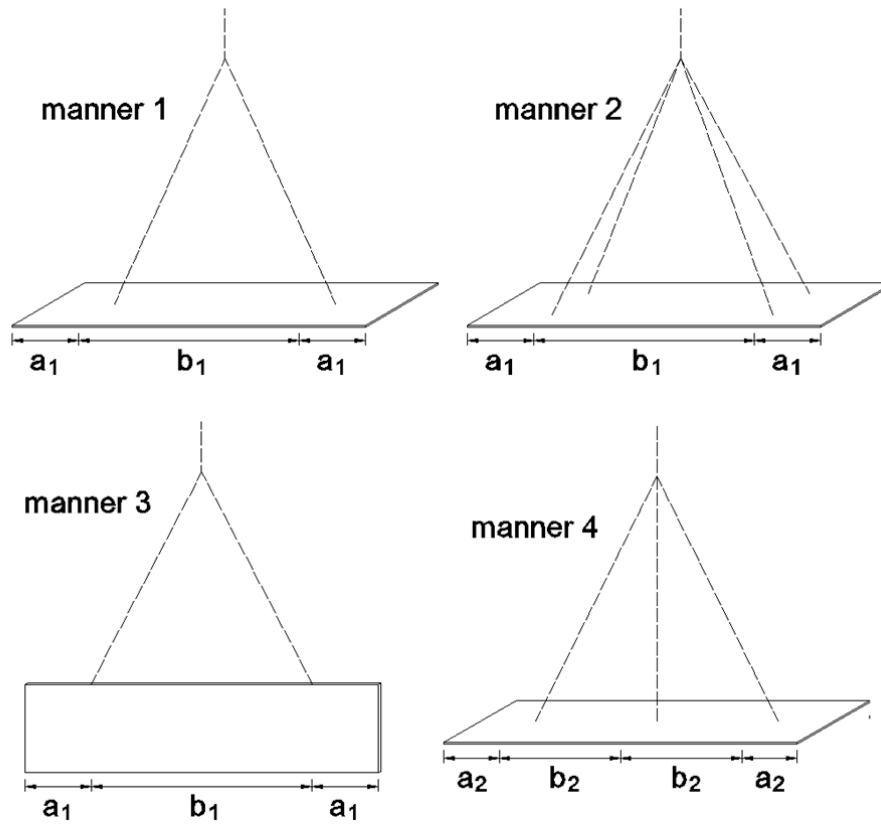


Figure 141: possible transportation manners assumed in place for the slabs

The heaviest values of strength due to self-weight are found in the wider slab, or else the one related to commercial background type, which has a span length of 8 m. We choose to proceed in the following order:

- We perform a finite elements analysis by using the software SAP2000 , with the aim of determining the maximum stress acting on the concrete slab
- We compare the stress obtained with the limit values of strength related to the material

5.1 EF analysis

The commercial background type slab measures 50 x 1600 x 8000 mm and, in the FE modeling, is considered simply supported on the points where it'll be lifted up. These points have been chosen in order to minimize the bending stresses on the slab (at the supports the stresses assume the same value). Since the experimental researches has been performed also on the slab measuring 50 x 1600 x 6000 mm, we evaluate, in next table 5, the position of these points also for this slab. In agreement with previous picture and calling with L the total length of the slab, the length of each span is:

$$a_1 = \frac{L}{2 \cdot (\sqrt{2} + 1)} \approx 0.207 \cdot L$$

$$b_1 = \frac{L \cdot \sqrt{2}}{\sqrt{2} + 1} \approx 0.586 \cdot L$$

$$a_2 = \frac{L}{2 \cdot (\sqrt{6} + 1)} \approx 0.145 \cdot L$$

$$b_2 = \frac{\sqrt{6}}{2} \cdot \frac{L}{\sqrt{6} + 1} \approx 0.355 \cdot L$$

n° of lifting points	L = 6 m		L = 8 m	
	2	a ₁ = 1.24 m	b ₁ = 3.52 m	a ₁ = 1.66 m
3	a ₂ = 0.87 m	b ₂ = 2.13 m	a ₂ = 1.16 m	b ₂ = 2.84 m

Table 5: distances of the points where the slab will be lifted up

The model we choose provides the plate subdivision in thin “shell” elements, square shaped with 20 cm sides and 5 cm thickness. In total there are 176 elements.

The plate is only subject to its own weight, amounting to: $\gamma_{k,FRC} = 22.93 \text{ KN/m}^3$.

The Young modulus of the material is: $E_{c,FRC} = 36210 \text{ N/mm}^2$.

Following Figures 142, 143, 144 and 145 show the software display with the trend of maximum stresses for each one of the three transportation manners considered.

First manner

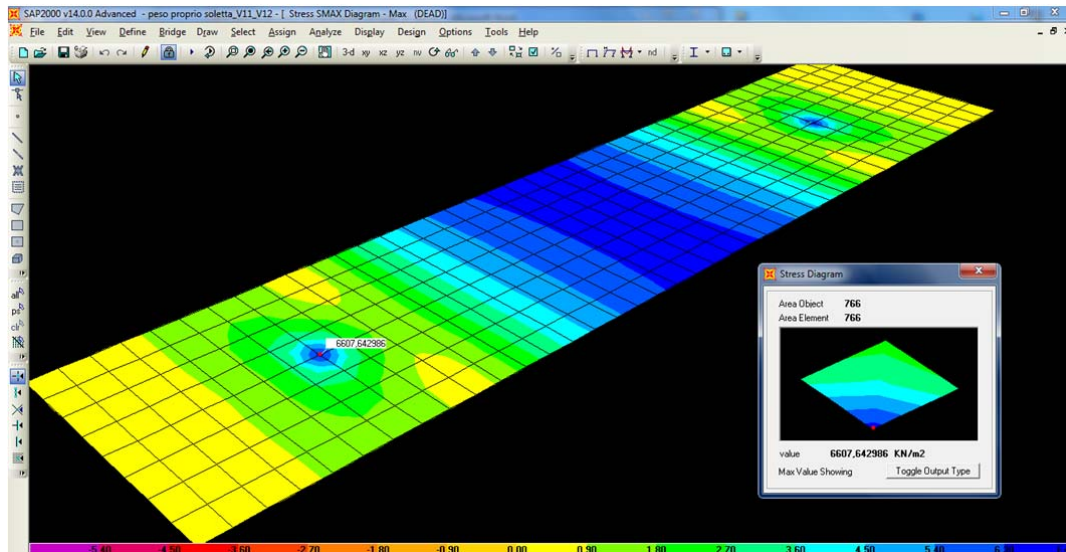


Figure 142: development of maximum stresses in the slab subject to its own weight, according to first way of carriage

The maximum stress at mid-span amounts to:

$$\sigma_{\max} \approx 6641 \left[\text{KN/m}^2 \right] = 6.64 \left[\text{MPa} \right]$$

Second manner

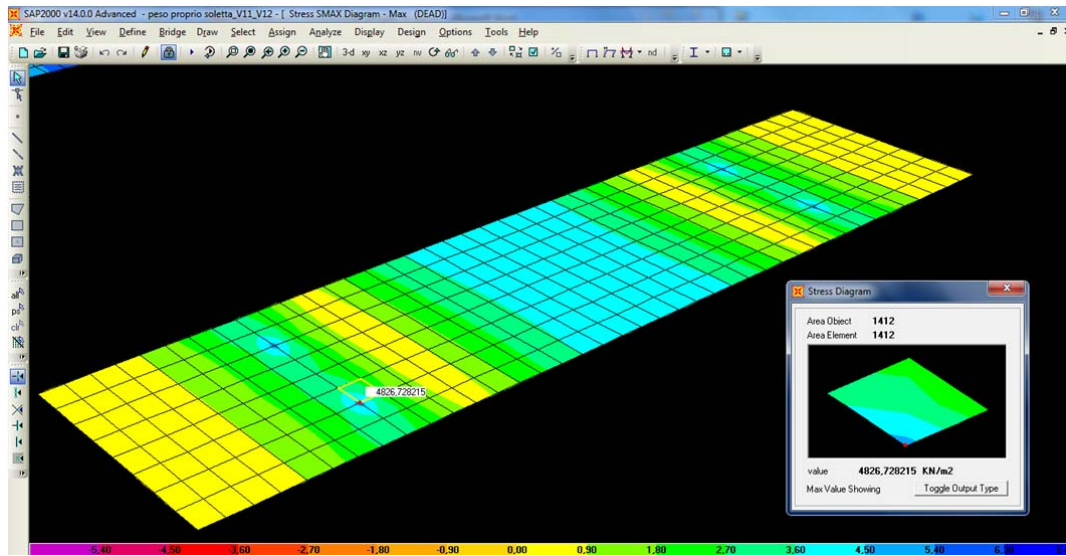


Figure 143: development of maximum stresses in the slab subject to its own weight, according to second way of carriage

The maximum stress at mid-span amounts to:

$$\sigma_{\max} \approx 4827 \left[\text{KN}/\text{m}^2 \right] = 4.83 \left[\text{MPa} \right]$$

Third manner

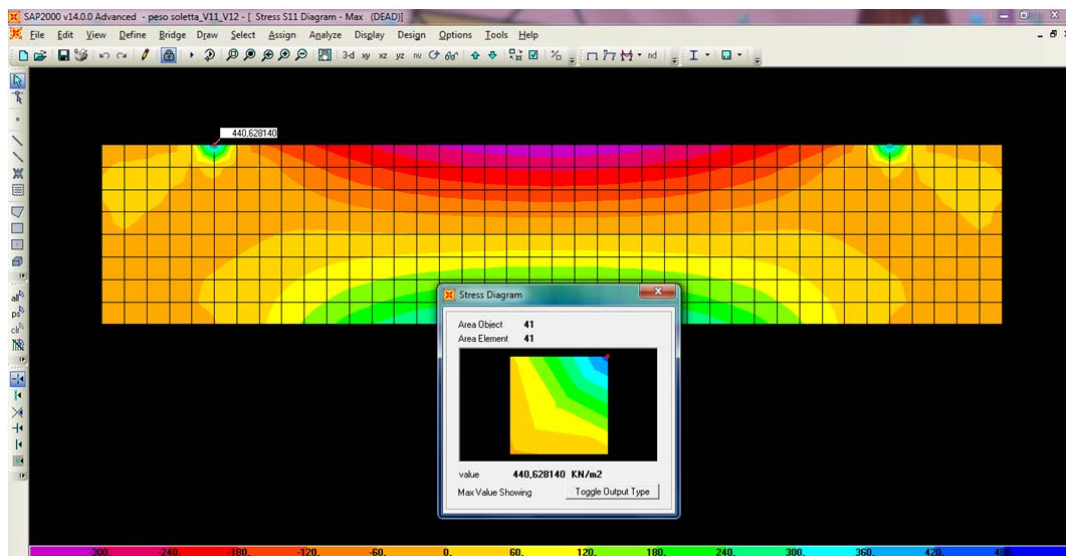


Figure 144: development of maximum stresses in the slab subject to its own weight, according to third way of carriage

The maximum stresses found at supports amounts to:

$$\sigma_{\max} \approx 442 \left[\text{KN}/\text{m}^2 \right] = 0.44 \left[\text{MPa} \right]$$

Fourth manner

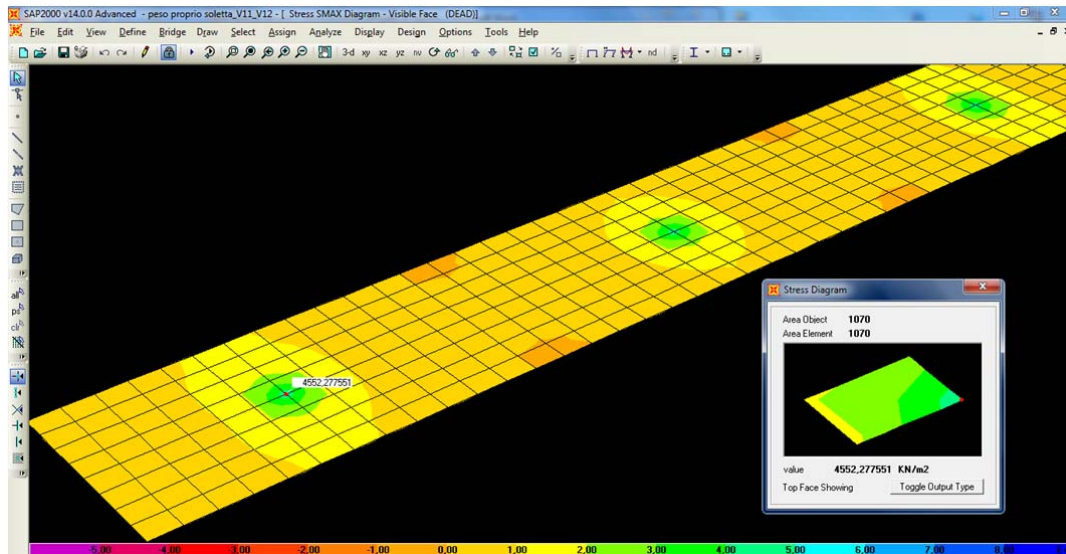


Figure 145: development of maximum stresses in the slab subject to its own weight, according to fourth way of carriage

The maximum stresses found at supports amounts to:

$$\sigma_{\max} \approx 4552 \left[\text{KN}/\text{m}^2 \right] = 4.55 \left[\text{MPa} \right]$$

5.2 Determination of strength limit values

A limit on the use of FRC is that mechanical properties of these materials are not collected and cataloged on theoretical grounds, and thus for their determination we have to rely on experimental tests results. To check the goodness of these results we won't rely to a single document but we'll use more than just one.

Now our target is to find the flexural strength limit value, for a fiber reinforced concrete containing $375 \text{ kg}/\text{m}^3$ of cement and $45 \text{ kg}/\text{m}^3$ of steel fibers type ZP30/.40 (Dramix), reported on next Figure 146. This is the same material used to perform the experimental tests described in Paper [1].

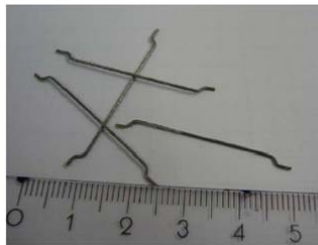


Figure 146: steel fibers ZP 30/.40

According to Table 4.1 of reference [3], the flexural strength of a fiber reinforced concrete containing $45 \text{ kg}/\text{m}^3$ (amounting to about 0.6% in volume) of steel fibers type ZP 30/.40 is equal to:

$$\sigma_{\text{lim}_{[3]}} = 859 \left[\text{Psi} \right] = 859 \times 6.895 \times 10^{-3} = 5.92 \left[\text{MPa} \right]$$

By referring now to Table 5 of Paper [4], the flexural strength for a fiber reinforced concrete similar to ours, or else containing 39 kg/m³ of steel fibers type ZP 50/.50 amounts to:

$$\sigma_{\text{lim}_{[4]}} = 850[\text{Psi}] = 850 \times 6.895 \times 10^{-3} = 5.86[\text{MPa}]$$

In Paper [5] there are reported laboratory tests performed to determine the flexural toughness. These experiments included to perform three points bending tests on some prismatic specimens of size 100 x 100 x 300 mm. The differences between each test concerned quantity and size of the fibers used to reinforce the concrete. In case of concrete with steel fibers type ZP 30/.50 in quantity of 75 lb/yd³ (or else equal to about a 45 kg/m³), the ultimate strength found amounted to about 3000 lb (13.35 KN), corresponding to following flexural strength:

$$\sigma_{\text{lim}_{[5]}} = \frac{F_{\text{lim}} \cdot L}{4} \cdot \frac{1}{W} = \frac{13.35 \times 10^3 \times 300}{4} \times \frac{6}{100 \times 100^2} = 6.01[\text{MPa}]$$

Paper [6], including disposition related to design of elements made of SFRC (Steel Fiber Reinforced Concrete), gives a range which contains the values of ultimate strength in bending (flexural strength). In particular, typical values found on the basis of three points bending tests on prismatic shaped standard specimens, made up with a quantity of steel fibers included between 0.5 % and 1.5 %, are contained in an interval between 5.5 e 7.5 MPa (variability is related to size and shape of the fibers and to water/cement ratio).

The same Paper [6] shows how the results of three points bending tests performed not on standard and prismatic specimens but on larger plates, respectively measuring 19 x 150 x 508 mm and 33 x 900 x 960 mm, depending on type, quantity and dimension of the steel fibers, provide a flexural strength included in a range of values between 6.2 and 7.6 MPa.

In accordance with Paper [8], flexural strength of a fiber reinforced concrete slab of dimensions 5000 x 600 x 50 mm, containing steel reinforcing fibers with length of 35 mm and in amount of 0.5 % in volume, is equal to:

$$\sigma_{\text{lim}_{[8]}} = 5.40[\text{MPa}]$$

5.3 Conclusions

We can see that, in agreement with the response of the software, the transportation way which have been used leads to high values of stress at the bottom of the slab. In general, we can observe that the third transportation manner is the least burdensome, leading to lower values of flexural stresses due only to self weight. So we can think, for future eventual researches and applications, that the slab first should be carried according to third transportation way, then lowered and made resting on one of the two the glulam beam over which it will lie to be finally rotated 90 degrees to assume horizontal position (as we can see from following figure 147).

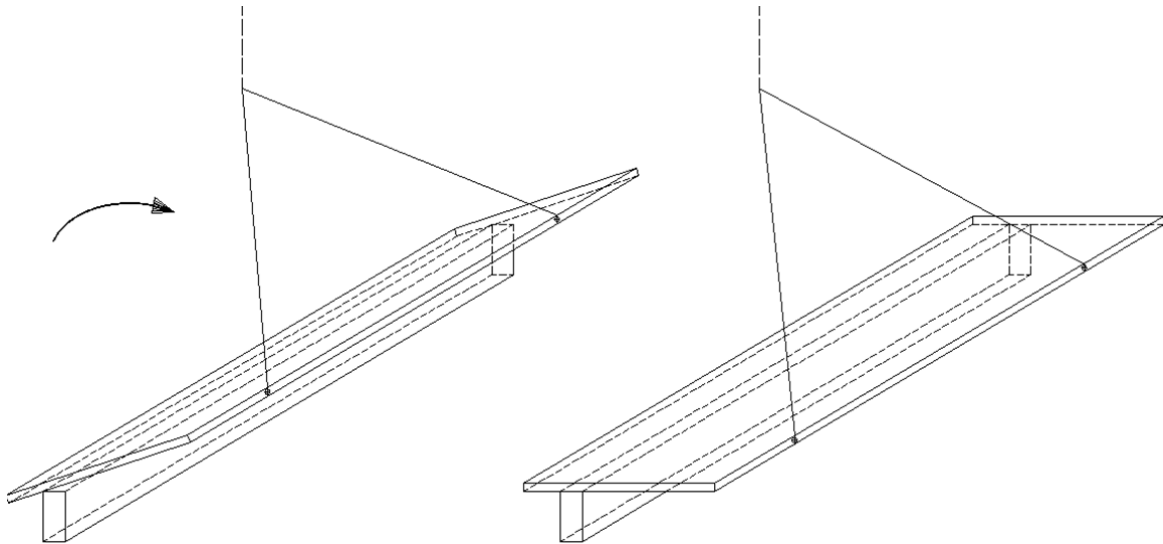


Figure 147: the slab is made rest on the glulam beam below and then rotated until horizontal position

In this phase the maximum stress due to self weight is found at the two supports (or else at the junction with the transport system cables).

Following Figure 148 shows the software display with the trend of maximum stresses for the slab at the limit moment in which it is almost horizontal, supported on one side by the glulam beam below and on the other side by the cables of the transport system.

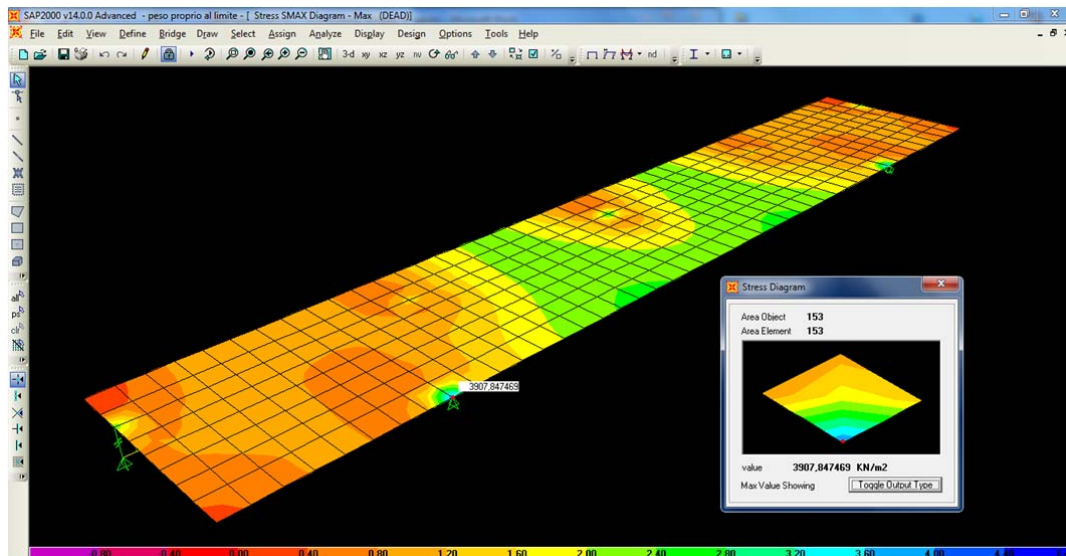


Figure 148: development of maximum stresses in the slab subject to its own weight, according to third way of carriage, with two supports

The maximum stresses found at supports (hangs) amounts to:

$$\sigma_{\max} \approx 3910 \left[\text{KN/m}^2 \right] = 3.91 \left[\text{MPa} \right]$$

Since this just described is the manner leading to the lowest values of tensile stress, and since this value is lower than the limits for the tensile strength carried above, this could be one smart way of transportation of the slab for eventual future applications.

However, to prevent damage during transport and reduce possible crackings due to shrinkage, as previously said on Chapter 7 (“Test results”) we provided a reinforcement system, made by fiber glass bars located longitudinally to the system and at about medium depth of the cross-section of the concrete slab (≈ 25 mm from the bottom).

APPENDIX 2

This annex shows the calculation of the horizontal load acting in a floor of a generic building. This action has to be transferred between adjacent slabs to reach first the resistant walls and then the foundations. Therefore, in order to have an idea about the possible slab to slab connections that we could use, we have to know the value of the maximum horizontal load acting on transversal slab connection.

1 HORIZONTAL LOAD ACTING ON THE SLAB TO SLAB CONNECTION

Before choosing the type of transversal connection between the slabs we must have an idea about the value of horizontal forces that have to be transmitted. To obtain a fairly accurate value we can proceed in the following order:

- We assume to have a building, with definite geometrical features, whose intermediate floors are made of the type described in this report (timber-concrete composite structure)
- For an esteem of the horizontal action, we choose two different locations for the building: first one will be in a high seismicity area, and second one in an area where wind action is dominant
- Choice, dimensioning and verification of the transversal connection system will be made on the basis of the heavier between the values obtained from the two previous situations

1.1 Building features

Assuming hypothetically a commercial background type, we choose a three floors building, with pitched wooden roof, wooden walls type XLAM 20 cm thickness and dimensions in plant equal to 8 x 15 m. We have a frame static scheme with six columns, regularly distributed in the plant construction and with 200 x 350 mm sides.

The height between two successive floors is 3 m.

We assume also that the load bearing walls are distributed along the perimeter of the building and that there is a further wall disposed in central position and parallel to the short side. For simplicity, we make the hypothesis that the area of the openings constitute about 20 % of total walls surface. Below there is the plant of the building, with the reference system whose we'll refer to and the dimensions in meters.

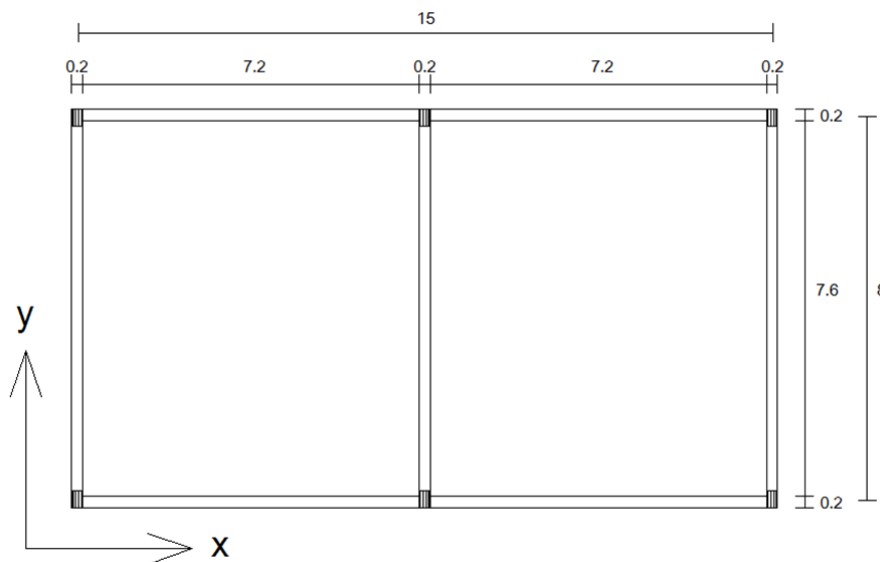


Figure 149: building plant

1.2 Locations of the buildings

According to the above-mentioned criterion, we choose to locate the building in the two following positions:

- Reggio Calabria (high seismic action value)
- Trieste (high wind action value)

We proceed now to the evaluation of the horizontal load in both cases.

1.3 Horizontal load evaluation

1.3.1 Building located in Reggio Calabria

The structure, as mentioned earlier, lies in a high seismicity area. We now calculate three fundamental items, depending on the type of building considered, and that will affect in different manners the calculation method and the building design and check, or else rated life, class of use and reference return period for seismic action.

1.3.1.1 Rated life, Class of use and reference return Period for seismic action

Our building is by definition an ordinary structure with normal importance, that is classified as type 2 building and thus, in accordance with paragraph 2.4.1 of Statement [1], its rated life is equal to:

$$V_N = 50 \text{ (years)}$$

For assumption, the construction provides normal crowding and thus, in accordance with paragraph 2.4.2 of Statement [1], the building belongs to the following Class of Use:

Class of Use: 2

The reference period V_R (years), for the evaluation of the seismic action, is given by the expression (2.4.1) of Statement [1]:

$$V_R = V_N \cdot C_U = 50 \times 1 = 50$$

where V_N and C_U is the use factor which amounts to 1.5 for Class of Use 3.

Tab. 2.4.II – Valori del coefficiente d'uso C_U

CLASSE D'USO	I	II	III	IV
COEFFICIENTE C_U	0,7	1,0	1,5	2,0

1.3.1.2 Loads Analysis

Loads due to intermediate floors

Floors structural load

In accordance with the summarizing table containing the geometrical dimensions of each element of the slab (and reported in previous point 5 of Appendix 1 "Geometrical dimensions achievable for the system"), for a commercial background type building we have the following structural load:

$$G_1 = \gamma_{k,CAP} \cdot h_1 + \gamma_{k,GL} \cdot \frac{h_2 \cdot b_2}{i} = 22.93 \times 0.05 + 3.82 \times \frac{0.45 \times 0.09}{0.8} = 1.40 \left[\frac{KN}{m^2} \right]$$

Floors non structural load

The permanent carried load, calculated in previous chapter 2.2 of Appendix 1 (“Non structural permanent load”) amounts to:

$$G_2 = 2.69 \left[\frac{KN}{m^2} \right]$$

Floors variable load

Variable load acting on the floor, related to a commercial background type building, is equal to:

$$Q_1 = 4.00 \left[\frac{KN}{m^2} \right]$$

According to point 2.5.3 of Statement [1], the seismic combination factor, related to variable loads on the floors, amounts to:

$$\psi_{2D} = 0.6$$

Loads due to the roof

As already stated we assume for the building a pitched wooden roof.

The evaluation of the loads is carried approximately referring to typical stratification and weights derived from literature. In particular we want an average and per unit of horizontal surface uniformly distributed load, or else a surface density of load on the projection of the roof to the horizontal plane. Thus, by the loads point of view, the roof can be considered as a flat slab.

To calculate the loads on the horizontal projection we choose an angle of approximate average slope of 30°.

The roof package stratification is shown in following Figure 150.

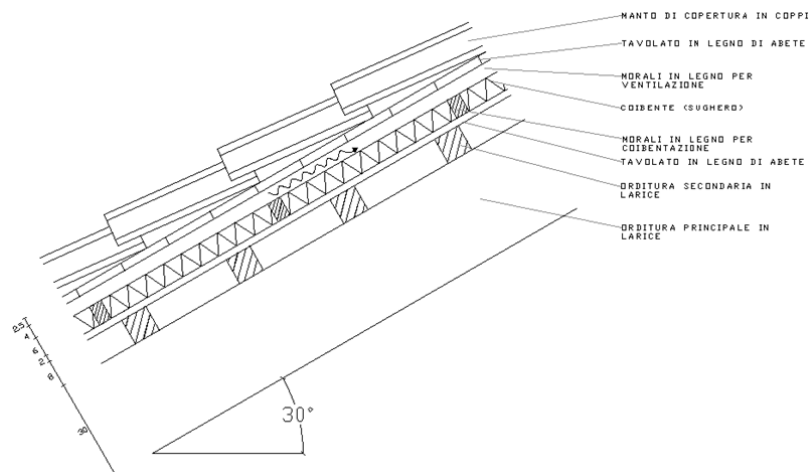


Figure 150: roof package stratification

Roof structural load

As structural loads we must consider all loads due to main and secondary warping.

Main warping is made up by 30 x 24 cm section and 150 cm spacing larch beams. Therefore, the load per unit area is given by:

$$P_{\text{main_warping}} = \frac{\gamma_{\text{LARCH}} \cdot 0.24\text{m} \cdot 0.3\text{m}}{i} \Big/ \cos \alpha = \frac{6 \times 0.24 \times 0.3}{1.5} \Big/ \cos(30^\circ) = 0.33 \left[\frac{\text{KN}}{\text{m}^2} \right]$$

Secondary warping is made by 8 x 8 cm section and 35 cm spacing larch joists. Therefore, the load per unit area is given by:

$$P_{\text{sec_ondary_warping}} = \frac{\gamma_{\text{LARCH}} \cdot 0.08\text{m} \cdot 0.08\text{m}}{i} \Big/ \cos \alpha = \frac{6 \times 0.08 \times 0.08}{0.35} \Big/ \cos(30^\circ) = 0.13 \left[\frac{\text{KN}}{\text{m}^2} \right]$$

Thus, structural load per horizontal unit area amounts to:

$$P_{\text{STRUCTURAL_ROOF}} = P_{\text{main_warping}} + P_{\text{sec_ondary_warping}} = 0.46 \left[\frac{\text{KN}}{\text{m}^2} \right]$$

Roof non structural load

Carried permanent loads are due to roofing, wood planking, morals (timber joists to create an aeration layer) and to insulating material.

The morals (timber joists required to create both ventilation and insulation layer) are made by 4 x 6 cm section and 60 cm spacing spruce frames. Therefore their weight per horizontal unit area amounts to:

$$P_{\text{morals}} = \frac{\gamma_{\text{SPRUCE}} \cdot 0.04\text{m} \cdot 0.06\text{m}}{i} \Big/ \cos \alpha = \frac{6 \times 0.04 \times 0.06}{0.6} \Big/ \cos(30^\circ) = 0.03 \left[\frac{\text{KN}}{\text{m}^2} \right]$$

To these we must add the weight of two spruce planking, respectively with 2.5 cm and 2 cm thickness,

$$P_{\text{planking}} = \gamma_{\text{SPRUCE}} \cdot (0.025\text{m} + 0.2\text{m}) \Big/ \cos \alpha = 6 \times (0.025 + 0.2) \Big/ \cos(30^\circ) = 0.31 \left[\frac{\text{KN}}{\text{m}^2} \right]$$

the weight of insulation material (cork), with 6 cm thickness,

$$P_{\text{insulation}} = \gamma_{\text{CORK}} \cdot 0.06\text{m} \Big/ \cos \alpha = 1 \times 0.06 \Big/ \cos(30^\circ) = 0.07 \left[\frac{\text{KN}}{\text{m}^2} \right]$$

and the weight of roofing, deducted from literature:

$$P_{\text{roofing}} = 0.8 \left[\frac{\text{KN}}{\text{m}^2} \right] \Big/ \cos \alpha = 0.8 \Big/ \cos(30^\circ) = 0.92 \left[\frac{\text{KN}}{\text{m}^2} \right]$$

Therefore the carried permanent load per horizontal unit area amounts to:

$$P_{NON-STRUCTURAL_ROOF} = P_{masonry} + P_{platings} + P_{insulation} + P_{roofing} = 1.33 \left[\frac{KN}{m^2} \right]$$

Roof variable load

In the analysis of the structure located in Reggio Calabria the roof accidental load is not considered. Below is reported the seismic load combination:

$$E + G_1 + G_2 + P + \sum_{i=1}^n \psi_{2i} \cdot Q_{ki}$$

In case of roof variable action, seismic combination factor ψ_{2H} is equal to, in accordance with Table 2.5.I of Statement [1]:

$$\psi_{2H} = 0.0$$

Snow action

In the analysis of the structure located in Reggio Calabria the snow action is not considered. Below is the seismic combination:

$$E + G_1 + G_2 + P + \sum_{i=1}^n \psi_{2i} \cdot Q_{ki}$$

In case of snow, seismic combination factor ψ_{2n} , under 1000 m s.l.m. is equal to, in accordance with Table 2.5.I of Statement [1]:

$$\psi_{2n} = 0.0$$

Wind action

In the analysis of the structure located in Reggio Calabria the wind action is not considered. Below is reported the seismic load combination:

$$E + G_1 + G_2 + P + \sum_{i=1}^n \psi_{2i} \cdot Q_{ki}$$

In case of wind, the seismic combination factor ψ_{2v} is equal to, in accordance with Table 2.5.I of Statement [1]:

$$\psi_{2v} = 0.0$$

Load due to columns

The columns measure 215 x 315 mm in section and they're built in glulam, with a density equal to 3.82 KN / m³.

Columns structural load

Total weight of each column is:

$$P_{COLUMN} = 3.82 \times 0.215 \times 0.315 \times 9 = 2.35 [KN]$$

Therefore, total weight of all columns is:

$$P_{COLUMNS} = 6 \cdot P_{COLUMN} = 6 \times 2.35 = 14.1 [KN]$$

Load due to XLAM walls

We make the hypothesis that all the walls are made of 1.5 cm thick plaster on both sides and 200 mm thick XLAM panels having a density of 5 KN / m³.

Walls structural load

In the case of the walls we evaluate load per vertical unit length:

$$P_{STRUCTURAL_WALLS} = 5 \times 0.2 = 1.0 \left[\frac{KN}{m^2} \right]$$

Walls non structural permanent load

It's the plaster load per vertical unit length (carried permanent load):

$$P_{NON-STRUCTURAL_WALLS} = 16 \left[\frac{KN}{m^3} \right] \times 2 \times 0.015m = 0.48 \left[\frac{KN}{m^2} \right]$$

1.3.1.3 Seismic action

Lateral force method of analysis

For the evaluation of the seismic action effects we provide, according to paragraph 7.3.3.2 of Statement [1], a simplified analysis called "lateral force method of analysis". This analysis will be implemented only with referring to ULS, in order to obtain the maximum value of horizontal load due to earthquake acting on building floors. The seismic action definition is preceded by the determination of "Primary Seismic Hazard" of the construction place, that must be evaluated through the method described at point 3.2 of Statement [1]. Here are the other parameters required to determinate the effect of the seismic action.

Exceedance probability

To ULS is associated the following exceedance probability in the reference return period V_R , presented in Table 3.2.1 of Statement [1]: $P_{V_R} = 10\%$.

Return period of seismic action

Once we have evaluate the reference period V_R and the exceedance probability P_{V_R} , we can obtain the return period of seismic action by the following relation:

$$T_R = -\frac{V_R}{\ln(1 - P_{V_R})} = -\frac{50}{\ln(1 - 0.10)} = 475[\text{years}]$$

Ground type

The ground type of the place where the building arises is B, characterized by the following stratigraphic profile description:

“Deposits of very dense sand, gravel, or very stiff clay, at least several tens of meters in thickness, characterized by a gradual increasing of the mechanical properties with depth”.

Topographical conditions

The topographical category of the place where the building arises is T1:

“Flat land, hillside and isolated peaks with average inclination under 15°”.

Primary Seismic Hazard

Primary Seismic Hazard of the construction place is defined throughout the design ground acceleration on type A and the corresponding elastic response spectrum $S_e(T)$.

Spectral shapes are defined, for each of the exceedance probability P_{V_R} , in the reference period V_R , from following parameters referred to the geographical position of the construction place:

a_g maximum horizontal acceleration of the place

F_0 maximum value for the amplification factor of the response spectrum in horizontal acceleration

T_C^* lower limit of the period of the constant spectral acceleration branch

Once we know the return periods of seismic action we are interested in, and both latitude and longitude of our construction place, Annex B of Statement [1] provides all above mentioned parameters for seismic hazard. In our case these parameters have been obtained through the software “Geostru PS 2010” (displayed in Figure 151) which automatically performs an interpolation of the values related to the geographical grid points identified by Statement [1], and straight gives us the numerical value of these parameters.

T_R [anni]	a_g [g]	F_0 [-]	T_C [s]
30	0,067	2,303	0,274
50	0,090	2,285	0,289
72	0,109	2,281	0,299
101	0,130	2,300	0,313
140	0,153	2,322	0,321
201	0,183	2,348	0,332
475	0,270	2,413	0,361
975	0,363	2,466	0,389
2475	0,512	2,513	0,442

Figure 151: display of the software "Geostru PS 2009" for evaluate seismic hazard parameters

Elastic response spectra in horizontal acceleration

Now we are in possession of all items needed to track the acceleration elastic response spectra at ULS. We recall that the parameters we will use are referred to a 475 years return period. They are expressed by spectral shape referred to a 5% conventional damping and multiplied by the value of the maximum horizontal acceleration a_g on a rigid and horizontal reference place. Obviously both spectral shape and a_g values vary according to the limit state considered, or else according to the exceedance probability considered. They allow to characterize the seismic motion in the horizontal building direction, along its two orthogonal and independent directions x and y .

For the horizontal components of the seismic action, the elastic response spectrum $S_e(T)$ is defined by the following expressions (3.2.4) of Statement [1], regardless of the limit state we are referring to:

$$0 \leq T < T_B \quad S_e(T) = a_g \cdot S \cdot \eta \cdot F_0 \cdot \left[\frac{T}{T_B} + \frac{1}{\eta \cdot F_0} \left(1 - \frac{T}{T_B} \right) \right]$$

$$T_B \leq T < T_C \quad S_e(T) = a_g \cdot S \cdot \eta \cdot F_0$$

$$T_C \leq T < T_D \quad S_e(T) = a_g \cdot S \cdot \eta \cdot F_0 \cdot \frac{T_C}{T}$$

$$T_D \leq T \quad S_e(T) = a_g \cdot S \cdot \eta \cdot F_0 \cdot \frac{T_C \cdot T_D}{T^2}$$

Where T and S_e are respectively vibration period of a linear single-degree-of-freedom system and horizontal spectral acceleration. We emphasize that the spectra thus defined can be used for structures with fundamental vibration period T less than 4 s.

The parameters appearing in all above mentioned expressions are calculated below for the limit state considered.

Horizontal elastic response spectrum at ULS

Now we calculate all the factors appearing in previous expressions (3.2.4), needed for the tracking of the spectrum:

S is the factor that takes account of ground type and topographical conditions by the following relation:

$$S = S_s \cdot S_T = 1.14 \times 1 = 1.14$$

Where:

- S_s is the stratigraphic amplification factor, given in Tab. 3.2.V of Statement [1]; for ground type B it amounts to:

$$1 \leq S_s = 1.4 - 0.4 \cdot \frac{F_0 \cdot a_g}{g} = 1.14$$

- S_T is the topographical amplification factor, given in Tab. 3.2.VI; for T1 category it amounts to:

$$S_T = 1.$$

η is a factor that takes account of energetic dissipation due to damping. If we assume a conventional viscous damping $\xi = 5\%$, we obtain (expression (3.2.6) of Statement [1]):

$$\eta = \sqrt{10/(5 + \xi)} = \sqrt{10/(5 + 5)} = 1$$

T_c is the upper limit of the period of the constant acceleration branch, given by (3.2.7) of [1] :

$$T_c = C_c \cdot T_c^* = 1.349 \times 0.361 = 0.487 [s]$$

where:

- C_c is a factor dependent on the ground type and for ground type B, according to the Table 3.2.V of Statement [1] it is equal to:

$$C_c = 1.1 \cdot (T_c^*)^{-0.2} = 1.1 \times (0.361)^{-0.2} = 1.349$$

T_B is the lower limit of the period of the constant spectral acceleration branch, given by expression (3.2.8) of [1]:

$$T_B = \frac{T_c}{3} = \frac{0.487}{3} = 0.162 [s]$$

T_D is the value defining the beginning of the constant displacement response of the spectrum, given by expression (3.2.9) of Statement [1]:

$$T_D = 4 \frac{a_g}{g} + 1.6 = 4 \times 0.270 + 1.6 = 2.680 [s]$$

By substituting these factors in expressions (3.2.4), previously reported, we can obtain the following elastic response spectrum in horizontal acceleration referred to ULS:

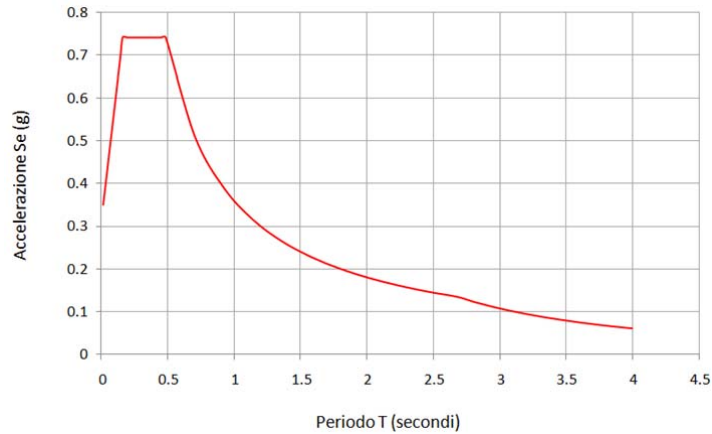


Figure 152: elastic response spectrum in horizontal acceleration referred to ULS

Design response spectrum at ULS

At the ultimate limit state it is expected that the structure is affected by a set of plasticizations that induce a significant Energy dissipation. Therefore, in order to design and check the structure, these dissipative resources can be put into account by reducing the elastic forces as provided in section 3.2.3.5 of Statement [1].

In this case the design spectrum $S_d(T)$ is obtained by scaling the elastic spectrum through the behavior factor q , depending on both material and type of structure, that takes into account of the building dissipation capacity. It is obtained by replacing in the above mentioned expressions (3.2.4) the constant η with the ratio $1/q$.

Anyway we have to verify the following inequality:

$$S_d(T) \geq 0.2 a_g$$

Behavior factor

Behavior factor q is given by expression (7.3.1) of Statement [1]:

$$q = q_0 \cdot K_R$$

where:

- q_0 is the basic value of the behavior factor, depending on the expected ductility level, on the structural typology and on the ratio α_u / α_1 between the seismic action value whereby a number of plastic hinges that turns the structure in a mechanism originates and the value whereby first an element reaches the bending plasticization.
- K_R is a reductive factor which depends on the elevation regularity characteristics of the structure, and is equal to 1 for buildings regular in elevation and to 0.8 for building non-regular in elevation.

The building can be regarded, according to paragraph 7.7.3 of Statement [1], as an “hyperstatic portal structure with cylindrical shanks, bolts, screws and nails as fastener”, belonging to high ductility class (CD A).

For this kind of structure Statement [1] provides, at point 7.7.3 and in Table 7.7.I, a value for q_0 equal to:

Tabella 7.7.I - Tipologie strutturali e fattori di struttura massimi q_0 per le classi di duttilità

Classe		q_0	Esempi di strutture
A	Strutture aventi una alta capacità di dissipazione energetica	3,0	Pannelli di parete chiodati con diaframmi incollati, collegati mediante chiodi e bulloni; strutture reticolari con giunti chiodati
		4,0	Portali iperstatici con mezzi di unione a gambo cilindrico, spinotti e bulloni (con le precisazioni contenute nei seguenti capoversi del § 7.7.3)
		5,0	Pannelli di parete chiodati con diaframmi chiodati, collegati mediante chiodi e bulloni
B	Strutture aventi una bassa capacità di dissipazione energetica	2,0	Pannelli di parete incollati con diaframmi incollati, collegati mediante chiodi e bulloni; strutture reticolari con collegamenti a mezzo di bulloni o spinotti; strutture cosiddette miste, ovvero con intelaiatura (sismo-resistente) in legno e tamponature non portanti
			Portali isostatici con giunti con mezzi di unione a gambo cilindrico, spinotti e bulloni (con le precisazioni contenute nei seguenti capoversi del § 7.7.3)
		2,5	Portali iperstatici con mezzi di unione a gambo cilindrico, spinotti e bulloni (con le precisazioni contenute nei seguenti capoversi del § 7.7.3)

$$q_0 = 4.0$$

The building can't be considered regular in elevation because doesn't respect all requirements provided at paragraph 7.2.2 of Statement [1]. In particular:

- The weight variation between intermediate floor and roof exceeds 25%

In fact, as previously calculated in this Appendix, floors and roof weight in seismic combination load respectively amount to:

$$P_{FLOOR} = (G_1 + G_2 + \psi_{2D} \cdot Q_1) \cdot A_{FLOOR} = (1.40 + 2.69 + 0.6 \cdot 4.00) \times 8 \times 15 = 779 [KN]$$

$$P_{ROOF} = (P_{STRUCTURAL_ROOF} + P_{NON-STRUCTURAL_ROOF}) \cdot A_{ROOF} = (0.46 + 1.33) \times 9 \times 16 = 258 [KN]$$

Thus we assume:

$$K_R = 0.8$$

Therefore the value of the behavior factor q that we have to adopt while evaluating the seismic action is:

$$q = q_0 \cdot K_R = 4.0 \times 0.8 = 3.2$$

By replacing in expressions (3.2.4) of Statement [1] the constant η with the ratio $1/q$ we can obtain the design response spectrum at ULS, carried below:

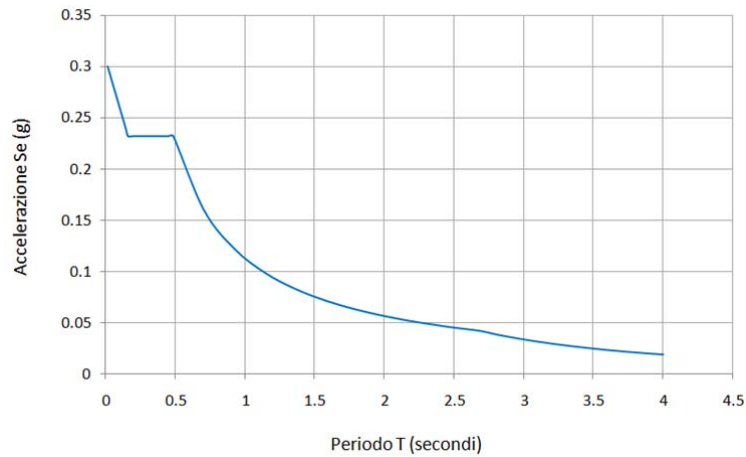


Figure 153: design response spectrum in horizontal acceleration at ULS

Lateral force method of analysis at ULS

We perform, according to paragraph 7.3.3.2 of Statement [1], a simplified analysis called “lateral force method of analysis” to determine the horizontal loads acting on the structure in seismic conditions. It consists in the application of horizontal static forces equivalent to inertia forces due to seismic action on building decks, and can also be adopted for non regular in elevation buildings (using $\lambda=1$) that respect following requirements:

$$T_1 \leq 2.5 \cdot T_c = 2.5 \times 0.487 [s] = 1.218 [s]$$

$$T_1 \leq T_D = 2.68[s]$$

where:

T_1 is the fundamental vibration period of the structure along the direction examined (in our case horizontal)

In this case, since the building is lower than 40 m in elevation and has weight approximately distributed in elevation, we can assume for the period T1 the expression 7.3.3.2 of Statement [1], reported below:

$$T_1 = C_1 \cdot H^{3/4} = 0.05 \times 11^{3/4} = 0.30[s]$$

where:

- H is the height of the building, in m, evaluated from the foundations level. In our case:

$$H \approx 11m$$

- C_1 is a factor equal to 0.05 for wood structures

All the requirements are thus respected:

$$T_1 = 0.30 [s] \leq 2.5 \cdot T_c = 1.218 [s]$$

$$T_1 = 0.30 [s] \leq T_D = 2.68 [s]$$

In the lateral force method of analysis we assume for the building a main vibration mode, characterized by a period T_1 evaluated approximately, and by displacements linearly increasing in elevation from the foundations level. To this mode is associated a certain percentage of the mass, 0.85 or 1, depending on the type of the building. Therefore we don't have to make any effects combination because we don't consider secondary vibration modes. The effects of seismic action shall be calculated only on the vibration mode considered.

For each of the two main directions the seismic forces are considered applied on decks levels, where we assume the seismic masses are concentrated, as shown in following Figure 154.

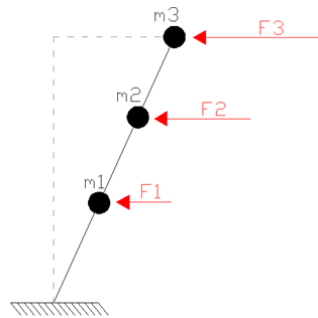


Figure 154: modeling of the structure according to lateral force method of analysis: displacements linearly increasing in elevation and masses concentrated at decks level

The load that must be applied to each mass (deck) of the construction can be evaluated by following expression (7.3.6) of Statement [1]:

$$F_i = F_h \cdot z_i \cdot W_i / \sum_j z_j \cdot W_j$$

where:

- F_h is the total horizontal action on the considered direction:

$$F_h = S_d(T_1) \cdot W \cdot \lambda / g$$

- F_i is the horizontal action to be applied to mass i
- W_i and W_j are the weights respectively of mass i and mass j
- z_i and z_j are the heights, with respect to foundations level, of mass i and mass j
- $S_d(T_1)$ is the design response spectrum corresponding to building fundamental vibration period T_1
- g is the gravity acceleration

- λ is a factor equal to 0.85 when the building has at least three floors and when $T_1 < 2 T_c$, and equal to 1 in all other cases. Since our construction is not regular in elevation we have:

$$\lambda = 1.0$$

Now we need to calculate the weights corresponding to each deck. They are evaluated according to the seismic load combination (3.2.4 of [1]):

$$W_i = G_{1,i} + G_{2,i} + \psi_2 \cdot Q_i$$

in which the reductive factor ψ_2 depends on the type of accidental action considered.

Seismic weights

The calculation of weights associated to different decks in seismic combination has already been performed at the beginning of this chapter. However, to those we must add the self weights of the vertical structural elements. Assuming a openings area equal to about 20% of the external wall surface, the weight of the walls on seismic masses associated to intermediate floors is:

$$\begin{aligned} P_{WALLS_FLOORS} &= (P_{STRUCTURAL_WALLS} + P_{NON-STRUCTURAL_WALLS}) \cdot (1 - 0.2) \cdot 3m \cdot (2 \cdot 15 + 3 \cdot 8)m + \frac{P_{COLUMNS}}{3} = \\ &= (1.0 + 0.48) \times 0.8 \times 3 \times 54 + \frac{14.1}{3} = 197 [KN] \end{aligned}$$

The weight of the walls associated to roof seismic mass is instead:

$$\begin{aligned} P_{WALLS_ROOF} &= (P_{STRUCTURAL_WALLS} + P_{NON-STRUCTURAL_WALLS}) \cdot (1 - 0.2) \cdot 1.5m \cdot (2 \cdot 15 + 3 \cdot 8)m + \frac{P_{COLUMNS}}{6} = \\ &= (1.0 + 0.48) \times 0.8 \times 1.5 \times 54 + \frac{14.1}{6} = 98 [KN] \end{aligned}$$

Here are the values for the weights of intermediate floors and roof, already calculated at previous paragraph of this Appendix "*Design response spectrum*":

$$P_{FLOORS} = (G_1 + G_2 + \psi_{2D} \cdot Q_1) \cdot A_{FLOORS} = (1.40 + 2.69 + 0.6 \cdot 4.00) \times 8 \times 15 = 779 [KN]$$

$$P_{ROOF} = (P_{STRUCTURAL_ROOF} + P_{NON-STRUCTURAL_ROOF}) \cdot A_{ROOF} = (0.46 + 1.33) \times 9 \times 16 = 258 [KN]$$

Now we can calculate the seismic masses.

Seismic masses associated to intermediate floors

$$P_{FLOORS_SEISMIC} = P_{FLOORS} + P_{WALLS_FLOOR} = 779 + 197 = 976 [KN]$$

Seismic masses associated to roof

$$P_{ROOF_SEISMIC} = P_{ROOF} + P_{WALLS_ROOF} = 258 + 98 = 356 [KN]$$

Total mass of the building in seismic combination

The total weight of the structure in seismic combination is obtained by adding the seismic weights related to the various decks and coverage. To those must be added the contribution of vertical elements at the ground level, equal to that provided at the cover:

$$P_{TOT_SEISMIC} = 2 \cdot P_{FLOORS_SEISMIC} + P_{ROOF_SEISMIC} + P_{WALLS_ROOF} = 2 \times 976 + 356 + 98 = 2406 [KN]$$

Evaluation of seismic loads acting at decks level

Once we know the seismic weights that form the structure, we can calculate the way in which the horizontal force equivalent to seismic action distribute itself, by using the above mentioned expressions.

Before performing the calculation of the horizontal forces acting on each deck we have to determine the value of the design acceleration corresponding to the period T_1 of the main vibration mode, and the value of the total shear load due to earthquake acting at ground level (total horizontal load acting on the building).

Since we have:

$$T_B = 0.162[s] \leq T_1 = 0.30[s] \leq T_C = 0.487[s]$$

the design acceleration value amounts to:

$$S_e(T) = a_g \cdot S \cdot F_0 \cdot \frac{1}{q} = 0.270 \times 1.14 \times 2.413 \times \frac{1}{3.2} = 0.232$$

The total horizontal load acting on the building is thus equal to:

$$F_h = S_d(T_1) \cdot W \cdot \lambda / g = (0.232 \cdot g \cdot 2406 \cdot 1.0 / g) [KN] = 558 [KN]$$

The resultant values are presented in the following table:

LEVEL	W_i [KN]	z_i [m]	$W_i \cdot z_i$ [KNm]	γ_i	W [KN]	$S_d(T_1)$	λ	F_h [KN]	F_i [KN]
ROOF	356	10	3560	0.288	2406	0.232	1.0	558	161
2° DECK	976	6	5856	0.474					265
1° DECK	976	3	2928	0.237					132
GROUND	98	0	0	0					-
TOTAL	2936	-	12344	1					558

It only remains to verify that the value of the design acceleration corresponding to period T_1 of the main vibration mode observes the inequality of section 3.2.3.5 of Statement [1]:

$$S_d(T_1) = 0.232 \cdot g > 0.2 \cdot a_g = 0.2 \times 0.270 \times g = 0.054 \times g$$

Therefore, as we can see from previous table, the maximum shear acting on a floor is equal to:

$$F_{MAX} = 265 [KN]$$

1.3.2 Building located in Trieste

The building now lies in an area where the wind action is very burdensome. With respect to the previous case, to determine the maximum horizontal load due to wind is not necessary the calculation of all loads acting on the building but it is sufficient to evaluate the characteristic wind action and to be aware of the external walls sizes.

1.3.2.1 Wind action

Here we calculate the significant values of the wind pressure on vertical facades of the building, as prescribed in paragraph 3.3 of Statement [1].

Wind velocity

With reference to wind action, the building is located in Zone 8. For this area Statement [1] provides the following parameters to evaluate the wind reference velocity.

$$V_{b,0} = 30 [m / s]$$

$$a_0 = 150 [m]$$

$$k_a = 0.01 [1/s]$$

The place where the construction arises is located at sea level:

$$a_s = 0m < a_0 = 150 [m]$$

Thus, the wind reference velocity is given by following expression (3.3.1) of Statement [1]:

$$V_b = V_{b,0} = 30 [m / s]$$

Peak velocity pressure

Peak velocity pressure is given by expression (3.3.4) of Statement [1]:

$$q_b = \frac{1}{2} \cdot \rho \cdot V_b^2 [N / m^2]$$

where:

ρ is the air density, conventionally assumed equal to 1.25 kg/m^3

V_b is the wind reference velocity

By substituting these values we obtain:

$$q_b = \frac{1}{2} \cdot \rho \cdot V_b^2 [N/m^2] = \frac{1}{2} \times 1.25 \times 30^2 = 562.5 [N/m^2]$$

Exposure factor

Exposure factor can be obtained in accordance with the method suggested at point 3.3.7 of Statement [1].

As hypothesis the building is located in an urban/industrial area and thus we choose for the ground the roughness class B.

The construction place is located in Zone 8 (Trieste) along the coast and thus at an elevation lower than 500 m on the sea level. Therefore, the exposure category of the place is the fourth (IV).

ZONE 7,8			
	mare		costa
	1.5 km	0.5 km	
A	--	--	IV
B	--	--	IV
C	--	--	III
D	I	II	*
* Categoria II in zona 8 Categoria III in zona 7			

At this category are associated the following parameters to define the exposure factor:

$$z_{\min} = 8[m]$$

$$z_0 = 0.3[m]$$

$$k_r = 0.22$$

We assume for the topographical factor the following value:

$$c_t = 1$$

Thus we have all items required to calculate the exposure coefficient. It is evaluated with reference both to the elevation $z < z_{\min}$ and to the average elevation between z_{\min} and the maximum building height (approximately 11 m), then at a height of 9.5 m:

$$c_e(z \leq z_{\min}) = k_r^2 \cdot c_t \cdot \ln\left(\frac{z_{\min}}{z_0}\right) \cdot \left[7 + c_t \cdot \ln\left(\frac{z_{\min}}{z_0}\right)\right] = 1.634$$

$$c_e(z = 9.5m) = k_r^2 \cdot c_t \cdot \ln\left(\frac{z}{z_0}\right) \cdot \left[7 + c_t \cdot \ln\left(\frac{z}{z_0}\right)\right] = 1.748$$

Dynamic factor

Since our building is regular in shape and doesn't exceed 80 m in height, the dynamic factor is conservatively assumed equal to 1, as provided at point 3.3.8 of Statement [1]: $c_d = 1$

Pressure coefficients

Shape factor can be evaluated according to point C3.3.10 of Statement [5]. It assumes values that rely on the wind direction and on location and inclination of the surface considered. From following Figures C3.3.2 and C3.3.3 of Statement [5] we can obtain shape factor values:

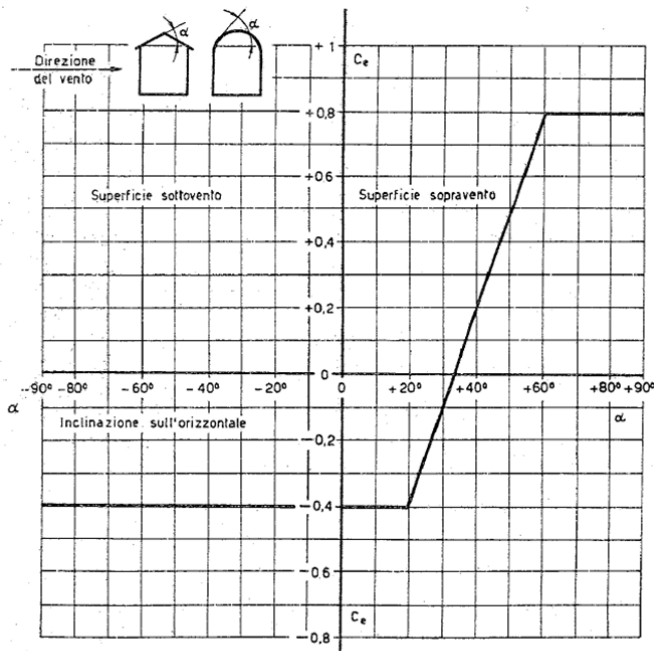


Figura C3.3.2 Valori assunti da c_{pe} al variare di α

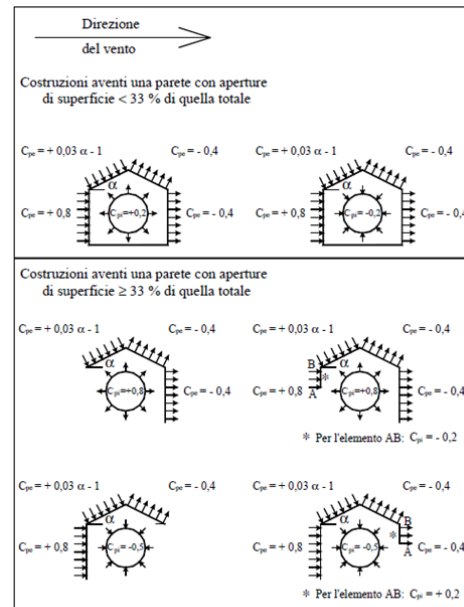


Figura C3.3.3 Coefficienti di forma per gli edifici.

In our case the building is made up by walls with area openings lower than 33 % of total external walls surface.

Thus, as shown in figure C3.3.3, we assume an external pressure coefficient equal to $C_{pe} = +0.8$ on the upwind wall and an external pressure coefficient equal to $C_{pe} = -0.4$ on the downwind wall.

Internal pressure coefficient is instead equal to: $C_{pi} = \pm 0.4$.

These values are graphically represented in following figure 155.

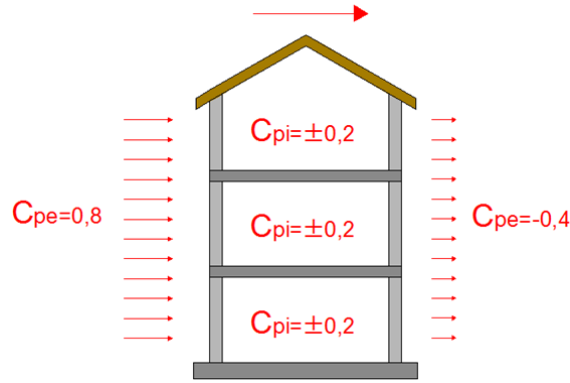


Figure 155: wind: pressure coefficient

Since we want to know the total load acting along the direction parallel to the building long side, with the aim of determining the horizontal action orthogonal to the floor warping and thus of dimensioning the transversal slab to slab connection, we calculate now only the horizontal force acting in direction parallel to the building long side, assuming (as indicated in previous Figure 155) that the slope of the roof is also parallel to the building long side.

Wind pressure

Wind pressure is given by expression (3.3.2) of Statement [1]:

$$P = q_b \cdot c_e \cdot c_p \cdot c_d$$

where:

q_b is the peak velocity pressure

c_e is the exposure factor

c_p is the pressure coefficient (or shape factor)

c_d is the dynamic factor

Since we have already evaluated all the above mentioned quantities we are then able to assess the wind pressure acting on the building walls. We neglect the internal pressure factor because in the following determination of wind global effects his contribution elides.

- On the upwind wall acts the following pressure, at an height $z < z_{\min}$:

$$p_v = q_b \cdot c_e(z = z_{\min}) \cdot c_{pe} \cdot c_d = 562.5 \times 1.634 \times 0.8 \times 1 = 735 [N/m^2] = 0.735 [KN/m^2]$$

- On the upwind wall acts the following pressure, at an height $z = 9.5$ m:

$$p_v = q_b \cdot c_e(z = 9.5m) \cdot c_{pe} \cdot c_d = 562.5 \times 1.748 \times 0.8 \times 1 = 787 [N/m^2] = 0.787 [KN/m^2]$$

- On the downwind wall acts the following pressure, at an height $z < z_{\min}$:

$$p_v = q_b \cdot c_e(z = z_{\min}) \cdot c_{pe} \cdot c_d = 562.5 \times 1.634 \times (-0.4) \times 1 = -368 [N/m^2] = -0.368 [KN/m^2]$$

- On the downwind wall acts the following pressure, at an height $z = 9.5$ m:

$$p_v = q_b \cdot c_e(z=9.5m) \cdot c_{pe} \cdot c_d = 562.5 \times 1.748 \times (-0.4) \times 1 = -393 \text{ [N/m}^2\text{]} = -0.393 \text{ [kN/m}^2\text{]}$$

Wind total load

Wind total load is given by:

$$F = p \cdot A$$

where:

A is the total area on which acts the wind

In our case we consider two surfaces, one located fully at an height $z < z_{\min}$ (called A_1) and the other (called instead A_2) located at an height $z > z_{\min}$ and for which we will refer to exposure factor evaluated at the height of 9.5 m. Here we calculate the values of these areas.

$$A_1 = 8m \cdot z_{\min} = 8 \times 8 = 64 \text{ m}^2$$

$$A_2 = 8 \times 1 + \frac{8 \times (8 \times \text{tg } 30^\circ)}{2} = 26.5 \text{ m}^2$$

Total wind force is obtained by subtracting the wind pressure acting on downwind wall from wind pressure acting on upwind wall:

$$F = p \cdot A = [0.735 - (-0.368)] \times 64 + [0.787 - (-0.393)] \times 26.5 = 102 \text{ [kN]}$$

To the just obtained value we must add the contribution given by tangential wind action. In our case, because of the geometrical properties of the building, this value is equal to zero. Indeed, in agreement with Figure 7.22 of Statement [1] (below), the reference surface on which the wind performs its tangential action is null, being positioned at a distance equal to the minimum between $2b$ and $4h$.

$$\min \{2b; 4h\} = \min \{2 \times 8; 4 \times 11\} \text{ m} = \min \{16; 44\} \text{ m} = 16 \text{ m} > d = 15 \text{ m}$$

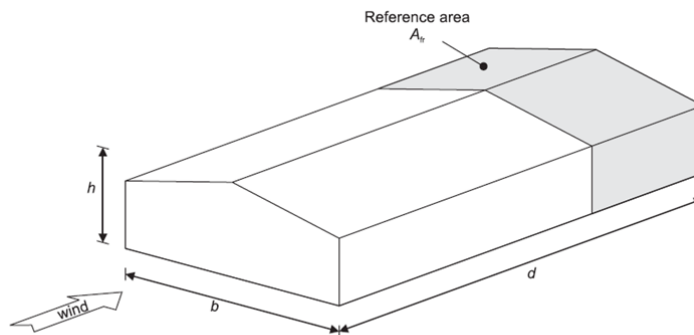


Figure 7.22 — Reference area for friction

The characteristic value of total wind load acting parallel to the building long side is thus:

$$F_{k,w} = 102 \text{ [KN]}$$

To obtain the design value is sufficient considering a load combination on which the wind action plays the role of main variable load and multiply the characteristic value for the partial safety factor $\gamma_Q = 1.5$ related to variable actions with unfavorable effect. Therefore we obtain:

$$F_{d,w} = \gamma_Q \cdot F_{k,w} = 1.5 \times 102 = 153 \text{ [KN]}$$

Maximum horizontal load acting on decks

The just obtained value distributes between intermediate floors according to the simplified static scheme of simple support (but we can reach similar results by using the method of influence areas related to each deck). In accordance with figure 156 carried below, maximum horizontal wind force acting on intermediate floors and parallel to the building long side amounts to:

$$F_{MAX} = \frac{F_{d,w}}{3} = \frac{153}{3} = 51 \text{ [KN]}$$

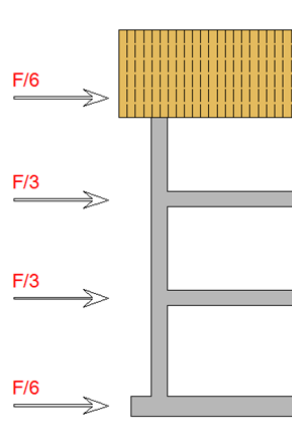


Figure 156: distribution of the horizontal wind force between the building decks

Maximum load acting on the connection system

The maximum design force through which we are going to choose, design and check the transversal slab to slab connection system is the higher value between the one obtained on the building located in Reggio Calabria and the other obtained on the building in Trieste, or else:

$$F_{MAX} = \max \{ F_{MAX_sisma} ; F_{MAX_w} \} = \max \{ 265 ; 51 \} \text{ [KN]} = 265 \text{ [KN]}$$

The force value that we'll use to design the connection system is equal to half of the just obtained value. In fact, as we can see from next figure 157, assuming the need to bring the load to two lateral shear walls, the horizontal load that must pass throughout the most stressed plate amounts to $F/2$.

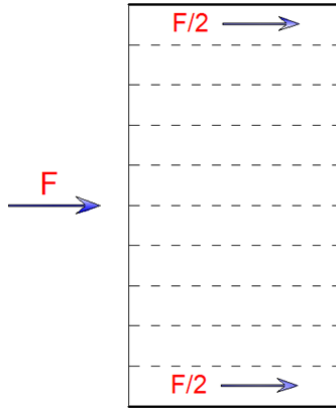


Figure 157: load path in the hypothesis of two lateral shear walls

Typology of connection system

We choose to make use of steel plates fixed to concrete elements throughout metal fasteners as screws or bolts. Each row has four connectors, two of which are positioned on one side with respect to the plate edge and the remaining two on the other edge, as shown in Figure 158. Below there is a table containing the type of metal fastener and the geometrical data of the possible connection made with this type of fastener, in addition to the explanation of the symbols used in the table.

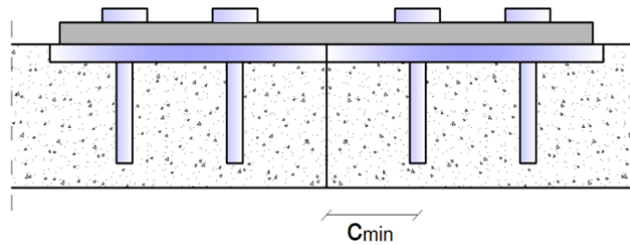


Figure 158: transversal slab to slab connection system

c_{min} is the minimum distance between fastener and slab edge (orthogonally to the slab warping) as indicated by the producer

s_{min} is the minimum spacing between fastener as indicated by the

s is the spacing at which we choose to locate fasteners

n_{min} is the minimum number of connections to be positioned, equal to $F_{MAX}/(2*2*F_{conn})$

n is the number of connectors that are positioned in each of the two slab edges (long sides)

F_{sd} is the design stress acting on each connector

F_{conn} is the average strength of each connector, as recommended by the producer

type	c_{min} [mm]	s_{min} [mm]	s [mm]	n_{min}	n	F_{sd} [kN]	F_{conn} [kN]
NWB 6-45 (Bossong)	45	45	170	44.2	47	1.41	1.50
NWB 10-60 (Bossong)	45	45	250	31.5	32	2.07	2.10
BRB 9-40 (Bossong)	45	45	440	17.4	18	3.68	3.80
DRB 9-40 (Bossong)	45	45	275	28.8	29	2.28	2.30
BRTS 9-45 (Bossong)	45	45	570	13.8	14	4.73	4.80
BPB 8-45 (Bossong)	45	45	170	17.4	18	3.68	3.80

Table 6: type and number of fasteners of the possible slab to slab connection

NWB 6-45: minimum thickness of the support = 80 mm; F_{conn} is the recommended shear strength ($\rho_{foro} < 50$ mm)

NWB 10-60: minimum thickness of the support = 90 mm; F_{conn} is the recommended shear strength ($\rho_{foro} < 50$ mm)

BRB 9-40: minimum thickness of the support = 80 mm; F_{conn} is the recommended shear strength ($\rho_{foro} < 50$ mm)

DRB 9-40: minimum thickness of the support = 80 mm; F_{conn} is the recommended shear strength ($\rho_{foro} < 50$ mm)

BRTS 9-45: minimum thickness of the support = 80 mm; F_{conn} is the recommended shear strength ($\rho_{foro} < 50$ mm)

BPB 8-45: minimum thickness of the support = 80 mm; F_{conn} is the recommended shear strength ($\rho_{foro} = 50$ mm)

ACKNOWLEDGEMENTS

First of all, I'd like to say that my study permanence in Lund has been absolutely one of the greatest experiences in my lifetime, not only for the fact that during this period I've been learning a lot of things related to the school, but also because I had the opportunity to live and be in contact with people with different culture, habits and way of thinking. I really recommend to everyone a similar experience, and I consider myself particularly lucky for this possibility I had.

Here there are some guys I really would like to thank to, in particular Roberto Crocetti, ordinary professor at Lunds Tekniska Högskola, who has always been kind with me, helpful and available for any problem and who even gave me hospitality during the first time in Sweden. He also provided all the material required for this research project and followed all the experimental tests. Per-Olof Rosenqvist, laboratory technician at Lunds Tekniska Högskola, who really helped me in everything concerning the work in the lab even if he was back-injury and couldn't move so much (construction of the formworks, pouring of the concrete, lifting of the slabs, fastening of the slabs to the beams, and execution of all the tests). Tiziano Sartori, PhD student at Trento University, who followed me in the whole theoretical part of this experimental research and brought me in Lund by car from Italy all the shear connectors required (steel pipes and screws). Maurizio Piazza, ordinary professor at Trento University, who gave me the possibility and allowed me to share this great experience in a foreign country. Peter Lungqvist, PhD student at Lunds Tekniska Högskola, who performed the dynamic tests in this experimental research. Daniel Honfi and Ivar Björnsson, PhD students at Lunds Tekniska Högskola, who have been my opponents during my presentation of this Master Thesis at the Lunds Universitet.

1	INTRODUCTION	5
1.1	<i>Background</i>	5
1.2	<i>Aims and scope</i>	6
1.3	<i>Outline of the thesis</i>	7
2	REFERENCES	9
3	SHEAR CONNECTORS IN TIMBER-CONCRETE COMPOSITE STRUCTURES	11
3.1	<i>“Oregon tests” – the first timber-concrete composite connectors</i>	11
3.2	<i>Strengthening of old timber structures and renovation of wooden bridges</i>	12
3.3	Timber-concrete connections	13
3.3.1	<i>Epoxy glue as a shear connector</i>	
3.3.2	<i>Epoxy glued-in continuous shear connectors</i>	
3.3.3	<i>Glued-in shear connectors</i>	
3.3.4	<i>Vertical, inclined nails, screws, bolts and horizontal shear connector types</i>	
3.3.5	<i>Punched metal plate fasteners</i>	
3.3.6	<i>Notch-type connectors with and without dowel</i>	
3.3.7	<i>Mechanical continuous shear connectors</i>	
3.4	<i>Different materials – from lightweight to high performance steel fiber reinforced concrete</i>	32
4	SLAB TO SLAB SHEAR CONNECTION	35
4.1	State of the art	35
4.1.1	<i>Why is cross connection so significant?</i>	
4.1.2	<i>Shear connections exploited so far</i>	
5	COMPOSITE ACTION OF TIMBER-CONCRETE COMPOSITE SYSTEMS	51
5.1	<i>Background</i>	51
5.2	<i>Theoretical models for incomplete composite action</i>	53
5.3	<i>Design procedure according to Eurocode 5 – γ-method</i>	55
5.4	<i>Short and long-term verification</i>	57
6	STIFFNESS OF THE TIMBER-CONCRETE CONNECTORS	61
6.1	Stiffness of the connection system type T12	61
6.1.1	<i>Stiffness evaluation</i>	
6.2	Stiffness of the connection system type F45	72
6.2.1	<i>Stiffness evaluation</i>	
6.3	Final values of stiffness	81
7	EXPERIMENTAL TESTS	83
7.1	Introduction	83
7.2	Shear tests program	83
7.2.1	<i>Test set-up</i>	
7.2.2	<i>Specimens design and preparation</i>	
7.2.3	<i>Optical full-field deformation measurement</i>	
7.2.4	<i>Test results</i>	

7.2.5	<i>Results and discussions</i>	
7.3	<i>Bending tests program</i>	89
7.3.1	<i>Specimens design and preparation</i>	
7.3.2	<i>Bending tests</i>	
7.3.2.1	<i>Evaluation of the load P</i>	
7.3.2.2	<i>Other tests performed</i>	
7.3.2.3	<i>Residential background type</i>	
7.3.2.4	<i>Commercial background type</i>	
7.3.2.5	<i>Comparison between the two systems</i>	
APPENDIX 1		117
1	<i>MATERIALS</i>	117
1.1	<i>Fiber reinforced concrete</i>	117
1.2	<i>Glulam</i>	120
2	<i>LOAD COMBINATIONS</i>	124
2.1	<i>Structural permanent load</i>	125
2.2	<i>Non structural permanent load</i>	126
2.3	<i>Variable load</i>	127
3	<i>DATA</i>	127
3.1	<i>Spans</i>	128
3.2	<i>Width of the glulam beams</i>	128
3.3	<i>Spacing between the glulam beams</i>	128
3.4	<i>Connection system</i>	128
3.5	<i>Check of the connection</i>	128
4	<i>CALCULATION EXAMPLE</i>	130
4.1	<i>Load combinations</i>	131
4.1.1	<i>External actions</i>	
4.2	<i>Properties of the connection system</i>	132
4.3	<i>Stiffness properties of the composite system</i>	132
4.4	<i>Strength verifications</i>	136
4.4.1	<i>Strength verifications at $t = 0$ with only permanent loads</i>	
4.4.2	<i>Strength verifications at $t = 0$ with all loads</i>	
4.4.3	<i>Strength verifications at $t = \infty$ with all loads</i>	
4.5	<i>SLS verifications</i>	147
4.5.1	<i>Mid span deflection check at $t = 0$</i>	
4.5.2	<i>Mid span deflection check at $t = \infty$</i>	
4.5.3	<i>Vibrations check at $t = 0$</i>	

4.5.4	<i>Vibrations check at $t = \infty$</i>	
5	LIFTING CHECK	153
5.1	<i>EF analysis</i>	154
5.2	<i>Determination of strength limit values</i>	157
5.3	<i>Conclusions</i>	158
APPENDIX 2		161
1	HORIZONTAL LOAD ACTING ON THE SLAB TO SLAB CONNECTION	161
1.1	<i>Buildings features</i>	161
1.2	<i>Locations of the buildings</i>	162
1.3	<i>Horizontal load evaluation</i>	162
1.3.1	<i>Building located in Reggio Calabria</i>	
1.3.1.1	<i>Rated Life, Class of Use and Reference Return Period for seismic action</i>	
1.3.1.2	<i>Loads analysis</i>	
1.3.1.3	<i>Seismic action</i>	
1.3.2	<i>Building located in Trieste</i>	
1.3.2.1	<i>Wind action</i>	
ACKNOWLEDGEMENTS		185